

TECHNISCHE UNIVERSITÄT MÜNCHEN
Lehrstuhl für Experimentelle Genetik

Molecular and functional analysis of the ERAD
effector VCP in cellular and Drosophila models
for retinitis pigmentosa

Ana Griciuc

Vollständiger Abdruck der von der Fakultät Wissenschaftszentrum Weihenstephan für Ernährung, Landnutzung und Umwelt der Technischen Universität München zur Erlangung des akademischen Grades eines

Doktors der Naturwissenschaften

genehmigten Dissertation.

Vorsitzender: Univ.-Prof. Dr. S. Scherer

Prüfer der Dissertation: 1. apl. Prof. Dr. J. Adamski
2. Univ.-Prof. Dr. D. Langosch
3. Univ.-Prof. Dr. M. Ueffing
(Eberhard-Karls-Universität Tübingen)

Die Dissertation wurde am 27.04.2010 bei der Technischen Universität eingereicht und durch die Fakultät Wissenschaftszentrum Weihenstephan für Ernährung, Landnutzung und Umwelt am 24.07.2010 angenommen.

To my dear parents Lidia and Ion

Table of contents

Abbreviations	1
Summary	5
Zusammenfassung	7
I. INTRODUCTION	9
Part one: The physiology and pathophysiology of Rhodopsin: Visual processing and <i>retinitis pigmentosa</i>	11
1.1 Vision in vertebrates and flies	11
1.1.1 The vertebrate retina	12
1.1.2 The <i>Drosophila</i> retina	12
1.2 Visual processing by vertebrate photoreceptor neurons	14
1.2.1 Vertebrate photoreceptor neurons	14
1.2.2 The visual transduction cascade	15
1.3 <i>Retinitis pigmentosa</i> : clinical and pathological features	17
1.4 Genetics of <i>retinitis pigmentosa</i>	18
1.4.1 Overview of genetic complexity in <i>retinitis pigmentosa</i>	19
1.4.2 Autosomal dominant <i>retinitis pigmentosa</i> caused by <i>Rhodopsin</i> mutations	21
1.4.3 <i>Retinitis pigmentosa</i> caused by <i>Rh</i> ^{P23H} mutations	23
1.5 Cellular models of <i>retinitis pigmentosa</i>	24
1.6 Rodent models of <i>retinitis pigmentosa</i>	25
1.7 <i>Drosophila</i> models of <i>retinitis pigmentosa</i>	27
1.7.1 The <i>Rh1</i> ^{P37H} model of <i>retinitis pigmentosa</i>	28
1.8 Mechanisms of photoreceptor cell death in <i>retinitis pigmentosa</i>	28
Part two: ER quality control and the ERAD effector VCP	32
A. ER quality control, ERAD and ER stress: mechanisms and impairment in disease	32
2.1 Overview of ER quality control	32
2.2 ERAD molecular machinery and ubiquitin proteasome system	33
2.3 Pathways activated during ER stress: relevance and mechanisms	39
2.4 Imbalanced ERAD and human disease	41
B. The ERAD effector VCP: biochemistry, genetics, pathology	42
2.5 VCP structure and cofactors	42
2.6 VCP is a major ERAD effector	44
2.7 ERAD-independent functions of VCP	45
2.8 VCP and human disease	46
2.9 Fine control of VCP/ERAD activity is required to avoid pathology	47
2.10 Disturbed quality control and ER stress as a cause for <i>retinitis pigmentosa</i> ?	47
2.11 Aims of the study	48

II. RESULTS	49
Part one: Clearance of Rh^{P23H} aggregates requires the ERAD effector VCP	51
1.1 VCP co-localizes with misfolded Rh ^{P23H} <i>in vitro</i>	51
1.2 VCP forms a complex with Rh aggregates	54
1.3 Proteasome inactivation enhances the interaction between VCP and misfolded Rh	56
1.4 VCP interaction with misfolded Rh requires its ND1 domains	57
1.5 VCP is required for degradation of misfolded Rh	58
1.6 D2 ATPase activity of VCP is required for degradation of misfolded Rh	60
1.7 Effect of Rh misfolding and of VCP expression on SK-N-SH cell viability	63
Part two: Genetic inactivation of VCP suppresses Rh1^{P37H}-induced retinal pathology in <i>Drosophila</i>	65
2.1 Rh1 ^{P37H} -mediated degeneration is light- and age-dependent	65
2.2 Loss of mature Rh1 in Rh1 ^{P37H} flies	68
2.3 Endogenous Rh1 is required for Rh1 ^{P37H} toxicity	69
2.4 VCP is required <i>in vivo</i> for clearance of misfolded Rh1 ^{P37H}	70
2.5 Partial VCP inactivation restores mature Rh1 levels in Rh1 ^{P37H} flies	72
2.6 Increased activation of the Ire1/Xbp1 UPR pathway in Rh1 ^{P37H} flies with decreased VCP function	74
2.7 Partial VCP inactivation increases the activation of the Ire1/Xbp1 pathway in GMR/UAS-Rh1 ^{G69D} and Rh1 ^{G69D} flies	76
2.8 VCP inactivation suppresses first signs of retinal degeneration in Rh1 ^{P37H} flies	78
2.9 Suppression of Rh1 ^{P37H} -induced retinal degeneration by VCP loss-of-function alleles	79
2.10 Dramatic suppression of the Rh1 ^{P37H} -mediated retinal degeneration after pharmacological inhibition of the VCP/ERAD/proteasome axis	81
2.11 Partial VCP inactivation restores visual processing in Rh1 ^{P37H} flies	83
2.12 Blindness in Rh1 ^{P37H} flies is rescued in a VCP hypomorphic background	85
2.13 VCP inactivation rescues the retinal pathology induced by a second class II Rhodopsin mutant, Rh1 ^{D1}	86
III. DISCUSSION	89
1. The ERAD effector VCP co-localizes and interacts with misfolded Rh <i>in vitro</i>	92
2. VCP is required for clearance of misfolded Rh <i>in vitro</i> and <i>in vivo</i>	94
3. Dramatic retinal degeneration and blindness are triggered by misfolded Rh in a light- and age-dependent manner in <i>Drosophila</i>	98
4. Endogenous Rh ^{WT} is recruited by misfolded Rh into aggregates	99
4.1 Misfolded Rh1 ^{P37H} forms aggregates in <i>Drosophila</i>	100
4.2 The endogenous Rh1 is required for Rh1 ^{P37H} toxicity	101
5. Dramatic rescue of blindness in Rh1 ^{P37H} flies by decreasing VCP activity	102
6. Upregulation of the Ire1/Xbp1 pathway might be protective in the Rh1 ^{P37H} retina	103
7. Potential pro-apoptotic effects of the VCP/ERAD/proteasome axis in the Rh1 ^{P37H} retina	104
8. How does decreased VCP/ERAD/proteasome activity prevent photoreceptor neuron cell death in the Rh1 ^{P37H} retina?	107

9. Interaction between misfolded Rh ^{P23H} , VCP activity, aging and light exposure might cause <i>retinitis pigmentosa</i>	111
10. Manipulation of Rh proteostasis via VCP/ERAD/proteasome axis as a therapeutic strategy for <i>Rh^{P23H}</i> -linked RP?	111
11. Perspectives	113
11.1 Ongoing and planned experiments	113
11.2 Towards differential (personalized) and integrative (multi-target) treatments of <i>retinitis pigmentosa</i> ?	113
IV. MATERIALS AND METHODS	115
A. Materials	117
A.1 Chemicals, reagents, commercial kits and enzymes	117
A.2 Consumable materials	118
A.3 Equipment	119
A.4 Oligonucleotides	120
A.5 Plasmids and constructs	121
A.6 Antibodies	122
A.7 Cell lines and bacteria	123
A.8 Media, buffers and standard solutions	123
A.8.1 Media and antibiotics for bacterial culture	123
A.8.2 Media and supplements for cell culture	124
A.8.3 Fly food	124
A.8.4 Buffers and standard solutions	124
A.8.5. Solutions and buffers for biochemistry, Western Blotting and histology	125
A.9 Fly stocks	127
A.10 Software and databases	128
B. Methods	129
B.1 Molecular biology	129
B.1.1 E. coli cultures	129
B.1.2 Chemical transformation of competent <i>E. coli</i>	129
B.1.3 Preparation of plasmid DNA	129
B.1.4 Enzymatic treatment of DNA	129
B.1.5 Agarose gel electrophoresis	130
B.1.6 DNA purification	130
B.1.7 DNA sequencing	130
B.1.8 Polymerase chain reaction	131
B.1.9 DNA cloning	131
B.1.10 Site-directed mutagenesis	133
B.1.11 Generation of VCP constructs	133
B.2 Analysis of mammalian cell cultures	134
B.2.1 Maintenance of mammalian cell cultures	134
B.2.2 Treatment and coating of coverslips	134
B.2.3 Transient transfection of mammalian cell cultures	134
B.2.4 Rh degradation and proteasome inhibition assay	135

B.2.5 Cell lysis	136
B.2.6 Lactate dehydrogenase assay	136
B.2.7 Immunofluorescence microscopy	136
B.2.8 Quantification of average levels of intracellular Rh aggregates	137
B.3 Protein chemistry and Western Blotting	137
B.3.1 Protein concentration measurement	137
B.3.2 Immunoprecipitation and chloroform-methanol precipitation	137
B.3.3 SDS-PAGE	138
B.3.4 Immunoblotting analysis	138
B.4 <i>Drosophila</i> genetics, biochemistry, immunohistochemistry, behaviour and ERG	139
B.4.1 <i>Drosophila</i> maintenance	139
B.4.2 The Gal4-UAS system	139
B.4.3 <i>Drosophila</i> heat-shock	140
B.4.4 <i>Drosophila</i> biochemistry	140
B.4.5 <i>Drosophila</i> histology, electron microscopy and immunohistochemistry	141
B.4.6 Pharmacological treatments	143
B.4.7 Behavioural assays	144
B.4.8 Electoretinogram recordings	145
B.4.9 Statistics	146
V. REFERENCES	147
VI. ANNEXES	163
1. Index of figures	165
2. Publications and poster presentations from the work presented in this thesis	166
2.1 Peer reviewed publications	166
2.2 Poster presentations	166
3. Acknowledgements	167
4. <i>Curriculum vitae</i>	168

Abbreviations

19S RP	19 S regulatory particle
AA	Amino acid
AAA	ATPase associated with a variety of activities
AD	Alzheimer's disease
ADRP	Autosomal dominant <i>retinitis pigmentosa</i>
APAF-1	Apoptotic protease activating factor 1
APS	Ammonium persulfate
Ask1	Apoptosis signaling-regulating kinase 1
Atf4	Activating transcription factor 4
Atf6	Activating transcription factor 6
ATP	Adenosine triphosphate
BCIP	5-bromo-4-chloro-3-indolyl phosphate
BiP	Binding immunoglobulin protein
bp	Base pair
BSA	Bovine serum albumin
β-Tub	β-Tubulin
Cdc48	Cell division cycle 48
CFTR	Cystic fibrosis transmembrane conductance regulator
CHOP	CCAAT enhancer-binding homologous protein
CHX	Cycloheximide
CLB	Cell lysis buffer
CNS	Central nervous system
CytC	Cytochrome c
DBD	DNA-binding domain
Der1	Derlin 1
Dle	Days of light exposure
DMEM	Dulbecco's modified Eagle's medium
DMSO	Dimethylsulfoxide
DN	Dominant-negative
DNA	Deoxyribonucleic acid
DsRed	<i>Discosoma sp.</i> red fluorescent protein
DTT	Dithiothreitol
DUB	Deubiquinating enzyme
ECL	Enhanced chemiluminescence
EDEM1	ER degradation-enhancing 1,2 mannosidase-like protein 1
EDTA	Ethylenediaminetetraacetate
EerI	Eeyarestatin I
e.g.	Example given
EIF2	Eukaryotic translation initiation factor
EMS	Ethyl methanesulfonate
EndoH	Endoglycosidase H
ER	Endoplasmic reticulum
ERAD	ER-associated degradation
ERG	Electroretinogram
ERO1	ER oxidase 1
ERQC	ER quality control
ex-polyQ	Expanded polyglutamine
FBS	Fetal bovine serum
FL	Full length
FTD	Frontotemporal dementia
GADD34	Growth arrest and DNA damage-inducible protein 34
GC	Guanylate cyclase

GCAP	Guanylate cyclase-activating protein
GFP	Green fluorescent protein
cGMP	Cyclic guanosine monophosphate
GMR	<i>Glass multimer reporter</i>
GOF	Gain-of-function
GPCR	G-protein coupled receptor
Gt	G-protein Transducin
GTP	Guanosine triphosphate
HD	Huntington's disease
HEK293	Human embryonic kidney 293
HMW	High molecular weight
Hrd1	3-hydroxy-3-methylglutaryl-coenzymA reductase degradation
HRP	Horseradish-peroxidase
Hs	Heat shock
Hsc3	Heat shock cognate 3
Hsp	Heat shock protein
Hsv	Herpes simplex virus
IB	Immunoblotting
IBM	Inclusion body myopathy
IBMPFD	IBM associated with Paget disease of bone and frontotemporal dementia
i.e.	<i>Id est</i> (that is)
IF	Immunofluorescence
IgG	Immunoglobulin G
IHC	Immunohistochemistry
IκBα	Inhibitor of NFκB
IP	Immunoprecipitation
Ire1	Inositol-requiring protein 1
Jnk	c-JUN N-terminal kinase
kb	Kilo base
kDA	Kilo Dalton
LB	Luria-Bertani
LCA	Leber congenital amaurosis
LDH	Lactate dehydrogenase
LGN	Lateral geniculate nucleus
LOF	Loss-of-function
LRAT	Lecithin retinol acyl transferase
MW	Molecular weight
NBT	Nitro blue tetrazolium
NFκB	Nuclear factor-kappa B
NP-40	Nonidet-P40
Npl4	Nuclear protein localization 4
ddNTP	Dideoxynucleotide triphosphate
dNTP	Deoxynucleotide triphosphate
n.s.	Non significant ($p>0.05$, Student's t test)
P1	Postnatal day 1
PBS	Phosphate-buffered saline
PBST	PBS-Triton
PCR	Polymerase chain reaction
PD	Parkinson's disease
PDB	Paget disease of bone
PDE	Phosphodiesterase
Perk	Protein kinase RNA (PKR)-like ER kinase
PFA	Paraformaldehyde
PN	Photoreceptor neuron
P/O	Photoreceptors per ommatidium
PQC	Protein quality control

PR	Proteostasis regulator
PS	Phototactic score
PVDF	Polyvinylidene difluoride
R1-8	Photoreceptor neuron 1-8
<i>rdgC</i>	<i>Retinal degeneration C</i>
RGC	Retinal ganglion cell
Rh	Rhodopsin
RING	Really interesting new gene
RIPA	Radio-immunoprecipitation assay
RNA	Ribonucleic acid
ROS	Reactive oxygen species
RP	<i>Retinitis pigmentosa</i>
RPE	Retinal pigment epithelium
rpm	Rounds per minute
RPN1	Regulatory particle non-ATPase1
RPT1	Regulatory particle ATPase1
RT	Room temperature
S1P	Site-1-protease
SAKS1	Stress-activated protein kinases substrate-1
SDS	Sodium dodecyl sulfate
SDS-PAGE	SDS-polyacrylamide gel electrophoresis
Sec61	<i>Saccharomyces cerevisiae</i> protein 61
siRNA	Small interfering RNA
SRH	Second region of homology
Strep	Streptavidin
Suc-LLVY-AMC	Succinyl-Leu-Leu-Val-Tyr-7-amino-4-methyl-coumarin
SVIP	Small VCP-interacting protein
TAE	Tris-acetate-EDTA
TAP	Tandem affinity purification
TBS	Tris-buffered saline
TBST	TBS-Tween
TCR	T-cell receptor
TEMED	N, N, N', N'-tetraethylmethylenediamine
Ter94	Transitional elements of the ER 94
TDP-43	TAR DNA-binding protein 43
Traf2	Tumor necrosis associated factor 2
Tris	Tris(hydroxymethyl)-aminomethane
TRP	Transient receptor potential
UAS	Upstream activating sequence
Ub	Ubiquitin
UBA	Ubiquitin-associated
UBL	Ubiquitin-like
UBX	Ubiquitin regulatory X
Ufd	Ubiquitin fusion degradation
UPR	Unfolded protein response
UPS	Ubiquitin proteasome system
VAT	VCP-like ATPase of <i>Thermoplasma acidophilum</i>
VCP	Valosin-containing protein
VIMP	VCP-interacting membrane protein
WB	Western blotting
WT	Wild-type
Xbp1	X-box binding protein-1

Summary

Vision is one of the most fascinating human experiences. The visual pigment, Rhodopsin (Rh) is the central mediator of vision and interacts with light particles to initiate the visual cascade; consequently, Rh conformational defects have dramatic effects on visual perception. *Retinitis pigmentosa* (RP) is often caused by *Rh* mutations and is characterized by the progressive loss of photoreceptor neurons (PNs) which ultimately causes loss of vision. The most common *Rh* mutation associated with autosomal dominant RP in North America is the substitution of proline 23 by histidine (Rh^{P23H}). Unlike the wild-type Rh, misfolded Rh^{P23H} accumulates within the endoplasmic reticulum (ER) and is degraded by the proteasome. Despite extensive research, the mechanisms responsible for Rh^{P23H} aggregate formation and clearance and PN degeneration remain obscure.

The conformation of membrane and secreted proteins is evaluated by a highly specialized quality control system within the ER. Misfolded proteins that do not pass ER quality control are cleared in a process called ER-associated degradation (ERAD) that involves their export from the ER to the cytosol (retrotranslocation) and degradation by the proteasome. The ATP-dependent chaperone Valosin-containing protein (VCP/ter94/p97/cdc48) is the driving force for the retrotranslocation of misfolded proteins. Although genetic evidence suggests that VCP dysfunction is associated with several neurodegenerative diseases, nothing was known about the role of VCP in Rh aggregate homeostasis and Rh-mediated retinal degeneration.

Using cellular models of RP, I provide the first evidence that misfolded Rh^{P23H} is a substrate of the ERAD effector VCP. VCP co-localizes with misfolded Rh^{P23H} in mammalian retinal and human neuroblastoma cells and requires functional N-terminal and D1 ATPase domains to form a complex with Rh^{P23H} aggregates. VCP is required and sufficient to promote degradation of misfolded Rh^{P23H} . Furthermore, VCP uses its D2 ATPase activity to promote retrotranslocation and proteasomal delivery of Rh^{P23H} .

To determine whether VCP activity modulates the retinal pathology caused by misfolded Rh *in vivo*, I performed experiments in *Drosophila* models of RP. Overexpression of $Rh1^{P37H}$ (the equivalent of mammalian Rh^{P23H}) in fly PNs leads to age- and light-dependent retinal degeneration and blindness. I found that the endogenous $Rh1^{WT}$ is required for $Rh1^{P37H}$ toxicity, as reducing the dosage of endogenous $Rh1$ strongly suppressed retinal pathology in $Rh1^{P37H}$ -expressing flies. Genetic inactivation of *VCP* increased the levels of Rh-containing aggregates in $Rh1^{P37H}$ flies, indicating that VCP is required *in vivo* for clearance of misfolded Rh. The increased level of Rh1-containing aggregates facilitated the activation of the Ire1/Xbp1 ER stress pathway. Despite this, $Rh1^{P37H}$ flies with decreased *VCP* function displayed a dramatic suppression of retinal degeneration and blindness, as assessed histologically, behaviorally and electrophysiologically. Pharmacological treatment of $Rh1^{P37H}$ flies with the VCP/ERAD inhibitor Eeyarestatin I or with the proteasome inhibitor MG132 also led to a strong suppression of retinal degeneration. Similar conclusions were reached using flies carrying another *Rh1* mutation, $Rh1^{S137F}$. Therefore, excessive retrotranslocation and/or proteasomal degradation of visual pigment might cause RP.

I suggest that pharmacologic manipulation of the VCP/ERAD/proteasome axis might prevent vision loss in RP patients carrying Rh^{P23H} mutations.

Zusammenfassung

Die Fähigkeit zu Sehen gehört zu den faszinierendsten Eigenschaften menschlicher Wahrnehmung. Dabei vermittelt das Sehpigment Rhodopsin (Rh) durch seine lichtabsorbierende Fähigkeit im Wesentlichen den Sehprozess. Folglich führen Defekte innerhalb des Proteins zu dramatischen Störungen bei der visuellen Wahrnehmung. Die erbliche Augenerkrankung *Retinitis pigmentosa* (RP) wird durch Mutationen im Rh-Gen ausgelöst, wobei es zu einem progressiven Verlust von Photorezeptor Neuronen (PN) der Netzhaut mit fortschreitender Erblindung kommt. Die häufigste *Rh* Mutation, der Austausch der Aminosäure Prolin 23 durch Histidin (Rh^{P23H}), steht im Zusammenhang mit autosomal dominanter RP in Nordamerika. Im Gegensatz zu gesundem Rh akkumuliert fehlgefaltetes Rh^{P23H} innerhalb des Endoplasmatischen Retikulums (ER) und wird vom Proteasom abgebaut. Trotz intensiver Forschung zur Aufklärung der komplexen Mechanismen, die schließlich zum Absterben der PN führen, konnten bisher keine zufriedenstellenden Ergebnisse erzielt werden.

Die Struktur von Membranen und sekretierten Proteinen wird durch ein hoch spezialisiertes System zur Qualitätssicherung innerhalb des ER vorgegeben. Fehlgefaltete Proteine unterlaufen einen Prozess, der als ERAD (ER-assoziierte Degradation) bezeichnet wird. Er steuert deren Export vom ER ins Zytosol (Retrotranslokation) und deren Abbau durch das Proteasom. Das ATP-abhängige Chaperon VCP/ter94/p97/cdc48 (Valosin-enthaltendes Protein) ist dabei hauptverantwortlich für die Retrotranslokation der strukturstörten Proteine. Obwohl es genetische Anhaltspunkte gibt, die eine Fehlfunktion des VCP mit dem Auftreten verschiedener neurodegenerativer Erkrankungen in Zusammenhang bringen, gibt es bisher keine Kenntnisse über die Rolle des VCP bei der Rh-Aggregat Homöostase und bei Rh-abhängiger Netzhautdegeneration.

Unter Anwendung zellulärer Modelle von RP, kann ich den ersten Hinweis liefern, dass fehlgefaltetes Rh^{P23H} ein Substrat des ERAD Effektors VCP darstellt. VCP kolokalisiert mit Rh^{P23H} in Säuger Netzhaut- und humanen Neuroblastomzellen und benötigt funktionale N-terminale und D1 ATPase Domänen um Komplexe mit Rh^{P23H} Aggregaten zu bilden. VCP ist dabei wichtig um den Abbau von fehlgefaltetem Rh^{P23H} voranzutreiben. Darüber hinaus nutzt VCP seine D2 ATPase Aktivität um die Retrotranslokation und der Transport des Rh^{P23H} zum Proteasom zu unterstützen.

Um zu untersuchen, ob die Aktivität von VCP *in vivo* einen Einfluss auf die, durch fehlgefaltetes Rh verursachte, Netzhautpathologie hat, habe ich verschiedene Experimente anhand eines RP-*Drosophila* Modells durchgeführt. Dabei konnte ich zeigen, dass die Überexpression von $Rh1^{P37H}$ (dem Equivalent von Säuger Rh^{P23H}) in PNs der Fliegen zu einer alters- und lichtabhängigen Netzhautdegeneration und Erblindung führt. Ich konnte darüber hinaus herausfinden, dass das endogene $Rh1^{WT}$ für das Zerstörungspotential von $Rh1^{P37H}$ benötigt wird, da eine Verminderung der verabreichten Dosis von endogenem $Rh1$ die Netzhautdegeneration in $Rh1^{P37H}$ exprimierenden Fliegen stark unterdrückte. Schließlich führte die genetische Inaktivierung von *VCP* zu einem Anstieg der Rh-Aggregate in $Rh1^{P37H}$ Fliegen. Somit kann man vermuten, dass VCP *in vivo* für den Abbau von fehlgefaltetem Rh notwendig ist. Die erhöhten Mengen an $Rh1$ -Aggregaten begünstigen zudem die Aktivierung des Ire1/Xbp1 ER Stress-Signalweg. Des Weiteren zeigen $Rh1^{P37H}$ Fliegen mit eingeschränkter *VCP* Funktion eine drastische Verminderung der Netzhautdegeneration und Erblindung. Dies konnte histologisch, elektrophysiologisch, sowie verhaltensphysiologisch bewertet werden. Pharmakologische Behandlung der $Rh1^{P37H}$ Fliegen mit dem VCP/ERAD Hemmstoff Eeyarestatin I oder

dem Proteasomhemmstoff MG132 führte ebenfalls zu starker Verminderung der Netzhautdegeneration. Ähnliche Ergebnisse konnten erzielt werden mit Fliegen, welche die *Rh1* Mutation *Rh1^{S137F}* trugen. Daraus kann geschlossen werden, dass für das Auftreten von RP der Prozess einer übermäßigen Retrotranslokation verbunden mit proteasomaler Degradation des Sehpigmentes Rhodopsin verantwortlich sein könnte.

Gestützt durch meine Forschungsergebnisse könnte eine pharmakologische Manipulation der VCP/ERAD/Proteasom Achse einer Erblindung von RP Patienten mit *Rh^{P23H}* Mutationen entgegen wirken.

I. INTRODUCTION

Introduction

Part one: The physiology and pathophysiology of Rhodopsin: Visual processing and *retinitis pigmentosa*

Vision is one of the most fascinating human experiences. The capacity to see the world around us results from the reception of light by photoreceptor neurons and its transduction and processing into a neural signal in the retina. The visual pigment, Rhodopsin (Rh) is the most important protein involved in visual processing. Rh directly interacts with light particles (photons) and its conformational change initiates the biochemical cascades that are responsible for the generation of electrical signals in photoreceptor neurons. Consistent with the fundamental role of Rh in visual processing, alterations in Rh structure and function lead to severe visual defects that culminate with the complete loss of vision (blindness).

This chapter deals with the physiology and pathophysiology of Rh and consists of three main parts. The first part (1.1 and 1.2) summarizes the most important features of visual processing and the cellular networks that process and convey visual information. It also describes the biochemical changes initiated by Rh after light absorption. The second part (1.3 and 1.4) describes the clinical and pathological characteristics of *retinitis pigmentosa* (RP), a disorder in which death of photoreceptor neurons (PNs) leads to blindness. It also deals with the genetic deficits that cause RP, in particular with Rh mutations. The third part (1.5 to 1.9) focuses on the generation and characterization of cellular and animal models for RP and on the molecular and cellular mechanisms of photoreceptor cell death in RP.

1.1 Vision in vertebrates and flies

In simple words, vision is the process by which the brain transforms energy into colours. This simple definition of vision hides an extremely complex group of networks that detect, process, relay, compare and integrate electric and biochemical signals. The fascination of people with the beauty and the mechanisms of vision makes the field of vision research one of the most advanced in terms of discoveries. The visual system is today the best understood part of the central nervous system (CNS).

Vision begins when light, entering the cornea, is sent to the inner surface of the eye, where it is transformed into an electric signal by a specialized sensory organ, the retina. This electric signal is then sent through the optic nerve to higher centers in the brain for further processing necessary for perception.

A century ago, Ramon y Cajal noticed striking similarities between vertebrate and fly visual systems. The visual systems of vertebrates and flies share i) a similar arrangement of cells and connections in parallel layers; ii) a regular spacing of neurons within each layer; iii) the existence of radial connections that run perpendicular to the layers; iv) similar modes of parallel processing; v) many shared molecular mechanisms that control development; and vi) conserved pathological mechanisms that underlie retinal degeneration. It is this last feature that justifies the development and use of *Drosophila* models for human retinal dystrophies, like *retinitis pigmentosa*.

1.1.1 The vertebrate retina

The retina is a light-sensitive neural tissue that has a relatively simple organization (Figure 1). During vertebrate embryonic development, the retina and the optic nerve originate as outgrowth of the developing brain, so the retina is considered part of the CNS. The retina is a multilayered tissue that contains several layers of neurons which synapse with each other. Five classes of neurons make up the retinal circuit: photoreceptor neurons, bipolar cells, horizontal cells, amacrine cells, and retinal ganglion cells (RGCs; Figure 1). In addition, one major type of glial cells (Müller glia) populates the retina. There are two types of PNs: rods and cones, and these cells are the only light-sensitive components of the retina. Incident light is detected by Rh expressed in PNs and the ensuing electric signal generated by PNs (see below for the details of phototransduction) is conveyed to bipolar cells; horizontal cells modulate the interaction between PNs and bipolar cells (lateral processing), and thus modify the activation of bipolar cells. The visual information generated by bipolar cells is relayed to RGCs; amacrine cells interact with both bipolar cells and RGCs (lateral processing) and modulate their responses.

The visual signal generated by RGCs in the retina is transmitted (in form of spatiotemporal patterns of action potentials) to several areas of the brain which include the thalamic lateral geniculate nucleus (LGN) and the midbrain-located superior colliculus and pretectum. The LGN is the major input to the visual cortex, and has a critical role in the processing of visual information sent by the retina. The projections from the retina to the superior colliculus are involved in the control of saccadic eye movements (movements that shift the gaze rapidly from one point of the visual scene to another); the projections to the pretectum control pupillary reflexes, which mediate the constriction of the eye pupils. The visual cortex is the major center for visual information processing. Neurons in the visual cortex perform complex computations, transform the visual information and redistribute it to various brain regions (Kandel et al., 2000).

1.1.2 The *Drosophila* retina

The fly retina (also called the compound eye) displays clear differences relative to the single lens eye of vertebrates. The *Drosophila* adult eye is composed of approximatively 800 independent ‘eyes’ or ommatidia. Each ommatidium contains eight PNs, which interact with light particles, and 6 non-neuronal cells (4 cone cells and 2 pigment cells) and is surrounded by a hexagonal lattice of 12 interommatidial cells (Mollereau and Domingos, 2005). The 8 PNs in each ommatidium are divided in 6 outer photoreceptors (R1-R6) and 2 inner PNs (R7 and R8) (Figure 2). These R1-R8 PNs express one of the six Rh genes (*Rh*). R1-R6 PNs have large rhabdomeres (light-sensing organelles) and express *Rh1*, a green-centered Rh with a broad spectrum of absorption. They are sensitive to light contrast, mediate motion detection and function well in dim light (Cook and Desplan, 2001). The inner PNs, R7 and R8, have smaller rhabdomeres and are mainly responsible for colour detection; they express a combination of *Rh3-6* genes, which divide the ommatidia into two subtypes: pale and yellow. 30 % of ommatidia are of pale type and express *Rh3* in R7 and *Rh5* in R8 PNs; 70% of ommatidia are of yellow type and express *Rh4* in R7 and *Rh6* in R8 PNs (Cook and Desplan, 2001; Sanes and Zipursky, 2010).

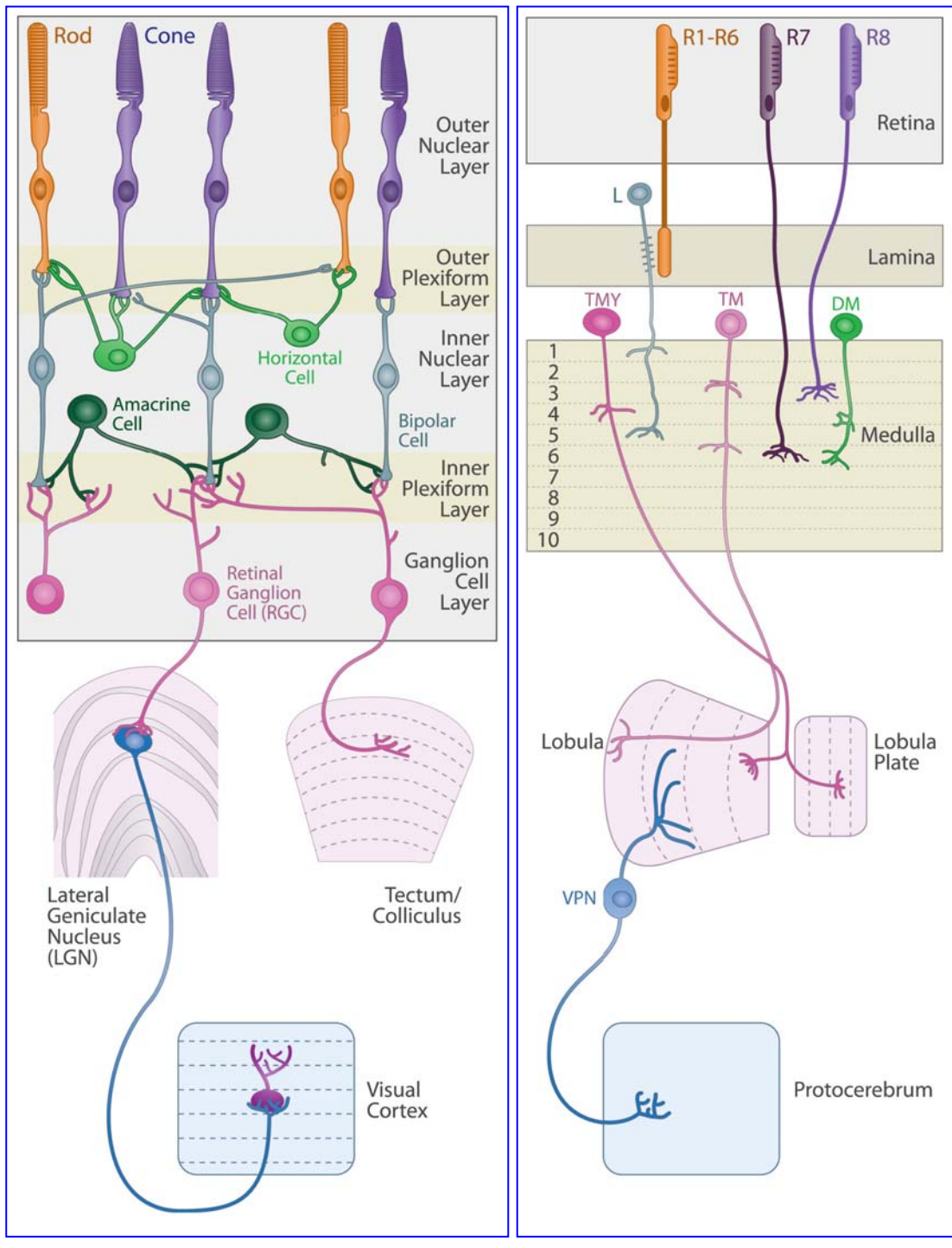


Figure 1. Components of the vertebrate (left) and *Drosophila* (right) visual systems. Left, the vertebrate retina has five major neuronal types: light reaches the PNs (rods and cones) which generate an electric signal; the signal is relayed to bipolar cells and then to retinal ganglion cells (RGCs). Horizontal and amacrine cells modulate this visual signal. RGCs then send most of their outputs to the thalamus (lateral geniculate nucleus [LGN]) or to the midbrain (pretectum/colliculus). LGN then sends its outputs to the visual cortex. Right, *Drosophila* visual system. Eight photoreceptor neurons (R1-R8) interact with light particles to initiate vision. R1-R6 PNs express the same Opsin (Rh1) and are sensitive to motion and light contrast; R7 and R8 are sensitive to colour. These PNs send signals to either the lamina (R1-R6) or the medulla (R7, R8). Transmedullary neurons (TM, TMY) project to the Lobula complex (Lobula and Lobula plate). Multiple pathways link the Lobula complex to regions of the central brain (protocerebrum). Adapted from Sanes and Zipserky (2010).

Introduction

Besides the retina, *Drosophila* has four major regions that process visual information: lamina, medulla, lobula and lobula plate (the latter two sometimes referred to as the lobula complex). The retina contains approx. 800 ommatidia; the lamina contains the same number of cartidrige; and the medulla also contains an equal number of columns. PNs R1-R6 project their axons to the lamina, while R7 and R8 PNs terminate in distinct layers of the medulla (Figure 1). Transmedullary neurons from the medulla further conduct visual information to the lobula plate complex. Finally, multiple pathways link the lobula plate complex with regions of the central brain (Otsuna and Ito, 2006; Sanes and Zipursky, 2010).

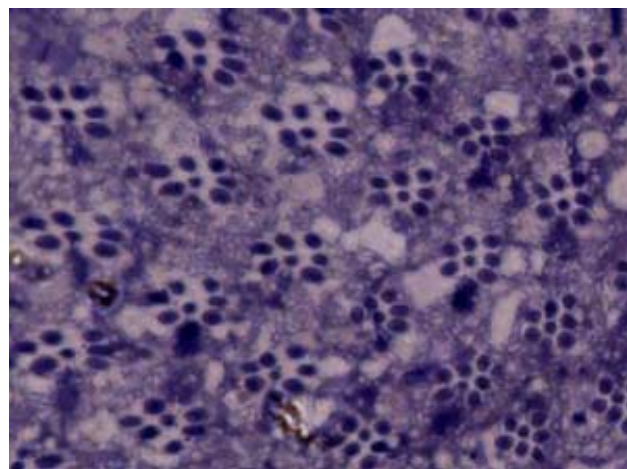


Figure 2. The *Drosophila* retina is made of ommatidia. The fly retina contains approximatively 800 units called ommatidia. Each ommatidium functions like an individual “eye” and contains 8 photoreceptor neurons. In this picture only 7 PNs are visible (R8 is under the plan of cutting). Each PN has a light-sensitive organelle, called rhabdomere (the dark dots), which contains the visual pigment Rh. R1-R6 PNs have one visual pigment (Rh1), while R7 and R8 express a combination of Rh3-Rh6 pigments. The cell bodies of PNs are in white, surrounding the rhabdomeres. PNs R1-R6 lie on the outside of each ommatidium, while R7 is smaller and is found in the center of all ommatidia. Besides 8 photoreceptors, each ommatidium has 18 non-neuronal cells, which are not visible here. The picture was obtained after cutting a *Drosophila* eye and staining with the contrasting agent toluidine blue.

1.2 Visual processing by vertebrate photoreceptor neurons

1.2.1 Vertebrate photoreceptor neurons

Two types of photoreceptor neurons (PNs) are responsible for light detection: rods and cones (Figure 3). These two cellular types have different characteristics and sensitivities. Thus, cones mediate daytime vision, while rods are responsible for night vision. The rods have a higher sensitivity to light, express more photopigment, but have a lower temporal resolution and a long integration time. In contrast, the cones have a lower sensitivity to light, contain less photopigment, but have a higher temporal resolution and a short integration time. All vertebrate rods express the same photopigment (Rhodopsin). In contrast, cone cells can be divided into several distinct groups according to which Opsin molecule they express; humans have three types of Opsins, which are the basis of our trichromatic vision: S (which absorb at short wavelengths, i.e. < 500 nm, blue), M (medium, approx. 530 nm, green), and L (long, approx. 560 nm, red).

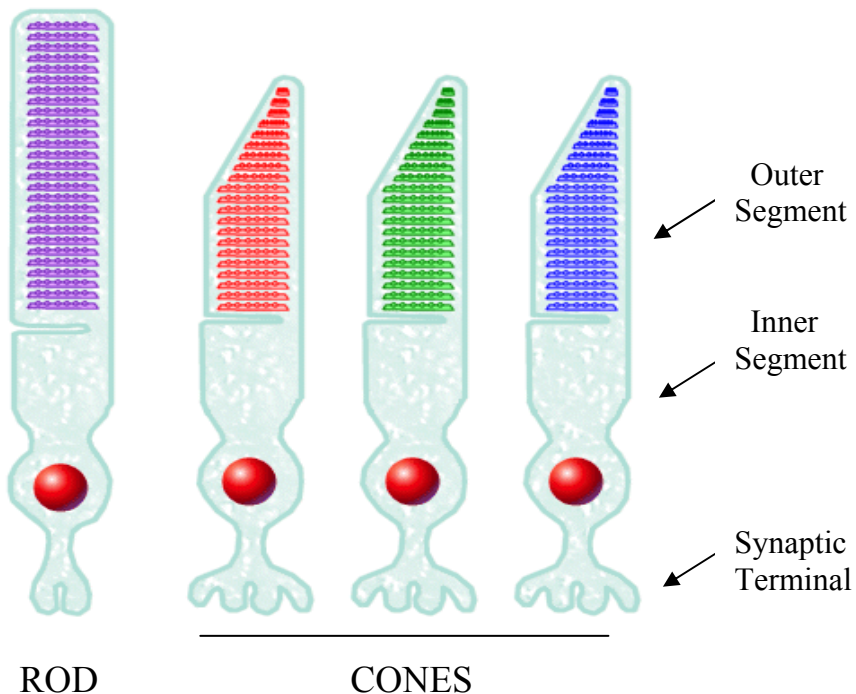


Figure 3. The two types of vertebrate photoreceptor neurons: rods and cones. Both rods and cones have inner and outer segments connected by a cilium (not shown). The inner segment contains the cell's nucleus (red) and most of the biosynthetic machinery of the cell. The outer segment contains the light-transducing apparatus. It consists of a stack of membranous discs, which contain light-absorbing pigments. All vertebrate rods express Rhodopsin. By contrast, the cones comprise three groups, distinguished by the Opsin they express (L-red, M-green and S-blue).

Most mammals have a dichromatic system (only S and M Opsins) while birds or fishes express four or more cone Opsins, together with filtering pigments, such as oil droplets (Ahnelt and Kolb, 2000). To discriminate between different light wavelengths, the *Opsin* gene family has been enriched via several rounds of duplications (Pichaud et al., 1999). Rods and cones share many cellular characteristics (Figure 3). Both neuron types are composed of a cell body, and of a ciliary outer segment, which is tightly packed with membrane discs full of visual pigment. The relative abundance of rods and cones is 90 % rods: 10 % cones in humans, the rods being more peripherally located, and the cones being concentrated in the fovea. Nocturnal animals like mice rely even more on rod-mediated vision (and have a 97 % rods: 3 % cones ratio; Cook and Desplan, 2001).

1.2.2 The visual transduction cascade

The visual pigment Rh is composed of a vitamin A-based chromophore (retinal) and a seven-transmembrane-helix apoprotein, Opsin. Rh is a prototypical seven-pass transmembrane protein, which is coupled to a heterotrimeric G protein (i.e. G-protein coupled receptor [GPCR]). Well over 1000 Opsins have been characterized so far in the animal kingdom, all arising from a common ancestor (Arendt, 2003). The arrival of one photon on a single PN, leads to photo-isomerisation of 11-cis retinal to *all trans*-retinal. This conformational change triggers a change in overall Rh structure (the active pigment is also called Meta II Rhodopsin or Rh*). As a result, active Rh (Rh*) activates the G-protein Transducin (G_t ; see Figure 4). Transducin in turn activates a phosphodiesterase (PDE) that catalyzes the hydrolysis of cGMP. In the dark, the levels of cGMP are high, and cGMP binds to non-selective cation channels, keeping them in an open state. The

Introduction

light-induced decrease in cGMP concentration leads to closure of these cationic channels and to a hyperpolarisation of the cell. In this state, the release of neurotransmitter (glutamate) from the synaptic region is inhibited, and a signal is sent (indirectly) to the visual cortex.

Activated Rhodopsin (Rh^*) is inactivated by Rhodopsin kinase and the phosphorylated Rh binds Arrestin. Transducin and PDE are inactivated and dissociate due to the hydrolysis of the bound GTP by the intrinsic GTPase activity of the Transducin α subunit. The reduced intracellular levels of Ca^{2+} , resulting from the closure of cGMP-gated channels cause the activation of the guanylate cyclase (GC) (via desinhibition of the guanylate-cyclase-activating protein [GCAP] due to decreased calcium levels) which synthesizes cGMP. As the intracellular levels of cGMP increase, the cGMP-gated cationic channels re-open and lead to influx of cations (Na^+ , Ca^{2+}), which re-establish the depolarized dark state. As the level of Ca^{2+} rises again, GC activity is inhibited (calcium inactivates GCAP) and cGMP synthesis returns to basal levels (Hims et al., 2003; Kandel et al., 2000).

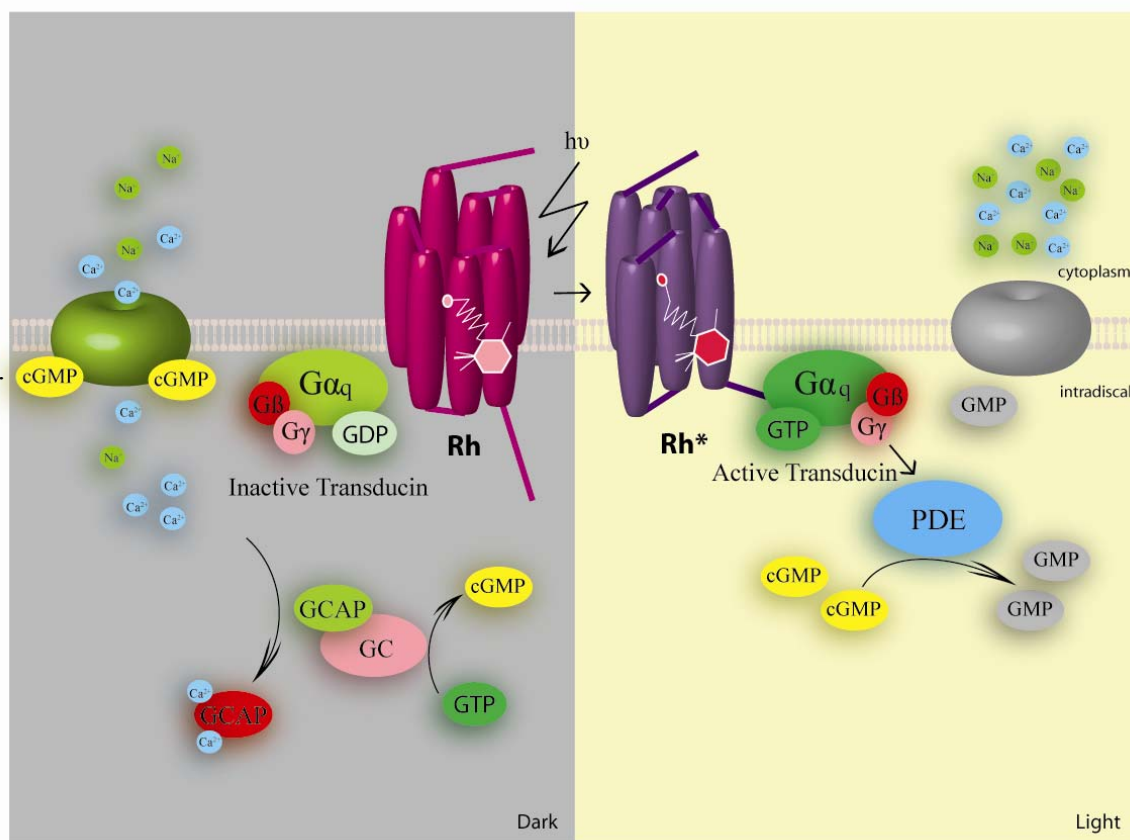


Figure 4. The vertebrate phototransduction cascade. In light (right): interaction between light particles and the chromophore 11-cis retinal leads to its transformation in all-trans retinal. This conformational change triggers a change in Rh conformation and to activation of the G protein Transducin. Transducin activates the phosphodiesterase (PDE) which transforms cGMP into GMP. Depletion of cGMP causes the cationic channels to close. In dark (left): Calcium and sodium ions flow through cationic channels, as the levels of cGMP are high. Calcium also regulates the production of cGMP - by binding to the guanylate-cyclase activating protein (GCAP) and preventing it from activating the guanylate cyclase.

1.3 *Retinitis pigmentosa*: clinical and pathological features

Loss of vision (blindness) has dramatic consequences for the affected individuals. One of the most common retinal dystrophies is *retinitis pigmentosa* (RP). RP comprises a group of extremely debilitating disorders that cause severe visual impairment. The prevalence of RP is 1 in 3.000 to 1 in 5.000 individuals; more than 1.5 million patients are affected worldwide (Shintani et al., 2009). As its name '*pigmentosa*' indicates, RP belongs to the group of pigmentary retinopathies, a generic name that covers all retinal dystrophies that present with loss of photoreceptor neurons and retinal pigment deposits (Hamel, 2006). The name '*retinitis*' is actually a misnomer, as inflammation is rarely present in RP. RP results primarily from the death of rod photoreceptor neurons, which mediate vision in conditions of dim light.

The RP symptoms typically start in the early teenage, while the severe visual deficits are predominant at the age of 40-50; some congenital forms display an early onset (Leber congenital amaurosis, see below) while some RP cases display late-onset or even nonpenetrant forms (Daiger et al., 2007). RP patients experience night-vision deficits, followed by decreasing visual fields and tunnel vision; in a second step, as many rod PNs are affected, the cone PNs (responsible for daylight vision) also become affected and eventually die, leading to loss of central vision. Subsequent to the loss of both rods and cones, there is degeneration of the retinal pigment epithelium (RPE) (Shintani et al., 2009).

RP displays the two major clinical hallmarks. First, in patients with the disease, a dramatic diminution of the electroretinogram (ERG) amplitudes can be seen. An ERG is an extracellular recording, which measures the summed responses of all retinal cells to light. As the disease becomes evident, the amplitudes of rod electroretinograms become reduced or are completely abolished (Figure 5A-C). Second, RP patients have an abnormal fundus, with attenuated retinal vessels and the accumulation of bone-spicule intra-retinal pigment deposits (Figure 5D,E) (Hims et al., 2003; Kalloniatis and Fletcher, 2004). The diagnostic criteria for RP are listed in the Table 1 below.

Functional signs

Night blindness (nyctalopia) is the earliest symptom

Photophobia appears later

Visual acuity is preserved in early and mid stages

Visual field

Patchy losses of peripheral vision, evolving to ring shape scotoma, and eventually tunnel vision

Fundus

Pigmentary deposits resembling bone spicules, initially in peripheral retina

Attenuation of retinal vessels

Waxy pallor of the optic disc

Various degrees of retinal atrophy

Electroretinogram (ERG)

Dramatic diminution in the amplitudes of a- and b-waves

Scotopic system (rods) predominates over photopic (cones) system

Table 1. Diagnostic criteria for *retinitis pigmentosa*. Adapted from Hamel (2006).

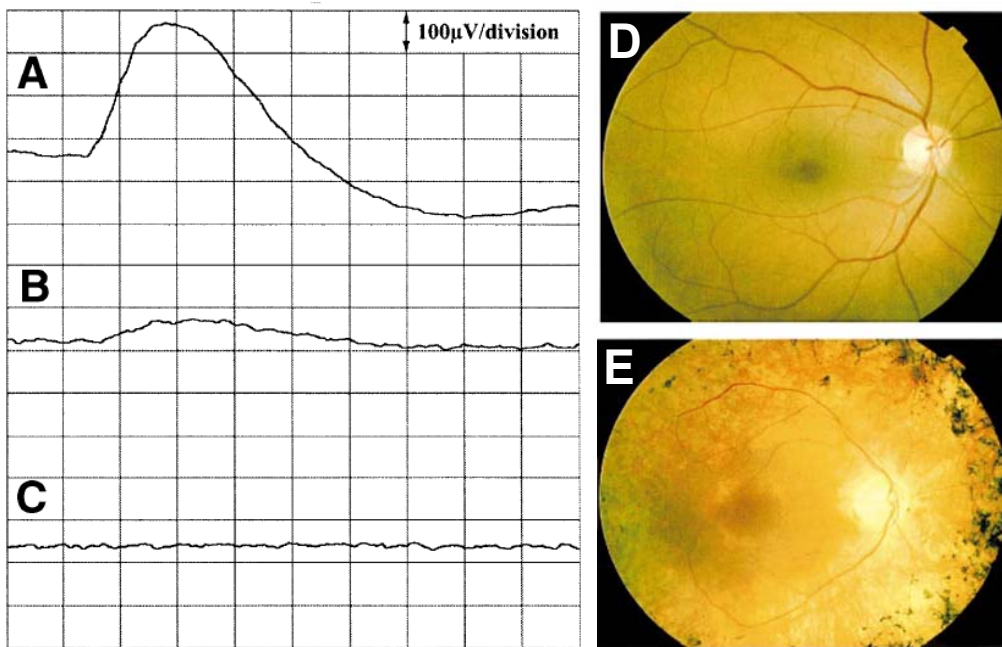


Figure 5. Clinical characteristics of *retinitis pigmentosa*. (A-C) Patients with moderately advanced RP have a reduced ERG amplitude (B) and patients with advanced RP have a dramatic reduction in the ERG amplitude (C) relative to healthy controls (A). The tracings show the rod responses to an intensity flash. (D,E) Photographs of a healthy (D) and a RP (E) retina. The RP retina exhibits typical features, including a marked pigment epithelial thinning, optic disc pallor, retinal vascular attenuation and intraretinal pigmentary deposits. Adapted from Farrar et al. (2002).

RP represents the most common cause of visual impairment among people of working age, while Leber congenital amaurosis (LCA), is the most prevalent cause of inherited visual handicap in children (Boughman and Fishman, 1983). RP has several classifications, made according to: distribution of affected PNs (central, pericentral, sector or peripheral subtypes); age of onset (congenital disease, juvenile, late onset); mode of inheritance (sporadic, dominant, recessive, X-linked); predominant PNs involved; primary (only the eye is affected) and syndromic (ocular degeneration is associated with abnormalities in one or more organ systems). More complex (and commonly used) classification systems divide RP into 2 main groups, primary and syndromic, with subclassifications involving inheritance patterns thereafter (Shintani et al., 2009).

1.4 Genetics of *retinitis pigmentosa*

About half of all RP cases are sporadic, i.e. no familial history or genetic defect was identified. The remaining 50 % of RP cases are caused by genetic alterations; they show dominant, recessive or X-linked patterns of inheritance. In addition, RP is also present in syndromes (which manifest concomitantly with several diseases), including Usher and Bardet-Biedl, which involve sensorineural deafness and vestibular dysfunction (Usher syndrome) or obesity and mental retardation (Bardet-Biedl syndrome) (Farrar et al., 2002). Several metabolic and neurological diseases also manifest with retinal degeneration, together with additional pathologies (Hamel, 2006). Table 2 lists the major RP subtypes and their prevalence.

Category	Type	% of total
Nonsyndromic RP	Autosomal dominant RP	20
	Autosomal recessive RP	13
	X-linked RP	8
	Insolated or unknown RP	20
	Leber congenital amaurosis	4
	Subtotal	65
Syndromic and systemic RP	Usher syndrome	10
	Bardet-Biedl syndrome	5
	Other	10
	Subtotal	25
Other or unknown types of RP		10
Total		100

Table 2. Prevalence of *retinitis pigmentosa* and estimated percentages of *retinitis pigmentosa* types. The total prevalence is 1 case per 3100 persons. Adapted from Daiger et al. (2007).

The autosomal dominant RP (ADRP) is usually the mildest form of RP, and starts generally after the age of 50. Autosomal recessive RP starts typically during the first decade, and X-linked RP also shows an early onset (Hamel, 2006). In summary, the term RP includes a wide spectrum of disorders with various chromosomal, metabolic and morphologic defects, many being genetically predetermined, and all associated with a progressive degeneration of PNs.

1.4.1 Overview of genetic complexity in *retinitis pigmentosa*

RP is arguably the most complex genetic disorder identified to date in humans. Several features make the genetics of RP extremely complicated. First, more than 181 genes causing inherited retinal diseases have been mapped to individual chromosomal locations, and the sequences of about 130 of these genes have been determined (see Table 3). Second, the inheritance forms are dominant, recessive and X-linked, and in addition, rare forms of mitochondrial inheritance and codominance have been detected. Third, mutations in the same gene might cause different diseases; even more surprisingly, the same mutation in different individuals of the same family may cause distinct symptoms (Daiger, 2004; Daiger et al., 2007; Shintani et al., 2009). Table 3 lists the number of genes linked to retinal disease. The classification of genes linked to retinal disease might be sometimes misleading, as some genes can cause several types of RP. A prominent example is the Rhodopsin gene: Rh mutations usually cause ADRP but some rare mutations also cause recessive RP. Mutations in NRL can also cause ADRP or recessive RP. In addition, mutations in some genes – like RDS – can cause ADRP, dominant macular degeneration or other distinct forms of retinopathy (Daiger et al., 2007).

Category	Mapped only	Cloned	Total
Total	51	130	181
Autosomal dominant RP	5	12	17
Autosomal recessive RP	15	10	25
X-linked RP	4	2	6
Usher syndrome	5	6	11
Bardet-Biedl syndrome	2	4	6
Leber congenital amaurosis	9	4	13
Autosomal dominant macular degeneration	4	4	8

Table 3. Summary of genes (mapped only or cloned) linked to retinal disease. Modified from Daiger (2004).

The genes linked to RP encode for proteins that generally localize in rods (sometimes in both rods and cones), and which are involved in various cellular pathways. They include proteins involved in rod visual transduction (*Rh*; alpha and β subunits of the rod phosphodiesterase; alpha and β subunits of the rod cGMP-gated channel; Arrestin; guanylate cyclase activating protein 1B), cytoskeleton proteins (Peripherin/RDS, ROM1, Fascin2), proteins involved in trafficking (RPGR, RP1, RP2, Prominin-like 1), in photoreceptor differentiation (NRL, NR2E3, CRX), in mRNA splicing (PRPC8, HPRP3, PRPF31, PAP1), components of the extracellular matrix (USH2A), and in lipid (ABCA4, CERKL), nucleotide (IMPDH1) or other (TULP1, CRB1, MITS2, CA4, SEMA4A) metabolic pathways. Moreover, RP is also caused by mutations of genes expressed in the photoreceptor supporting tissue (the retinal pigment epithelium), and which encode for proteins involved in retinol metabolism (retinol isomerase RPE65; 11-cis retinol transporter CRALBP; the lecithin retinol acyl transferase LRAT; RGR) or for proteins controlling the phagocytosis of the photoreceptor outer segments (cMERTK) (Daiger et al., 2007; Hamel, 2006). The most common mutations associated with RP are listed in Table 4.

Gene symbol	Mutation	% of total per gene
Rh	Pro23His	40
	Arg135Trp	3
	5 others	6
RDS	Pro210Arg	25
	IVS2A>T	12
RP1	Arg677ter	50
	Leu726dd5	16
	Gly723ter	16
IMPDH1(RP10)	Asp226Asn	50
	Gly324Asp	25

Table 4. Common retinal disease mutations. The *Pro23His* mutation in the *Rh* gene (*Rh*^{P23H}) mutation is the most common *Rh* mutation (accounts for 40 % of all *Rh* mutations). From Daiger (2004).

These genetic findings suggest that a molecular definition of each RP subtype, combined with a careful clinical description might be extremely useful for the development of

specific therapies. It is also interesting to note that, although most of the genes linked to RP are expressed in several neuronal populations in the retina, the PNs are particularly affected (Farrar et al., 2002). This raises the hope that some factors underlying the specific vulnerability of PNs might be uncovered.

1.4.2 Autosomal dominant *retinitis pigmentosa* caused by *Rhodopsin* mutations

The first *Rh* mutation that was shown to cause RP was identified in 1990 by Thaddeus Dryja in a Scandinavian family (Dryja et al., 1990) and found to be a single amino acid substitution (Ala135Leu). Today, more than 100 mutations have been identified in the *Rh* gene, and they appear to cause cell dysfunction and degeneration in different ways. Collectively, these *Rh* mutations account for more than 25 % of all ADRP cases (Kennan et al., 2005). Rhodopsin accounts for more than 70 % of the total rod outer segment protein and is expressed predominantly in the membranes of rod cell outer segment stacked discs, where it is covalently bound to 11-cis retinal (Kennan et al., 2005). Huge amounts of *Rh* are expressed in PNs (about 4×10^7 molecules of *Rh* are present in one rod) and since the apex of the rod outer segment is phagocytosed daily by the retinal pigment epithelium, this means that an intense activity of mRNA and protein synthesis, and trafficking (from the rod inner segment, through the connecting cilium, to the rod outer segment) takes place in each rod PN (Hamel, 2006).

The human *Rh* gene was mapped in 1986 to chromosome 3q21 (Nathans et al., 1986). The 3D structure of bovine *Rh* was determined in 2000 by Palczewski, from diffraction data extending to 2.8 Å resolution (see Figure 6 top panel) (Palczewski et al., 2000). The extracellular region of *Rh* has a highly organized structure and forms the basis for the arrangement of the 7-helix transmembrane motif (Helices HI-VII). The carbohydrate moieties are attached at the aminoacid residues Asn2 and Asn15. The ground-state chromophore, 11-cis-retinal (in purple) holds the transmembrane region of the protein in the inactive conformation. Interactions between the chromophore and a cluster of key residues determine the wavelength of the maximum absorption. Changes in these interactions among Rhodopsins facilitate colour discrimination. A set of residues (not shown) were identified which mediate interactions between the transmembrane helices and the cytoplasmic surface, where G protein activation occurs, suggesting a possible structural change upon photoactivation (Bourne and Meng, 2000; Palczewski et al., 2000). Using infrared-laser atomic-force microscopy, Fotiadis revealed the native arrangement of *Rh*, which forms paracrystalline arrays of dimers in mouse disc membranes (Fotiadis et al., 2003).

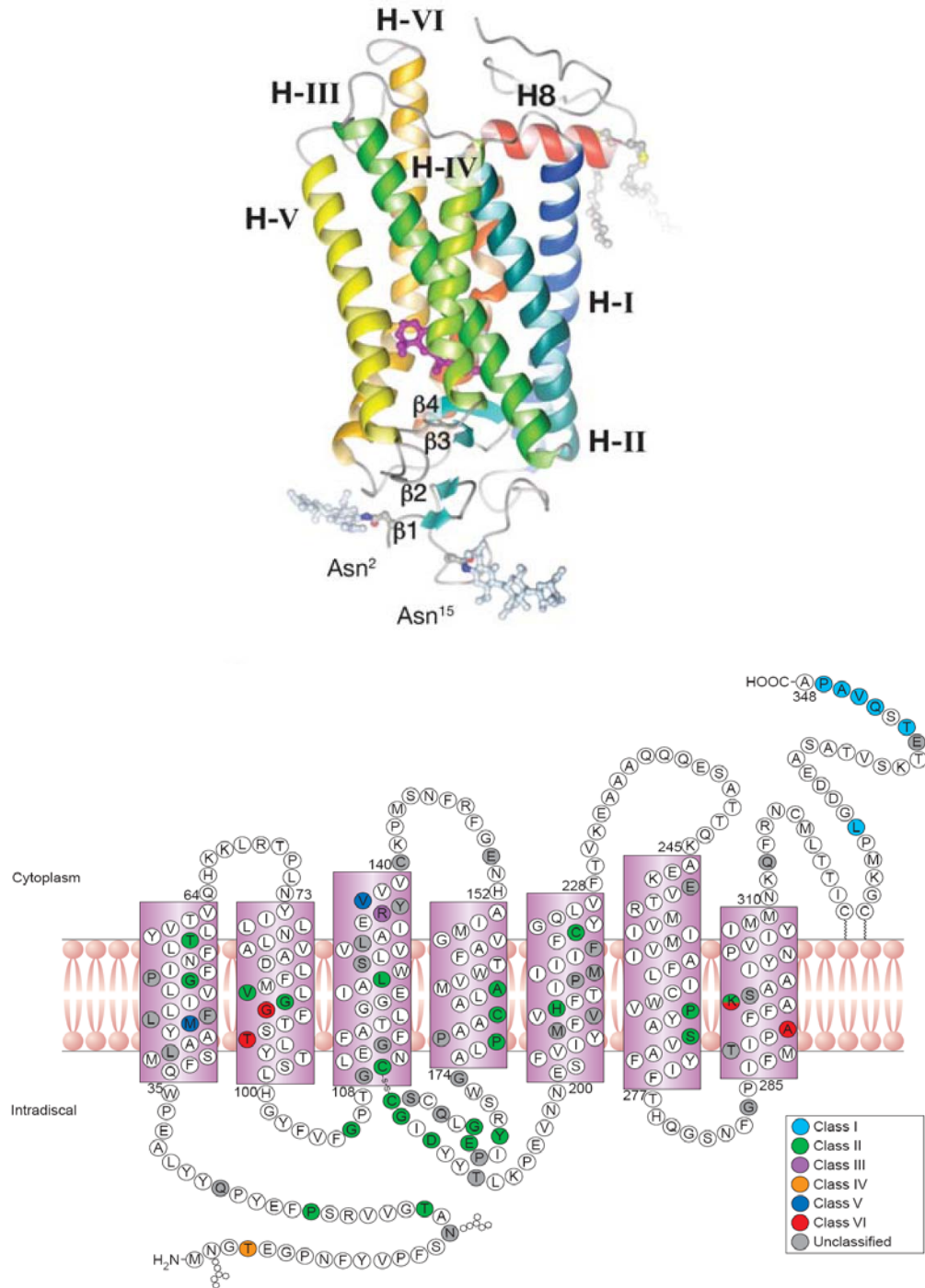


Figure 6. Structure of the visual pigment Rh and the localization of RP-linked mutations. The top panel shows a three-dimensional model of Rhodopsin. The ribbon drawing of Rh is parallel to the plane of the membrane. The carbohydrate moieties are attached at the aminoacid residues Asn2 and Asn15. The pairs of β 1- β 2 and β 3- β 4 hairpins, the transmembrane helices (H-I-VII) and the cytoplasmic helix 8 (H8) are indicated. The chromophore (11-cis-retinal) is shown in purple. From Palczewski (2006). The lower panel shows a schematic diagram of Rh structure, with the transmembrane regions marked in purple. The localization of Rh mutations is indicated. Each class of mutants is represented in a different colour (according to the colour code on the right). From Mendes et al. (2005).

More than 100 *Rh* mutations have been identified throughout the *Rh* transcript (Farrar et al., 2002; Sohocki et al., 2001) and they have been recently classified based on their biochemical and subcellular properties and localization (see Figure 6 lower panel and Table 5). Class I mutations comprise Rh mutants that fold normally but are not transported correctly to the outer segment. Class II refers to mutations that misfold, are retained within the endoplasmic reticulum (ER) and cannot easily reconstitute with 11-cis retinal. Class III mutations affect endocytosis; class IV mutations have little folding defects but have impaired post-translational modifications and altered stability. Similarly, class V mutations have no obvious folding defects but show an increased rate of Transducin activation. Finally, mutants that appear to fold correctly but lead to constitutive activation of Opsin, in the absence of chromophore and in the dark constitute the class VI (Kennan et al., 2005; Mendes et al., 2005). The fact that this diversity of mutations, which have different consequences on Rh conformation and function, all cause RP suggests that several independent mechanisms cause cell death in the retina (see below).

Classification	Behaviour	Site of point mutation
Class I	Fold normally but are not transported to the outer segment	L328, T342, Q344, V345, A346, P347
Class II	Are retained in the ER and cannot reconstitute with 11-cis-retinal	T17, P23 , G51, T58, V87, G89, G106 C110, L125, A164, C167, P171, Y178 E181, G182, C187, G188, D190, H211 C222, P267, S270, K296
Class III	Affect endocytosis	R135
Class IV	Do not necessarily affect folding but affect Rh stability	T4
Class V	Mutants show increased activation rate for Transducin	M44, V137
Class VI	Show constitutive activation of Opsin in the absence of chromophore	G90, T94, A292
Unclassified	No observed defect or not studied in detail	N15, Q28, L40, F45, L46, P53, G109 G114, S127, L131, Y136, C140, E150 P170, G174, P180, Q184, S186, T193 M207, V209, P215, M216, F220, E249 G284, T289, S297, E341

Table 5. Classification of mutant Rhodopsins. The P23H (P23) Rh mutation is in bold. Adapted from Mendes et al. (2005).

1.4.3 *Retinitis pigmentosa* caused by Rh^{P23H} mutations

The most common mutation associated with ADRP in North America is a C-to-A transversion in the codon 23 of the *Rh* transcript. It leads to a proline-to-histidine substitution near the amino acid terminus of Rh (see Figure 6 lower panel; the mutation [P] is in green), in an intradiscal region of the protein. This mutation has therefore been termed Rh^{P23H} (Berson et al., 1991; Dryja et al., 1991; Heckenlively et al., 1991; Stone et al., 1991; Sung et al., 1991a). The Rh^{P23H} mutation has been classified as a class II mutation, as it is retained within the ER and it fails to reconstitute with 11-cis retinal (see Table 5). It is unclear how this misbehaviour of Rh^{P23H} causes photoreceptor neurons in the retina to die in RP. One of the major aims of the current Ph.D. work was to understand the pathology associated with this Rh mutation.

Why do the PNs die in *retinitis pigmentosa*? This is a simple, yet unanswered, question and a major challenge for RP research. The extreme diversity of mutations linked to RP, the fact that sporadic RP is also common, but also the existence of several RP subtypes suggest at least three general principles of PN cell death: i) PN cell death follows the same routes in all RP cases, irrespective of the initial triggers (mutations or other environmental factors) that initiate the cell death program ii) the different mutations or environmental triggers lead to cell death via different molecular and cellular mechanisms iii) there might be some partial overlap between the molecular and cellular processes mediated by the different triggers that cause RP; this raises the possibility that the identification of both common and distinctive cell death features might promote successful therapies for RP in general, and for different RP subgroups. It remains to be determined to what extent the PN cell death relies on one of these three above principles.

In the following, I will focus on the mechanisms of photoreceptor neuron cell death in *Rh*-linked autosomal dominant RP. I will first describe progress in understanding the pathology of mutant Rh in two major research areas: the study of cellular models for RP, and the use of animal models for RP (I focus on rodent and *Drosophila* models). Finally, I discuss the pathogenic mechanisms in retinal degeneration, which emerged from these studies.

1.5 Cellular models of *retinitis pigmentosa*

Overexpression of mutant Rh in different cell culture systems is one way of understanding the pathological events induced by mutant Rh. Classical studies, in which diverse Rh mutants were expressed in tissue culture cells (like 293S and COS cells) have shown that class II mutants (including the Rh^{P23H} mutant) are retained within the ER, regenerate poorly when 11-cis retinal is added and fail to reach the plasma membrane; in contrast, several class I mutations displayed a behaviour similar to Rh^{WT} (Kaushal and Khorana, 1994; Sung et al., 1993; Sung et al., 1991b). These initial studies allowed therefore the delineation of at least 2 classes of Rh mutations. The fact that class II Rh mutants (including Rh^{P23H}) failed to accumulate at high levels in transfected cells (as wild-type Rh) suggests that they are subject to enhanced intracellular degradation. Therefore, the pathogenesis of RP associated with class II Rh mutations might involve the ER/proteasome axis. In 2004, Chuang transfected HEK cells with three Rh mutants in which Arg135 was substituted by leucine, tryptophan or glycine (i.e. R135L, R135W and R135G); he found that these mutant Rh species are hyperphosphorylated and bind with high affinity to visual Arrestin. Moreover, mutant Rh recruited Arrestin to the plasma membrane, and the Rhodopsin-Arrestin complex was internalized into the endocytic pathway. The Rhodopsin-Arrestin complexes altered the morphology of endosomal compartments and severely damaged receptor-mediated endocytic functions (Chuang et al., 2004). Because the biochemical and cellular defects of Arg135 mutant Rh were distinct from those previously described for class I and class II RP mutations, they were classified as class III mutations; thus, impaired endocytic activity may underlie the pathogenesis of RP caused by this novel class of Rh mutations.

During its maturation, Rh is first N-glycosylated, followed by the addition of high-mannose core oligosaccharides in the ER and the subsequent trimming of these added parts in the Golgi apparatus (Kornfeld and Kornfeld, 1985). Maturation through the ER-Golgi pathway (towards the plasma membrane) is therefore associated with the acquisition of a trimmed and elaborated glycosylation. The use of endoglycosidases, endoF and endoH allows distinguishing between mature and immature Rh; thus, endoF

cleaves all N-linked oligosaccharides from the protein, while endoH cleaves the high-mannose ER forms but not the complex Golgi forms. When employing these enzymatic treatments, the mutant Rh^{P23H} was cleaved by both the endoF and endoH (in contrast to Rh^{WT} which was cleaved only by endoF), suggesting that Rh^{P23H} is not trafficked through the Golgi, but is retained within the ER (Sung et al., 1991b). These observations suggest that the quality control system of the ER did not allow the further traffic of mutant Rh^{P23H} through the secretory pathway.

Overexpression of Rh^{P23H} in several cell types led to the formation of high molecular weight (HMW) aggregates, as evidenced by western blotting and immunofluorescence techniques (Illing et al., 2002; Mendes and Cheetham, 2008; Saliba et al., 2002; Sung et al., 1991b). Interestingly, the mutant Rh^{P23H} was found to recruit the wild-type (WT) Rh in these aggregates (Mendes and Cheetham, 2008; Rajan and Kopito, 2005; Saliba et al., 2002), suggesting a mechanism of selective impairment of Rh^{WT} maturation by the mutant Rh^{P23H}. Cells expressing Rh^{P23H} also exhibited an impairment of the ubiquitin proteasome system, and both Rh^{P23H} and Rh^{WT} were found to be degraded by the proteasome (Illing et al., 2002). Therefore, impairment of the proteasome system (by overloading with Rh) could represent a cell death mechanism for RP caused by Rh^{P23H}.

Taken together, these observations suggest that mutant Rh^{P23H} is specifically retained in the ER, is subject to enhanced proteasomal degradation and might cause toxicity by impairing the activity of the proteasome. The fact that the wild-type Rh is also found in Rh^{P23H}-containing aggregates raises the possibility that both WT and P23H Rh are excessively degraded in cells expressing mutant Rh^{P23H}.

1.6 Rodent models of *retinitis pigmentosa*

While the above-mentioned studies in cell culture systems gave important hints about the pathogenic mechanisms initiated by mutant Rh, they largely failed to reproduce an important feature of RP: cell death. It is therefore difficult to understand the relevance of these pathogenic mechanisms initiated by mutant Rh to cell degeneration. Moreover, in most cases, the cells used to study the pathobiology of Rh were not photoreceptor neurons, the cellular population most affected in RP. In a few cases, retinal cells (like 661W mouse retinal cells) were used, but their transfection efficiency was very low, and thus prevented a thorough analysis of Rh-mediated toxicity.

The use of animal models allows overcoming these important limitations, and allows the investigation of the mechanisms mediating mutant Rh toxicity in an appropriate cellular environment.

To investigate the pathophysiologic and molecular events that contribute to retinal degeneration in *Rh*-linked RP, transgenic animals expressing *Opsin* genes containing defined mutations were generated and analyzed. Although most studies used rodents such as rats and mice, some teams used the pig, thanks to the striking resemblance of its eye to the human eye (the pig eye has a similar size and a similar distribution of rod and cone cells, when compared to the human eye). In a heroic undertaking, Petters et al. produced a porcine model expressing mutant (Pro347Leu) Rh and found an early rod loss, followed by slower cone degeneration (Petters et al., 1997). This pig model might therefore be attractive for defined preclinical trials.

Introduction

Studies using genetically engineered mice (and to a less extent rats) have succeeded in modelling and characterizing several aspects of mutant *Rh*-induced retinal pathology. This is mainly due to the availability of diverse genetic tools in the mouse (including the existence of routine gene targeting technologies). Transgenic mice expressing the most common *Rh* mutation associated with ADRP, *Rh*^{P23H}, have been generated by the Thaddeus Dryja laboratory at the Harvard Medical School in 1992. Three transgenic lines expressing mutant human *Rh*^{P23H} (P23H-D, P23H-E and P23H-L) and two lines expressing wild-type human *Rh* (NHR-A and NHR-E) were generated. To obtain these transgenic mice, human genomic fragments that encompassed the entire *Rh* transcriptional unit as well as 4,8 kb upstream and 6,2 kb downstream DNA (for the wild-type allele) and 4,2 kb upstream and 8,4 kb downstream DNA (for the *P23H* allele) were used. These genomic fragments were derived from an ADRP patient carrying one WT and one *P23H Rh* allele (Olsson et al., 1992). Transgenic mice expressing the *P23H* allele developed photoreceptor neurodegeneration, which was revealed histologically but also by an altered fundus and severely reduced ERG amplitudes. Interestingly, the degree of degeneration correlated with the expression level of the mutant *P23H* allele, i.e. two lines expressing *Rh*^{P23H} at high levels displayed more severe degeneration. Of the two transgenic lines expressing the WT *Rh* allele, one expressed equal amounts of transgenic and endogenous murine *Rh* levels, while the other expressed 5 times more transgenic than murine Opsin. The former line was relatively unaffected, while the latter developed retinal degeneration similar to the *P23H*-expressing lines (Olsson et al., 1992). Therefore, these mice recapitulate important features of ADRP. Although these experiments indicate that increased levels of *Rh* are pathologic, they do not allow determining whether the two (WT and *P23H*) *Rh* variants cause disease by a similar mechanism when overexpressed.

The fact that increased levels of WT *Rh* cause PN degeneration suggests that overexpression of WT *Rh* can be toxic for cells. To overcome this limitation, investigators reasoned that reducing the levels of the endogenous murine *Rh* might prevent the toxicity associated with WT *Rh* overexpression. Mice were thus generated in which the expression of the endogenous *Rh1* was reduced or eliminated by targeted gene disruption.

In the absence of any transgenic *Rh*, mice lacking both *Rh* alleles (*Rh*^{-/-}) displayed a normal initial development of the retina, however, the rod outer segments failed to form. Within months of birth, photoreceptor neurons degenerated completely. In contrast, mice carrying a single copy of the *Rh* gene (*Rh*^{+/+}) developed with normal retinas, and rods elaborated outer segments of normal size despite the presence of only 50 % *Rh* relative to the normal situation. Photoreceptor neurons in these retinas also showed some signs of dysfunction (i.e. the outer segments become shorter in older mice), but the severity of this phenotype was drastically reduced relative to *Rh*^{-/-} mice (Humphries et al., 1997; Lem et al., 1999). These observations indicated that the endogenous *Rh* has a crucial role in the development of photoreceptor neurons, and raised the possibility that loss of endogenous *Rh* function (which might be caused in RP by mutant *Rh*) might also contribute to PN degeneration in RP.

To examine the contribution of the endogenous *Rh* (or the loss of endogenous *Rh*) to the degeneration triggered by dominant *Rh* mutations, a transgenic mouse expressing three *Rh* mutations (V20G, P23H, P27L, termed GHL mutant) was made (Frederick et al., 2001). When *Rh*^{GHL} is expressed in the presence of the two endogenous *Rh*^{WT} alleles (i.e. *Rh*^{GHL}; *Rh*^{+/+}), the retinal degeneration was found to be moderate. When, however, *Rh*^{GHL} is expressed in a *Rh* heterozygous (i.e. *Rh*^{GHL}; *Rh*^{-/-}) or homozygous (i.e. *Rh*^{GHL}; *Rh*^{-/-})

knockout background, retinal degeneration was severely accelerated (Frederick et al., 2001). These results suggest that the presence of the endogenous Rh is required for maintaining the viability of PNs that express mutant Rh^{GHL}, and raise the possibility that the Rh^{GHL} allele causes RP via a dominant-negative (DN) mechanism (i.e. mutant Rh^{GHL} might recruit the endogenous Rh into ER aggregates and might thus prevent its delivery to the plasma membrane where it is required for structural and functional stability).

1.7 Drosophila models of retinitis pigmentosa

One major advantage when using *Drosophila* as a model system for RP is the ability to perform a rapid screening of visual mutants in order to identify genes important for normal *Drosophila* vision. Besides that, *Drosophila* has a very short generation time (about 10 days at 25° C), is cost effective and has a well characterized visual system.

In 1985 O'Tousa et al. isolated a *Drosophila* gene that showed similarity to bovine *opsin* cDNA. This gene encoded the major visual pigment found in *Drosophila* R1-6 PNs and showed a significant homology to vertebrate *Opsins*, suggesting its conservation during evolution (O'Tousa et al., 1985). In the following we will refer to this *ninaE* gene as *Rh1*. The first *Rh1* mutants in *Drosophila* were characterized in 1986 and shown to display both physiological (Johnson and Pak, 1986) and histological defects (Leonard et al., 1992; O'Tousa et al., 1989).

In 1995, Kurada and O'Tousa performed ethyl methanesulfonate (EMS) mutagenesis to isolate various dominant mutations (single base substitutions) in the *Drosophila Rh1* gene (Kurada and O'Tousa, 1995). Two of these mutations, *Rh1*^{S137F} called *Rh1*^{D1} and *Rh1*^{S95F} called *Rh1*^{D2}, were characterized in more detail. These dominant alleles in flies (genotypes: *Rh1*^{D1}/*Rh1*⁺ and *Rh1*^{D2}/*Rh1*⁺) were found to impair the maturation of the endogenous WT *Rh1* and to trigger retinal degeneration (assessed in retinal morphological studies) and blindness (as assessed by reduced ERG amplitudes). Remarkably, the degeneration was drastically reduced in these *Rh1*^{D1} or *Rh1*^{D2} flies after eliminating the endogenous *Rh1* (genotypes: *Rh1*^{D1}/*Rh1*⁻ and *Rh1*^{D2}/*Rh1*⁻), suggesting that the presence of the endogenous *Rh1* is pathologic (Kurada and O'Tousa, 1995). Mutant *Rh1*^{D1} and *Rh1*^{D2} might recruit the endogenous *Rh1* into ER aggregates and might thus implicate *Rh1* in the toxic effects generated by aggregate formation.

Abnormal activation of the visual cascade (e.g. by enhancing the phosphorylation of *Rh1* after interaction with light particles, or by enhancing its interaction with Transducin) was found to be a major mechanism for ADRP, especially for mutations of class V and VI (Mendes et al., 2005). In *Drosophila*, mutation of a Ca²⁺-dependent protein phosphatase (called *rdgC*, from *retinal degeneration*), which acts on phosphorylated *Rh1* leads to excessive activation of the visual cascade and to retinal degeneration. Interestingly, mutations like *Rh1*^{D1} and *Rh1*^{D2} rescue the degeneration caused by the *rdgC* mutation, since they reduce the levels of mature *Rh1* (see above) and thus decrease the overall activation of the visual cascade in *rdgC* mutants (Kurada and O'Tousa, 1995). Alloway and colleagues demonstrated the existence of stable, persistent complexes between *Rh1* and its regulatory protein Arrestin (which normally binds active and phosphorylated *Rh1* and inactivates it) in several different retinal degeneration mutants in *Drosophila*. Elimination of these *Rh1*-Arrestin complexes by removing either *Rh1* or Arrestin rescued the degeneration phenotype. Furthermore, accumulation of these complexes triggers apoptotic cell death and the observed retinal degeneration requires the endocytic machinery (Alloway et al., 2000). Thus, the endocytosis of *Rh1*-Arrestin complexes may

Introduction

be a molecular mechanism for the initiation of retinal degeneration. In a subsequent study it was found that internalized Rh1 is not degraded by the lysosomes but instead accumulates in late endosomes, forming insoluble aggregates that cause cell death (Chinchore et al., 2009). Dominant *Rh1* mutations that lead themselves to excessive visual processing have also been characterized in *Drosophila*. The *Rh1^{pp100}* mutant shows a prolonged interaction with Arrestin and leads to constitutive activation of the phototransduction cascade, but also (independently) to elevated levels of the α subunit of Transducin (Iakhine et al., 2004).

Besides the abnormal gain-of-function (GOF) (e.g. aggregate formation, excessive activation of the visual cascade, mislocalization, etc.), loss of mature Rh from the plasma membrane can also lead to severe dysfunction of the cell and to cell demise. *Drosophila* and rodent studies, as well as mutations in humans that abolish Rh function suggest that Rhodopsin is essential for photoreceptor morphogenesis (Mendes et al., 2005). Chang and Ready (2000) found that transgenic expression of a constitutively active *Drosophila* Rho guanosine triphosphatase, Rac1 rescued photoreceptor morphogenesis defects in *Rh1 null* mutants. Expression of a dominant-negative version of *Rac1* caused a phenotype similar to that seen in *Rh1 null* mutants. Rac1 was localized in a specialization of the photoreceptor cortical actin cytoskeleton, which was lost in *Rh1 null* mutants (Chang and Ready, 2000). Thus, Rh appears to organize the actin cytoskeleton through Rac1, providing a structural support essential for photoreceptor morphogenesis.

1.7.1 The *Rh1^{P37H}* model of *retinitis pigmentosa*

The laboratory of Angela Giangrande at the Institute of Genetics and Molecular and Cellular Biology (IGBMC) Strasbourg generated a *Drosophila* model of *Rh^{P23H}*-linked RP. They overexpressed *Rh1^{P37H}*, the equivalent of mammalian *Rh^{P23H}*, in PNs R1-6 using the endogenous *Rh1* promoter (Galy et al., 2005). In these flies, mutant *Rh1^{P37H}* triggered light- and age-dependent retinal degeneration. Mutant *Rh1^{P37H}* was found to be partially mislocalized (it was present in rhabdomeres, but a part of the mutant protein was retained in the ER), however, no major effects on the maturation of the WT Rh1 were detected. After 20 days of light exposure, massive loss of PNs was detected. This degeneration was also accompanied by progressive blindness. The degenerative process was likely caused by abnormal activation of JNK and p38 signaling, two well-known pro-apoptotic effectors. Finally, the retinal pathology induced by mutant *Rh1^{P37H}* was rescued by the overexpression of the anti-apoptotic gene *p35* (Galy et al., 2005). Therefore, the *Rh1^{P37H}* flies recapitulate important features of RP, and can be used to understand the mechanisms causing *Rh^{P23H}*-linked RP. Most of our *Drosophila* work was performed on these flies (and the corresponding controls).

1.8 Mechanisms of photoreceptor cell death in *retinitis pigmentosa*

The above-mentioned genetic findings in RP together with studies in animal models of RP have led to the delineation of several pathogenic mechanisms that might be responsible for PN degeneration in RP (Figure 7). As previously mentioned, it appears that each class of Rh mutations has specific pathogenic features that might distinguish it from the other classes. Therefore, one major conclusion regarding Rh-linked RP is that several mechanisms might initiate the cell death cascade. However, these mutations might have at least two things in common. First, they cause cell death either via a DN mechanism or via a toxic GOF mechanism. Second, despite the differences in initiating

the disease, all classes of Rh mutants might share common cell death effectors, that lead to cell demise once the initiating dysfunctions are amplified.

The DN mechanisms that might cause RP are: i) interference with the maturation of the endogenous Rh; ii) lack of structural support in the outer segment, leading to outer segment instability.

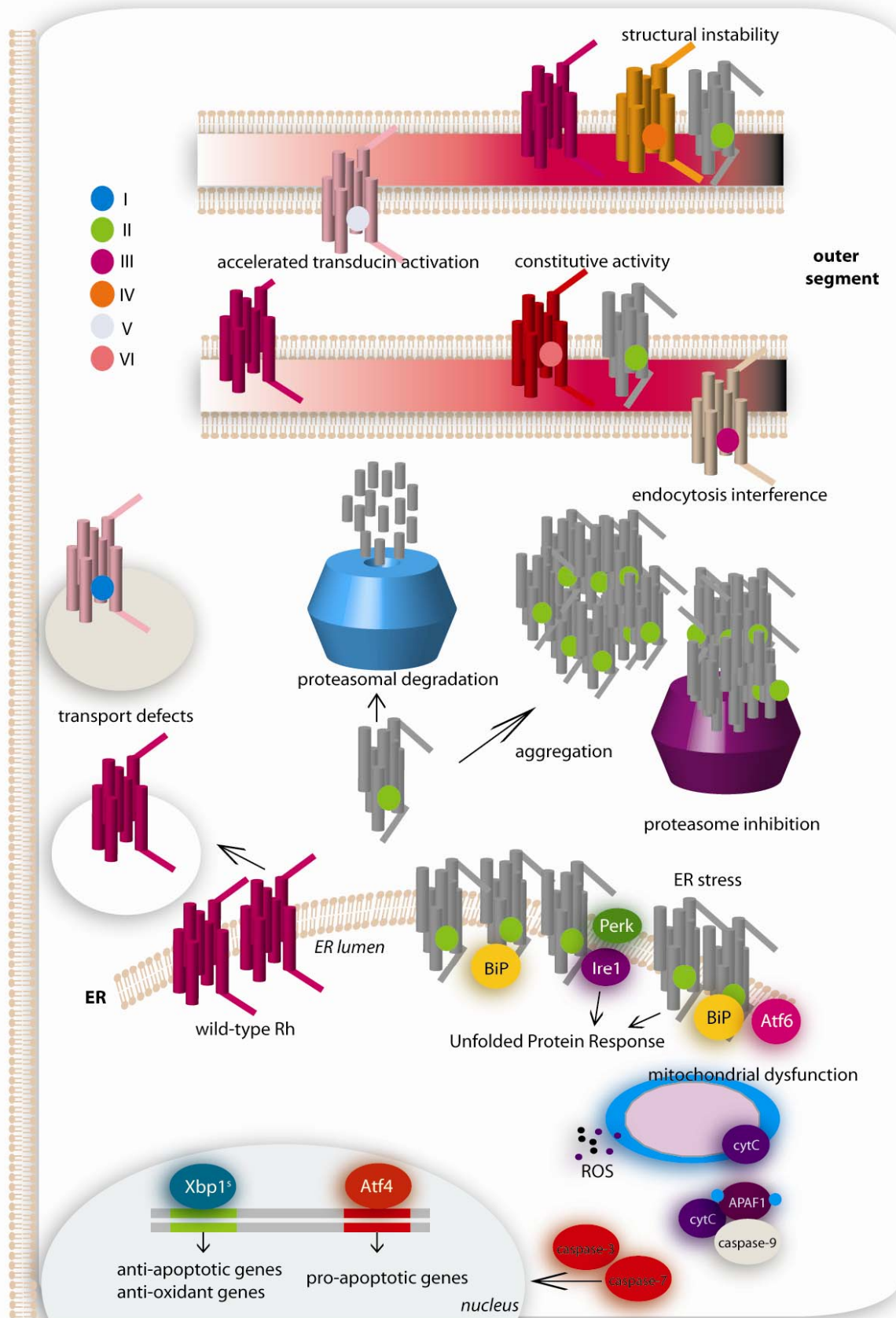
How do these DN effects lead to cell death? The absence of Rh from the plasma membrane not only impairs visual processing but might also compromise the stability of the outer segment; indeed, the studies mentioned above found that Rh has an important role in the maintenance of the outer segment structure (Humphries et al., 1997; Lem et al., 1999; Mendes et al., 2005) (Figure 7).

The GOF mechanisms that might cause RP are: i) Rh aggregation and inclusion formation; ii) activation of the unfolded protein response; iii) Rh mis-sorting and interference with the traffic machinery; iv) endocytosis and Arrestin binding; v) constitutive or dysregulated activation; vi) structural instability within the outer segment.

These GOF effects might have the following consequences (Figure 7): i) Misfolded Rh (class II) is extracted from the ER and delivered to the proteasome for degradation. If the protein is not timely degraded, it might accumulate and aggregate in the cytosol, where it causes toxicity by recruiting other proteins or by interfering with diverse cellular processes ii) Class II Rh mutants are retained within the ER and are subsequently extracted from the ER and degraded. If the presence of these mutants in the ER is prolonged, they might induce an ER stress response, called the unfolded protein response (UPR; see below; Introduction 2.3). Excessive UPR activation might lead to cell death iii) Class I Rh mutants are not properly targeted to the plasma membrane and might interfere with the normal vesicular traffic machinery iv) Class III Rh mutants bind Arrestin in a dysregulated fashion and might lead to impairment of the endocytic pathway. This might lead to a general failure in internalizing photoactivated Rh and might lead to severe outer segment imbalance v) Several classes of Rh mutants, if not all, can lead to constitutive activation of phototransduction (in specific circumstances) and this might be very deleterious for PNs vi) Class IV Rh mutants (and some class II mutants that reach the plasma membrane) might cause structural instability in the outer segment, via a GOF effect (Adler, 1996; Mendes et al., 2005; Sancho-Pelluz et al., 2008; Stone et al., 1999; Travis, 1998).

A better understanding of the molecular mechanisms mediating these DN and GOF effects and their potential interplay is therefore required in order to understand RP. Since both DN and GOF effects might underlie the Rh^{P23H} -linked RP, it is crucial to determine i) the mutual interactions between Rh^{P23H} and its wild-type counterpart (that are implicated in the DN effect) and ii) the molecular interactions between Rh^{P23H} and the cellular machinery responsible for protein refolding and degradation (which are involved in the GOF effect). These aspects of Rh^{P23H} pathogenicity represent the major aim of the present thesis.

Figure 7. Mechanisms of photoreceptor cell death mediated by mutant Rh in *retinitis pigmentosa*. Rh mutations were classified (class I to VI; see top left for the color code) based on their biochemical and cellular behaviour. **Class I** mutants (blue circle) are not properly transported to the outer segment; they might also impair other transport processes, thereby leading to severe cell dysfunction. **Class II** mutants (which include Rh^{P23H}; green circles) are retained within the ER and subsequently delivered to the proteasome for degradation. In order to be degraded, class II Rh mutants must be extracted from the ER (retrotranslocated). However, excess retrotranslocation might lead to proteasome overwhelming and to accumulation of misfolded Rh in the cytosol (and subsequent aggregation). Both ER-located and cytosolic Rh aggregates might be toxic for the cell. Misfolded Rh in the ER might induce the unfolded protein response (UPR) that might trigger cell death under conditions of chronic UPR activation. UPR activation could be both beneficial (via activation of the Ire1/Xbp1 pathway and generation of the Xbp1S transcription factor; not shown) and deleterious (e.g. via production of the pro-apoptotic factor CHOP). A part of class II mutant Rh might reach the outer segment; however, this mutant Rh might lead to defects in outer segment stability or might lead to abnormal activation of the visual cascade. It is therefore not clear how class II mutant Rh triggers cell death and how deleterious is the ER vs. cytosolic localization of mutant Rh, or its presence in the outer segment. Another potential pathologic mechanism induced by class II mutant Rh is the recruitment of WT Rh into aggregates and the subsequent loss of WT Rh (not shown). **Class III** Rh mutants (purple circle) display defects in endocytosis and might trigger cell death by inducing alterations of the endosomal compartments. **Class IV** mutants (orange circle) localize to the outer segment but these mutants are instable; they might therefore destabilize the outer segments, leading to severe structural and functional defects. **Class V** mutants (grey circle) lead to constitutive transducing activation and might trigger cell death via excessive visual activation that might deplete the cell of energy and cause metabolic imbalances. **Class VI** Rh mutants (pink circle) display constitutive Rh activity in the absence of retinal, and trigger continuous activation of the visual cascade, thereby destabilizing the cell. Please note that some Rh mutations remained unclassified. It remains to be determined whether the cell death mechanisms triggered by these mutant classes share some common downstream effectors. A possible common pro-apoptotic pathway could be the release of cytochrome c (cytC) from the mitochondria and formation of the apoptosome complex (cytC, APAF-1 and caspase-9) which leads to activation of caspases. Dysfunctional mitochondria also produce reactive oxygen species (ROS) and lead to calcium imbalance (not shown), which cause severe cell dysfunction.



Part two: ER quality control and the ERAD effector VCP

A. ER quality control, ERAD and ER stress: mechanisms and impairment in disease

The acquisition of an optimal three dimensional conformation is a critical requirement for proteins in order to exert their functions in the cell. Conformational defects in a single protein might have devastating consequences for the entire cell, and might lead to its demise. This chapter describes the mechanisms responsible for the quality control in the ER and the consequences of protein misfolding in the ER. The first part (2.1 to 2.4) examines the mechanisms of ER quality control, with particular emphasis on ER-associated degradation (ERAD). The second part (2.5 to 2.10) deals with the ERAD effector VCP, and in particular with the mechanisms by which VCP promotes the degradation of ER-localized misfolded proteins.

2.1 Overview of ER quality control

The eukaryotic cell environment is extremely complex and most proteins, after synthesis, rapidly fold to perform their biological activities. Although protein folding is assisted by chaperones, this process is sometimes characterized by errors and some polypeptides remain in a non-native intermediate state instead of reaching their final native conformation (Jahn and Radford, 2005). Spontaneous errors during transcription and translation, genetic mutations, toxic compounds or cellular stress (e.g. increased temperature) can compromise the efficiency of cellular protein folding (Vembar and Brodsky, 2008). Although in many instances defects in protein conformation are tolerated by the cell, in numerous cases these conformational defects cause disease. Thus, inherited mutations that lead to protein misfolding are responsible for a wide range of diseases, such as cystic fibrosis, antitrypsin deficiency or neurodegenerative disorders like Alzheimer's (AD), Parkinson's (PD) or Huntington's disease (HD) (Gregersen et al., 2005) and many mutations causing defects in Rh folding cause *retinitis pigmentosa* (Mendes et al., 2005).

Misfolded proteins are deleterious in various ways, and they often form insoluble aggregates that are toxic to cells. It is therefore essential that such abnormal proteins are detected and cleared by the cell. To prevent the toxicity associated with protein misfolding, cells have developed several protein quality control (PQC) systems. The central task of a PQC system is to supervise folding, to prevent aggregation and to discard unfolded polypeptides from the compartment where it acts. Three major PQC systems evolved in eukaryotic cells, and are located in three main subcellular compartments: cytosol, ER and mitochondria (Anelli and Sitia, 2008).

The ER hosts a huge variety of proteins that are destined to the plasma membrane or to the extracellular space. The ER is thus an important source of membrane and secreted proteins, which often regulate various aspects of cell metabolism or intra/intercellular communication. These proteins are co-translationally inserted in the ER membrane or translocated in the ER lumen and must be free of conformational errors in order to exit the ER and reach their final destinations. The PQC system that acts in the ER (ER quality control [ERQC] system) is therefore highly specialized in detecting errors in protein conformation, and functions with amazing precision and rapidity (Ellgaard and Helenius, 2003). The central players of ERQC are molecular chaperones that help polypeptides fold and assess the conformations of their substrates. Important characteristics for recognition

of non-native polypeptides are exposure of hydrophobic regions, unpaired cysteine residues and the tendency to aggregate. The ER lumen is a more oxidizing environment compared to the cytosol and contains various chaperones and folding enzymes, such as heat shock protein (Hsp)40, Hsp70, Hsp90, Calnexin, Calreticulin or thiol-disulphide oxidoreductases (Hebert and Molinari, 2007). Binding immunoglobulin protein (BiP) is the most important member of the Hsp70 family and it is considered to be a master regulator of protein folding in the ER (Hendershot, 2004). BiP binds to extended hydrophobic domains in different nascent polypeptides and prevents immature proteins from aggregation, detects conditions of stress in the ER to activate stress response pathways and participates in the targeting of misfolded proteins for degradation (Vembar and Brodsky, 2008).

The ER is also the site of extensive co-translational modifications. Thus, most proteins that travel through the secretory pathway (including Rh) are co-translationally modified with N-linked oligosaccharides. Two ER resident lectin chaperones, which recognize these sugar-modified proteins, are Calnexin and Calreticulin. These chaperones interact with trimmed intermediates of the N-linked glycans from almost all glycoproteins (Hebert et al., 1995; Spiro et al., 1996) and promote their folding. At the end of this folding process, also called Calnexin/Calreticulin cycle, most glycoproteins are released in native, transport-competent state. However, proteins with folding defects (non-native) are subjected to additional folding cycles until they are correctly folded. Should these additional folding cycles remain unsuccessful, the misfolded proteins (called terminally misfolded) are targeted for degradation, in a process termed ER-associated degradation (Hirsch et al., 2004; Meusser et al., 2005).

The process of ERAD culminates with the degradation of misfolded proteins by the ubiquitin proteasome system (UPS). Another major pathway for intracellular proteolysis is represented by lysosomes, in a process called autophagy. The process of autophagy involves the recognition and engulfment of targeted proteins or organelles into autophagosome vesicles that become fused with lysosomes (Knecht et al., 2009). Therefore, the combined action of both ERAD/UPS and lysosome'autophagy systems is responsible for clearance of most misfolded proteins. In some cases, however, the ERAD/UPS and autophagy pathways cannot cope with misfolded proteins, and many misfolded proteins form large perinuclear aggregate inclusions called aggresomes. These intracellular aggregates are often toxic for cells, causing cell dysfunction and cell death (Kopito, 2000).

2.2 ERAD molecular machinery and ubiquitin proteasome system

If proteins do not succeed to fully mature in the ER and do not fulfill all the requirements established by ERQC, they are subjected to ERAD (Romisch, 2005). The process of ERAD involves the selective export of misfolded proteins from the ER to the cytosol (retrotranslocation), followed by proteasomal degradation (Vembar and Brodsky, 2008).

The history of ERAD. The notion of ERAD was introduced in 1988 by the Klausner laboratory that investigated the degradation of subunits in the heptameric T-cell receptor (TCR) complex (Lippincott-Schwartz et al., 1988). Assembly of TCR subunits into a hetero-oligomeric complex is required for trafficking out of the ER. Klausner and colleagues showed that isolated α and μ subunits of TCR were degraded in a non-lysosomal, pre-Golgi compartment (Klausner and Sitia, 1990). In 1993, the work of Sommer and Jentsch provided the first link between the UPS and the quality control of a

Introduction

mutated membrane protein in the yeast ER (Sommer and Jentsch, 1993). Studies performed in the mid-1990s showed that mutant secretory proteins (that were initially located in the ER) were degraded by the proteasome and it became clear that these misfolded proteins are retrotranslocated into the cytosol for degradation (Hebert and Molinari, 2007). Therefore, extraction of misfolded proteins from the ER (retrotranslocation) is a critical step during the ERAD process, as it allows the delivery of ER misfolded proteins to the cytosolic UPS.

ERAD steps. During ERAD, substrates are first recognized as being terminally misfolded, and then they are targeted to the retrotranslocation machinery, retrotranslocated into the cytosol, ubiquitinated and finally delivered to UPS for degradation (Vembar and Brodsky, 2008). Each of these individual steps is detailed below. Figure 8 summarizes the major interactions that promote substrate selection, retrotranslocation, ubiquitination and proteasomal degradation.

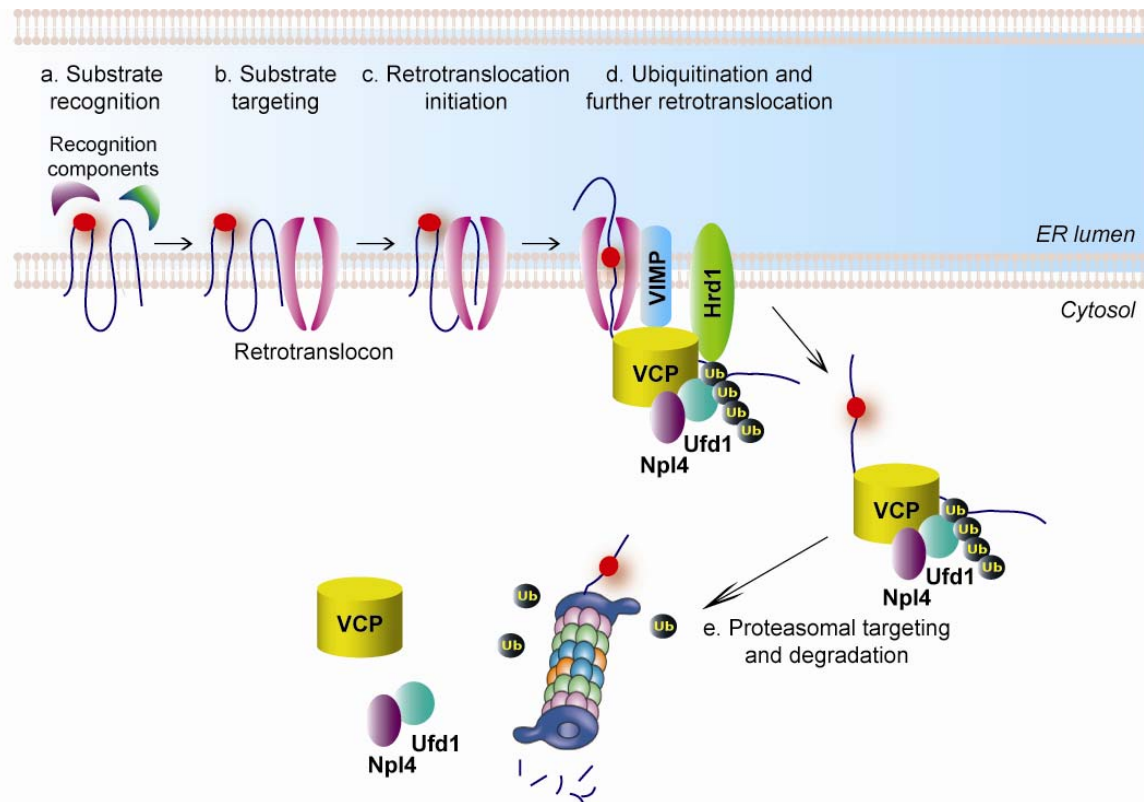


Figure 8: The main steps of the ERAD process. (A) Substrate recognition. ER membrane misfolded proteins containing ER luminal lesions are recognized by ER recognition components/chaperones (such as Hsp70, Calnexin, Calreticulin, and protein disulphide isomerases). (B) Substrate targeting. Substrates are targeted to the retrotranslocation machinery (the retrotranslocon). (C) Retrotranslocation initiation. Substrate retrotranslocation into the cytosol starts when the polypeptide is partially moved out of the ER through the retrotranslocon which might be represented by Derlin1 or Sec61 channel, or by transmembrane E3 ubiquitin ligases. (D) Ubiquitination and further retrotranslocation. As proteins exit the retrotranslocon, they are polyubiquitinated by E3 ubiquitin ligases (such as Hrd1). This promotes further retrotranslocation and the emerging polypeptide is captured by the cytosolic VCP-Ufd1-Npl4 complex, which is recruited to the ER membrane by an ER membrane protein (like VIMP or Erasin). The energy derived from ATP hydrolysis by VCP, is used for retrotranslocation. (E) Proteasomal targeting and degradation. Once a polyubiquitinated substrate is dislocated into the cytoplasm, it is recognized by receptors in the 19S cap of the proteasome. Deubiquitinating enzymes (not shown) remove the polyubiquitin tag, and peptide N-glycanase (not shown) might also be required for efficient degradation. The substrate is then threaded into the 20S catalytic core of the proteasome where it is degraded into small peptide fragments.

Substrate recognition. The machinery responsible for substrate recognition is able to specifically recognize mutant proteins and decide whether they are terminally misfolded and must be targeted to ERAD. The Hsp70s have a general role in ERAD substrate selection. It is believed that prolonged interaction between an ERAD substrate and an Hsp70 is sufficient to recruit a E3 ligase (Vembar and Brodsky, 2008). The Hsp70 BiP has a critical role during selection of many substrates; consistent with that, BiP knock-in mice have profound defects in ERQC and display many defects in brain development (Mimura et al., 2008). Calnexin and Calreticulin are also involved in the recognition of misfolded substrates, and it is thought that a crosstalk exists between BiP and Calnexin/Calreticulin systems; for example, BiP can compensate for the absence of the Calnexin/Calreticulin cycle by binding to glycosylated substrates, for which it normally has a reduced affinity (Zhang et al., 1997).

Substrate targeting. Soluble ERAD substrates must be first selected for retrotranslocation to the cytoplasm as the enzymes required for ubiquitination of these substrates reside in the cytoplasm. For ERAD substrates that belong to the ER membrane (like mutant Rh), ubiquitination precedes or can take place concomitant with retrotranslocation. It was suggested that the location of a misfolded site dictates the factors that are required for ERAD substrate targeting. Proteins with lesions in the cytoplasmic, luminal and transmembrane domains follow the ERAD-C, ERAD-L and ERAD-M pathways, respectively (Carvalho et al., 2006; Denic et al., 2006). Up to now, these ERAD pathways were defined only in yeast. ERAD-C substrates use for ERAD targeting a complex that contains the yeast Doa10 ubiquitin ligase. Substrates of the ERAD-L pathway, soluble or integral membrane proteins that contain a luminal lesion, interact with the Hrd1 ubiquitin ligase complex. Less is known about the ERAD-M pathway, but it appears that its substrates are also ubiquitinated by the Hrd1 complex (Vembar and Brodsky, 2008). The different ERAD pathways are summarized in the Figure 9.

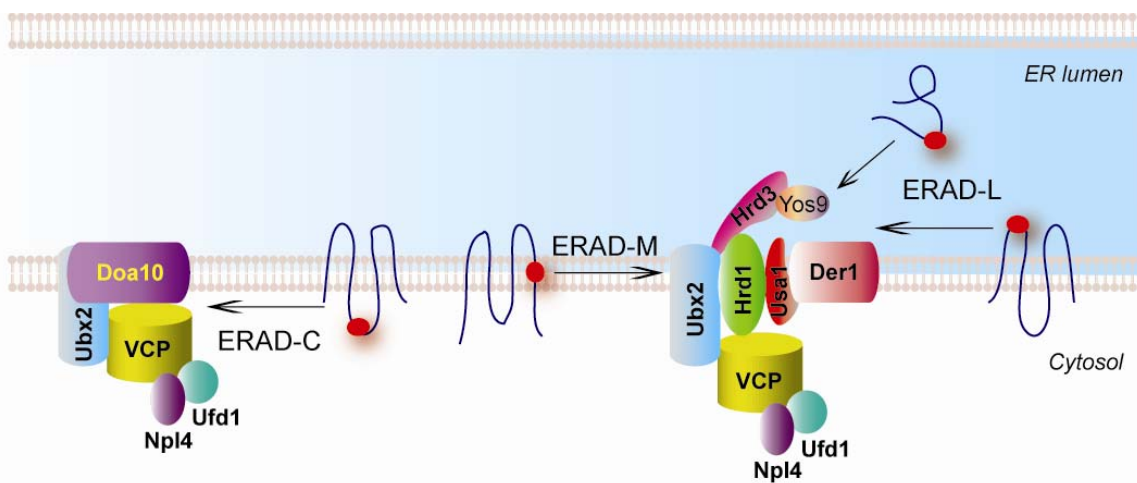


Figure 9. Distinct ERAD pathways and machineries. Misfolded proteins containing cytosolic, intramembrane or ER luminal lesions are targeted to different ERAD machineries and follow ERAD-C, ERAD-M and ERAD-L pathways, respectively. The right panel shows the Hrd1/Hrd3 complex in the ERAD-L and ERAD-M pathways. Yos9 recognizes N-glycans on misfolded proteins which are then ubiquitinated by Hrd1 in the cytosol and degraded by the proteasome. The left panel shows the Doa10 complex of the ERAD-C pathway. For both Hrd1 and Doa10 complexes, the yeast cytosolic Cdc48/VCP complex is recruited to the ER membrane by the intramembrane protein Ubx2. Please note that the three ERAD pathways were defined until now only in yeast.

Introduction

Several ER resident targeting factors that recognize glycoproteins (like Rhodopsin) have been characterized (Kosmaoglou et al., 2009). These include the family of ER degradation-enhancing 1,2 mannosidase-like protein (EDEM). Trimming of terminal mannoses by ER mannosidase-I might act as a timer for glycoproteins, making them enter ERAD (Fagioli and Sitia, 2001). EDEM proteins facilitate the disposal of glycoproteins from the ER by operating in two different ways: accelerating mannose removal and preventing aggregation of terminally misfolded glycoproteins released from the Calnexin/Calreticulin cycle. It appears that the EDEM factors deliver ERAD substrates to the retrotranslocation channel (Hebert and Molinari, 2007).

Cytoplasmic Hsp70s and Hsp40s participate in the substrate targeting of membrane proteins that present misfolded domains to the cytoplasm and contain short folded luminal segments. They mediate the interaction between membrane substrates and the Doa10 ubiquitin ligase in yeast (Vembar and Brodsky, 2008).

Retrotranslocation initiation. Following substrate recognition and targeting, ERAD substrates are retrotranslocated across the ER membrane to the cytosol. In order to undergo retrotranslocation, ERAD substrates must be soluble and dissociated from oligomeric complexes, and their disulfide bonds need to be reduced (Fagioli et al., 2001). This requirement for unfolding during retrograde transport was nonetheless questioned by other studies that showed that substrates can be retrotranslocated in a folded state (Tirosh et al., 2003).

Dislocation of misfolded proteins to the cytosol may involve the Sec61 translocation channel that appears to have a secondary role as retrotranslocation channel (the retrotranslocon). Mutations in the gene encoding yeast Sec61 partially impaired the ERAD of soluble and membrane substrates (Plempfer et al., 1997) and interactions between proteasome subunits and Sec61 were detected (Kalies et al., 2005). Members of the Derlin family have also been implicated as putative components of the retrotranslocon (Ye et al., 2004).

The E3 ubiquitin ligases Doa10 and Hrd1, which mediate ERAD in yeast, are multi-spanning membrane proteins and are believed to be integral components of retrotranslocation channels (Kostova et al., 2007). Ubiquitination and retrotranslocation activities in a single E3 enzyme might be the most efficient way to target ERAD substrates to the proteasome.

Ubiquitination and further retrotranslocation. Almost all ERAD substrates are ubiquitinated before they are targeted to the proteasome. Protein ubiquitination requires the action of an E1 ubiquitin-activating enzyme, E2 ubiquitin-conjugating enzymes and E3 ubiquitin ligases (Figure 10) (Vembar and Brodsky, 2008). For ubiquitin (Ub) conjugation, a thioester linkage is formed between the E1 Ub-activating enzyme and Ub. Ub is then transferred to an E2 Ub-conjugating enzyme through the formation of another thioester linkage. The covalent attachment of Ub to substrates is catalysed by E3 ligases, such as RING, U-box and HECT domain-containing proteins (Figure 10). The attached polyubiquitin chain must reach a crucial length before a substrate can be retrotranslocated. It is believed that the minimal signal necessary for proteasome targeting is a chain of four Ub molecules linked through Lys48 (Thrower et al., 2000).

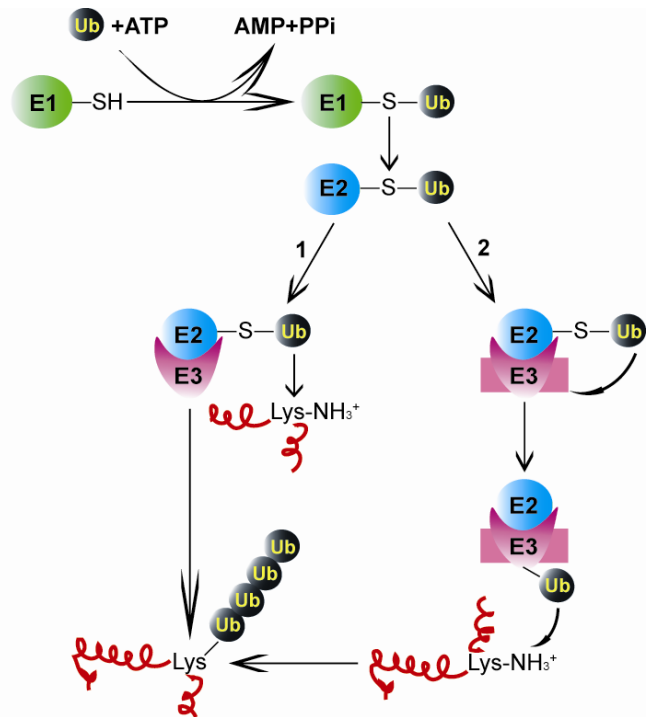


Figure 10. The ubiquitination process. Proteins destined for proteasomal degradation are first polyubiquinated in a multi-step process. The C-terminal Gly of Ub is adenylated by the E1 Ub-activating enzyme and then displaced following the nucleophilic attack of a conserved Cys residue in the E1, resulting in a thioester linkage between the E1 and Ub. In the next step, the transfer of Ub to an E2 Ub-conjugating enzyme takes place through formation of another thioester linkage. The covalent attachment of Ub to substrates is catalysed by the E3 Ub ligases, such as RING, U-box and HECT domain-containing ligases. The E3 ligases containing RING or U-box domains facilitate the transfer of Ub from the E2 to selected substrates (step 1). The E3 ligases containing the HECT domain are covalently coupled to Ub by a thioester bond in the HECT domain. The subsequent interaction with substrates is required for Ub modification (step 2).

With few exceptions, retrotranslocation of ERAD candidates is inhibited upon proteasome inactivation, thus indicating that retrotranslocation and degradation are coupled events (Chillaron and Haas, 2000; Mancini et al., 2000). Once a membrane protein is polyubiquitinated, it is extracted from the membrane and targeted to the proteasome. In some cases, the proteasome is sufficient to retrotranslocate substrates (Lee et al., 2004; Mayer et al., 1998).

For almost all ERAD substrates, a cytoplasmic protein complex, the Valosin-containing protein (VCP) complex, has a crucial role in substrate retrotranslocation in both yeast and mammals (Jentsch and Rumpf, 2007). In yeast, this retrotranslocation complex contains the VCP ortholog, cell division cycle 48 protein (Cdc48) and two associated factors, ubiquitin fusion degradation (Ufd1) and nuclear protein localization (Npl4). In mammals, VCP associates with conserved Ufd1 and Npl4 homologues. VCP is an ATPase and the energy produced by VCP-mediated ATP hydrolysis is used for substrate extraction from the ER (retrotranslocation). In yeast, the VCP complex might be recruited to the ER membrane in part through its interaction with the ubiquitin regulatory X (UBX) domain-containing ER membrane protein Ubx2 (Schuberth and Buchberger, 2005); in mammals, the VCP complex is recruited through its interaction with the VCP-interacting membrane protein (VIMP) (Ye et al., 2004). The VCP complex also binds to several other ER-resident components, including the E3 ligase gp78, Derlin1 and the Hrd1 complex (Carvalho et al., 2006; Denic et al., 2006). VCP extracts ubiquitinated substrates from the

Introduction

ER membrane and then directs them to the proteasome (Ye et al., 2001). The mechanism of this process is discussed below (also see Figure 8).

Proteasomal targeting and degradation. VCP was found to associate with the proteasome (Dai et al., 1998; Verma et al., 2000), suggesting that soluble and integral membrane substrates might be transported directly from the membrane-associated VCP complex to the proteasome. Moreover, an important percentage of proteasomes reside at the surface of the ER membrane (Kalies et al., 2005; Rivett and Knecht, 1993) and are therefore positioned to receive and degrade ERAD substrates. Other studies suggest nonetheless that different VCP- and proteasome-interacting factors take the role of shuttle between VCP and the proteasome during substrate degradation. These adaptors are proteins that contain both UBA and UBL domains; ubiquitin-associated (UBA) domains bind poly-Ub chains of the ubiquitinated substrates in the VCP complex, while ubiquitin-like (UBL) domains interact with the proteasome. Two proteasome adaptor proteins, Rad23 and Dsk2, containing both UBA and UBL domains have been shown to increase the efficiency of ERAD (Medicherla et al., 2004).

Recent evidence suggests that additional mechanisms of shuttling allow ERAD substrates to be targeted to the proteasome. The UBX domain-containing protein Erasin is an integral membrane protein of the ER and serves as a platform for binding the cytoplasmic VCP (Liang et al., 2006). Erasin was suggested to bind to both Ubiquilin and VCP, forming a complex involved in ERAD (Lim et al., 2009). The polyubiquitinated chain of the ERAD substrate might be recognized by the UBA domain of Ubiquilin; once the substrate bound to it, Ubiquilin might recruit proteasomes using its UBL domain (Lim et al., 2009). Thus, Ubiquilin might serve as a shuttle between VCP substrates and the proteasome.

Once targeted to the proteasome, substrate proteins are cleaved to small peptides that are quickly hydrolyzed by cytosolic peptidases. The proteasome is composed of a 20S core particle capped by a 19S regulatory particle (19S RP) at one or both ends (thus forming 26S or 30S proteasomes). The 20S core particle is a stack of four heptameric rings (28 subunits), which are assembled to form a cylindrical structure. The outer two rings are composed of α subunits while the inner two rings are composed of β subunits, which contain the proteolytic active sites in a central cavity. The degradation chamber can be reached through a narrow channel that runs along the axis of the core particle. Therefore, folded proteins need to be partially unfolded before they can be translocated into the 20S catalytic core and degraded (Pickart and Cohen, 2004).

The 19S RP is composed of at least 19 subunits arranged into two sub-complexes: the lid and the base. The 19S RP controls the activity of the complex, gates the entrance to the degradation channel and plays a role in substrate recognition, unfolding and translocation into the 20S core particle (Finley, 2009). The 19 subunits of the 19S cap comprise 6 regulatory particle ATPase1 (RPT1–RPT6), 13 regulatory particle non-ATPase1 (RPN1–RPN13), besides peripheral factors (Knecht et al., 2009).

Another important activity of the 19S RP is the interaction with ubiquitinated substrates via its ubiquitin receptors. Some of the Ub receptors have been identified and include RPN13, RPN10 and RPT5. The 19S cap also removes Ub from substrates via the action of proteasome-associated deubiquinating enzymes (DUBs) either by sequential trimming or by removal of the total polyubiquitin chain, allowing Ub to escape from the

proteasome and to be recycled; removal of poly-Ub chains might be essential for a substrate to enter the proteasome (Amerik and Hochstrasser, 2004).

2.3 Pathways activated during ER stress: relevance and mechanisms

ER stress and the unfolded protein response. An imbalance between the load of unfolded proteins that enter the ER and the capacity of the cellular machinery that handles this load leads to the generation of ER stress (Schroder and Kaufman, 2005). The presence of ER stress signifies that misfolded proteins accumulate in the ER beyond a certain tolerated limit. Accumulation of unfolded proteins in the ER (ER stress) induces a series of signalling pathways termed the unfolded protein response (UPR; Figure 11). The main goal of the UPR is to make the ER return to its physiological state and adjust the ER protein folding capacity of the cell according to need (Bernales et al., 2006). In metazoans, accumulation of unfolded proteins activates signalling cascades in the cytosol via three classes of ER transmembrane sensor proteins: inositol-requiring protein 1 (Ire1), activating transcription factor 6 (Atf6) and protein kinase RNA (PKR)-like ER kinase (Perk). Each class of ER stress sensors defines a distinct arm of the UPR, senses the protein folding status in the ER lumen and transmits this information to the cytosol (Ron and Walter, 2007). These pathways are described in more detail below (see Figure 11).

Ire1. Ire1 encodes an ER transmembrane protein with a luminal domain and a cytoplasmic portion that contains a protein kinase domain. When misfolded proteins accumulate in the ER, Ire1 oligomerizes allowing the trans-autophosphorylation of juxtaposed kinase domains. Oligomerization of Ire1 can be induced by binding of misfolded proteins to the Ire1 luminal domain or by the release of oligomerization-inhibiting chaperones (e.g. BiP), or both. In the next step, trans-autophosphorylation of the kinase domain of Ire1 leads to the activation of its endoribonuclease function, which leads to the precise endonucleolytic cleavage of the X-box binding protein-1 (*Xbp1*) mRNA. *Xbp1* encodes a transcription factor that regulates UPR target genes. Unspliced *Xbp1* mRNA (*Xbp1U*) encodes a labile transcription factor that represses the expression of UPR target genes, while excision of an intron from *Xbp1* mRNA by the Ire1-mediated unconventional splicing results in a frameshift in the *Xbp1* transcript (*Xbp1S*; see also Materials and Methods for further details). The *Xbp1S* transcript is translated into a stable transcription factor *Xbp1S*, which upregulates UPR target genes (including ER chaperones and components of the ERAD machinery) (Rutkowski and Kaufman, 2007; Figure 11).

Perk. The activation of Perk is also controlled by interaction with BiP and upon ER stress, BiP dissociates from the Perk luminal domain. This leads to Perk dimerization, subsequent trans-autophosphorylation and activation of the cytosolic kinase domain. Perk phosphorylates the alpha subunit of the heterotrimeric eukaryotic translation initiation factor (eIF2 α) leading to inhibition of the eIF2B complex and attenuation of protein translation. Surprisingly, eIF2 α phosphorylation specifically promotes translation of the activating transcription factor 4 (Atf4) mRNA which activates expression of genes encoding amino acid transporters, redox enzymes and the pro-apoptotic transcription factor CCAAT enhancer-binding homologous protein (CHOP) (Schroder and Kaufman, 2005; Figure 11).

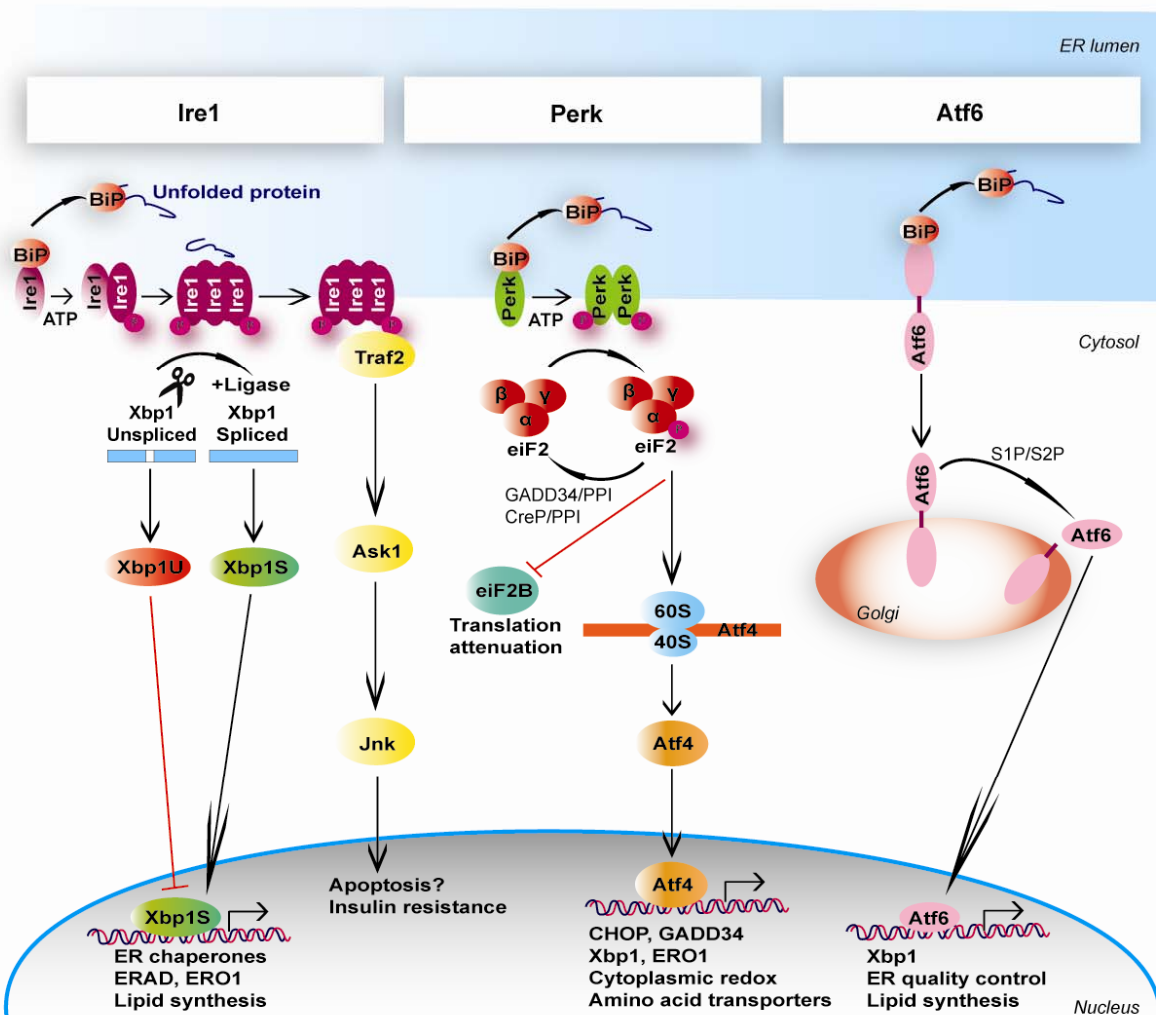


Figure 11. The Unfolded Protein Response. Mammalian UPR consists of three branches, each regulated by distinct transmembrane proteins in the ER: Ire1, Perk, and Atf6. Upon accumulation of misfolded proteins in the ER, Ire1 oligomerizes and is trans-autophosphorylated. Its endoribonucleolytic activity leads to cleavage of the Xbp1 by excising a small RNA fragment (intron). The two ends of the mRNA are ligated by a tRNA ligase. A frame shift in the coding sequence takes place and the spliced *Xbp1* mRNA encodes a potent transcriptional activator (*Xbp1S*), whereas the unspliced *Xbp1* mRNA encodes *Xbp1U*, an inhibitor of the UPR. *Xbp1* regulates UPR target genes that encode for ER chaperones and ERAD effectors. Phosphorylated Ire1 can also recruit tumor necrosis associated factor 2 (Traf2) and allows it to signal to apoptosis signaling-regulating kinase 1 (Ask1) and c-JUN N-terminal kinase (Jnk). The Ire1–Traf2 complex has been linked to caspase-12 activation and cell death. In response to ER stress, Perk also oligomerizes and is activated by trans-autophosphorylation. Active Perk phosphorylates the α subunit of eIF2 on Ser51, thus inhibiting the pentameric guanine nucleotide exchange factor eIF2B from recycling eIF2 to its active GTP-bound form. Inhibition of eIF2B leads to translation attenuation. However, translation of only Atf4 is increased under conditions of limiting eIF2. The transcription factor CHOP is activated transcriptionally by Atf4 and its target genes include growth arrest and DNA damage-inducible protein 34 (GADD34), a regulatory subunit of phosphatase PP1 that dephosphorylates eIF2 α and terminates signalling, and ER oxidase 1 (ERO1) which is required for disulphide bond formation in protein folding. Atf6 is a transmembrane protein with a cytoplasmic portion that, when liberated from its transmembrane tether, can bind to DNA and activate target genes. In unstressed cells, Atf6 resides in the ER membrane. Atf6 trafficking is prohibited by binding of BiP to its luminal domain. ER stress disrupts BiP binding and Atf6 is trafficked to the Golgi apparatus. In the Golgi, Atf6 is cleaved first by luminal S1P and then by the intramembrane S2P, which liberates the cytosolic effector portion of Atf6 from the membrane and allows its import into the nucleus. Atf6 might activate UPR target genes involved in ERQC.

Atf6. Atf6 is synthesized as inactive precursor, localized to the ER membrane by a transmembrane domain and having a stress-sensing domain that emerges into the ER lumen. Atf6 is regulated by interaction with BiP in the ER lumen. Under ER stress conditions, dissociation of BiP from Atf6 allows Atf6 trafficking to the Golgi. In the Golgi apparatus, Atf6 is sequentially cleaved by the site-1-protease (S1P) and S2P, to release a cytosolic DNA-binding domain of Atf6. Atf6 traffics to the nucleus to activate genes encoding ER chaperones and Xbp1 (Ron and Walter, 2007).

The activation of the three UPR branches leads to an initial acute response that reduces the protein load entering the ER. This transient adaptation is achieved by translational attenuation of protein synthesis, as a consequence of eIF2 α phosphorylation by Perk. Ire1-dependent degradation of a subset of ER-associated mRNAs might also contribute to the reduction of protein load. After this initial response, an adaptive, long-term response ensues; it consists of the transcriptional activation of UPR target genes by Xbp1, Atf6 and Atf4. UPR target genes encode proteins of the ER protein folding machinery, ERAD factors and other ER proteins that are involved in protein translocation and protein trafficking. If the ER homeostasis cannot be re-established by the actions of the UPR, apoptosis is triggered as a final irreversible step (Rutkowski and Kaufman, 2007).

Since one of the main goals of the UPR is to remove the misfolded proteins from the ER, the processes of UPR activation and ERAD are tightly coupled. UPR induction increases the capacity of the cell for ERAD, while a strong decrease in ERAD efficiency leads to constitutive UPR induction. Simultaneous impairment of ERAD and of the UPR leads to a significant decrease in cell viability (Travers et al., 2000). It is poorly understood how the UPR allows the selection of a pro-survival or of a pro-apoptotic cellular program. A better understanding of the connections between UPR, ERAD, the pro-survival adaptive stress response to aggregate imbalance and cell death induction might uncover new targets for the treatment of diseases caused by proteins that misfold in the ER, like RP-linked Rh.

2.4 Imbalanced ERAD and human disease

Conformational disorders are often due to mutations which cause protein folding defects. Some diseases are known to be caused by mutations that lead to protein degradation and therefore to protein loss-of-function (LOF). For example, folding-deficient V2 vasopressin receptors are retained in the early secretory pathway and subject to VCP- and Derlin1-mediated ERAD, thereby causing X-linked nephrogenic *diabetes insipidus* (Schwieger et al., 2008). Other diseases are caused by mutations in proteins that lead to abnormal protein retention in the ER (or accumulation in the cytosol) and acquire toxic GOF properties. For example, α -synuclein accumulation is cytotoxic and its expression in yeast causes ER stress and inhibits the ER-Golgi vesicular trafficking (Cooper et al., 2006). A transmembrane protein like Rh might lose its membrane localization when mutated (especially class II Rh mutations), and thus fails to exert its normal function. Mutated Rh can also acquire new properties, like abnormal retention in the ER, the capacity to aggregate or to inhibit the proteasome (GOF effects). It is therefore important to distinguish between these possibilities and to determine the exact molecular and cellular mechanisms of proteostasis defects caused by each type of mutation.

B. The ERAD effector VCP: biochemistry, genetics, pathology

2.5 VCP structure and cofactors

The chaperone VCP is a member of the type II AAA (ATPases associated with a variety of activities) ATPases (Dreveny et al., 2004). It is best known for its activity that promotes ERAD of misfolded proteins, but VCP also performs many other functions in eukaryotic cells, including membrane fusion, cell cycle regulation and transcriptional control (Wang et al., 2004).

VCP is a ubiquitous and highly conserved protein. VCP homologues are found in archaeabacteria (VCP-like ATPase of *Thermoplasma acidophilum* [VAT]), yeast (cell division cycle 48 [Cdc48]), *Caenorhabditis elegans* (C41C4.8 and C06A1.1), *Drosophila melanogaster* (transitional elements of the ER 94 [Ter94], where 94 denotes the apparent molecular weight), *Xenopus laevis* (p97) and mammals (VCP) (Wang et al., 2004). VCP was first characterized in *Saccharomyces cerevisiae*, in a genetic screen for mutants that cause cell cycle arrest and it was named cell division cycle protein 48 (Cdc48) (Moir et al., 1982). The mammalian homolog of Cdc48 was first characterized as a 97 kDa precursor protein for valosin, a small peptide isolated from pig intestine and was named valosin-containing protein (VCP) (Koller and Brownstein, 1987). Later on, it was showed that valosin is an artifact of purification and has nothing in common with the identified 97 kDa protein. However, the name VCP is still widely used in the literature.

VCP is one of the most highly evolutionarily conserved proteins. A 69 % sequence identity was found between yeast Cdc48 and human VCP. VCP is also one of the most abundant proteins in cells and represents approximately 1 % of the cytosolic proteins (Wang et al., 2004). It is ubiquitously expressed in all eukaryotic cells and is mainly localized in the cytosol, but an important fraction of the protein is also associated with ER and Golgi membranes (Latterich et al., 1995; Rabouille et al., 1995); VCP expression was also detected in the nucleus (Madeo et al., 1998).

Structure of VCP and its domains. VCP is characterized by the presence of two conserved ATPase domains, also named AAA domains (Lupas and Martin, 2002). Human VCP consists of 806 amino acids and can be divided into N-terminal (1-187), D1 (209-460), D2 (481-761), and C-terminal (762-806) domains, with the N-D1 linker (188-208) and D1-D2 linker (461-480) joining the respective domains (see Figure 12). The D1 and D2 ATPase domains comprise the conserved AAA motifs Walker A, Walker B and the second region of homology (SRH). Similar to other AAA proteins, VCP catalyzes ATP hydrolysis to generate energy and uses most of this energy to perform mechanical work in cells (Wang et al., 2004).

VCP forms a barrel-like, stable homo-hexameric structure that comprises two ring-shaped layers made of the respective D1 and D2 AAA modules (Zhang et al., 2000; Figure 12). The two-layer VCP structure has a central channel running through the entire span of the hexamer. The D1 and D2 rings have similar shapes and are positioned above each other in a head-to-tail manner (Huyton et al., 2003). The N-terminal domain, important for cofactor binding, resides at the periphery of the D1 ring, is oriented towards the exterior of the hexamer and is flexible in most nucleotide states except during ATP hydrolysis. VCP was found to undergo conformational changes during its nucleotide hydrolysis cycle (Wang et al., 2004).

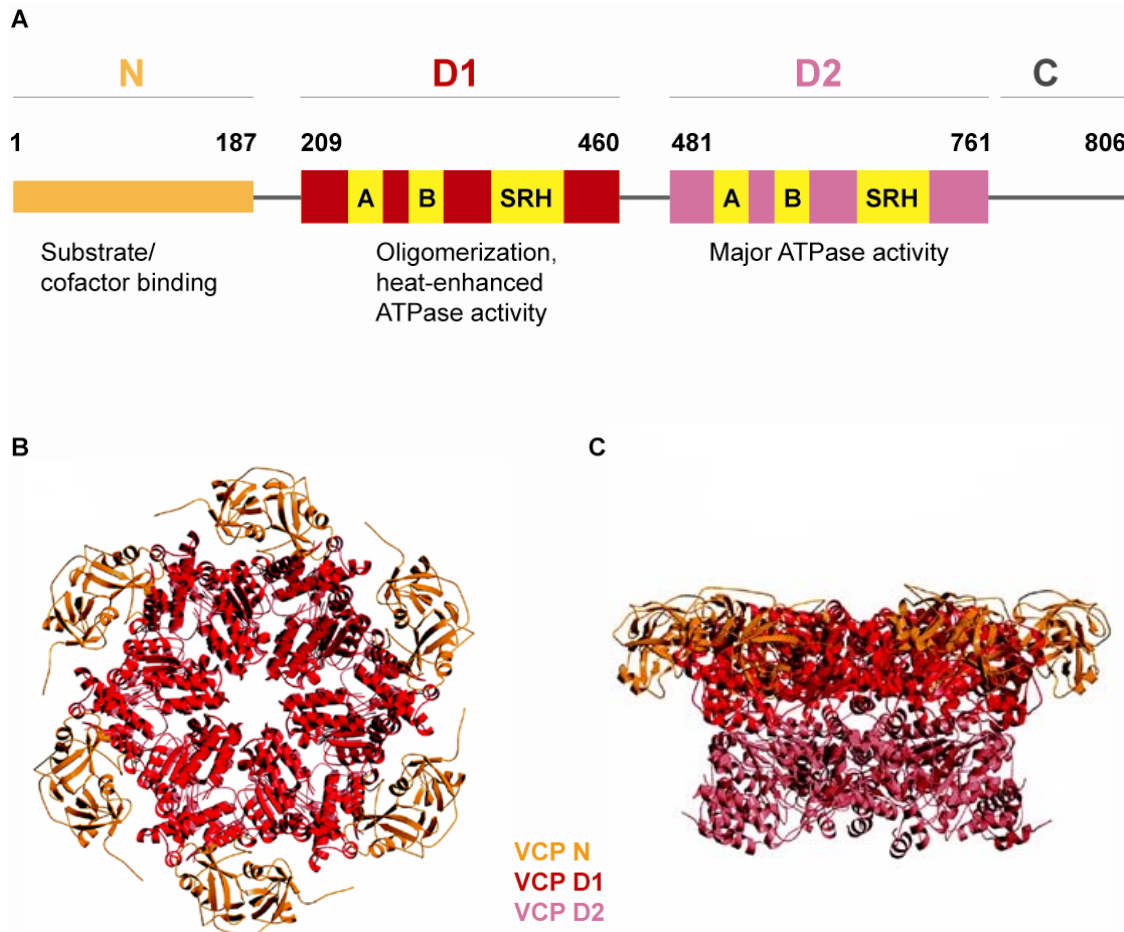


Figure 12. VCP structure. (A) VCP domain structure. VCP consists of four domains, the N-terminal domain, the ATPase domains D1 and D2, both characterized by Walker A, Walker B and the ‘second region of homology’ (SRH) motifs, and the C-terminal domain. (B, C) Crystal structure of VCP. Ribbon representation of full-length murine VCP is shown in top (B) and side view (C). VCP forms stable barrel-like, homo-hexameric that comprises two ring-shaped layers made of the D1 and D2 AAA modules aligned above each other in a head-to-tail manner. A central pore runs through the entire span of the hexamer. The six N domains are sticking out at positions ~30° from the apex of the D1 and D2 domains. Adapted from Dreveny et al. (2004).

The N-terminal domain of VCP is involved in binding to cofactors and substrates of VCP and is crucial for target specificity. The N domain has been shown to bind to almost all adaptors of VCP, except for the ubiquitin fusion degradation protein 2 and 3 (Ufd2 and Ufd3) (Ye, 2006). The N domain is also required for binding to polyubiquitinated target proteins, thus mediating VCP functions in ubiquitin-proteasome pathway (Dai and Li, 2001).

The D1 ATPase domain was shown to be the major domain responsible for VCP oligomerization (Wang et al., 2003; Zhang et al., 2000). VCP is exceptionally stable in hexameric form and its oligomerization in hexamer is required for its ATPase and biological activities (Wang et al., 2003). The D1 domain seems to display a marked ATPase activity only under elevated temperatures (Song et al., 2003) and might have aggregation-preventing activity *in vitro* (Song et al., 2007).

The major ATPase activity of VCP has been assigned to the D2 domain (Song et al., 2003). Overexpression of VCP^{K524A}, a dominant-negative VCP variant that is ATPase deficient, in cultured cells induced ER-derived large vacuolization followed by ER stress

Introduction

and cell death, demonstrating that the ATPase activity of VCP is essential for cell survival (Hirabayashi et al., 2001; Kobayashi et al., 2002). It was also shown that the Arg586 and Arg599 amino acid residues of the D2 domain are essential for substrate interaction during ERAD (DeLaBarre et al., 2006), suggesting that substrate binding might take place not only at the N-terminal, but also at the D2 domain of VCP.

The C-terminal domain of VCP binds the cofactors Ufd2 and Ufd3 and a specific characteristic of this domain is the presence of a stretch of Tyr phosphorylation sites. Tyr phosphorylation of VCP might regulate VCP activity during ERAD (Li et al., 2008; Zhao et al., 2007).

VCP cofactors and adaptors. A large number of VCP-associated cofactors have been identified to date. Four groups of VCP cofactors can be distinguished: major substrate-recruiting cofactors, additional substrate-recruiting cofactors, substrate-processing cofactors and miscellaneous interactors. The major and additional substrate-recruiting cofactors direct VCP to different cellular pathways. Substrate-processing adaptors accelerate and/or regulate the fate of substrates after recruitment, by exerting additional enzymatic activities. Miscellaneous interactors are believed to regulate VCP activity by other mechanisms (Schuberth and Buchberger, 2008).

The major substrate-recruiting cofactors lead to the separation of fundamentally distinct cellular functions of VCP. The VCP-p47 and VCP-p37 complexes control the fusion of homotypic membranes, while the cofactors Ufd1 and Npl4 direct VCP towards Ub-dependent protein degradation and ERAD. p47 and the Ufd1–Npl4 complex bind to VCP in a mutually exclusive manner, thus directing VCP to a specific cellular pathway (Meyer et al., 2002).

Additional substrate-recruiting cofactors often join major substrate-recruiting cofactors and contribute to a better regulation of VCP in a specific cellular pathway. For example, the ER membrane proteins Erasin and stress-activated protein kinases substrate-1 (SAKS1) act as additional recruitment factors of VCP-Ufd1-Npl4 during ERAD. VIMP and Derlin proteins also recruit VCP to the ER membrane and improve the efficiency of substrate turnover (Schuberth and Buchberger, 2008).

2.6 VCP is a major ERAD effector

VCP is required for retrotranslocation of ERAD substrates. VCP was first found to be required for the degradation of an unstable substrate containing an amino-terminal ubiquitin fusion (Ghislain et al., 1996). Later, it was shown that VCP interacts with Ufd1, Ufd2 and Ufd3, suggesting that it is a central component of the Ub fusion degradation pathway (Meyer et al., 2000). The activity of VCP as ERAD effector is one of the best understood aspects of VCP biology.

During ERAD, retrotranslocation is initiated when a segment of a substrate is inserted into the retrotranslocation channel. The extraction of most polypeptides into the cytosol requires both polyubiquitination (Flierman et al., 2003) and the function of the VCP–Ufd1–Npl4 complex (Meyer et al., 2002; Ye et al., 2001). A dual recognition model was suggested, in which the VCP complex first joins the retrotranslocation complex containing an unfolded substrate emerging from the ER lumen. Then VCP itself binds to a non-ubiquitinated polypeptide segment of the substrate. Once Ub moieties are attached to

the substrate by E3 ligases, the poly-Ub conjugates can be recognized by both VCP and Ufd1-Npl4 and the substrate can be extracted into the cytosol (Ye et al., 2003).

Interfering with the recognition of poly-Ub chains by the VCP complex leads to inhibition of substrate retrotranslocation (Flierman et al., 2003). Retrotranslocation of a substrate is also inhibited by expression of mutant VCP lacking ATPase activity. Mutations of Lys524, Arg586, Arg599 and Phe552 residues in the D2 domain lead to loss of ATPase activity and subsequently to impaired ERAD (DeLaBarre et al., 2006; Kobayashi et al., 2002). Since abolishing polyubiquitination leads to a similar defect to that caused by ATPase-deficient VCP, it was suggested that Ub binding to the VCP complex may activate VCP ATPase activity, leading to the dislocation of substrates into the cytosol (Ye, 2006).

Regulation of VCP activity during ERAD. VCP function during ERAD is regulated by several mechanisms, including: Tyr phosphorylation; Akt phosphorylation on Ser residues; and by an endogenous regulator small VCP-interacting protein (SVIP). Tyr phosphorylation of VCP was shown to modulate its activity during ERAD. Phosphorylation of VCP on Tyr805 suppresses VCP binding to PNGase and Ufd3 (Zhao et al., 2007) and causes accumulation of the ERAD substrate TCR α -GFP and ubiquitin-conjugated substrates (Li et al., 2008). Akt-mediated phosphorylation of VCP on Ser352, Ser746 and Ser748 regulates its interaction with ubiquitinated substrates. VCP phosphorylation on these residues releases it from ubiquitinated substrate proteins and allows the substrates to be degraded by the proteasome (Klein et al., 2005). Besides the interaction with the Ufd1-Npl4 complex, VCP was also shown to participate in ERAD by binding to the E3 ligase gp78 (Ballar et al., 2006). SVIP might be a negative regulator of VCP/ERAD by interfering with the formation of the gp78-VCP-Derlin1 complex, thereby inhibiting ERAD (Ballar et al., 2007).

A pharmacologic way to manipulate VCP function was developed by Fiebiger and colleagues who identified two large, hydrophobic, and structurally related ERAD inhibitors: Eeyarestatin I and II (EerI/II) (Fiebiger et al., 2004). A recent work shows that EerI associates with the VCP complex and seems to negatively influence the deubiquitinating process that is mediated by VCP-associated DUB enzymes (such as Ataxin-3) (Wang et al., 2008).

2.7 ERAD-independent functions of VCP

VCP is an essential gene in unicellular and multicellular organisms and VCP total gene disruption is lethal (Leon and McKearin, 1999; Muller et al., 2007). Numerous studies have revealed that VCP is involved in different cellular functions. Besides ERAD, VCP participates in cell cycle regulation by mediating the degradation of cell cycle regulators such as cyclin E (Dai and Li, 2001); VCP is involved in transcriptional control by targeting I κ B α , an inhibitory factor of NF κ B, to proteasome degradation (Dai et al., 1998); it also regulates membrane fusion by interacting with p47 (Wang et al., 2004; Ye, 2006). It appears that, although different, these diverse cellular functions all share the capacity of VCP to interact with either mono-Ub or poly-Ub substrates. VCP itself contains a Ub-binding site in its N-terminal domain and binds preferentially to poly-Ub conjugates, although with low affinity (Dai and Li, 2001; Ye et al., 2003). Adaptors of VCP also contain Ub-binding sites that enhance the affinity of the VCP complex to poly-Ub chains (e.g. Ufd1) (Ye et al., 2003) or to monoubiquitinated substrates (e.g. p47) (Meyer et al., 2002).

2.8 VCP and human disease

VCP was shown to be implicated in the pathogenesis of human diseases linked to protein aggregation such as inclusion body myopathy (IBM) associated with Paget disease of bone (PDB) and frontotemporal dementia (FTD) (IBMPFD) (Kimonis et al., 2008; Watts et al., 2004) and several types of neurodegenerative diseases (Mizuno et al., 2003).

Mutant VCP and the pathogenesis of IBMPFD. IBMPFD is a progressive autosomal dominant disorder that is caused by point mutations in the *VCP* gene (Kimonis and Watts, 2005). Patients suffering of IBMPFD display adult-onset myopathy, early onset of PDB (characterized by abnormal rates of bone growth) and premature FTD (Kimonis et al., 2008). Ten point mutations were identified in the *VCP* gene and most of them cluster in the N-domain responsible for cofactor binding and substrate specificity. Arg155 is the most common amino acid affected (e.g. R155H and R155C) (Watts et al., 2004). In IBMPFD patients, VCP co-localizes with protein aggregates in affected muscle fibers (Watts et al., 2004) and is present in neuronal nuclear inclusions consisting of ubiquitinated protein aggregates (Schroder et al., 2005). The mechanism of IBMPFD pathogenesis is unknown and therefore, animal models expressing mutant VCP were generated. Skeletal muscle-restricted expression of *VCP*^{R155H} in mice recapitulates many of the features seen in IBMPFD muscle, such as ubiquitinated inclusions and progressive muscle weakness (Weihl et al., 2007). A recent study shows that these mice also display impaired autophagy characterized by accumulation of non-degradative autophagosomes and failure to degrade aggregated proteins (Ju et al., 2009). *VCP*^{R155H} and *VCP*^{A232E} were also ubiquitously expressed in mice and it was shown that these mice exhibit progressive muscle weakness, accumulation of TAR DNA-binding protein 43 (TDP-43) in the muscle and in the brain, and severe defects of the skeleton, thus recapitulating the spectrum of disease in humans with IBMPFD (Custer et al., 2010). However, it is still not clear whether the IBMPFD pathology is a direct consequence of VCP/ERAD impairment (Weihl et al., 2006), of autophagy impairment, of the imbalance between VCP and HDAC6 which promotes aggresome formation (Ju et al., 2008), or if a combination of these defects leads to disease.

Wild-type VCP and protein aggregation disorders. Formation of protein aggregates, intranuclear or cytoplasmic inclusion bodies and extracellular plaques are characteristic for human neurodegenerative disorders such as AD, PD and HD (Lansbury and Lashuel, 2006). Interestingly, wild-type VCP was found to co-localize and interact with protein aggregates in patients with neurodegenerative disease. It co-localizes with Ataxin-3 and ubiquitin in neuronal nuclear inclusions in spinocerebellar ataxia type 3 patients (Boeddrich et al., 2006). VCP also forms complexes with TDP-43, in both control and AD patients (Gitcho et al., 2009). Moreover, VCP co-localizes with ubiquitin-positive inclusions in patients with Creutzfeldt–Jakob disease, AD and PD (Mizuno et al., 2003), raising the possibility that VCP plays an important role in aggregate clearance in different neuronal populations. Thus, VCP was proposed to be a sensor for aggregated proteins associated with human degenerative disorders.

HD and Machado–Joseph disease are both neurodegenerative disorders characterized by the expansion of polyglutamine stretches (ex-polyQ). Ex-polyQ lead to aggregate formation and VCP was found to be an ex-polyQ interacting protein *in vitro* and *in vivo* (Hirabayashi et al., 2001). The role of VCP in fibrillogenesis caused by Ataxin-3 containing an ex-polyQ tract was addressed *in vitro* and in *Drosophila* (Boeddrich et al., 2006). It was shown that VCP suppresses the fibrillogenesis of pathogenic forms of

Ataxin-3 and leads to suppression of Ataxin-3-induced neurodegeneration (Boeddrich et al., 2006). However, the role of VCP in neuron cell loss induced by polyglutamine aggregation still remains elusive. The *Drosophila* homologue of *VCP* (*Ter94*) might act as a cell death effector in the pathology caused by ex-polyQ aggregation (Higashiyama et al., 2002).

2.9 Fine control of VCP/ERAD activity is required to avoid pathology

Improper VCP/ERAD functioning is associated with several pathologies. For example, excessive degradation of misfolded ΔF508-CFTR, which is less prone to aggregation, is deleterious for airway epithelial cell function. *In vitro*, decreasing VCP activity allows some of the mutant CFTR to escape ERQC and reach the plasma membrane, leading to a partial rescue of Cl⁻ efflux mediated by CFTR (Vij et al., 2006). On the other hand, mutant proteins like Huntingtin, Ataxin-3 or TDP-43 are extremely prone to aggregation and cause neurodegeneration (Orr and Zoghbi, 2007). It was shown that neuron-like PC12 cells expressing polyQ-expanded Huntingtin fragments display a drastic impairment of ERAD caused mainly by the entrapment of VCP, Ufd1 and Npl4 by ex-polyQ (Duennwald and Lindquist, 2008). VCP was also found to co-localize and interact with Ataxin-3, TDP-43 and ubiquitin-positive aggregates in patients with neurodegenerative disease (Boeddrich et al., 2006; Gitcho et al., 2009; Mizuno et al., 2003), raising the possibility that VCP and ERAD impairment might have broad pathological consequences.

For diseases caused by excessive protein degradation (such as cystic fibrosis), VCP activity should be decreased to suppress pathology (Vij et al., 2006). In contrast, methods to enhance ATPase activity or unfoldase function of VCP can be developed as a therapeutic approach in disorders characterized by protein aggregates. For example, VCP overexpression was shown to suppress mutant Ataxin-3-induced neurodegeneration by preventing the accumulation of large Ataxin-3 inclusion bodies (Boeddrich et al., 2006).

2.10 Disturbed quality control and ER stress as a cause for *retinitis pigmentosa*?

Although mutations in the visual pigment Rh are the major cause of photoreceptor loss and blindness in RP, the pathological mechanisms linking misfolded Rh to cell death are poorly understood (Kennan et al., 2005). Class II mutant Rh^{P23H} forms insoluble aggregates in the ER, induces ER stress (Galy et al., 2005; Lin et al., 2007) and impairs the proteasome (Illing et al., 2002). These observations suggest that misfolded Rh might induce cell death via a toxic GOF effect. However, since mutant Rh might recruit the endogenous Rh into aggregates, lack of functional Rh from the plasma membrane (DN effect) might lead to disease as well. Thus, it is still unclear what causes cell death in Rh^{P23H}-linked RP. The identification of molecular and cellular pathways responsible for Rh quality control and Rh homeostasis will help define the role of misfolded Rh in RP.

2.11 Aims of the study

Dominant mutations in the visual pigment Rh are the most common genetic defects in autosomal dominant RP. This thesis investigates the pathogenic mechanisms mediated by mutant Rh^{P23H} , the most common Rh mutation associated with autosomal dominant RP in North America. Although misfolded Rh^{P23H} was found to accumulate in the ER and to be degraded by the proteasome, the mechanisms linking Rh^{P23H} misfolding and degradation to photoreceptor neuron degeneration in RP remained elusive.

The ATP-dependent chaperone VCP is part of a highly specialized cellular system responsible for protein quality control in the ER. Proteins that fail to fold properly are cleared during a process called ER-associated degradation (ERAD). VCP has a central role during ERAD, as it extracts misfolded proteins from the ER (a process called retrotranslocation) and delivers them to the proteasome for degradation. Mounting evidence suggests that VCP participates in the quality control of aggregation-prone proteins, including those that cause neurodegeneration (e.g. Alzheimer's or Parkinson's diseases). A role for VCP in RP has thus far not been described.

The major aim of the present work was to determine the relevance of VCP to the cellular pathology induced by misfolded Rh^{P23H} . To achieve this, genetic, biochemical, pharmacological, behavioural and electrophysiological studies were conducted, using cellular and *Drosophila* models of Rh^{P23H} -induced toxicity.

The objectives of this thesis were the following:

1. To assess whether misfolded Rh^{P23H} is a substrate of the ERAD effector VCP *in vitro* and *in vivo*.
2. To evaluate whether VCP interacts with misfolded Rh^{P23H} *in vitro* and to characterize the structural and functional aspects of this interaction
3. To investigate the interaction between mutant $Rh1^{P37H}$ and endogenous $Rh1^{WT}$ in *Drosophila* photoreceptor neurons.
4. To determine whether the genetic inactivation of *VCP* mitigates the $Rh1^{P37H}$ -mediated retinal pathology and visual processing defects in *Drosophila* photoreceptor neurons.
5. To investigate the consequences of *VCP* inactivation on $Rh1^{P37H}$ aggregate dynamics and the activation of the Unfolded Protein Response in *Drosophila* photoreceptor neurons.
6. To determine whether pharmacological inhibition of the VCP/ERAD/proteasome axis suppresses the retinal pathology induced by misfolded $Rh1^{P37H}$ in *Drosophila* photoreceptor neurons.

II. RESULTS

Results

Part one: Clearance of Rh^{P23H} aggregates requires the ERAD effector VCP

A single amino acid substitution (Pro23His) in the visual pigment Rhodopsin is sufficient to cause massive retinal degeneration and blindness in *retinitis pigmentosa*. The P23H mutation is the most common Rh mutation associated with ADRP in North America (Mendes et al., 2005). Unlike the wild-type Rh, misfolded Rh^{P23H} forms aggregates within the ER and is subsequently degraded by the proteasome (Illing et al., 2002; Saliba et al., 2002). The mechanisms linking Rh^{P23H} aggregate formation/clearance to photoreceptor neuron degeneration remain elusive.

Given the fact that mutant Rh^{P23H} accumulates in the ER, we hypothesized that it might be a substrate of the ERAD machinery, whose function is to clear misfolded proteins from the ER. We focused our study on the ERAD effector VCP, the driving force for the extraction of misfolded proteins from the ER and delivery to the proteasome (Ye et al., 2001).

In a first set of experiments (Part one) performed in cellular models for *retinitis pigmentosa*, I found that VCP is required and sufficient to promote clearance of Rh^{P23H} aggregates. VCP co-localizes and interacts with misfolded Rh^{P23H} in retinal cells and requires functional N-terminal and D1 ATPase domains to form a complex with Rh^{P23H} aggregates. Furthermore, VCP uses its D2 ATPase activity to promote Rh^{P23H} aggregate retrotranslocation and proteasomal delivery.

In a second set of experiments (Part two), I used *Drosophila* genetics and found that genetic inactivation of *VCP/ter94* suppresses the Rh1-induced retinal pathology. In flies expressing mutant Rh1^{P37H} (the equivalent of mammalian Rh^{P23H}), I found that the endogenous WT Rh1 is recruited into Rh1^{P37H} aggregates and is required for Rh1^{P37H} toxicity. Genetic inactivation of *VCP* in *Rh1^{P37H}* flies increased the level of Rh1-containing aggregates and further activated the Ire1/Xbp1 UPR pathway. Despite this, *Rh1^{P37H}* flies with decreased *VCP* function displayed a dramatic suppression of retinal degeneration and blindness (assessed with histology, behaviour and electrophysiology assays). Pharmacological treatment of *Rh1^{P37H}* flies with the VCP/ERAD inhibitor EerI or with the proteasome inhibitor MG132 also led to a potent suppression of retinal degeneration. In summary, excessive retrotranslocation and/or proteasomal degradation of visual pigment might cause RP.

Taken together, these experiments suggest that inhibition of the VCP/ERAD/proteasome axis might prevent vision loss in RP patients carrying Rh^{P23H} mutations.

1.1 VCP co-localizes with misfolded Rh^{P23H} *in vitro*

It remained unclear how misfolded Rh is able to trigger the death of PNs. The fact that misfolded Rh^{P23H} accumulated in the ER and was subsequently degraded by the proteasome (Illing et al., 2002; Saliba et al., 2002) suggested to us that misfolded Rh might be a substrate of the ERAD machinery. In this set of experiments, I determined whether misfolded Rh^{P23H} interacts with the ERAD effector VCP.

To see whether misfolded Rh is a substrate of the ERAD effector VCP, I manipulated Rh aggregate formation and VCP function in different cell lines. For this purpose, I employed

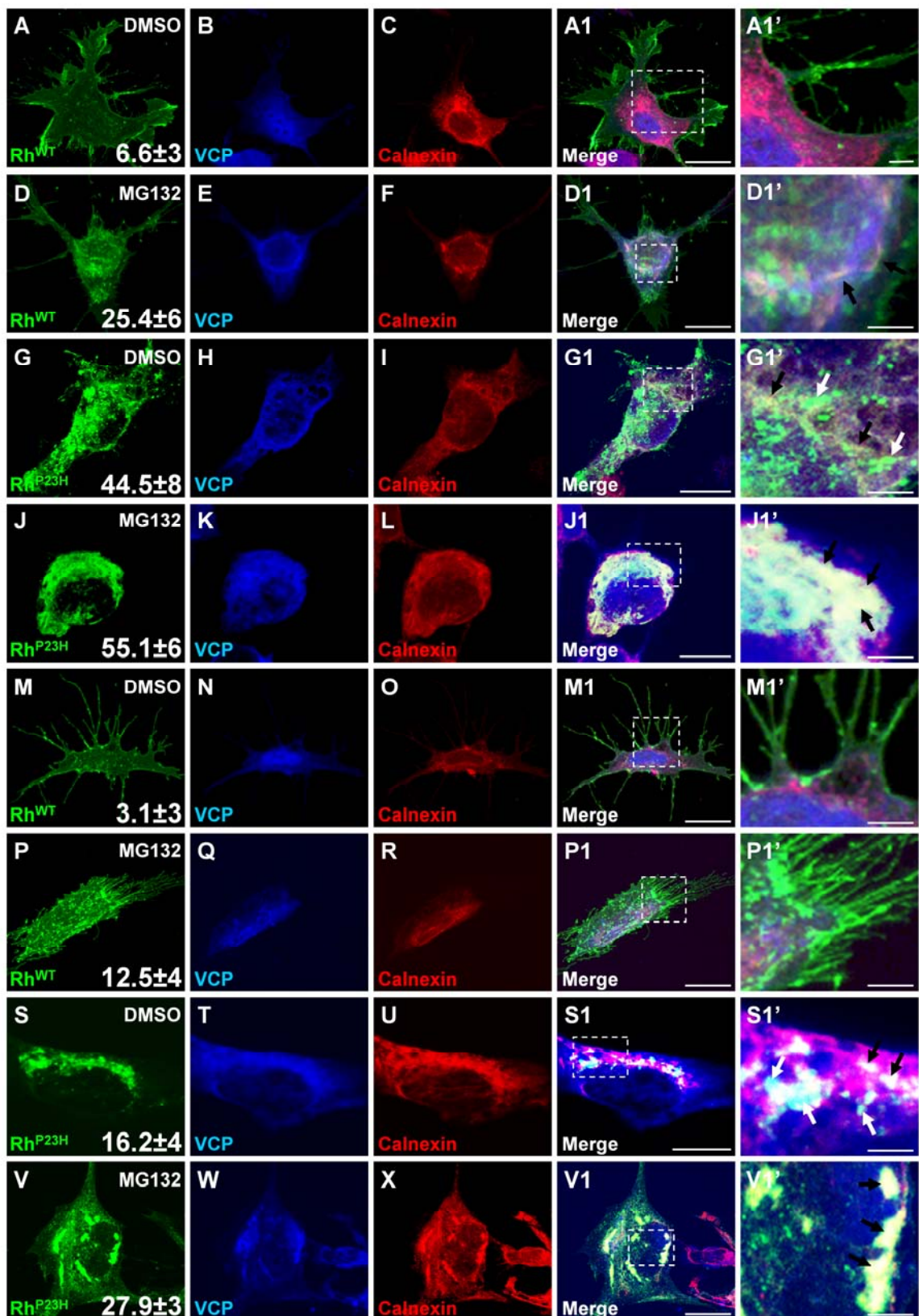
Results

three cellular models: HEK293 cells, human SK-N-SH neuroblastoma cells and 661 mouse retinal cells. HEK293 cells are easy to culture, are characterized by high transfection efficiency (80 %) and allow a very good study of large cell populations required for biochemistry purposes. SK-N-SH human neuroblastoma cells are more difficult to culture, are characterized by low transfection efficiency (15 %), but resemble PNs more closely. They have been used extensively as a model for other protein aggregation diseases, including polyglutamine expansions (Westhoff et al., 2005) and have been established as an appropriate cell model for identifying and characterizing new modulators of Rh^{P23H} processing and aggregation (Chapple and Cheetham, 2003; Mendes and Cheetham, 2008). 661W cells are an immortalized mouse cell line derived from transgenic mice expressing the SV40 T antigen under the control of the human interphotoreceptor retinol-binding protein promoter. They express mostly cone photoreceptor markers, display a neuronal shape and protrusion formation, and show the highest resemblance to PNs (Tan et al., 2004). 661W retinal cells have been successfully used for studies of Rh^{P23H} aggregation (Surgucheva et al., 2005); however, although they are easy to culture, they have very low transfection efficiency (10 %).

Using immunofluorescence labeling, I first determined the subcellular localization of Rh-containing aggregates and of endogenous VCP in cultured cells. I transfected mouse retinal 661W or human neuroblastoma SK-N-SH cells with plasmids encoding either Rh^{WT} or mutant Rh^{P23H}, tagged with GFP. I used a VCP-specific antibody (Gitcho et al., 2009) to label the endogenous VCP (in blue) and a Calnexin-specific antibody to highlight the ER (in red; Figure 13).

In 661W and SK-N-SH cells treated with DMSO as control, I found that Rh^{WT} was correctly targeted to the plasma membrane (Figure 13A,M), although some Rh^{WT}-containing aggregates were also detected, probably as a result of overexpression, in agreement with previous studies (Illing et al., 2002; Saliba et al., 2002). In contrast, Rh^{P23H} formed many cytoplasmic aggregates (Figure 13G,S). To follow Rh aggregation in a more quantitative way, I quantified the average signal intensity corresponding to these cytoplasmic Rh-containing aggregates (values indicated in column 1) in at least 15 cells per condition. The maximum signal intensity of the nucleus (devoid of aggregates) was subtracted from these aggregate intensity values, to correct for background effects. I found a significant increase in signal intensity in cells expressing Rh^{P23H} vs. Rh^{WT} (661W cells: Rh^{P23H} vs. Rh^{WT} p<0.001; SK-N-SH cells Rh^{P23H} vs. Rh^{WT} p<0.01, Student's t-test).

Figure 13. VCP co-localizes with aggregated Rh in mouse retinal 661W and SK-N-SH cells. Immunofluorescence pictures revealing localization of transfected Rh-GFP (green, first column), endogenous VCP (blue, second column) and the ER marker Calnexin (red, third column) in mouse retinal 661W (A-L,A1,A1'-J1,J1') or SK-N-SH cells (M-X,M1,M1'-V1,V1') treated with either DMSO (rows 1,3,5,7) or the proteasome inhibitor MG132 dissolved in DMSO (rows 2,4,6,8). Co-localization is revealed in merged pictures (fourth column) while higher magnification of insets from merged pictures is shown in column 5. The average intensity of the green signal within the cytoplasm is a measure of Rh aggregates and is indicated in the first column. Rh^{WT} is mainly localized at the plasma membrane in 661W cells (row 1). Proteasome inhibition leads to accumulation of Rh^{WT} aggregates within the cytoplasm (row 2); Rh^{WT}-containing ER aggregates co-localize with VCP (black arrows in D1'). Mutant Rh^{P23H} accumulates in the ER (black arrows in G1') and the cytosol (white arrows in the G1') and partially co-localizes with VCP in the ER (G1,G1'). Proteasome inhibition increases the pool of Rh^{P23H} aggregates within the ER (J-L,J1) and the co-localization between Rh^{P23H} and VCP (J1', black arrows). In SK-N-SH cells, Rh^{WT} localizes to the plasma membrane (row 5), while proteasome inhibition increases the pool of cytoplasmic Rh^{WT} aggregates (row 6). Rh^{P23H} localizes to the ER (S1', black arrows) and outside of the ER (S1', white arrows), while proteasome inhibition increases the pool of Rh^{P23H} aggregates within the ER (V1', black arrows). Scale bar in A1-V1 is 20 μm and in A1'-V1' is 5 μm.



Results

The Rh^{P23H}-containing aggregates partially co-localized with the ER marker Calnexin and with VCP (Figure 13G1,S1 and black arrows in Figure 13G1',S1'). Some of these Rh^{P23H}-containing cytoplasmic aggregates were not found within the ER (Figure 13G1,S1 and white arrows in Figure 13G1',S1'), suggesting that they were extracted from the ER and delivered to the cytosol, probably during their processing for ERAD. While the localization of endogenous VCP was mainly nuclear in both cell types transfected with Rh^{WT} (Figure 13B,N), VCP was localized to the ER in cells expressing mutant Rh^{P23H} (Figure 13H,T). In additional control experiments, I determined that transfection with a plasmid encoding only GFP did not lead to aggregate formation and that under these conditions, VCP expression remained nuclear (data not shown). Thus, mutant Rh forms aggregates in the ER and partially co-localizes with endogenous VCP.

Proteasome inhibition increases the retention of Rh^{P23H} aggregates within the ER, suggesting that the proteasome is required for the efficient retrotranslocation of the misfolded Rh (Saliba et al., 2002). To determine whether Rh-containing aggregates are degraded by the proteasome and whether proteasome inactivation leads to increased co-localization between VCP and misfolded Rh, I used the proteasomal inhibitor MG132 to inhibit this degradation pathway in 661W or SK-N-SH cells. I treated transfected cells with the proteasome inhibitor MG132 dissolved in DMSO, or with DMSO only. Inhibition of the proteasome significantly increased the load of cytoplasmic Rh-containing aggregates (Figure 13: D vs. A, J vs. G, P vs. M and V vs. S); the quantification of average signal intensity corresponding to these cytoplasmic Rh-containing aggregates also confirmed a significant increase in Rh aggregate load after proteasomal inhibition (661W cells: Rh^{WT} vs. Rh^{WT}+MG132 p<0.001; Rh^{P23H} vs. Rh^{P23H}+MG132 p<0.05; SK-N-SH cells : Rh^{WT} vs. Rh^{WT}+MG132 p<0.05; Rh^{P23H} vs. Rh^{P23H}+MG132 p<0.01; Student's t-test; at least 15 cells were used/condition). The levels of both Rh^{WT}- and Rh^{P23H}-containing aggregates increased, suggesting that both Rh^{WT} and Rh^{P23H} were degraded by the proteasome. Proteasomal inhibition led to the accumulation of Rh^{P23H}-containing aggregates within the ER (Figure 13J1',V1', black arrows) and interestingly, the co-localization between these aggregates and the endogenous VCP increased (Figure 13J1,J1',V1,V1'). Taken together, these results suggest that expression of Rh^{P23H} leads to the formation of cytoplasmic aggregates that are substrate of the proteasome and that partial co-localization between Rh^{P23H} aggregates and endogenous VCP is substantially enhanced after proteasome inhibition.

1.2 VCP forms a complex with Rh aggregates

The observation that misfolded Rh was degraded by the proteasome raises the possibility that misfolded Rh is a substrate of the ERAD machinery, the cellular system responsible for the extraction of misfolded proteins from the ER and their delivery to the proteasome. Given the co-localization between Rh^{P23H} aggregates and the ERAD chaperone VCP, we asked whether aggregated Rh^{P23H} and VCP are found in a complex. To this aim, I performed immunoprecipitation (IP) experiments in HEK293 cells.

I transfected cells with either Rh^{WT} or Rh^{P23H}, and found that Rh^{P23H}, in contrast to Rh^{WT} led to the formation of HMW aggregates, the major species migrating at >170 kDa. (Figure 14A). I then immunoprecipitated the endogenous VCP from these cells and tested for presence of Rh using a Rh-specific antibody (Saliba et al., 2002). The analysis revealed that Rh^{P23H} aggregates formed a complex with VCP; VCP also interacted with Rh^{WT} aggregates, which displayed reduced levels compared to Rh^{P23H}. Although Rh^{WT} at

endogenous levels does not form aggregates *in vivo*, aggregates have been reported as a result of overexpression in cell culture systems (Illing et al., 2002).

No interaction between Rh monomers and VCP was seen, suggesting that only misfolded and oligomeric Rh is a substrate of VCP. I found VCP to interact with other non-Rh containing aggregates (Figure 14A), suggesting that VCP has a broader role in aggregate recognition that extends beyond misfolded Rh, and in agreement with former studies (Boeddrich et al., 2006; Gitcho et al., 2009; Mizuno et al., 2003). Another possibility is that VCP itself might be ubiquitinated. No signal was detected when the anti-VCP antibody was replaced with Immunoglobulin G (IgG) (negative control; Figure 14A). Thus, endogenous VCP forms a complex with Rh-containing aggregates.

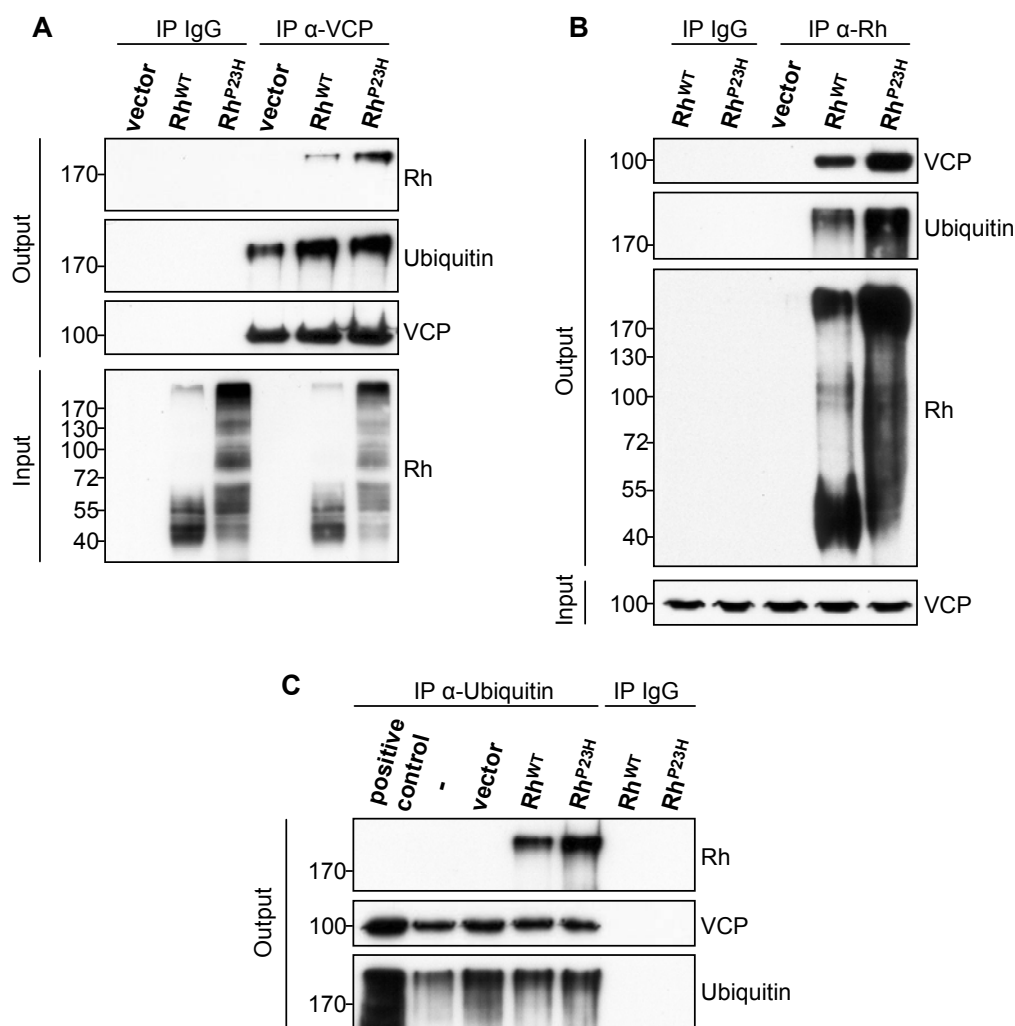


Figure 14. VCP forms a complex with Rh aggregates in vitro. HEK293 cells were transfected with Rh^{WT} or Rh^{P23H} and endogenous VCP (A) or total Rh (B) or ubiquitin (C) were immunoprecipitated with anti-VCP (A) or anti-Rh (B) antibody, or with polyubiquitin-affinity resin, while Immunoglobulin G (IgG) was used as negative control (A,B,C). The immunoprecipitates were analyzed by WB for (A) Rh (output, upper panel), ubiquitin (output, middle panel) and VCP (output, lower panel) or for (B) VCP (output, upper panel), ubiquitin (output, middle panel) and Rh (output, lower panel), or for (C) Rh (output, upper panel), VCP (output, middle panel) and ubiquitin (output, lower panel). The presence of Rh (A) or VCP (B) was revealed in input lysates (Input). Rh^{P23H} and Rh^{WT} aggregates form a complex with VCP, while no interaction between VCP and Rh monomers was observed (A). (C) Both Rh^{WT} and Rh^{P23H} aggregates are polyubiquitinated and there is accumulation of Rh^{P23H} compared to Rh^{WT}. VCP is found in a complex with polyubiquitinated proteins and a very strong ubiquitin signal is observed for the polyubiquitin positive control provided by the manufacturer.

Results

I then performed the reverse experiment and transfected HEK293 cells with either Rh^{WT} or Rh^{P23H}, after which I precipitated Rh aggregates with a Rh antibody and assessed for the presence of VCP (Figure 14B). Similarly, I found that both WT and mutant Rh aggregates form a complex with VCP, although more aggregates were formed when Rh^{P23H} was transfected. I then used an ubiquitin-specific antibody to label polyubiquitinated proteins. I found that the Rh aggregates are polyubiquitinated, and as expected, I detected a stronger signal for Rh^{P23H} than Rh^{WT} aggregates (Figure 14B). This raises the possibility that the interaction between VCP and polyubiquitinated Rh aggregates might promote their proteasomal delivery.

Given that VCP is found in a complex with polyubiquitinated aggregates, I performed an independent set of experiments in which I transfected cells with either Rh^{WT} or Rh^{P23H} and then pulled down polyubiquitinated proteins using a polyubiquitin affinity resin. I found similarly, that polyubiquitinated aggregates, including Rh aggregates, interact with VCP (Figure 14C), in line with the results from Figure 14A. Taken together, these experiments indicate that VCP forms a complex with polyubiquitinated Rh^{P23H} aggregates, probably during their processing by the ERAD machinery.

1.3 Proteasome inactivation enhances the interaction between VCP and misfolded Rh

The observation that the co-localization between VCP and Rh^{P23H}-containing aggregates is enhanced upon proteasome inhibition (Figure 13) suggested to us that the interaction between endogenous VCP and Rh^{P23H}-containing aggregates might be enhanced after proteasome inhibition. To test this possibility, I assessed the interaction between Rh aggregates and VCP after inhibition of the proteasome with MG132.

I overexpressed Rh^{WT} or Rh^{P23H} in HEK293 cells and treated the cells with MG132 dissolved in DMSO or with DMSO as control, after which I precipitated Rh aggregates with a Rh-specific antibody and tested for the presence of endogenous VCP (Figure 15A). I found that both Rh^{WT} and Rh^{P23H} aggregates form a complex with VCP, and that more VCP is co-immunoprecipitated with Rh^{P23H}-containing aggregates after proteasome inhibition. I then used a ubiquitin-specific antibody that labels polyubiquitinated proteins and found that these Rh aggregates are polyubiquitinated; moreover, Rh^{P23H} aggregates showed increased polyubiquitination relative to Rh^{WT} aggregates (Figure 15A), in line with the results from Figure 14. I also determined the levels of VCP, ubiquitin and Rh in input lysates and found that proteasome inhibition leads to accumulation of polyubiquitinated Rh aggregates, while VCP levels are not affected by proteasome inactivation (Figure 15B). Proteasome inhibition led to a significant accumulation of Rh^{P23H}-containing aggregates and to a slight accumulation of Rh^{WT}-containing aggregates (Figure 15B), in line with our immunofluorescence results shown in Figure 13. Taken together, these results further suggest that endogenous VCP forms a complex with the ER-retained misfolded Rh^{P23H} and the interaction is substantially increased after proteasome inhibition.

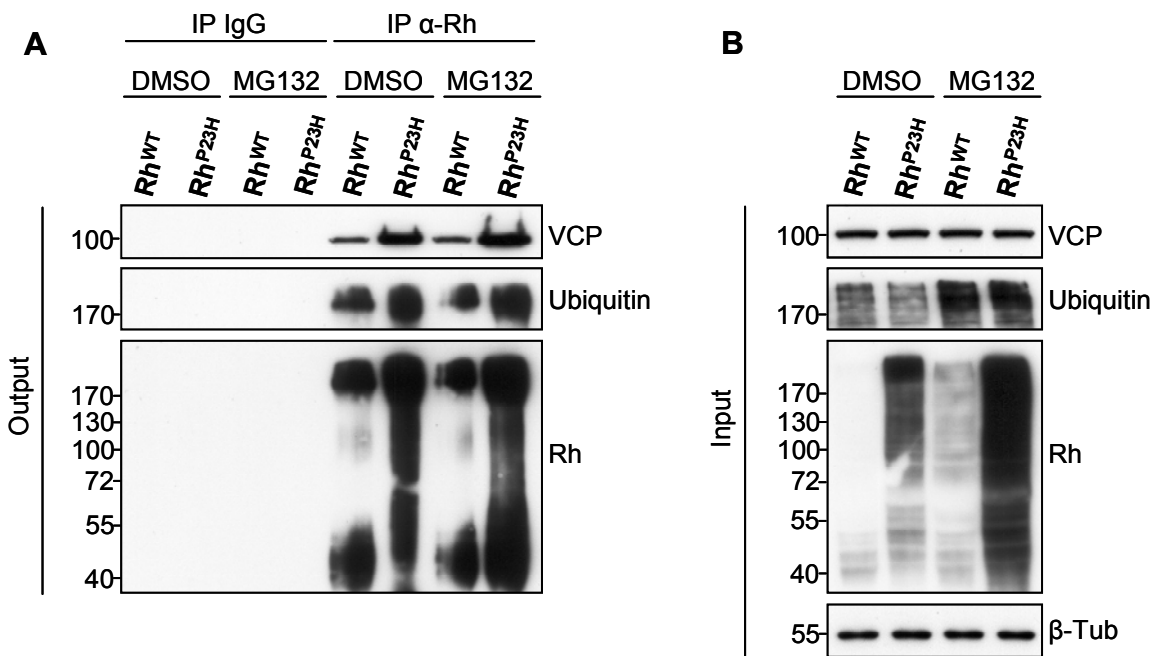


Figure 15. The interaction between VCP and Rh aggregates is enhanced after proteasome inhibition. (A,B) HEK293 cells were transfected with Rh^{WT} or Rh^{P23H} and 32h after transfection were treated with MG132 or with DMSO as control. (A) Rh was immunoprecipitated with anti-Rh antibody, while Immunoglobulin G (IgG) was used as negative control. The immunoprecipitates were analyzed by WB for VCP (output, upper panel), ubiquitin (output, middle panel) or Rh (output, lower panel). Rh^{P23H} and Rh^{WT} aggregates form a complex with VCP and formation of the complex between VCP and Rh^{P23H}-containing aggregates is enhanced after proteasome inhibition. (B) The presence of VCP, ubiquitin and Rh was revealed in input lysates (Input). Proteasome inhibition leads to formation of ubiquitin and Rh aggregates, while VCP levels remain constant. β-Tubulin (β-Tub) served as loading control.

1.4 VCP interaction with misfolded Rh requires its ND1 domains

Given that endogenous VCP forms a complex with Rh^{P23H}-containing aggregates, I next analyzed the structural requirements of VCP for its interaction with aggregated Rh. I generated several Flag-tagged constructs for full length (FL) VCP and deletion constructs representing domains of VCP: N-terminal, D1, D2, ND1, ND2 and D1D2 (Figure 16A). To determine which domains of VCP mediate the interaction with Rh aggregates, I performed IP experiments in HEK293 cells transfected with these tagged constructs and with Rh^{P23H}. As expected, FL VCP formed a complex with Rh^{P23H} aggregates. The individual N and D2 domains were dispensable for the interaction between VCP and Rh^{P23H} aggregates, while D1 and D1D2 domains displayed weaker binding, showing that the D1 domain of VCP is necessary for interaction with aggregates (Figure 16B). Furthermore, the ND1 domain displayed the same binding efficacy as the FL VCP suggesting that the presence of both D1 and N-terminal domains of VCP is required for maximal binding of VCP to Rh^{P23H} aggregates. To rule out that the lack of interaction between VCP deletion constructs and Rh^{P23H} was caused by the absence of these truncated proteins from the ER, I determined their subcellular localization in cultured HEK293 cells using immunofluorescence. I found that all FL and truncated VCP forms (in green) show extensive co-localization with the DsRed-ER tracker (in red), indicating that they localized to the ER (Figure 16C). Thus, all VCP deletion constructs localize to the ER and the lack of interaction between N-terminal or D2 ATPase domains with Rh^{P23H} aggregates is not due to their absence from the ER.

Results

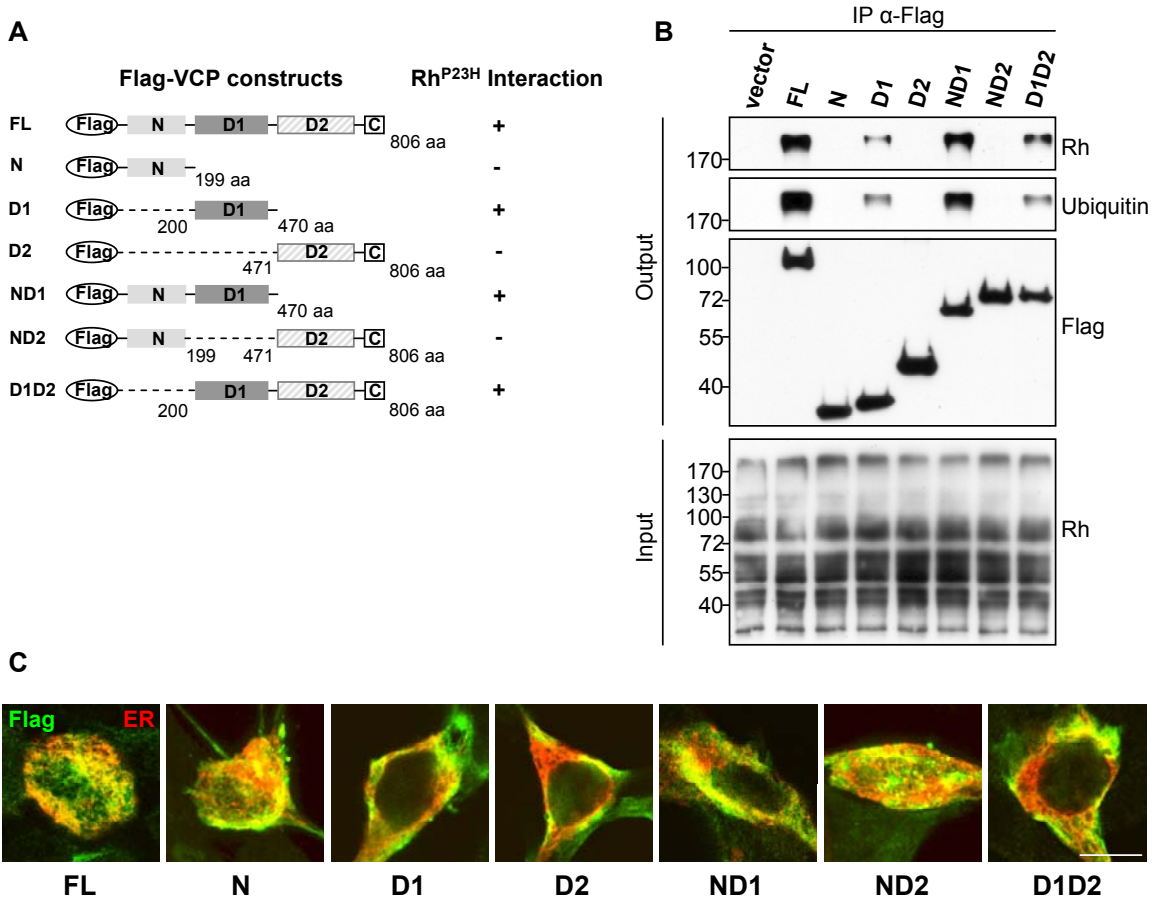


Figure 16. The D1 domain of VCP is required for interaction with Rh^{P23H} aggregates. (A) Schematic representation of Flag-VCP fusion proteins and summary of binding results with Rh^{P23H} aggregates. (B) Flag pull-down experiments in HEK293 cells using an anti-Flag antibody. Bound Rh^{P23H} aggregates were detected using Rh (output, upper panel) or ubiquitin (output, middle panel) antibodies. Flag antibody was used to detect immobilized Flag bait proteins (output, lower panel). Full-length VCP (FL) was found in a complex with Rh^{P23H} aggregates. Weaker binding was seen for the D1 and D1D2 domains, while the ND1 domain displayed the same binding efficacy as the FL VCP. The N and D2 domains of VCP are dispensable for its interaction with Rh^{P23H} aggregates. (C) HEK293 cells were transfected with the indicated Flag-VCP fusion constructs (detected with anti-Flag antibody, green) and with DsRed-ER tracker (red), and the localization of the Flag signal and the ER tracker is shown in merged pictures. The different Flag-VCP fusion constructs localize mainly within the ER. Scale bar is 20 μ m.

These experiments suggest that the D1 ATPase and N-terminal domains of VCP are required for optimal interaction between VCP and Rh^{P23H}-containing aggregates. Because the D1 domain regulates the hexamerization of VCP, which is required for proper functioning during ERAD (Wang et al., 2003) and the N-terminal domain binds the aggregate-recruiting complex Ufd1-Npl4 (Ye et al., 2003), it appears that both a proper higher-order structure and proper interaction with adaptor complexes are needed for VCP to recognize its substrates during ERAD.

1.5 VCP is required for degradation of misfolded Rh

The finding that misfolded Rh^{P23H} co-localizes and forms a complex with VCP led us to hypothesize that misfolded Rh^{P23H} is a substrate of VCP during ERAD. To test this hypothesis, I modified VCP levels *in vitro* and evaluated the consequences of altered VCP levels on the clearance of misfolded Rh. To determine whether VCP is required for degradation of misfolded Rh^{P23H}, I knocked down VCP function in HEK293 cells expressing mutant Rh^{P23H} (Figure 17A). I used a previously published VCP siRNA (Ballar

et al., 2007) and a nonsense sequence as negative control and found that cells treated with VCP siRNA, but not negative control, displayed a strong reduction of VCP protein levels (Figure 17A). 40 hours after knock-down, I added cycloheximide (CHX) to suppress *de novo* protein synthesis and analyzed the samples collected at various time points. Knock-down of VCP led to the accumulation of HMW Rh-containing oligomers and aggregates, indicating that VCP activity is required for degradation of Rh^{P23H} aggregates. I reached similar conclusions when VCP function was decreased in cells overexpressing Rh^{WT} (data not shown). Thus, VCP is required for degradation of misfolded Rh^{P23H}.

I then investigated whether VCP activity is sufficient to promote degradation of Rh^{P23H} aggregates (Figure 17B). For this purpose, I transfected cells with Rh^{P23H} and with increasing amounts of VCP plasmid. I found that these cells displayed a dose-dependent reduction of Rh^{P23H} aggregates, suggesting that VCP activity is sufficient to promote clearance of misfolded Rh.

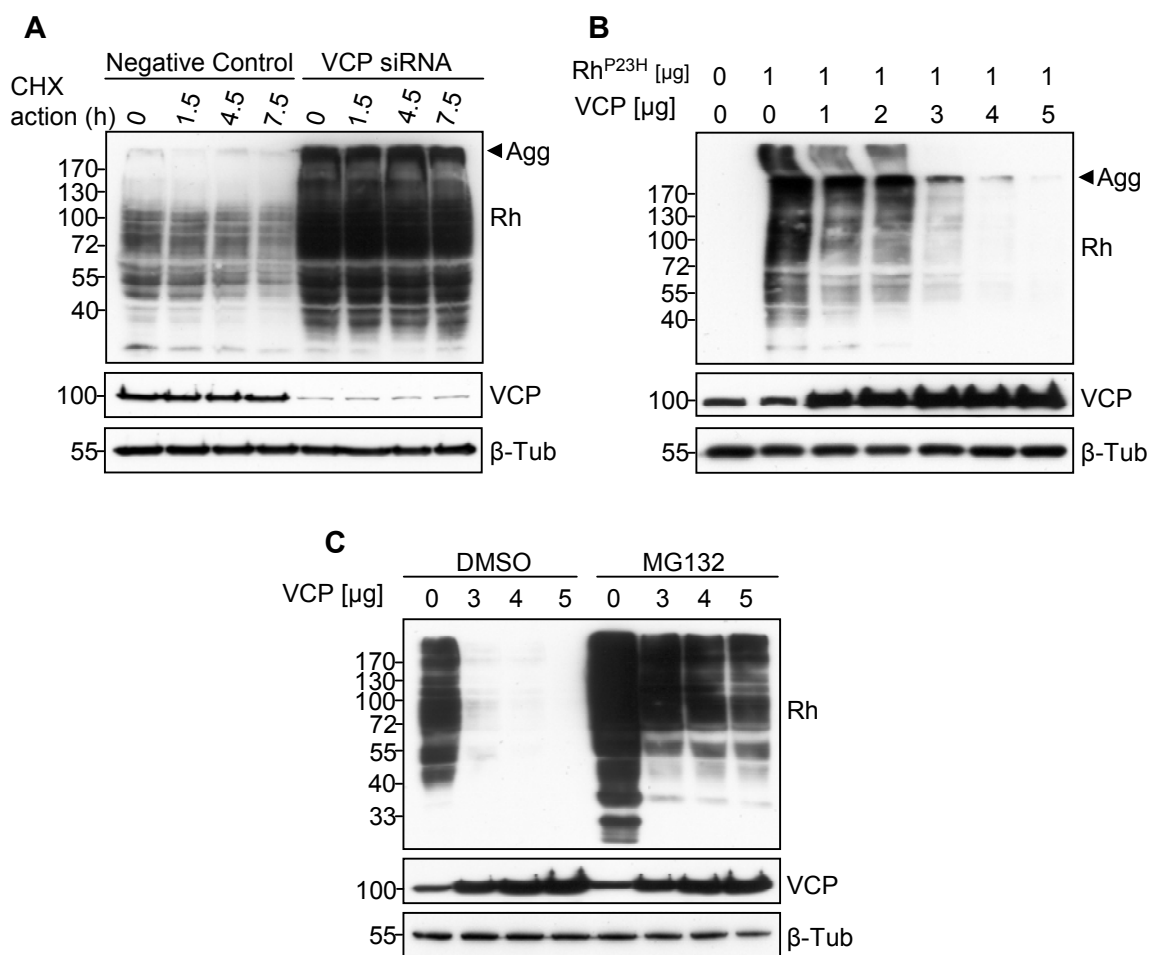


Figure 17. VCP is required for degradation of Rh aggregates *in vitro*. (A,B) HEK293 cells were transfected with Rh^{P23H} together with either VCP or control siRNA (A), or with increasing amounts of VCP^{WT} construct (B). (A) Cell lysates were collected after different durations of cycloheximide (CHX) treatment and probed for Rh. siRNA of VCP strongly decreases degradation of Rh^{P23H}, and high molecular weight (HMW) Rh aggregates are formed. (B) Dose-dependent mediated degradation of Rh^{P23H} aggregates by VCP. Increasing VCP levels (revealed by VCP antibody, middle panel) leads to a decrease in Rh^{P23H} aggregates (upper panel). (C) VCP-mediated degradation of Rh^{P23H} requires a functional proteasome. HEK293 cells were co-transfected with Rh^{P23H} and with increasing amounts of VCP^{WT} followed by treatment with the proteasome inhibitor MG132 (or with DMSO as control). Proteasome inhibition severely impairs degradation of Rh aggregates. Rh HMW aggregates (Agg, arrowhead) are indicated. β-Tubulin (β-Tub) served as loading control.

Results

We then asked whether Rh aggregates are degraded by the proteasome and whether VCP-mediated degradation of misfolded Rh requires the proteasome. I used the proteasome-specific inhibitor MG132 that I added to cells transfected with the mutant Rh^{P23H} and with increasing amounts of VCP plasmid. Proteasomal inhibition severely impaired the VCP-mediated degradation of Rh^{P23H} aggregates, and led to a massive accumulation of Rh^{P23H} oligomers and HMW aggregates (Figure 17C), indicating that degradation of Rh^{P23H} aggregates requires the proteasome; this result is in line with the previous results (Figures 13 and 15), in which proteasome inhibition led to the accumulation of both Rh^{WT} and Rh^{P23H} aggregates and to enhanced interaction between misfolded Rh^{P23H} and VCP. Taken together, these results suggest that VCP is both required and sufficient to promote the degradation of misfolded Rh, in a proteasome-dependent manner.

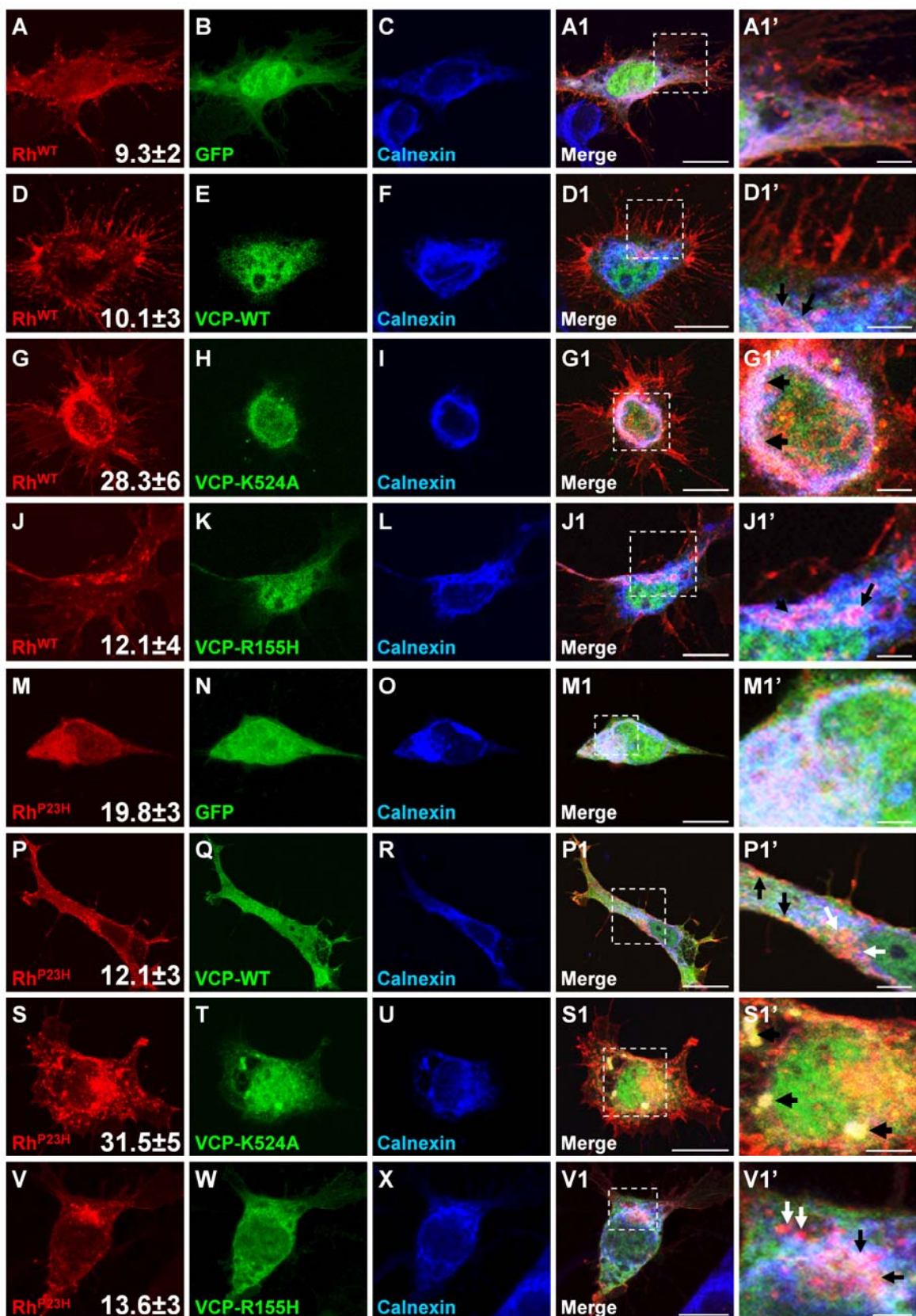
1.6 D2 ATPase activity of VCP is required for degradation of misfolded Rh

Previous studies suggested that VCP uses ATP hydrolysis (via its D2 ATPase domain) to promote substrate retrotranslocation from the ER to the cytosol and delivery to the proteasome (Song et al., 2003; DeLaBarre et al., 2006). The K524A mutation in the D2 domain of VCP was shown to abolish the ATPase activity associated with this domain and to induce accumulation of misfolded ΔF508-CFTR (Kobayashi et al., 2002), whereas the R155H mutation in the N-terminal domain of VCP did not impair the ATPase activity (Weihl et al., 2006).

To test whether degradation of Rh aggregates requires the D2 ATPase activity of VCP, I transfected mouse retinal 661W cells with either Rh^{WT} or Rh^{P23H} plasmids and with GFP or GFP-tagged plasmids encoding WT, K524A or R155H mutant VCP. I used a Rh-specific antibody (Saliba et al., 2002) to label Rh (in red) and a Calnexin-specific antibody to reveal the ER (in blue).

In cells transfected with Rh^{WT} and with either GFP, VCP^{WT} or VCP^{R155H}, most of the overexpressed Rh^{WT} properly localized at the plasma membrane and few intracellular aggregates were detected (Figure 18 rows 1,2 and 4); the intracellular Rh^{WT} aggregates showed a limited co-localization with VCP^{WT/R155H} (Figure 18D1',J1', black arrows). Interestingly, cells co-transfected with VCP^{K524A} and Rh^{WT} displayed numerous intracellular aggregates that showed an extensive co-localization with the ER and VCP (Figure 18G1,G1', black arrows), suggesting that inhibition of VCP D2 ATPase activity impairs clearance of the Rh^{WT} aggregates, which result from Rh overexpression (Figure 18 row 3).

Figure 18. D2 ATPase activity of VCP is required for clearance of Rh^{P23H} aggregates. Immunofluorescence pictures revealing the localization of overexpressed WT (rows 1-4) or P23H Rh (rows 5-8) in 661W mouse retinal cells transfected with GFP (rows 1,5), or with WT (rows 2,6), D2 domain ATPase K524A mutant (rows 3,7) or N-terminal R155H mutant (rows 4,8) VCP-GFP constructs. Rh was detected with anti-Rh antibody (red, first column), VCP was visualized through GFP (green, second column) and the ER network was revealed using an anti-Calnexin antibody (blue, third column). Co-localization is shown in merged pictures (fourth column) while higher magnification of insets from merged pictures is shown in column 5. The average intensity of the red signal within the cytoplasm is a measure of Rh aggregates and is indicated in the first column. Expression of the VCP^{WT} construct leads to a decreased Rh^{P23H} aggregate load (row 6) compared to cells transfected with Rh^{P23H} and GFP (row 5) and some of the remaining aggregates do not co-localize with the ER marker nor with VCP (P1 and P1', white arrows). Expression of VCP ATPase deficient construct leads to an increase in the amount of cytoplasmic Rh^{WT} (row 3) and Rh^{P23H} (row 7), in contrast to WT and R155H VCP overexpression. All VCP forms co-localized with aggregated Rh^{P23H} (P1,S1,V1), either mainly outside the ER (P1',V1' white arrows) or inside the ER (P1',S1',V1' black arrows). Thus, the D2 ATPase activity of VCP is not required for interaction with Rh^{P23H} but is required for degradation of aggregated Rh. Scale bar is 20 μm (A1-V1) and 5 μm (A1'-V1').



Results

To derive a quantitative estimation of aggregate formation, I quantified the average signal intensity corresponding to intracellular Rh aggregates (in red) in at least 15 cells for each condition (using the signal intensity from the nucleus to correct for background effects) and found a significant increase in aggregate incidence in cells transfected with VCP^{K524A} (column 1, Rh^{WT}+VCP^{K524A} vs. Rh^{WT}+VCP^{WT} p<0.05, Student's t-test). These experiments suggest that the D2 ATPase activity of VCP is required for clearance of Rh^{WT}-containing aggregates, which were probably formed as a result of overexpression.

I then investigated the effect of WT and mutant VCP overexpression on the clearance of misfolded Rh^{P23H}. Retinal cells transfected with Rh^{P23H} and GFP displayed numerous intracellular aggregates (Figure 18M vs. A, Rh^{WT}+GFP vs. Rh^{P23H}+GFP p<0.001) that showed extensive co-localization with the ER (Figure 18 row 5). When VCP^{WT} was co-transfected with Rh^{P23H}, the load of Rh^{P23H} aggregates decreased (Rh^{P23H}+GFP vs. Rh^{P23H}+VCP^{WT} p<0.05) and some of the remaining aggregates did not co-localize with the ER marker nor with VCP (Figure 18P1 and P1', white arrows) suggesting that they were extracted from the ER and accumulated in the cytosol. Co-transfection with Rh^{P23H} and VCP^{R155H} led to a similar situation: less aggregates were detected (Figure 18M,V) and some of these aggregates did not co-localize with the ER marker nor with VCP (Figure 18V1', white arrows), suggesting that they were extracted from the ER. When the ATPase deficient VCP^{K524A} was co-transfected with Rh^{P23H}, the level of intracellular aggregates was significantly increased (Figure 18M,P,S Rh^{P23H}+GFP or Rh^{P23H}+VCP^{WT} vs. Rh^{P23H}+VCP^{K524A} p<0.0001) and these aggregates showed extensive co-localization with the ER marker and VCP^{K524A} (Figure 18S1,S1', black arrows). Thus, inhibition of D2 domain ATPase activity of VCP does not abolish co-localization between VCP^{K524A} and aggregated Rh^{P23H}, but strongly impairs aggregate clearance.

To provide more quantitative evidence for a requirement of VCP ATPase activity during ERAD of misfolded Rh and because of the low transfection efficacy of mouse retinal 661W cells, I performed the same experiments in HEK293 cells (Figure 19). Similarly, I observed that in the presence of VCP^{K524A}, both Rh^{WT} and Rh^{P23H}-expressing cells accumulate Rh aggregates (Figure 19A). In agreement with the data obtained from transfected 661W retinal cells, the presence of the N-terminal mutant VCP^{R155H} had no significant effect on the turnover of Rh aggregates (Figure 19A). I then quantified the average intensity of bands corresponding to Rh oligomers and aggregates (molecular weight [MW]>60 kDa) and found that while VCP^{WT} or VCP^{R155H} overexpression promoted aggregate clearance, transfection with VCP^{K524A} strongly impaired aggregate clearance (Figure 19B). In summary, the D2 domain-associated ATPase activity of VCP is dispensable for interaction with misfolded Rh, yet appears to be specifically required for its proper delivery to the proteasome for degradation.

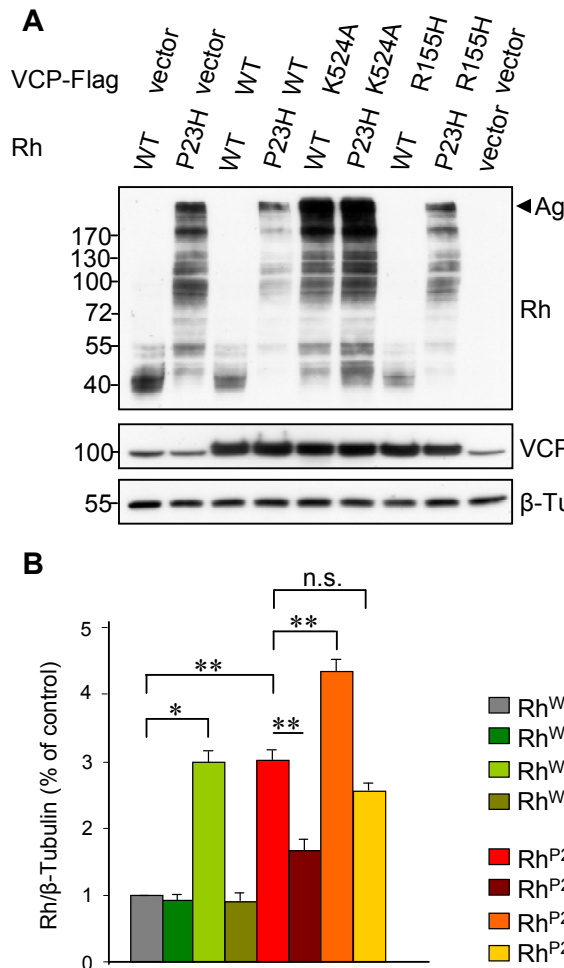


Figure 19. Clearance of misfolded Rh^{P23H} requires the D2 ATPase activity of VCP. (A) Immunoblot revealing the levels of Rh in HEK293 cells transfected with WT or P23H Rh and with WT, K524A or R155H VCP. Transfection with VCP^{WT} leads to increased degradation of Rh^{P23H} aggregates, while VCP^{R155H} has the same potent effect in promoting Rh^{P23H} aggregate clearance. Expression of ATPase-deficient VCP^{K524A} strongly impairs aggregate clearance of both Rh^{WT} and Rh^{P23H}. Rh aggregates (Agg, arrowhead) are indicated. β -Tubulin (β -Tub) served as loading control. (B) Quantification of the level of Rh-containing oligomers and aggregates (MW>60 kDa); the intensity of high molecular weight bands was averaged from three different experiments (* p<0.05 and ** p<0.01 Student's t-test).

1.7 Effect of Rh misfolding and of VCP expression on SK-N-SH cell viability

Given the requirement of VCP in mutant and WT Rh aggregate clearance, we asked whether modulation of VCP function could rescue cells from mutant Rh-induced cell death. For this purpose, I used human neuroblastoma SK-N-SH cells that were previously used to characterize the process of Rh-induced cell death (Mendes and Cheetham, 2008). To determine the toxic effects of manipulating Rh and/or VCP function, I quantified the release of cytoplasmic lactate dehydrogenase (LDH) into the cell culture supernatant. An increased LDH release is indicative of cell dysfunction, as membrane-damaged cells release increased amounts of LDH in the cell culture supernatant (Mendes and Cheetham, 2008).

Decreasing VCP function by expression of ATPase-deficient VCP^{K524A} led to a significant increase in cytotoxicity, while expression of VCP^{WT} or VCP^{R155H} variants had no significant effect on cell viability (Figure 20A). Inactivation of VCP by siRNA also

Results

led to a pronounced decrease in SK-N-SH viability, in contrast to cells transfected with a non-targeting sequence (negative control; Figure 20B). As previous evidence suggests, a decrease of VCP function probably leads to cell dysfunction via both ERAD-dependent (Hirabayashi et al., 2001; Kobayashi et al., 2002) and ERAD-independent (e.g. effects on cell proliferation and strong inhibition of NF κ B activation by FGF-2) mechanisms (Vandermoere et al., 2006; Wojcik et al., 2004).

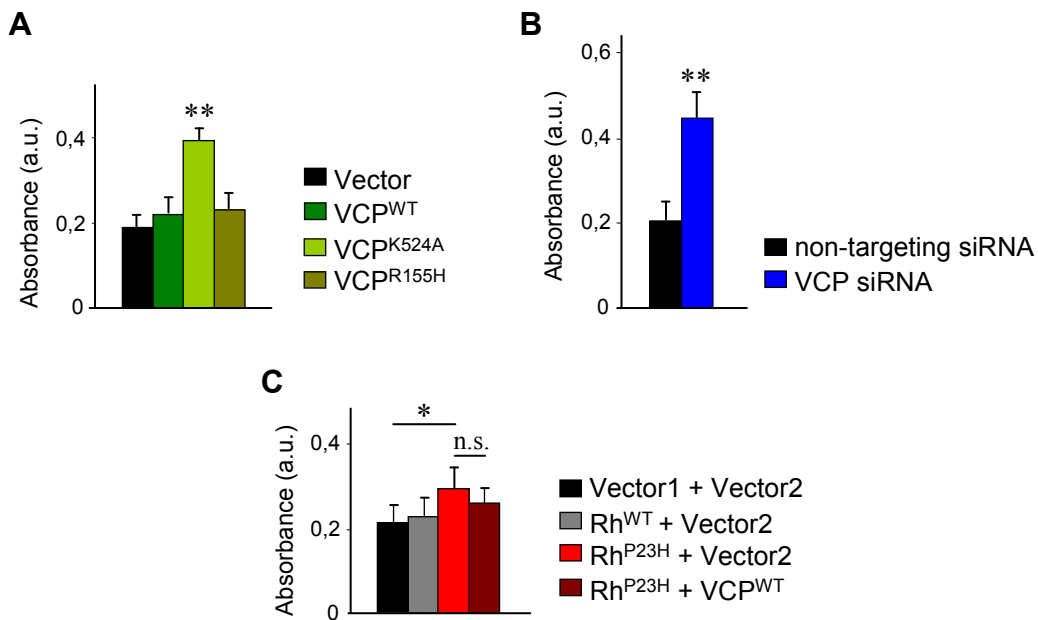


Figure 20. Effect of Rh misfolding and of VCP expression on SK-N-SH cell viability. (A) LDH release was measured in cells transiently expressing empty vector, VCP^{WT}, VCP^{K524A} or VCP^{R155H}. Expression of ATPase-deficient VCP^{K524A}, but not of VCP^{WT/R155H} leads to increased cytotoxicity. (B) Knock-down of VCP 48h after transfection with VCP siRNA leads to significantly increased LDH release compared to cells transfected with non-targeting siRNA. (C) LDH release in cells expressing Rh^{P23H} is significantly increased compared to cells expressing Rh^{WT} or empty vector. Co-expression of VCP^{WT} and Rh^{P23H} leads to a non-significant decrease in cell death compared to cells expressing Rh^{P23H} and empty vector. Absorbance (a direct readout of LDH activity) was expressed in arbitrary units. LDH release was averaged from three independent experiments (* p<0.05 and ** p<0.01 Student's t-test).

When transfecting SK-N-SH cells with either WT or P23H Rh, I observed only a minor decrease in cell viability in the Rh^{P23H} vs. Rh^{WT} case (Figure 20C). These moderate defects prevented me from analyzing the rescuing effects of VCP^{WT} overexpression in this system (Figure 20C). The effect of VCP inactivation on Rh^{P23H}-induced cell dysfunction could also not be assessed because decreasing VCP function induced cell death (Figure 20A,B). Taken together, these results suggest that further improvements of the existent cell-based assays appear to be necessary in order to address the connection between Rh aggregates, VCP function and cell dysfunction *in vitro*.

Part two: Genetic inactivation of VCP suppresses $Rh1^{P37H}$ -induced retinal pathology in *Drosophila*

Our experiments in mammalian cell culture provided important insights into the interaction between misfolded Rh and the ERAD effector VCP. They did not, however, allow us to establish a mechanistic link between misfolded Rh, VCP activity and cell death.

To determine the relevance of VCP function to the retinal pathology triggered by misfolded Rh, we used the fruit fly *Drosophila melanogaster*. *Drosophila* has a long and successful history in *retinitis pigmentosa* studies and has already been used to characterize the pathological events in *Rh*-linked RP (see Introduction). We used a newly established *Drosophila* model of RP, generated in the laboratory of Dr. Angela Giangrande at IGBMC, in Strasbourg-France. In this fly model, $Rh1^{P37H}$ (the equivalent of mammalian Rh^{P23H}) is ectopically expressed in PNs R1-6, under the control of a promoter identical to the endogenous $Rh1$ promoter. $Rh1^{P37H}$ -expressing flies exhibit light- and age-dependent retinal degeneration and progressive blindness, thus providing a very close model of Rh^{P23H} -linked RP (Galy et al., 2005). Another important advantage of this model is the fact that the $Rh1^{P37H}$ transgene bears an hsv tag (which does not modify its properties), thus allowing us to follow the fate of both the ectopic and the endogenous $Rh1$. I used these flies and the corresponding controls ($Rh1^{WT}$ -expressing flies, $Rh1$ -Gal4 and WT flies) to address the role of VCP during the process of retinal dysfunction and retinal degeneration mediated by misfolded $Rh1^{P37H}$. I found that partial *VCP* inactivation led to a dramatic suppression of retinal degeneration and to an almost complete rescue of blindness in $Rh1^{P37H}$ flies, thereby establishing a critical role for VCP in $Rh1$ proteostasis.

2.1 $Rh1^{P37H}$ -mediated degeneration is light- and age-dependent

To confirm that retinal degeneration induced by $Rh1^{P37H}$ in *Drosophila* is light- and age-dependent (Galy et al., 2005), I raised flies overexpressing either $Rh1^{WT}$ (genotype: +/+; $Rh1$ - $Rh1^{WT}$, in short $Rh1^{WT}$) or mutant $Rh1^{P37H}$ (genotype: +/+; $Rh1$ - $Rh1^{P37H}$ /+, in short $Rh1^{P37H}$) in either complete darkness or exposed to moderate and constant illumination, for durations between 1-30 days after birth. Constant illumination was obtained by using photosynthetic fluorescent tubes (see Materials and Methods). After defined durations, I sacrificed the animals and collected their heads. I then sectioned the eyes and highlighted the retinal ultrastructure using toluidine blue as a contrasting agent (see Materials and Methods for details). I found, as previously reported, that both $Rh1^{P37H}$ and $Rh1^{WT}$ flies display no signs of retinal degeneration when reared in the presence of light at postnatal day 1 (P1) or reared in the dark at P30 (Figure 21). The retinas of these flies had an intact ultrastructure, with their ommatidia (hexagonal units) containing all seven visible rhabdomeres (functional equivalents of the rod and cone outer segments; blue dots in Figure 21) and intact cell bodies (in white) surrounding the rhabdomeres. Thus, $Rh1^{P37H}$ flies raised in the dark for 30 days or exposed to light for very short periods do not show signs of retinal degeneration.

Results

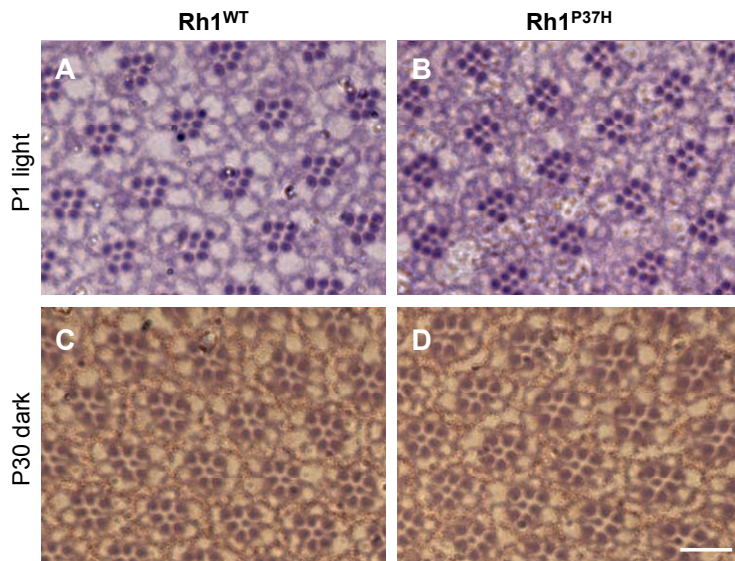
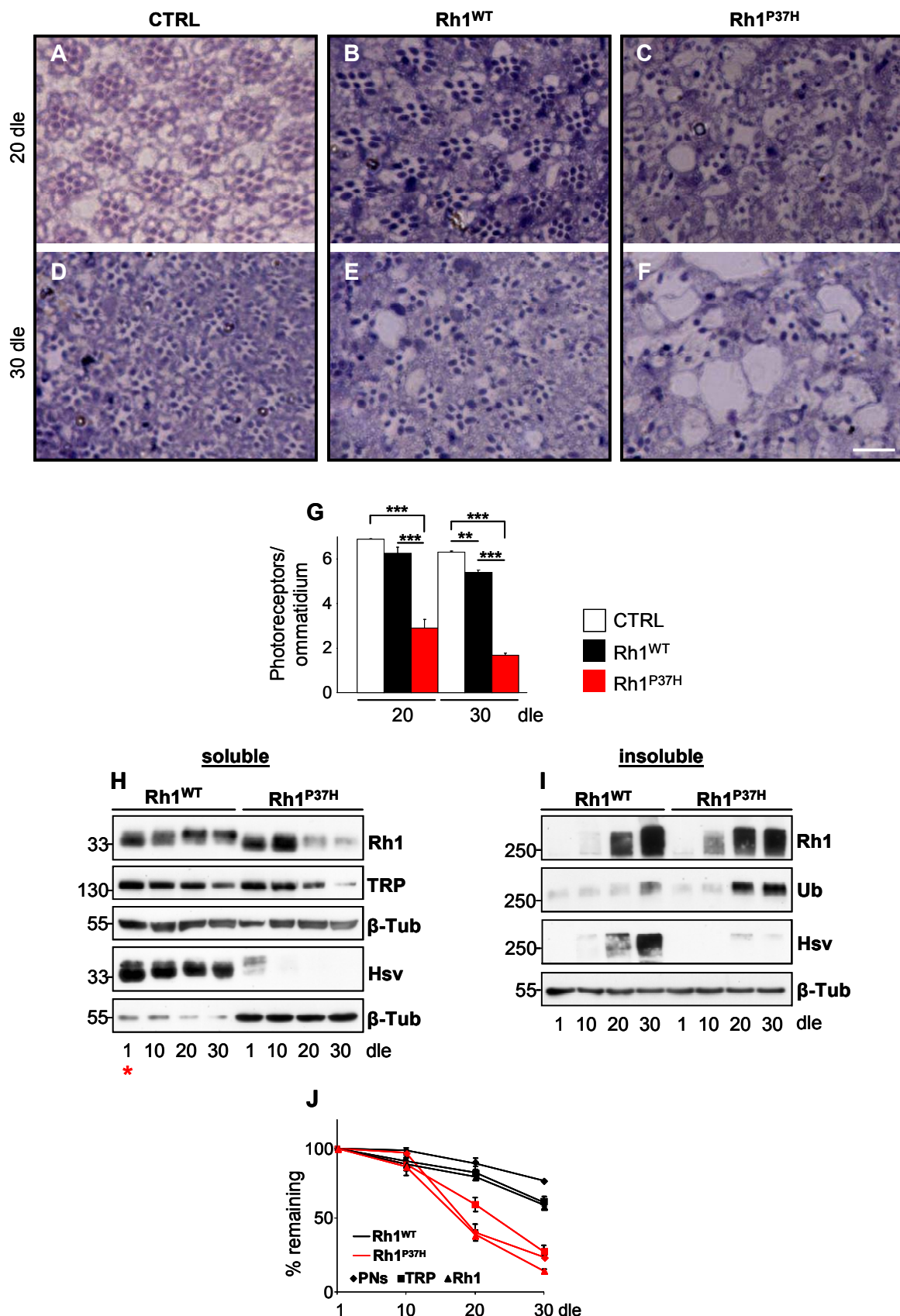


Figure 21. Retinal degeneration in *Rh1*^{P37H} flies is light- and age-dependent. (A-D) Photomicrographs of toluidine blue-stained semithin adult eye sections of *Rh1*^{WT} (A,C) and *Rh1*^{P37H}-overexpressing flies (B,D) reared at light until postnatal day 1 (P1) (A,B) or reared in the dark until P30 (C,D). No signs of retinal degeneration (such as vacuolization or loss of photoreceptor neurons) are observed in *Rh1*^{P37H} flies reared in the dark for long periods of time (up to 30 days) or exposed to light for a short periods. Ommatidia (hexagonal, functional units of the eye) consist of 7 rhabdomeres in the same plane (the R8 photoreceptor is not visible here) and highlighted in blue and their cell bodies are represented in white. Scale bar is 50 μ m.

I then reared the *Rh1*^{P37H} flies and the corresponding controls in constant and moderate light for different durations (up to 30 days). I found that *Rh1*^{P37H} flies, in contrast to *Rh1*^{WT} flies and to control (*Rh1-Gal4*) flies display a dramatic loss of PNs, leading to an overall disruption of the retinal integrity and to pronounced eye vacuolization after 20 and 30 days of light exposure (dle) (Figure 22A-F). Using multiple pictures from several eyes/group, I quantified the average number of photoreceptor neurons found in each ommatidia. After 20 dle, ommatidia from *Rh1*^{P37H} retinas displayed 2.9 photoreceptors left on average, compared to 6.8 in *Rh1*^{WT} and 7.0 in *Rh1-Gal4* flies; after 30 dle, ommatidia from *Rh1*^{P37H} retinas displayed 1.7 photoreceptors on average, compared to 5.5 in *Rh1*^{WT} and 6.5 in *Rh1-Gal4* flies (n>7 eyes/genotype and at least 150 ommatidia were analyzed/eye; ** p<0.01 and *** p<0.001 Student's t-test) (Figure 22G). Photoreceptor R7 remained in many ommatidia intact as it does not express *Rh1*^{P37H}. Thus, *Rh1*^{P37H} induces light- and age-dependent retinal degeneration in *Drosophila* PNs.

Figure 22. Progressive retinal degeneration and Rh1 loss in *Rh1*^{P37H} flies exposed to light. (A-F) Photomicrographs of toluidine blue stained semithin eye sections of control (*Rh1-Gal4*) (A,D), *Rh1*^{WT}- (B,E) and *Rh1*^{P37H}- (C,F) overexpressing flies kept at light for 20 days (A-C) or for 30 days (D-F). Dle: days of light exposure. Scale bar is 50 μ m. (G) Quantification of average number of photoreceptors/ommatidium (P/O) in different mutant groups (n>7 animals in each group, ** p<0.01 and *** p<0.001 Student's t-test). *Rh1*^{P37H} flies display a dramatic loss of P/O after 20 dle. (H,I) Immunoblots revealing the abundance of total (endogenous and ectopic, Rh1 antibody) and ectopic (hsv antibody) Rh1 in detergent-soluble (H) or insoluble (I) fractions obtained from retinas of *Rh1*^{WT} or *Rh1*^{P37H} flies exposed to light for the indicated durations. The rhabdomeric marker TRP was used to independently assess rhabdomere loss (H) while aggregates were independently labeled with a ubiquitin antibody (I). β -Tubulin (β -Tub) served as loading control. * Please note that 5-fold less protein was loaded for *Rh1*^{WT} flies for the hsv WB (H, lanes 1-4; red star). (J) Evolution of mature Rh1 (triangles), TRP levels (squares) and retinal degeneration (P/O; rhombus) in *Rh1*^{WT} and *Rh1*^{P37H} flies exposed to light for increasing durations. Results from 3 independent crosses were averaged.



Results

2.2. Loss of mature Rh1 in $Rh1^{P37H}$ flies

To characterize the temporal evolution of mature and aggregated Rh1 forms in $Rh1^{P37H}$ -overexpressing flies, I collected fly heads and following lysis, I separated them into detergent-soluble and insoluble fractions, containing mature Rh1 and Rh1 aggregates, respectively. To specifically detect the overexpressed protein, I used flies in which ectopically expressed Rh1^{P37H} (or Rh1^{WT}) was hsv-tagged (Galy et al., 2005; Kurada et al., 1998); in the following, all $Rh1^{P37H-hsv}$ and $Rh1^{WT-hsv}$ flies are named $Rh1^{P37H}$ and $Rh1^{WT}$ respectively, unless otherwise stated.

I found a dramatic loss of mature Rh1 (endogenous and ectopic) levels in $Rh1^{P37H}$ but not $Rh1^{WT}$ flies after 20 dle (Figure 22H, Rh1 blot). I used an hsv-specific antibody to label the ectopic protein and found a complete loss of hsv signal in the soluble fraction of $Rh1^{P37H}$ flies after 10 dle, while no loss of mature Rh1 occurred in $Rh1^{WT}$ flies (Figure 22H, hsv blot). These experiments suggest that the mature (endogenous and ectopic) Rh1 is completely lost from $Rh1^{P37H}$ flies after 20 days of light exposure.

To determine whether the loss of mature Rh1 is the cause or the consequence of retinal degeneration in $Rh1^{P37H}$ flies, I compared the evolution of mature (rhabdomeric) Rh1 levels, relative to the rhabdomeric marker transient receptor potential (TRP) (Lee and Montell, 2004) and to PN degeneration in the $Rh1^{P37H}$ retina (Figure 22J; results from 3 independent crosses were averaged). The loss of rhabdomeric marker TRP should provide an independent measure of retinal degeneration. As expected, death of PNs paralleled the decrease in TRP levels, consistent with the rhabdomeres being lost during retinal degeneration; moreover, I found that no loss of mature Rh1 preceded the loss of PNs/TRP (Figure 22J). Therefore, the onset of retinal degeneration in $Rh1^{P37H}$ flies is not caused by loss of mature Rh1; the reverse is true, i.e. loss of mature Rh1 is the result of rhabdomere loss, which takes place during retinal degeneration.

To determine whether the endogenous Rh1 is recruited into Rh1-containing aggregates, I next assessed the situation of insoluble Rh1-containing species and found a significant increase in Rh1 aggregates in both $Rh1^{WT}$ and $Rh1^{P37H}$ flies after 20 dle; I reached similar conclusions using an ubiquitin-specific antibody to label aggregates (Figure 22I). Remarkably, hsv labeling was absent in the insoluble fraction from $Rh1^{P37H}$, but not $Rh1^{WT}$ flies indicating that endogenous Rh1 is the major component of insoluble aggregates in the $Rh1^{P37H}$ retina (Figure 22I). Accumulation of endogenous Rh1 in the insoluble fraction suggests that mutant $Rh1^{P37H}$ recruits its endogenous WT counterpart into aggregates (Colley et al., 1995; Kurada and O'Tousa, 1995; Kurada et al., 1998). Furthermore, given the similar levels of Rh1 aggregates in $Rh1^{WT}$ and $Rh1^{P37H}$ flies, the formation of Rh1 aggregates is probably not a primary cause of retinal degeneration in $Rh1^{P37H}$ flies.

Taken together, these experiments suggest that $Rh1^{P37H}$ flies display light- and age-dependent retinal degeneration, characterized by loss of mature Rh1 (as a result of cell and rhabdomere loss) and recruitment of endogenous Rh1 into insoluble aggregates after long durations of light exposure. The fact that both $Rh1^{WT}$ and $Rh1^{P37H}$ flies display similar levels of Rh1 aggregates after 30 dle, but completely different levels of retinal degeneration, suggests that the presence of these aggregates is not by itself pathogenic.

2.3 Endogenous Rh1 is required for $Rh1^{P37H}$ toxicity

The recruitment of endogenous Rh1 into insoluble aggregates prompted us to investigate the relevance of endogenous Rh1 to the retinal pathology initiated by $Rh1^{P37H}$. To reduce the dosage of the endogenous Rh1 in $Rh1^{P37H}$ flies, I used the *Rh1* null allele *ninaE^{II}* (here called $Rh1^{KO}$). I found, remarkably, that PN degeneration is strongly suppressed in $Rh1^{P37H};Rh1^{KO/+}$ flies (Figure 23A,B). After 20 dle, ommatidia from $Rh1^{P37H}$ retinas displayed 2.8 photoreceptors on average, compared to 5.5 in $Rh1^{P37H};Rh1^{KO/+}$ flies, while after 30 dle, ommatidia from $Rh1^{P37H}$ retinas displayed 1.7 photoreceptors on average, compared to 5.05 in $Rh1^{P37H};Rh1^{KO/+}$ flies ($n>7$ eyes/genotype and at least 150 ommatidia were analyzed/eye; *** $p<0.001$ Student's t-test) (Figure 23C). These results suggest that endogenous Rh1 contributes to $Rh1^{P37H}$ -induced retinal degeneration, probably following recruitment by $Rh1^{P37H}$.

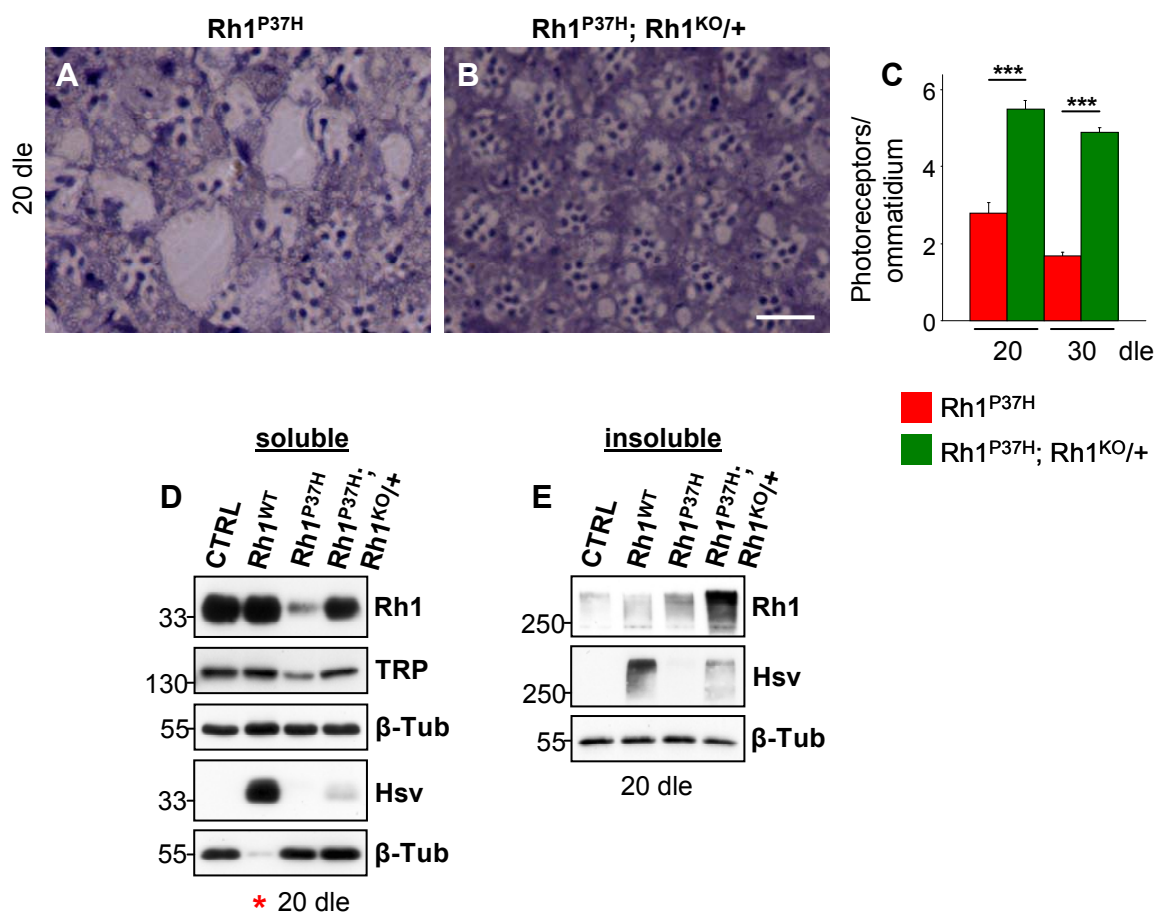


Figure 23. Dominant effects in $Rh1^{P37H}$ flies exposed to light. (A-C) Reducing the dosage of endogenous *Rh1* rescues retinal degeneration in $Rh1^{P37H}$ flies, suggesting that endogenous Rh1 is required for $Rh1^{P37H}$ toxicity. Photomicrographs of toluidine blue sections of $Rh1^{P37H}$ (A) and $Rh1^{P37H};Rh1^{KO/+}$ (B) flies and (C) quantification of the average number of photoreceptors/ommatidium (P/O) ($n>7$ animals/group, *** $p<0.001$ Student's t-test) after 20 and 30 days of light exposure (dle). Scale bar is 50 μ m. (D,E) Immunoblots showing the levels of total and ectopic mature (D) and aggregated Rh1 (E), as well as TRP levels (D) in flies of indicated genotypes, after 20 dle. Loss of mature Rh1 and of TRP is rescued in $Rh1^{P37H};Rh1^{KO/+}$ flies (D). $Rh1^{P37H};Rh1^{KO/+}$ flies display increased endogenous and ectopic Rh1 aggregate levels compared to $Rh1^{P37H}$ flies (E). β -Tubulin (β -Tub) served as loading control. * Please note that 10-fold less protein was loaded for $Rh1^{WT}$ flies for the hsv WB (D; red star).

Results

The observation that retinal degeneration is rescued in $Rh1^{P37H};Rh1^{KO}/+$ raised the possibility that TRP and Rh1 levels might be also restored in these flies. Consistent with the rescue of PN degeneration, I found that the levels of TRP were partially restored in $Rh1^{P37H};Rh1^{KO}/+$ flies (Figure 23D). The level of total mature (Rh1 blot), but not P37H ectopic (hsv blot) Rh1 was partially restored (Figure 23D), indicating that rescue of retinal degeneration in $Rh1^{P37H}$ flies correlates with decreased degradation of endogenous Rh1.

Given the recruitment of the endogenous Rh1 into Rh1-containing insoluble aggregates, we hypothesized that removal of one allele of endogenous Rh1 would lead to less Rh1 insoluble aggregates in $Rh1^{P37H};Rh1^{KO}/+$ flies. To our surprise, increased dosage of the mutant $Rh1^{P37H}$ transgene relative to endogenous $Rh1$ led to an increased level of Rh1 aggregates (that contained a large fraction of endogenous Rh1; Figure 23E, compare Rh1 and hsv blots) in $Rh1^{P37H};Rh1^{KO}/+$ flies. This is probably due to the indirect effect of this manipulation on PN viability, i.e. the increased levels of Rh1-containing aggregates reflect the increased survival of aggregate-containing PNs.

These results suggest that the endogenous Rh1 is required for $Rh1^{P37H}$ toxicity and that reduced clearance of endogenous Rh1 is associated with decreased retinal degeneration in the $Rh1^{P37H}$ retina; moreover, these results raise the possibility that Rh1-containing aggregates might exert protective effects in $Rh1^{P37H}$ PNs.

2.4. VCP is required *in vivo* for clearance of misfolded $Rh1^{P37H}$

To investigate the relevance of aggregate formation and clearance to $Rh1^{P37H}$ -mediated pathology, we focused our attention on the ERAD effector VCP/Ter94, the driving force for extraction of misfolded proteins from the ER and delivery to the proteasome (Dai and Li, 2001; Wang et al., 2004; Ye et al., 2001). Total knock-out of VCP is lethal in flies and in mice (Leon and McKearin, 1999; Müller et al., 2007). To reduce VCP function, I used the hypomorphic allele VCP^{26-8} that was generated by ethyl methanesulfonate (EMS)-induced mutagenesis (Ruden et al., 2000). This EMS allele contains a missense mutation (E450A) in the D1 ATPase domain (Ruden et al., 2000). I determined that the expression levels of VCP are decreased in $VCP^{26-8}/+$ flies (genotype: $VCP^{26-8}/+;+/+$, in short $VCP^{26-8}/+$) as compared to control flies (Figure 24A) suggesting that the mutant VCP is unstable, probably as a result of its failure to constitute a functional hexameric complex (Wang et al., 2004). Thus, the presence of the VCP^{26-8} allele leads to reduced VCP levels.

I crossed flies carrying the VCP^{26-8} allele to flies overexpressing either $Rh1^{P37H}$ or $Rh1^{WT}$ (and to additional controls). I then selected the right progeny (e.g. $VCP^{26-8}/+;Rh1^{P37H}/+$ flies, in which mutant $Rh1^{P37H}$ is expressed in a VCP hypomorphic background) and exposed these flies to light for different durations (10, 20 and 30 dle). I then anesthetized the flies and collected heads for biochemical experiments. Using these fly heads, I extracted the total proteins which were used for Western blotting (WB) experiments using diverse antibodies.

Using Rh1- and ubiquitin-specific antibodies to label aggregates, I found that $VCP^{26-8}/+;Rh1^{P37H}/+$ flies, in contrast to $Rh1^{P37H}$ and control flies, display a strong increase in total levels of Rh1 aggregates at 10 dle (Figure 24B) and similarly at 20 (Figure 24C) and 30 dle (Figure 24D).

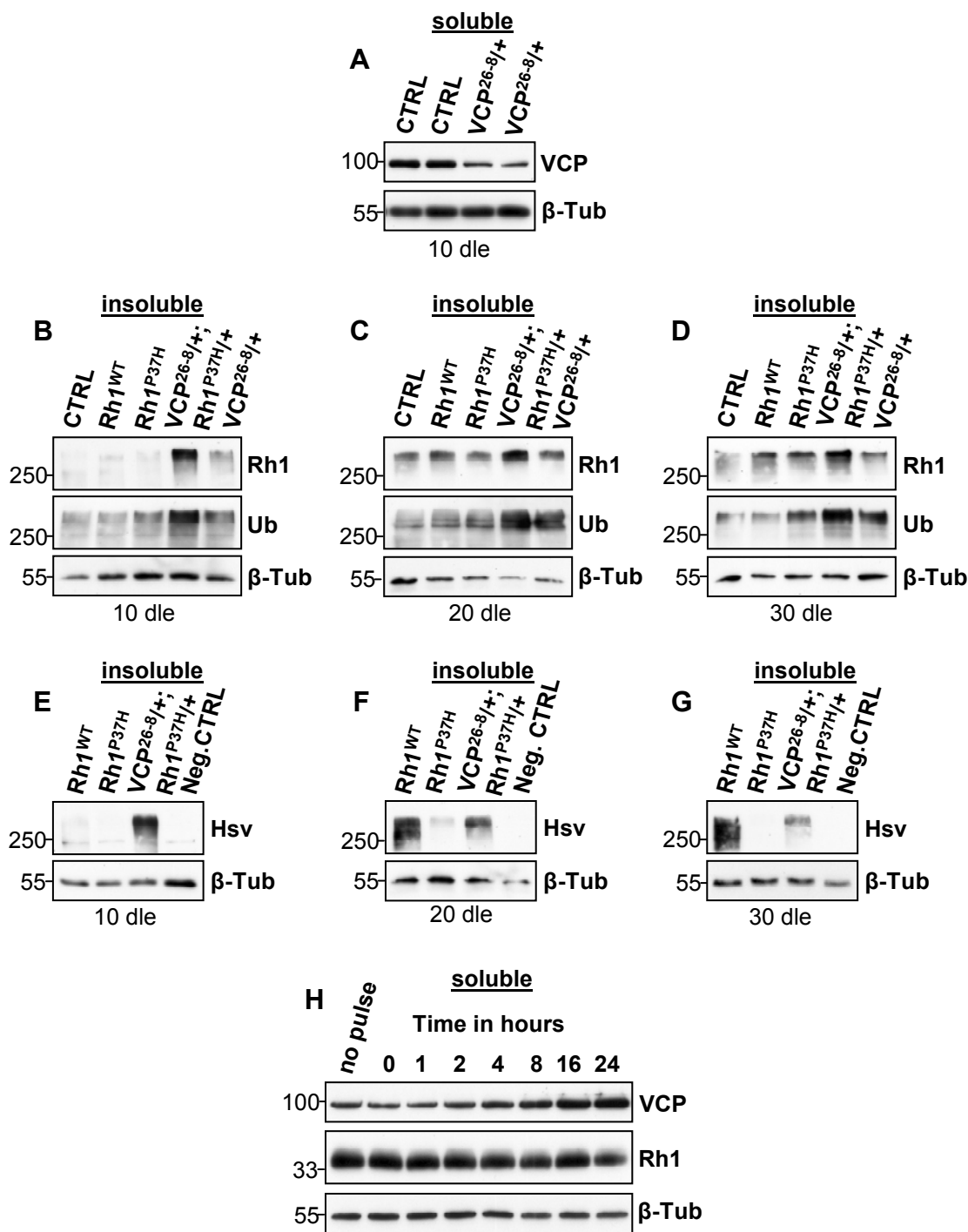


Figure 24. Decreasing VCP function increases Rh1 aggregate load in Rh1^{P37H} flies. (A) Adult control and VCP^{26-8/+} (genotype: VCP^{26-8/+};+/+) flies were tested for VCP expression using a VCP-specific antibody. Flies carrying the VCP hypomorphic allele VCP²⁶⁻⁸ have reduced levels of VCP. (B-G) Immunoblots showing the levels of total (B-D, endogenous and ectopic, Rh1 antibody) and ectopic (E-G, hsv antibody) Rh1 aggregates in flies of indicated genotypes after 10 days of light exposure (dle) (B,E), 20 dle (C,F) or 30 dle (D,G). A ubiquitin antibody was used to independently label aggregates. VCP^{26-8/+};Rh1^{P37H/+} flies display increased aggregate levels (endogenous and ectopic) compared to the other mutant flies (B-D). Aggregates containing the ectopic Rh1^{P37H} are also rescued from degradation after partial VCP inactivation (E-G). Overexpressed WT or P37H Rh1 was hsv-tagged and WT flies, lacking hsv, served as negative control for the hsv antibody. (H) VCP is not sufficient for degradation of mature Rh1. Animals carrying a UAS-VCP transgene and a Hs-Gal4 driver (heat shock promoter coupled to Gal4) were given a 90 min heat-pulse at 37°C and assayed at the indicated times after being shifted to 25°C. Numbers across the top refer to time in hours of chase. Lane 1 represents animals sampled prior to heat-pulse (no pulse), lane 2 represents animals sampled directly after the heat-pulse, and lane 3 represents animals that were given the heat-pulse followed by 1 hour chase. Immunoblots show the levels of VCP and Rh1. β -Tubulin (β -Tub) served as loading control.

Results

Flies carrying the *VCP²⁶⁻⁸* allele in an otherwise WT background (*VCP^{26-8/+}*) also displayed slightly more aggregates relative to control flies (Figure 24B-D) suggesting that VCP is involved in the quality control of endogenous Rh1, which undergoes repeated cycles of endocytosis and degradation during visual processing (Satoh and Ready, 2005). Thus, VCP activity is required *in vivo* for degradation of Rh1-containing aggregates.

The observation that VCP is required *in vivo* for degradation of total Rh1-containing aggregates prompted us to determine whether this effect applied to the mutant Rh1^{P37H}, or the WT Rh1, or both. The fact that the ectopic Rh1 was hsv-tagged facilitated this analysis. Hsv labeling indicated that partial *VCP* inactivation also prevents degradation of insoluble mutant Rh1^{P37H}-containing aggregates (Figure 24E-G), indicating that VCP is required for the degradation of ectopic mutant Rh1^{P37H}. The fact that after 10 dle, *VCP^{26-8/+;Rh1^{P37H/+}}* displayed many Rh1^{P37H-hsv} aggregates, in contrast to *Rh1^{P37H}* flies, suggests that VCP was responsible for the degradation of these aggregates in *Rh1^{P37H}* flies, before they began to accumulate (after 20 dle).

To assess whether VCP is sufficient to degrade mature endogenous Rh1 in PNs, I performed an independent experiment and induced acute overexpression of VCP in the whole fly body. For this, I used the heat-shock (Hs) promoter which allows ubiquitous transgene overexpression after exposure of flies to an increased temperature (heat shock; see Materials and Methods). Animals carrying the *UAS-VCP* transgene and the *Hs-Gal4* driver (also a transgene) were given a 90 minutes heat-pulse at 37 °C and assayed at various times after being shifted back to 25 °C. I prepared head lysates from these flies and determined the total VCP and Rh1 levels by WB (Figure 24H). As expected, the heat shock led to the activation of the Hs promoter and to VCP overexpression. However, I found that these increased levels of VCP did not influence the stability of mature Rh1, suggesting that mature Rh1 is not a substrate of VCP. These observations are in line with our previous *in vitro* results which suggested that VCP does not interact with mature monomeric Rh (see Figure 14A).

Therefore, VCP is required *in vivo* for clearance of misfolded Rh1^{P37H}.

2.5 Partial *VCP* inactivation restores mature Rh1 levels in *Rh1^{P37H}* flies

I next set up to determine whether decreasing VCP activity has any effect on the fate of mature Rh1 in *Rh1^{P37H}* flies. To determine the levels of mature (soluble) Rh1 in retinas derived from *VCP^{26-8/+;Rh1^{P37H/+}}*, *Rh1^{P37H}* or control flies, I extracted detergent-soluble head fractions and used the Rh1-specific antibody to reveal their content of mature Rh1. I also used the TRP antibody to determine the presence or absence of rhabdomeres.

While the levels of mature total (endogenous and ectopic) Rh1 were similar for all groups after 10dle (Figure 25A), I found a dramatic loss of mature Rh1 in *Rh1^{P37H}* flies after 20 dle (Figure 25B) and after 30 dle (Figure 25C,G, see also Figure 22H). Remarkably, partial *VCP* inactivation leads to an almost complete rescue of mature Rh1 and TRP levels after 20 dle (Figure 25B). *VCP* inactivation also allowed an almost complete rescue of mature Rh1 levels after 30 dle (Figure 25C,G; results from 3 independent crosses were averaged) and similarly, restored the levels of the rhabdomeric marker TRP (Figure 25C,H), suggesting decreased retinal degeneration in the *VCP^{26-8/+;Rh1^{P37H/+}}* retina after 30 dle. Thus, partial *VCP* inactivation leads to an almost complete rescue of total mature Rh1 in *Rh1^{P37H}* flies.

The restoration of total (ectopic and endogenous) mature Rh1 in $Rh1^{P37H}$ flies after *VCP* inactivation prompted us to investigate the fate of mutant $Rh1^{P37H}$ specifically. Using the Hsv-specific antibody, I observed a similar, although moderate, rescue of the soluble mature ectopic $Rh1^{P37H}$ (hsv-labeled) at 10 dle (Figure 25D), 20dle (Figure 25E) and 30 dle (Figure 25F). Taken together, these experiments suggest that inactivation of *VCP* leads to recovery of mature (both endogenous and P37H mutant) Rh1 in $Rh1^{P37H}$ flies exposed to light.

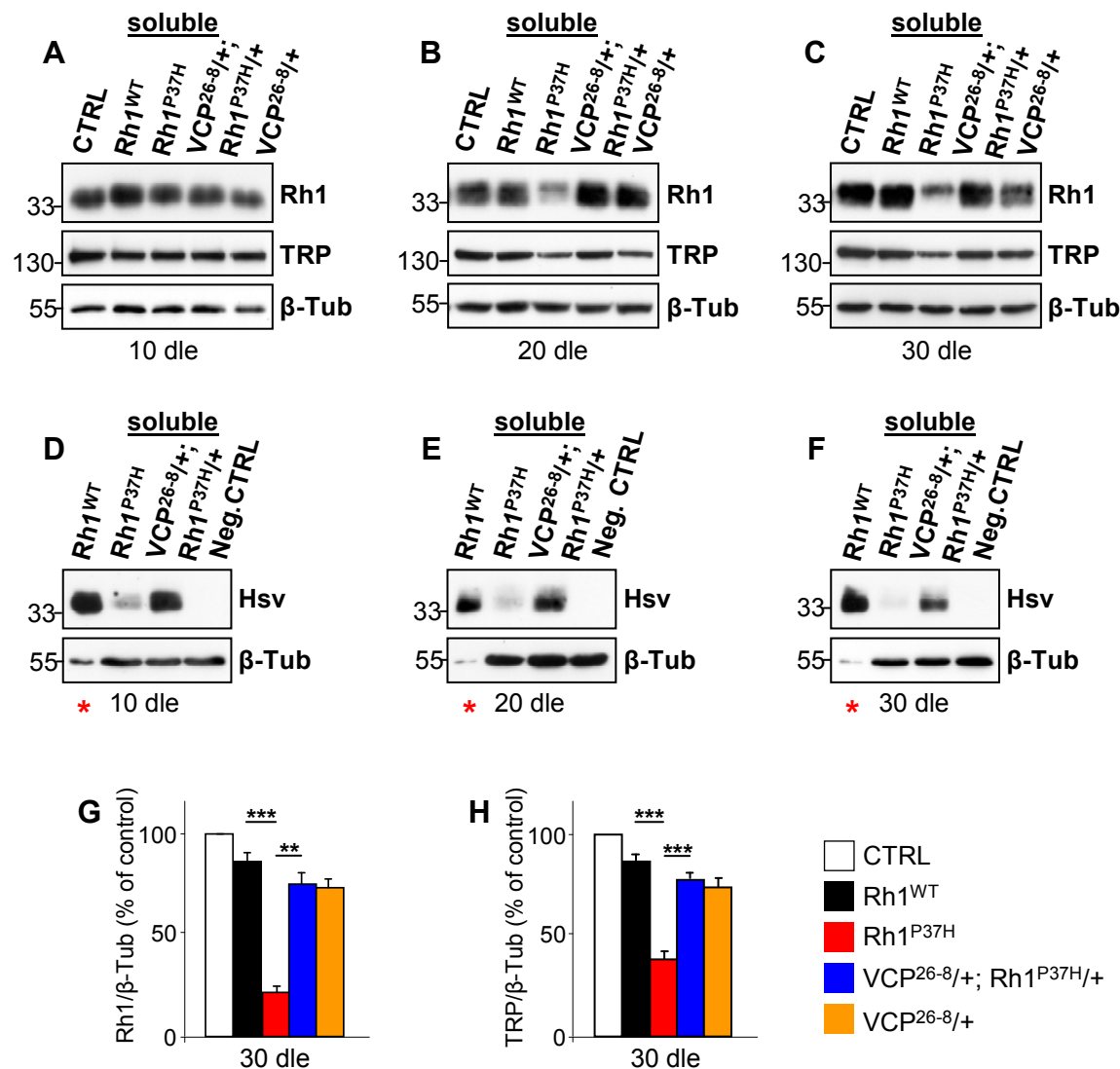


Figure 25. Decreasing *VCP* function restores mature Rh1 levels in $Rh1^{P37H}$ flies. (A-F) Immunoblots revealing the levels of total (A-C, endogenous and ectopic, Rh1 antibody) and ectopic (D-F, hsv antibody) mature Rh1, as well as TRP levels in flies of indicated genotypes after 10 days of light exposure (dle) (A,D), 20 dle (B,E) and 30 dle (C,F). Loss of endogenous and ectopic mature Rh1 in $Rh1^{P37H}$ flies is rescued in $VCP^{26-8/+}; Rh1^{P37H/+}$ flies. Overexpressed WT or P37H Rh1 was hsv-tagged and WT flies, lacking hsv, served as negative control for the hsv antibody. * Please note that 10-fold less protein was loaded for the $Rh1^{WT}$ flies (D-F) and β -Tubulin (β -Tub) served as loading control. (G,H) Quantifications of Rh1 levels (G) and of TRP levels (H) in flies of indicated genotypes, after 30 dle. Values from three independent experiments were averaged (** p<0.01 and *** p<0.001 Student's t-test).

Results

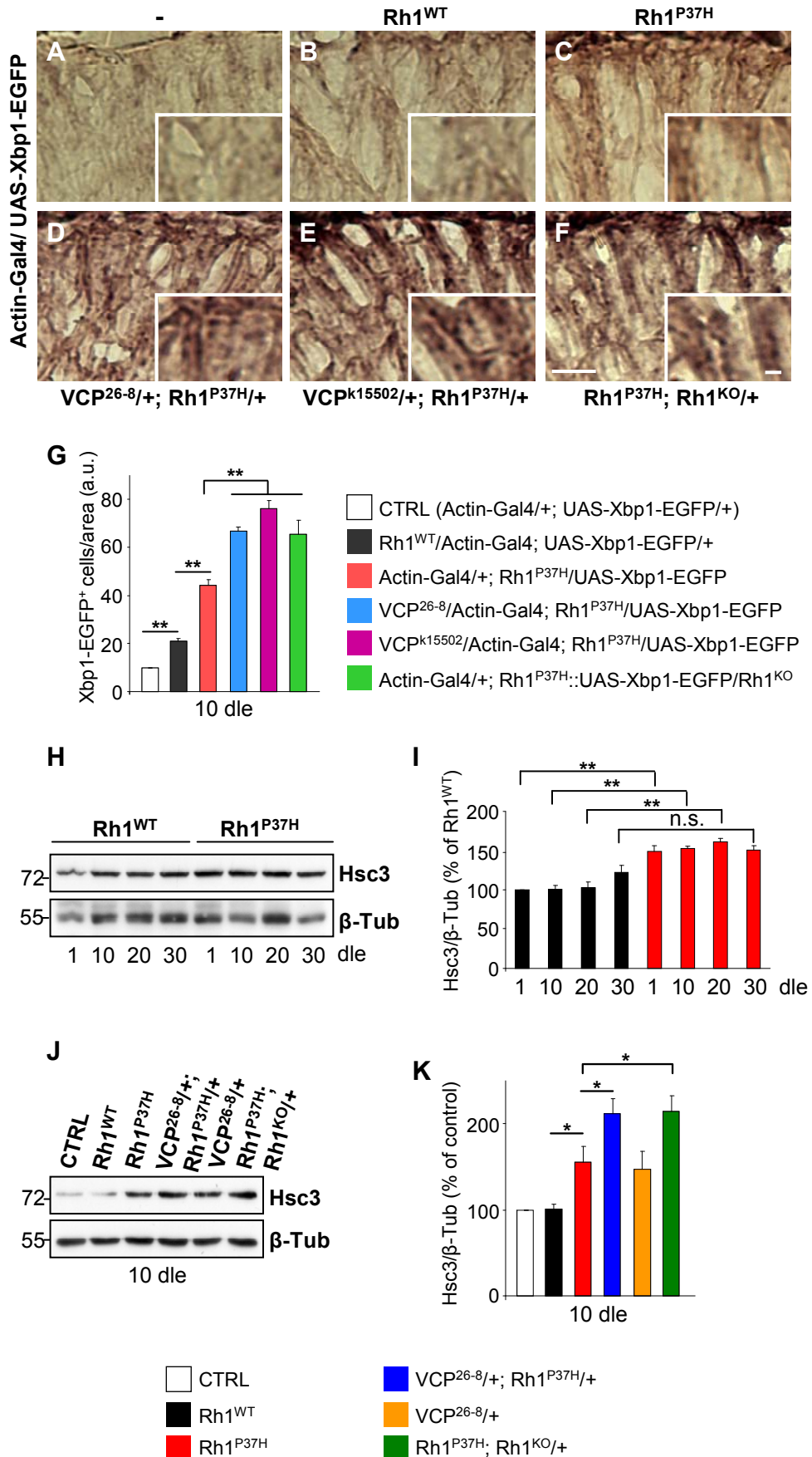
2.6 Increased activation of the Ire1/Xbp1 UPR pathway in $Rh1^{P37H}$ flies with decreased VCP function

Accumulation of misfolded proteins in the ER activates the UPR which is mediated by the ER stress sensors Ire1, Perk and Atf6. In *Drosophila*, the activation of the Ire1/Xbp1 pathway can be assessed using available genetic tools and antibodies; in contrast, no tools exist that allow the assessment of Perk and Atf6 activation. The unconventional splicing of *Xbp1* mRNA is favoured during the UPR/ER stress, generating a transcription factor that activates stress response genes, including the ER stress sensor and chaperone Hsc3/BiP (Ryoo et al., 2007). The splicing of a 23-nucleotide sequence by Ire1 is predicted to cause a frame shift during protein translation of *Xbp1*. The property of unconventional slicing of *Xbp1* was used to develop a specific ER stress reporter, Xbp1-EGFP, in which EGFP is expressed in frame only after ER stress (developed by the Ryoo laboratory; Ryoo et al., 2007; see Materials and Methods).

Given that *VCP* inactivation leads to an increased load of Rh1 aggregate levels, we wondered whether $VCP^{26-8}/+;Rh1^{P37H}/+$ flies display differences in the activation of the Xbp1/Ire1 pathway. For that, I determined the occurrence of *Xbp1* mRNA unconventional splicing by inducing ubiquitous expression (using the *Actin-Gal4* driver) of the *UAS-Xbp1-EGFP* transgene construct, which activates EGFP expression only after unconventional splicing. I stained retinas using a GFP-specific antibody (Mendes et al., 2009; Ryoo et al., 2007) followed by alkaline phosphatase staining (see Materials and Methods) and I determined the density of GFP-positive profiles for the different genotypes.

I found that Xbp1-EGFP activation is increased in $Rh1^{P37H}$ retinas relative to $Rh1^{WT}$ and control retinas after 10 dle (Figure 26A-C,G). $Rh1^{P37H}$ flies carrying VCP^{26-8} , $Rh1^{KO}$ or the stronger *VCP LOF* allele VCP^{k15502} (a P-element allele; see below; Ruden et al., 2000) displayed an increased density of GFP positive profiles in the retina (Figure 26D-F,G; n>5 eyes/genotype), consistent with them having increased levels of Rh1 aggregates (see Figures 23E, 24B-G). Therefore, the increase in Rh1 aggregate load in $VCP^{26-8}/+;Rh1^{P37H}/+$ flies correlates with an increased activation of the Ire1/Xbp1 UPR pathway. To assess the activation status of the Ire1/Xbp1 UPR pathway in $Rh1^{P37H}$ flies independently of the Xbp1-EGFP reporter, I determined the levels of the Hsc3/BiP chaperone in the retina, as a second read-out for ER stress (Mendes et al., 2009; Ron and Walter, 2007; Ryoo et al., 2007).

Figure 26. Increasead activation of the Ire1/Xbp1 UPR pathway in $VCP^{26-8}/+;Rh1^{P37H}/+$ flies. (A-F) Horizontal retinal cryosections from flies after 10 days of light exposure (dle) were stained with an anti-GFP antibody. *Xbp1-EGFP* is expressed under the control of *Actin* promoter. Unconventional *Xbp1* mRNA splicing is increased in the $Rh1^{P37H}$ (C) retina while further removal of *VCP* (D,E) or endogenous *Rh1* function (F) strongly enhances *Xbp1* unconventional splicing, revealed by EGFP expression. Scale bar is 75 μ m and inset is 10 μ m. (G) Quantification of Xbp1-EGFP positive nuclei. Results are expressed as number of EGFP-positive nuclei per area from five different flies/group (** p<0.01 Student's t-test). (H) Immunoblot revealing the levels of Hsc3 in $Rh1^{WT}$ and $Rh1^{P37H}$ retinas, exposed to light for increasing durations. A 1.5-fold increase of Hsc3 levels is seen in $Rh1^{P37H}$ vs. $Rh1^{WT}$ retinas starting at day 1. β -Tubulin (β -Tub) served as loading control. (I) Quantification of Hsc3 expression levels. The results are expressed as mean percentage compared to Hsc3 levels in $Rh1^{WT}$ at 1 dle (100 %) and were obtained from three independent experiments (** p<0.01 Student's t-test). (J) Immunoblot showing the levels of Hsc3 in flies of indicated genotypes after 10 dle. $Rh1^{P37H}$ retinas exhibit more Hsc3 compared to control and $Rh1^{WT}$ retinas, while further removal of *VCP* or endogenous *Rh1* function leads to a further increase in Hsc3 levels. β -Tub served as loading control. (K) Quantification of Hsc3 levels was averaged from three independent experiments (* p<0.05 Student's t-test).



Results

Using a Hsc3-specific antibody (Ryoo et al., 2007), I found that $Rh1^{P37H}$ retinas display a 50 % increase in Hsc3 levels relative to $Rh1^{WT}$ retinas, starting from P1 (Figure 26H,I). Interestingly, after 30 dle no difference in Hsc3 levels between $Rh1^{WT}$ and $Rh1^{P37H}$ flies was detected (Figure 26H,I, see also Figure 22I). These results suggest that $Rh1^{P37H}$ induces UPR at earlier time points (before onset of the retinal degeneration) while during aging, the levels of Rh1 aggregates become equal in both fly lines, leading to similar Hsc3 levels.

I then used the Hsc3 antibody to determine the activation of the Ire1/Xbp1 UPR pathway in $VCP^{26-8}/+;Rh1^{P37H}/+$ or $Rh1^{P37H};Rh1^{KO}/+$ flies, relative to $Rh1^{P37H}$ and control flies. As previously seen for Xbp1-EGFP activation, $Rh1^{P37H}$ flies carrying VCP^{26-8} or $Rh1^{KO}$ alleles displayed increased Hsc3 levels compared to $Rh1^{P37H}$ and control flies after 10 dle (Figure 26J,K; results from 3 independent crosses were averaged). Therefore, the increase in Rh1-containing aggregates following partial removal of VCP or endogenous $Rh1$ function is associated with increased activation of the Ire1/Xbp1 UPR pathway.

2.7 Partial VCP inactivation increases the activation of the Ire1/Xbp1 pathway in $GMR/UAS-Rh1^{G69D}$ and $Rh1^{G69D}$ flies

Given that decreasing VCP function leads to enhanced activation of the Ire1/Xbp1 pathway in $Rh1^{P37H}$ flies and the $Rh1^{P37H}$ mutation belongs to the class II of Rh1 mutations that cause RP, we asked whether VCP has similar effects on other class II $Rh1$ mutants. For this purpose, we chose to investigate the G69D Rh1 mutation. The G69D mutation represents a glycine-to-aspartic acid substitution in a transmembrane domain of Rh. I used two lines of flies, one in which mutant $Rh1^{G69D}$ is overexpressed in PNs ($GMR-Gal4;UAS-Rh1^{G69D}$, in short $GMR/UAS-Rh1^{G69D}$), and a second line carrying an EMS allele, $Rh1^{G69D}$ (Ryoo et al., 2007)

I first assessed the $Xbp1$ unconventional splicing in $GMR/UAS-Rh1^{G69D}$ flies. Targeted expression of this allele in the eye was found to induce UPR via activation of Ire1/Xbp1 pathway (Ryoo et al., 2007). I induced the expression of this $UAS-Rh1^{G69D}$ transgene together with the reporter $UAS-Xbp1-EGFP$ transgene in PNs using the PN-specific *glass multimer reporter* (*GMR*), which allows transgene expression in post-mitotic PNs in the developing retina, starting in late larval stages (Read et al., 2005). I then collected the fly heads and stained the retinas using a GFP-specific antibody, followed by the quantification of GFP-positive profiles for the different genotypes.

As expected, I found that the $Xbp1$ -EGFP unconventional splicing was increased in $GMR/UAS-Rh1^{G69D}$ retina relative to control retina at postnatal day 1 (Figure 27A,B,D). $GMR/UAS-Rh1^{G69D}$ flies carrying the stronger VCP LOF allele VCP^{k15502} displayed an increased density of GFP positive profiles compared to $GMR/UAS-Rh1^{G69D}$ flies (Figure 27C,D; n>5 eyes/genotype), consistent with the above-mentioned results showing that $VCP^{26-8}/+;Rh1^{P37H}/+$ flies display increased activation of Ire/Xbp1 pathway (see Figure 26). Thus, these experiments suggest that decreasing VCP function leads to enhanced activation of Ire1/Xbp1 pathway in $GMR/UAS-Rh1^{G69D}$ flies.

In a second set of experiments, I determined the levels of the Hsc3/BiP chaperone in the retinas of flies carrying the other G69D mutant Rh1 allele (generated by EMS-induced mutagenesis). $Rh1^{G69D}/Rh1^+$ flies (genotype: $+/+;Rh1^{G69D}/+$, in short $Rh1^{G69D}$) were found to have defects in Rh1 maturation and ER-to-Golgi transport (Colley et al., 1995; Kurada and O'Tousa, 1995). I found that $Rh1^{G69D}$ flies had increased Hsc3 levels

compared to WT flies after 10 and 20 dle (Figure 27E,F), as previously reported (Ryoo et al., 2007). Moreover, $Rh1^{G69D}$ flies carrying the VCP^{26-8} allele displayed increased Hsc3 levels compared to $Rh1^{G69D}$ flies after 10 dle (Figure 27E) and 20 dle (Figure 27F). Therefore, partial removal of VCP function leads to increased activation of the Ire1/Xbp1 UPR pathway in other two models of RP, $GMR/UAS-Rh1^{G69D}$ and $Rh1^{G69D}$.

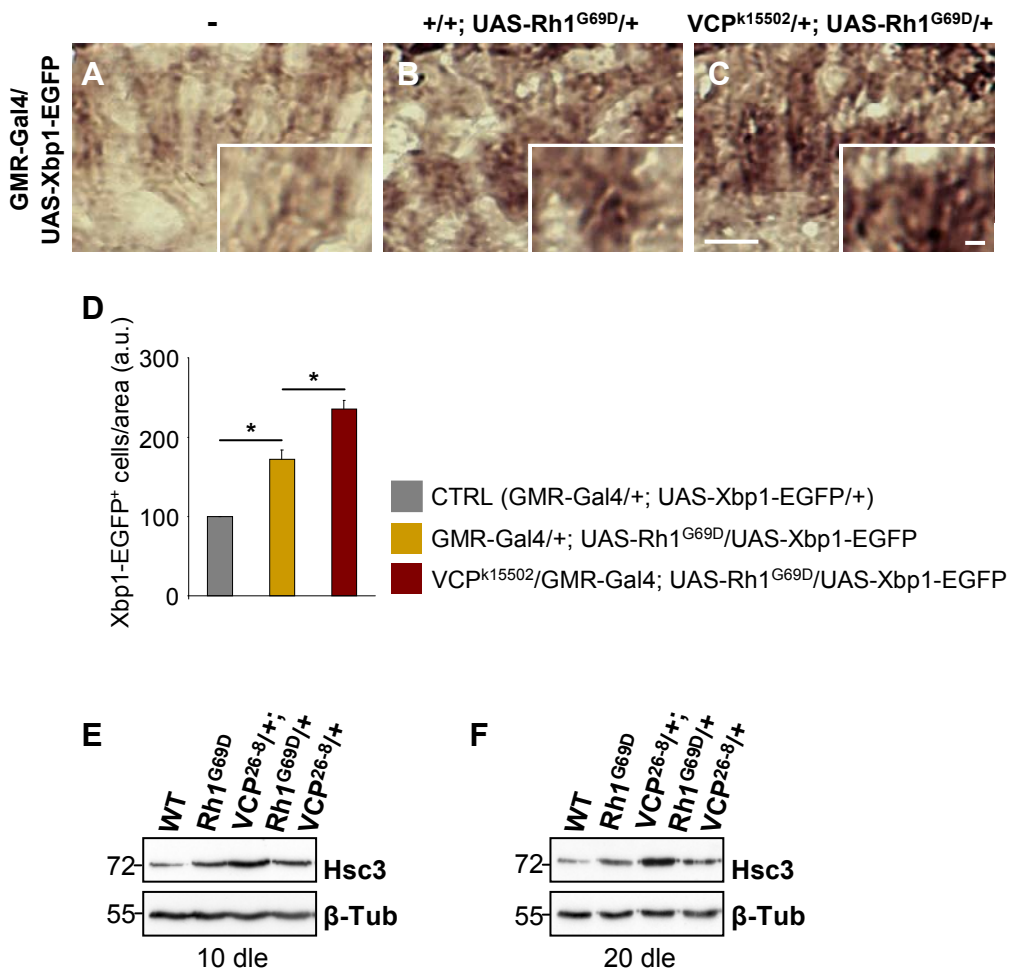


Figure 27. VCP inactivation increases ER stress in $GMR/Rh1^{G69D}$ flies and in $Rh1^{G69D}$ flies. (A-C) Horizontal retinal cryosections stained with a GFP specific antibody in 1-day old flies. Control photoreceptors expressing $Xbp1$ -EGFP driven by the GMR promoter (GMR -Gal4; UAS - $Xbp1$ -EGFP) show weak GFP staining (A) while GMR ; UAS - $Rh1^{G69D}$ / UAS - $Xbp1$ -EGFP flies expressing mutant $Rh1^{G69D}$ and the $Xbp1$ -EGFP constructs in PNs show an increased number of GFP positive profiles (B); VCP^{k15502} / GMR -Gal4; UAS - $Rh1^{G69D}$ / UAS - $Xbp1$ -EGFP retinas show a further increase in the number of GFP positive profiles (C). Scale bar is 75 μ m and inset is 10 μ m. (D) Quantification of $Xbp1$ -EGFP positive profiles for the indicated genotypes. Results are expressed as number of EGFP-positive profiles per area ($n = 4$ animals/group, * $p < 0.05$ Student's t-test). (E,F) Immunoblots showing the levels of Hsc3 in flies of indicated genotypes after 10 days of light exposure (dle) (E) or after 20 dle (F). $Rh1^{G69D}$ (genotype: +/+/ $Rh1^{G69D}$ /+) retinas exhibit an increase in Hsc3 levels compared with WT retinas, and Hsc3 levels are further increased in VCP^{26-8} /+; $Rh1^{G69D}$ /+ retinas, both after 10 and 20 dle (E,F).

2.8. VCP inactivation suppresses first signs of retinal degeneration in $Rh1^{P37H}$ flies

After establishing that partial *VCP* inactivation prevents the loss of mature Rh1 in $Rh1^{P37H}$ flies, we wondered whether *VCP* inactivation has any effects on the retinal degeneration process mediated by misfolded Rh1. To this end, I analyzed the retinal ultrastructure of flies at early stages of light exposure (10 dle), at which $Rh1^{P37H}$ -mediated retinal degeneration was found to be very mild (Galy et al., 2005). Fly eyes were tangentially sectioned and ultrathin cuts (75 nm) were contrasted for electron microscopy using uranium and lead derivatives (Figure 28).

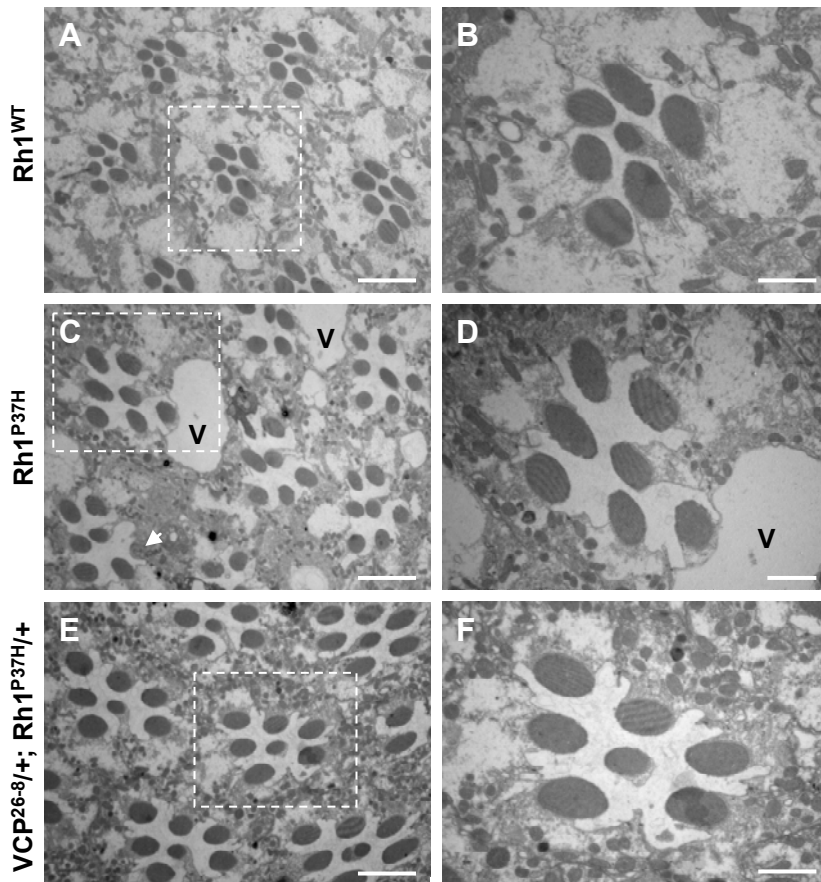


Figure 28. VCP inactivation suppresses first signs of retinal degeneration in $Rh1^{P37H}$ flies. (A-F) Electron micrographs of ultrathin tangential eye sections of $Rh1^{WT}$ (A,B), $Rh1^{P37H}$ (C,D) and $VCP^{26-8/+}; Rh1^{P37H}/+$ (E,F) flies after 10 days of light exposure (dle). Higher magnification pictures of the insets from pictures (A,C,E) are shown in column 2 (B,D,F) and reveal the ultrastructure of a single ommatidium. (A) $Rh1^{WT}$ flies show intact retinal ultrastructure. (B) All 7 rhabdomeres are present in each ommatidium and are surrounded by a well-preserved cell body (white). (C,D) $Rh1^{P37H}$ flies display first signs of retinal degeneration, such as large vacuoles (V) and missing rhabdomeres (arrowhead). (E,F) *VCP* inactivation leads to the suppression these degenerative signs in $Rh1^{P37H}$ flies. No vacuoles are seen and all rhabdomeres remain intact in each ommatidium. Scale bar is 10 µm (A,C,E) and 2 µm (B,D,F).

Ultrastructural analysis of the $Rh1^{WT}$ retina revealed an intact ultrastructure, with entirely preserved rhabdomeres (highlighted in black) in each ommatidium (Figure 28A). High magnification electron micrographs also revealed that the PN cell bodies, which surround the rhabdomeres, displayed a normal morphology (in white; Figure 28B). In contrast, the ultrastructure of the $Rh1^{P37H}$ retina was moderately affected after 10 dle; these mutant retinas displayed degenerative signs, including the presence of a considerable number of vacuoles (highlighted with V) and mild loss of rhabdomeres (arrowhead, Figure 28C).

Moreover, the PN cell bodies (in white) also had a partially altered morphology (Figure 28D).

Remarkably, inactivation of *VCP* in *Rh1^{P37H}* flies suppressed these degenerative signs in the retina (Figure 28E,F). Each ommatidium displayed a normal complement of rhabdomeres, and no vacuoles were detected in these retinas. These initial observations suggested to us that partial *VCP* inactivation was able to mitigate the neurodegenerative process mediated by misfolded *Rh1^{P37H}* in *Drosophila*. These observations raised the possibility that *VCP* inactivation might protect fly PNs from the toxic effects of misfolded *Rh1^{P37H}*.

2.9 Suppression of *Rh1^{P37H}*-induced retinal degeneration by *VCP* loss-of-function alleles

The finding that the hypomorphic allele *VCP²⁶⁻⁸* suppresses the initial signs of retinal degeneration in *Rh1^{P37H}* flies, prompted us to investigate the protective role of *VCP* inactivation at later time points, during the degenerative process. To this purpose, I investigated the effect of decreasing *VCP* function on *Rh1^{P37H}*-induced PN degeneration at 20 and 30 dle, using semithin (2 μm) sections stained with the contrasting agent toluidine blue.

I found that *VCP^{26-8/+;Rh1^{P37H}/+}* and *Rh1^{P37H}* retinas showed a similar degree of PN degeneration after 20 dle (Figure 29A,B,G; 2.9 photoreceptors/ommatidium (P/O) in *Rh1^{P37H}* flies vs. 3.3 P/O in *VCP^{26-8/+;Rh1^{P37H}/+}* flies; n>7 animals/group). Remarkably, further degeneration (after 30 dle) was prevented in the *VCP^{26-8/+;Rh1^{P37H}/+}* retina (Figure 29D,E,G; 1.6 P/O in *Rh1^{P37H}* flies vs. 3.2 P/O in *VCP^{26-8/+;Rh1^{P37H}/+}* flies, * p<0.05 Student's t-test) despite the increased levels of Rh1 aggregates.

I then analyzed the retinal integrity of *Rh1^{P37H}* flies carrying the stronger *VCP* LOF allele, *VCP^{k15502}*. Remarkably, PN degeneration was strongly suppressed in *Rh1^{P37H}* flies carrying the stronger *VCP* LOF allele (genotype: *VCP^{k15502/+;Rh1^{P37H}/+}*), both after 20 and 30 dle (Figure 29A,C,D,F,G; 2.9 P/O in *Rh1^{P37H}* flies vs. 4.3 P/O in *VCP^{26-8/+;Rh1^{P37H}/+}* flies after 20 dle, **p<0.01 Student's t-test and 1.6 P/O vs. 4.2 P/O after 30 dle, *** p<0.001 Student's t-test).

Since the decrease in *VCP* function suppressed the *Rh1^{P37H}*-induced cell death, we asked whether *VCP* acts as a cell death effector; if this were the case, we would expect VCP levels and/or activity to closely parallel the neurodegenerative process. Therefore, I assessed the levels of VCP in *Rh1^{P37H}* vs. *Rh1^{WT}* flies and found that they increased 2-fold at day 1 in *Rh1^{P37H}* flies, after which they dropped; in *Rh1^{WT}*, VCP levels remained inferior to levels in *Rh1^{P37H}* retinas (Figure 29H,I; results from 3 independent crosses were averaged). Although we were not able to measure the activity of VCP in these retinas and an initial increase in VCP levels might induce long-term cellular changes that contribute to PN degeneration, our results suggest that differences in VCP levels (and activity) probably play a minor, if any, direct pro-apoptotic role in *Rh1^{P37H}*-mediated retinal degeneration.

Thus, partial inactivation of *VCP* exerts a strong protective role in the *Rh1^{P37H}* retina.

Results

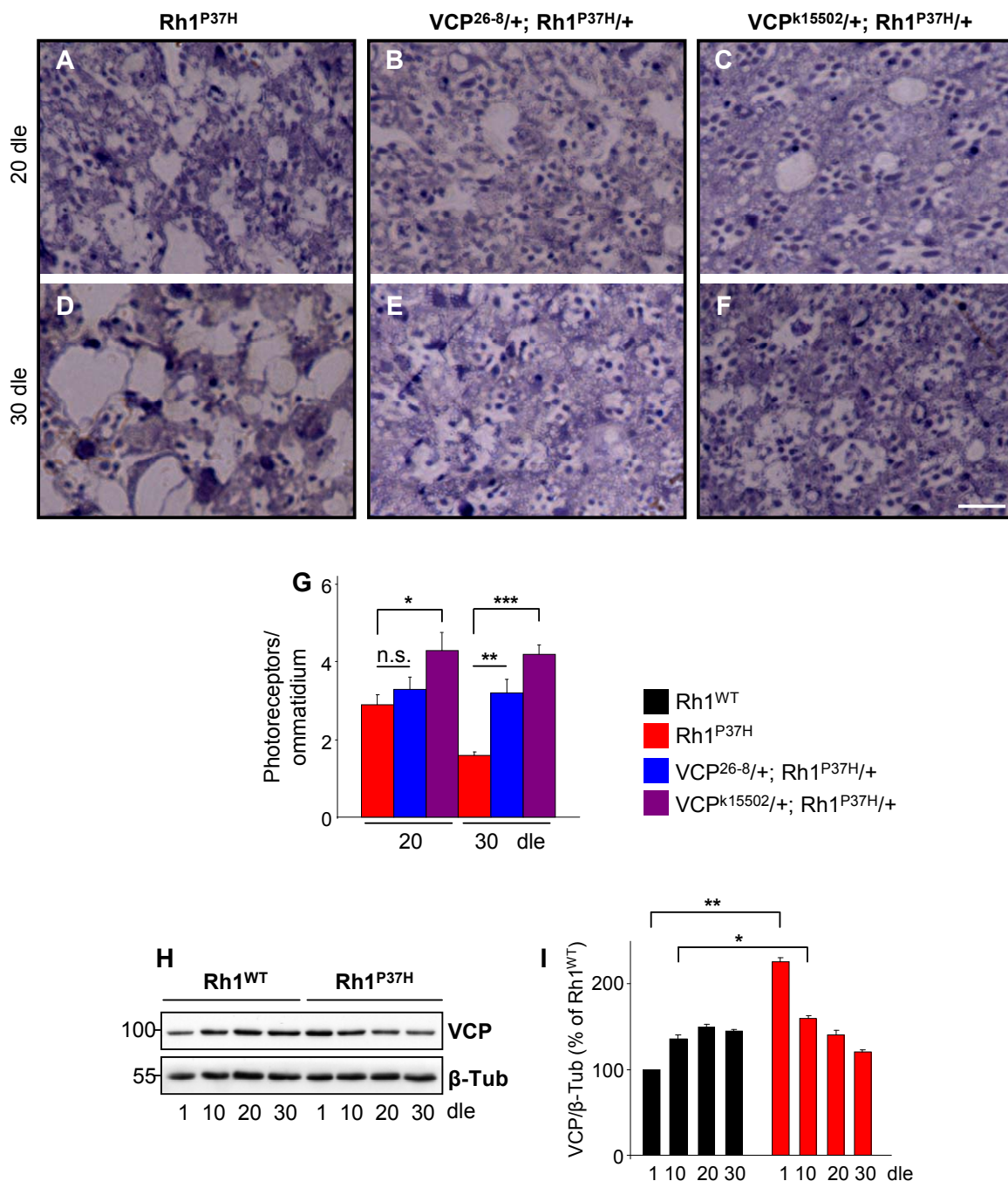


Figure 29. Suppression of *Rh1*^{P37H}-induced retinal degeneration by *VCP* loss-of-function alleles. (A-F) Photomicrographs of toluidine blue-stained semithin eye sections of *Rh1*^{P37H} (A,D), *VCP*^{26-8/+; Rh1}^{P37H/+ (B,E) and *VCP*^{k15502/+; Rh1}^{P37H/+ (C,F) flies after 20 (A-C) or 30 (D-F) days of light exposure (dle). Scale bar is 50 μ m. (G) Quantification of average number of photoreceptors/ommatidium (P/O) (n>7 animals/group, * p<0.05, ** p<0.01 and *** p<0.001 Student's t-test). Decreasing *VCP* function potently suppresses retinal degeneration caused by *Rh1*^{P37H}. (H) Immunoblot revealing the levels of *VCP* in *Rh1*^{WT} and *Rh1*^{P37H} retinas, exposed to light for increasing durations. *Rh1*^{P37H} display a 2.25-fold increase of *VCP* levels relative to *Rh1*^{WT} retinas after 1 dle. β -Tubulin (β -Tub) served as loading control. (I) Quantification of *VCP* expression levels revealed higher *VCP* levels in *Rh1*^{P37H} flies after 1 and 10 dle. *VCP* levels were averaged from three independent experiments (* p<0.05 and ** p<0.01 Student's t-test).}}

2.10 Dramatic suppression of the *Rh1^{P37H}*-mediated retinal degeneration after pharmacological inhibition of the VCP/ERAD/proteasome axis

The finding that VCP inhibition rescues retinal degeneration in *Rh1^{P37H}* flies suggests that inhibition of the ERAD activity might exert long-term protective effects in *Rh1^{P37H}* PNs. Our experiments in mammalian cell culture suggested that misfolded Rh^{P23H} is a substrate of the proteasome (Figures 13 and 15). Moreover, the tight coupling between VCP and proteasome activities is essential for substrate delivery and clearance during ERAD (Dai and Li, 2001) and interestingly, proteasome activity is required for proper substrate retrotranslocation (Chillaron and Haas, 2000; Saliba et al., 2002). To independently test whether inhibition of the VCP/ERAD/proteasome axis is protective for *Rh1^{P37H}*-expressing PNs, I employed the VCP/ERAD inhibitor EerI and the proteasome inhibitor MG132 that I dissolved in fly food. EerI acts on deubiquitinating enzymes that function downstream of VCP during ERAD and therefore inhibits ERAD-associated VCP functions (Fiebiger et al., 2004; Wang et al., 2008). MG132 is a classical proteasome inhibitor and potently inhibits the proteasome in *Drosophila* S2 cells (Lundgren et al., 2005; Muro et al., 2002). To determine whether the inhibitory effect of MG132 extends to the fly proteasome, I obtained crude extracts from *Drosophila* heads and measured the proteasome activity of control flies, in the presence or absence of MG132 (Figure 30A). I found that MG132 potently inhibits the activity of the proteasome; after addition of 50 μM MG132 (final concentration), the fly proteasome retained only 4.28 % of its initial activity (Figure 30A). Thus, MG132 inhibits the *Drosophila* proteasome and could be used as a pharmacological tool to assess the role of proteasome inhibition in *Rh1^{P37H}*-mediated retinal pathology in *Drosophila*.

Using two doses of EerI (1 mM and 10 mM), I found that partial VCP/ERAD inhibition potently suppressed retinal degeneration in *Rh1^{P37H}* flies after 30 dle (Figure 30C-E,H; n>7 flies/genotype, 1.55 P/O in *Rh1^{P37H}* flies reared on control food vs. 4.05 P/O in *Rh1^{P37H}* flies treated with 1 mM EerI and 4.24 P/O in *Rh1^{P37H}* flies treated with 10 mM EerI, *** p<0.01 Student's t-test). Both doses displayed the same (partial) suppression of PN degeneration, suggesting that a higher dose is required to achieve a more complete rescue or that EerI only inhibits some, but not all, ERAD-related VCP functions. *Rh1^{WT}* flies kept on control food were not affected after 30 dle and displayed 5.5 photoreceptors per ommatidium in average (Figure 30B,H). Thus, pharmacological inhibition of VCP/ERAD activity exerts protective effects in the *Rh1^{P37H}* retina.

I then investigated the effect of proteasome inhibition on the *Rh1^{P37H}*-mediated retinal pathology. I transferred newly emerged *Rh1^{P37H}* flies to food containing 5 μM MG132 and analyzed their retinal integrity after 30 dle. Using this low MG132 dose, I found a striking suppression of PN degeneration in *Rh1^{P37H}* flies after 30 dle (Figure 30C,F,H; 1.55 P/O in *Rh1^{P37H}* flies reared on control food vs. 4.2 P/O in *Rh1^{P37H}* flies treated with 5 μM MG132, *** p<0.001 Student's t-test). Remarkably, treatment of *Rh1^{P37H}* flies with the higher (50 μM) MG132 dose led to a very dramatic rescue of retinal degeneration, the average number of photoreceptors/ommatidium reaching 5.5 (Figure 30C,G,H; *** p<0.001 Student's t-test, n>7 flies/genotype and >150 ommatidia scored/animal). A comparison of the rescuing efficiency of the two MG132 doses revealed that MG132 rescued retinal degeneration in the *Rh1^{P37H}* retina in a dose-dependent manner (4.2 P/O in *Rh1^{P37H}* flies treated with 5 μM MG132 vs. 5.5 in *Rh1^{P37H}* flies treated with 50 μM MG132, ** p<0.01 Student's t-test).

Results

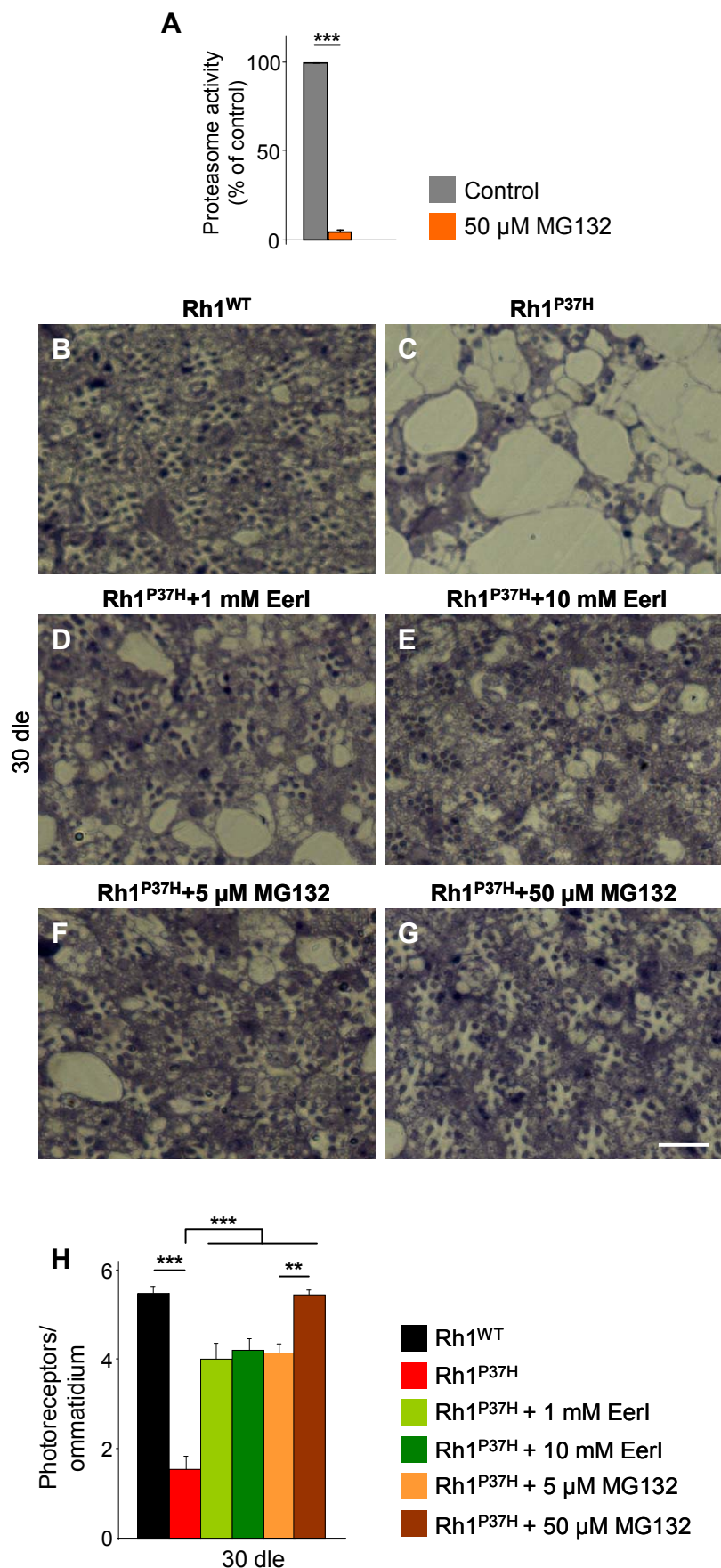


Figure 30. VCP/ERAD/proteasome inhibition rescues $Rh1^{P37H}$ -mediated retinal degeneration. (A) The proteasome inhibitor MG132 potently suppresses proteasome activity in *Drosophila*. Head fly lysates were assayed for the proteasome activity in the absence (control, 0.5 % DMSO) or presence of the proteasome inhibitor MG132 (50 μ M MG132 in 0.5 % DMSO). The results are shown as mean percentage compared to proteasome activity levels in fly lysates treated with DMSO (set as 100 %) and were averaged from three independent experiments (**p<0.001 Student's t-test). (B-G) Photomicrographs of toluidine blue-stained semithin eye sections of $Rh1^{WT}$ flies fed on control food (B); $Rh1^{P37H}$ flies fed on control food (C); $Rh1^{P37H}$ flies fed on food containing 1 mM (D), or 10 mM (E) EerI; $Rh1^{P37H}$ flies fed on food containing 5 μ M (F) or 50 μ M (G) MG132 after 30 dle. Dle: days of light exposure. Scale bar is 50 μ m. (H) Quantification of average number of photoreceptors/ommatidium (P/O) (n>7 animals/group, ** p<0.01 and *** p<0.001 Student's t-test).

Taken together, these pharmacological experiments provide independent evidence that inhibition of the VCP/ERAD/proteasome axis is protective for $Rh1^{P37H}$ PNs. These experiments further suggest that excessive retrotranslocation and/or proteasomal degradation of visual pigment cause retinal degeneration.

2.11 Partial VCP inactivation restores visual processing in $Rh1^{P37H}$ flies

The almost complete restoration of mature Rh1 levels in $VCP^{26-8}/+;Rh1^{P37H}/+$ flies prompted us to investigate visual processing in these flies. To assess the capacity of different mutants to process visual information, I performed fast phototaxis measurements (Galy et al., 2005). This analysis reflects the average visual functioning of a fly population and scores the percentage of flies that successfully respond to five consecutive light stimulations. WT flies are normally attracted by light, and the analysis of light responses in different groups of mutants serves as an indicator of their retinal integrity. After 20 dle, I found that $Rh1^{WT}$, $Rh1^{WT}/VCP^{26-8};+/+$ and $VCP^{26-8}/+$ flies display a normal and highly reproducible response to light, i.e. most of these flies move towards the light source (positive phototaxis) in all five consecutive light stimulations (Figure 31A; n=277-451 flies/genotype). In contrast, $Rh1^{P37H}$ flies were seriously impaired in their light processing capability (Figure 31A) and had a significantly lower phototactic score (PS, defined in Materials and Methods) as compared to $Rh1^{WT}$ and control flies (Figure 31B; and in line with the results of Galy et al. [2005]). Remarkably, in $VCP^{26-8}/+;Rh1^{P37H}/+$ flies, positive phototaxis was dramatically improved, consistent with these flies having normal levels of mature Rh1 (Figure 31A,B; see Figure 25B). I obtained similar results after 30 dle (Figure 31C,D).

To confirm these results, I employed the stronger VCP allele VCP^{k15502} and analyzed the visual processing of $VCP^{k15502}/+;Rh1^{P37H}/+$ flies after 20 dle. I found a similar rescue of visual processing in these flies relative to $Rh1^{P37H}$ flies (Figure 31E,F; n=150-200 flies/genotype in 3 independent experiments). Most of the $VCP^{k15502}/+;Rh1^{P37H}/+$ flies reached the tubes 5 and 6 and displayed a higher PS compared to $Rh1^{P37H}$ flies. To rule out that other non-visual related impairments accounted for the performance of $Rh1^{P37H}$ flies in the phototaxis test, I used geotaxis to measure motor functioning in these and all other fly groups, and found that all had a similar motor ability after 20 and 30 dle (Figure 31G-I). This indicated that the differences seen in the phototaxis test are due to differences in visual acuity. Therefore, $Rh1^{P37H}$ -induced blindness is suppressed in a background of reduced VCP activity.

Results

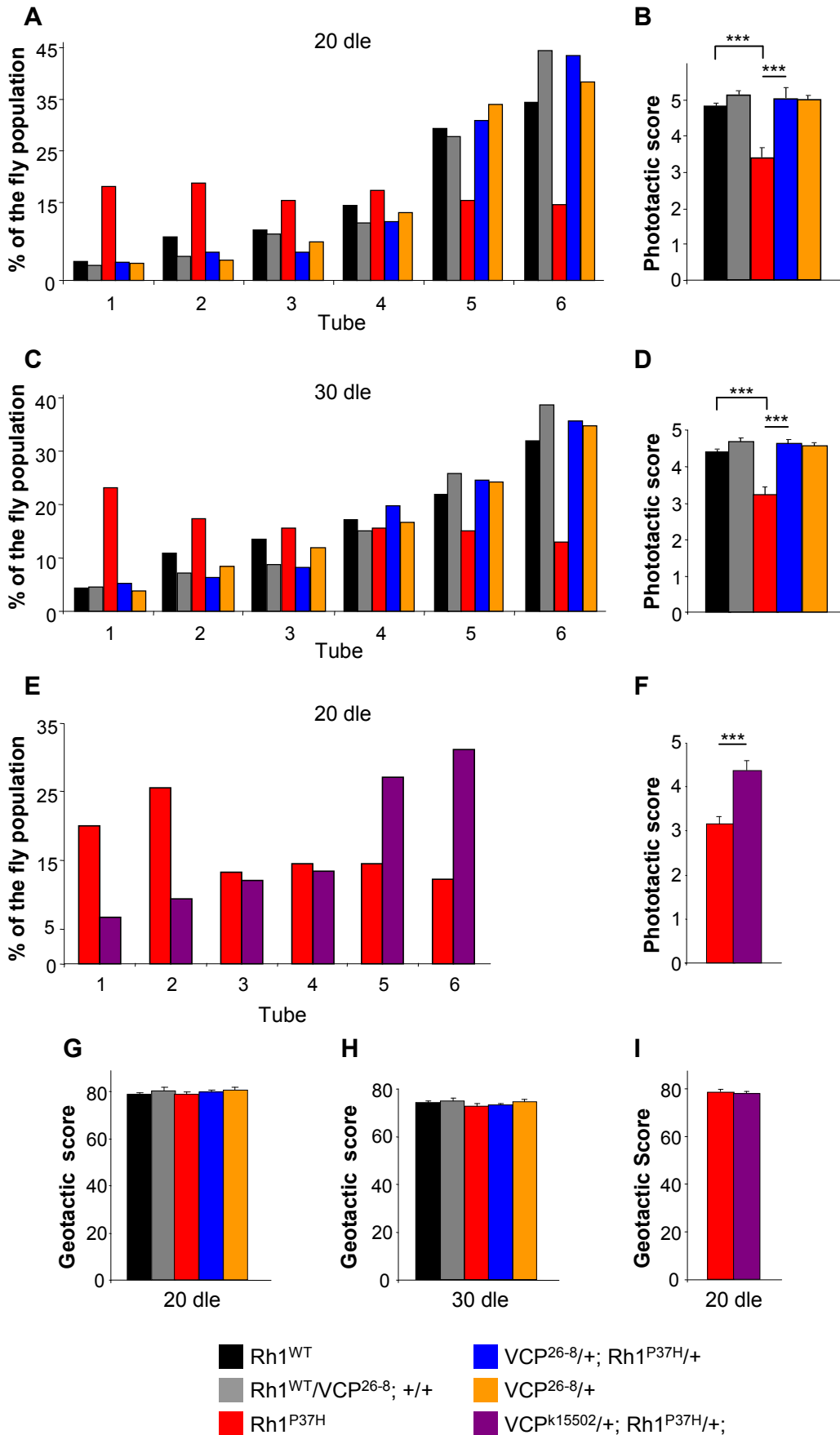


Figure 31. Altered phototaxis in $Rh1^{P37H}$ flies is rescued by VCP loss-of-function alleles. (A,C) Phototaxis histograms after 20 (A) or 30 (C) days of light exposure (dle) revealing the light response of flies of indicated genotypes. (B,D) Phototactic scores (PS) after 20 (B) or 30 (D) dle reveal impairment of light response in $Rh1^{P37H}$ flies and rescue after decreasing VCP function (n=277-451 flies/genotype, in 3 independent experiments, *** p<0.001 Student's t-test). (E) Phototaxis histogram after 20 dle revealing the light response of flies of indicated genotypes. While $Rh1^{P37H}$ flies show visual impairment, $VCP^{k15502/+}; Rh1^{P37H}/+$ flies have an improved visual acuity. (F) Phototactic score (PS) of $Rh1^{P37H}$ and $VCP^{k15502/+}; Rh1^{P37H}/+$ flies after 20 dle (n=150-200 flies/genotype in 3 independent experiments, *** p<0.001 Student's t-test). (G,H,I) No differences in motor performance in mutant vs. control flies chronically exposed to light. Geotactic score of flies of indicated genotypes after 20 (G,I) or 30 (H) dle. Flies from all genotypes display similar geotactic scores after 20 and 30 dle.

2.12 Blindness in $Rh1^{P37H}$ flies is rescued in a VCP hypomorphic background

Partial VCP inactivation in the $Rh1^{P37H}$ retina led to i) a strong suppression of retinal degeneration, ii) to a complete restoration of the mature Rh1 levels and iii) to a strong recovery of visual acuity, as assessed behaviourally. To complement these observations, we searched for more direct evidence of visual recovery in our $VCP^{26-8/+}; Rh1^{P37H}/+$ flies. Analysis of PN depolarization after light stimulation using electroretinogram (ERG) measurements is a common clinical test to detect alterations in retinal processing (Paskowitz et al., 2006). Similarly, ERG measurements are employed on animal models of RP, to assess the severity of the retinal pathology (Humphries et al., 1997; Wang and Montell, 2007). In collaboration with Dr. Michel Roux from IGBMC Strasbourg, I performed ERG measurements on our different groups of flies.

We determined that, in contrast to $Rh1^{WT}$, $Rh1^{WT}/VCP^{26-8}; +/+$ and $VCP^{26-8}/+$ retinas which displayed a normal photoreceptor depolarization following light stimulation, $Rh1^{P37H}$ photoreceptors had a decreased amplitude of photoreceptor depolarization (Plateau), both after 30 and 45 dle, reflecting their defective phototransduction (Figure 32; n=12-20 flies/genotype; -6.74 mV in $Rh1^{P37H}$ flies vs. -9 mV in $Rh1^{WT}$ flies, ** p<0.01 after 30 dle and -5.4 mV in $Rh1^{P37H}$ flies vs. -7 mV in $Rh1^{WT}$ flies, ** p<0.01 Student's t-test after 45 dle).

In contrast, light processing in $VCP^{26-8}/+; Rh1^{P37H}/+$ photoreceptors was largely rescued, the ERG amplitude values for these flies reaching control levels, both after 30 dle (Figure 32A,B; -6.74 mV in $Rh1^{P37H}$ flies vs. -8.57 mV in $VCP^{26-8}/+; Rh1^{P37H}/+$ flies, * p<0.05 Student's t-test) and after 45 dle (Figure 32C,D; -5.4 mV in $Rh1^{P37H}$ flies vs. -6.93 mV in $VCP^{26-8}/+; Rh1^{P37H}/+$ flies, * p<0.05 Student's t-test). Thus, the deleterious effects of mutant $Rh1^{P37H}$ on light transduction and photoreceptor depolarization are almost completely suppressed by inactivating the function of the ERAD effector VCP, suggesting that specific inhibition of VCP function has potential therapeutic significance for Rh^{P23H} -linked RP.

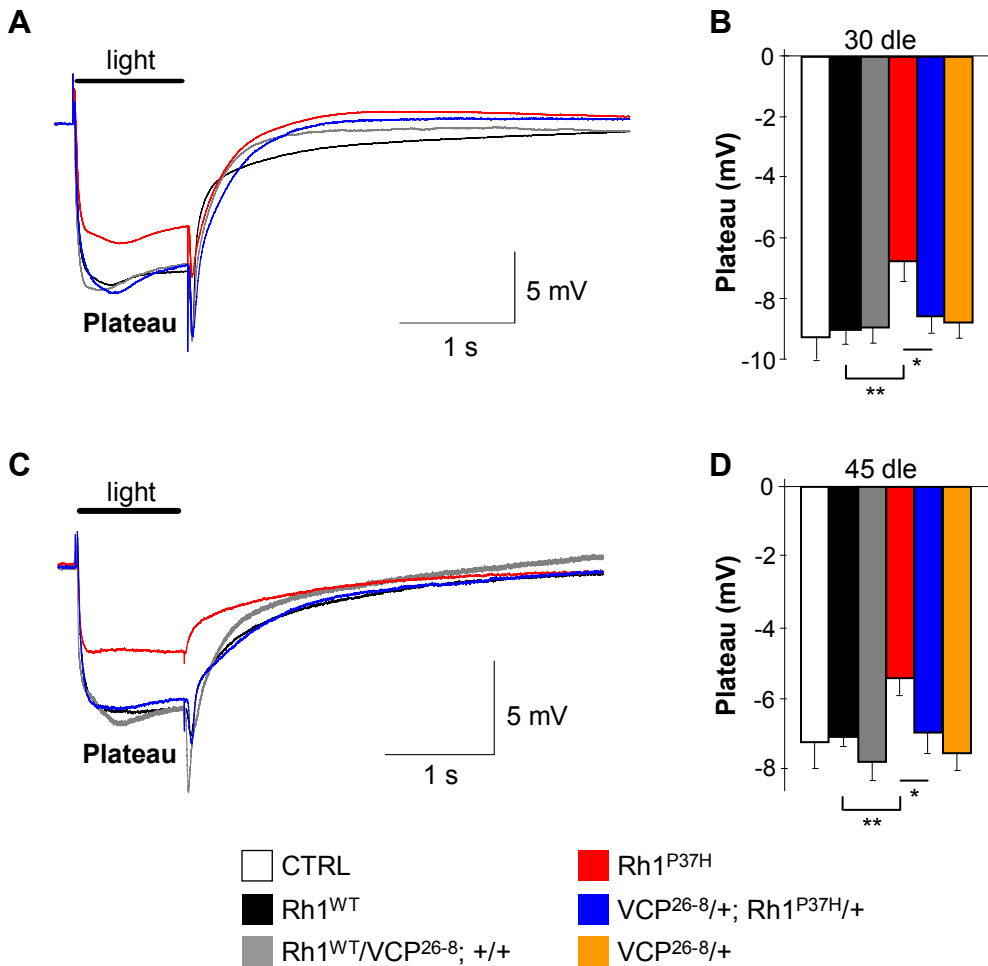


Figure 32. Blindness in *Rh1^{P37H}* flies is rescued in a hypomorphic *VCP²⁶⁻⁸* background. (A,C) ERG after 30 (A) or 45 (C) days of light exposure (dle). Plateau represents photoreceptor depolarization. *Rh1^{P37H}* flies (red tracing) display reduced plateau amplitude, while partial *VCP* inactivation restores their light transduction almost to control levels. Time scale: 1 s and stimulus intensity scale: 5 mV. (B,D) Average depolarization amplitudes after 30 (B) or 45 (D) dle. Impaired light transduction in *Rh1^{P37H}* flies is rescued in a *VCP²⁶⁻⁸* background (n=12-20 flies/group, * p<0.05 and ** p<0.01 Student's t-test).

2.13 *VCP* inactivation rescues the retinal pathology induced by a second class II Rhodopsin mutant, *Rh1^{D1}*

The *Drosophila* experiments presented so far dealt with the P37H *Rh1* mutation, the equivalent of the mammalian P23H Rh mutation. We hypothesized that the rescuing effect after *VCP* inactivation extends to other class II Rh mutations. We therefore decided to investigate the effect of *VCP* inactivation on another class II type mutant, *Rh1^{S137F}* (*Rh1^{S137F}/Rh1⁺* hereafter referred to as *Rh1^{D1}*). The *Rh1^{D1}* allele (generated by EMS-induced mutagenesis) leads to retinal degeneration and to a progressive decline in visual acuity; mutant *Rh1^{D1}* accumulates in the ER and impairs the maturation of the endogenous *Rh1* (Kurada and O'Tousa, 1995). I generated and assayed the retinal integrity of WT, *Rh1^{D1}* (genotype: *+/+; Rh1^{D1}/+*, in short *Rh1^{D1}*) and *VCP^{26-8/+; Rh1^{D1}/+}* flies after 30 dle.

I found that *Rh1^{D1}* retinas underwent degeneration and displayed only 3.75 photoreceptors on average after 30 dle. In WT flies the retinal degeneration was very mild, and 6.0

photoreceptors were preserved in average ($n>6$ eyes/genotype and at least 150 ommatidia were analyzed/eye; *** $p<0.001$ Student's t-test) (Figure 33A,B,D). Remarkably, partial genetic inactivation of *VCP* activity partially suppressed the loss of PNs in the *Rh1^{D1}* retina, as 5.12 photoreceptors were left on average in the *VCP^{26-8/+;Rh1^{D1/+}}* retina (3.75 P/O in *Rh1^{D1}* flies vs. 5.12 P/O in *VCP^{26-8/+;Rh1^{D1/+}}* flies, ** $p<0.01$ Student's t-test) (Figure 33B-D). Thus *VCP* inactivation leads to rescue of retinal degeneration induced by another class II *Rh1* allele, *Rh1^{D1}*.

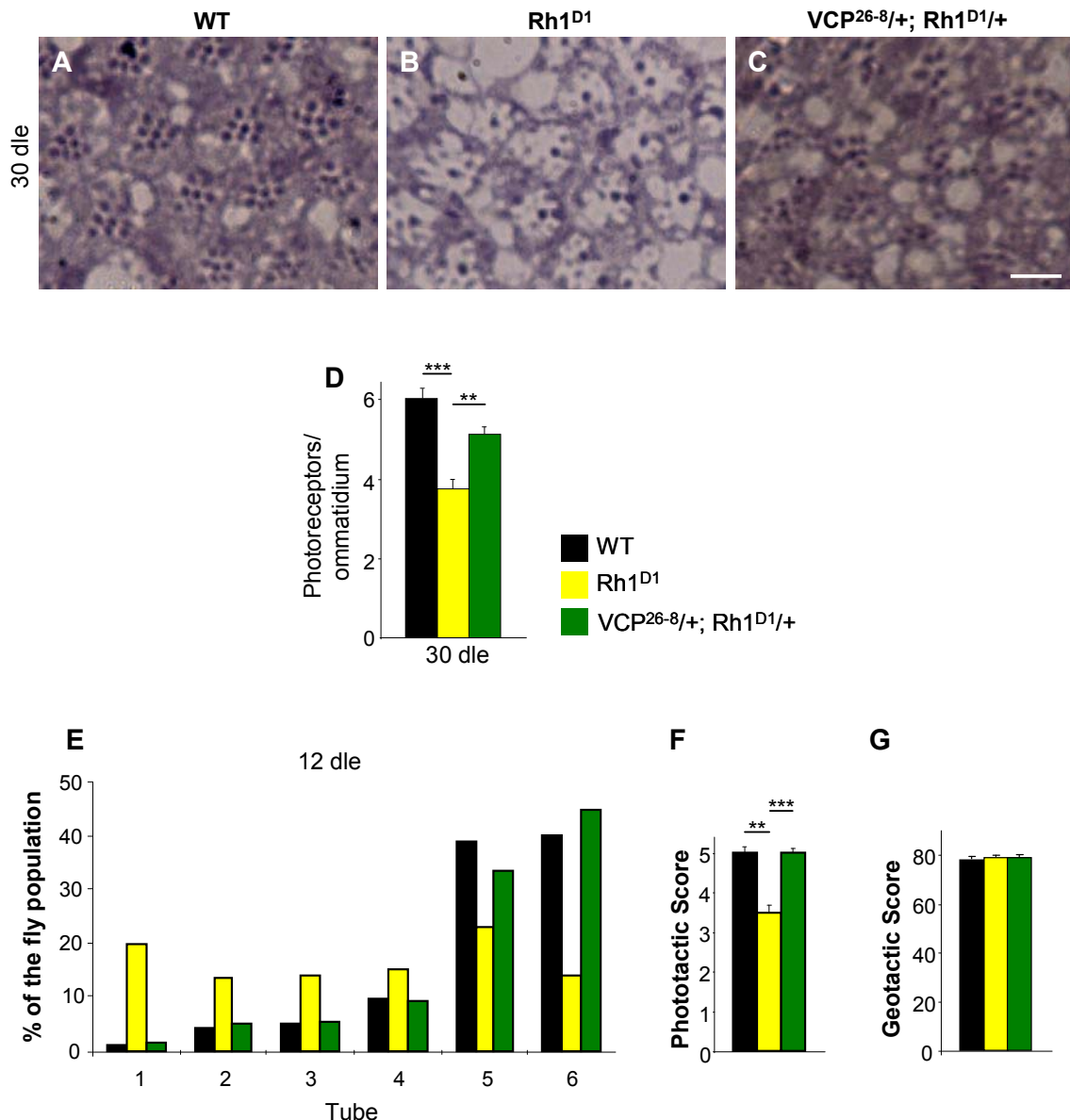


Figure 33. Rescue of *Rh1^{D1}*-induced retinal degeneration and visual impairment by *VCP²⁶⁻⁸*. (A-C) Photomicrographs of toluidine blue-stained semithin eye sections of WT (A), *Rh1^{D1}* (genotype: $+/+$; *Rh1^{D1/+}*) (B), *VCP^{26-8/+;Rh1^{D1/+}}* (C) flies after 30 days of light exposure (dle). Scale bar is 50 μ m. (D) Quantification of average number of photoreceptors/ommatidium (P/O) ($n>6$ animals/group, ** $p<0.01$ and *** $p<0.001$ Student's t-test). Decreasing *VCP* function suppresses retinal degeneration caused by *Rh1^{D1}*. (E) Phototaxis histogram after 12 dle revealing the light response of flies of indicated genotypes. *Rh1^{D1}* flies show visual impairment relative to WT flies, while *VCP^{26-8/+;Rh1^{D1/+}}* flies display a rescue of visual acuity. Between 250-300 flies were scored/genotype, in 3 independent experiments. (F) PS of WT, *Rh1^{D1}* and *VCP^{26-8/+;Rh1^{D1/+}}* flies after 12 dle ($n=250-300$ flies/group, ** $p<0.01$ and *** $p<0.001$ Student's t-test). (G) Geotactic score of WT, *Rh1^{D1}* and *VCP^{26-8/+;Rh1^{D1/+}}* flies after 12 dle. Flies from all genotypes display similar geotactic scores.

Results

We next tested whether the partial inactivation of *VCP* also rescued the progressive blindness in *Rh1^{D1}* flies. I performed phototaxis experiments and found that, after 12 dle, *Rh1^{D1}* flies have a seriously impaired visual acuity (Figure 33E). *Rh1^{D1}* flies displayed a significantly lower phototactic score as compared to WT flies (Figure 33F), in line with previous observations (Kurada and O'Tousa, 1995). As expected, positive phototaxis was significantly improved in *VCP^{26-8/+;Rh1^{D1}/+}* flies (Figure 33E,F) relative to *Rh1^{D1}* flies (n=250-300 flies/group, ** p<0.01 and *** p<0.001 Student's t-test), consistent with these flies having rescued retinal morphology.

To exclude that other non-visual related defects accounted for the performance of *Rh1^{D1}* flies in the phototaxis test, I used geotaxis to measure motor abilities in these fly groups. I found that all groups had a similar motor ability after 12 dle (Figure 33G). Therefore, partial *VCP* inactivation rescues *Rh1^{D1}*-induced blindness.

In summary, the excessive retrotranslocation and/or proteasomal degradation of visual pigment, mediated by the VCP/ERAD/proteasome axis might cause RP. Inhibition of this axis potently suppressed the retinal degeneration and blindness induced by misfolded *Rh1^{P37H}* in *Drosophila*.

Collectively, the results presented in this thesis suggest that inhibition of the VCP/ERAD/proteasome axis might prevent vision loss in RP patients carrying *Rh^{P23H}* mutations.

III. DISCUSSION

Discussion

The mechanisms underlying degeneration of photoreceptor neurons in RP are incompletely understood. Although several symptomatic therapies for RP exist, none of them is able to prevent or cure RP, suggesting that a better understanding of the molecular mechanisms regulating maintenance and degeneration of PNs is needed in order to successfully fight against RP.

The most common mutation linked to RP in North America is the substitution of proline 23 by histidine (Rh^{P23H}). Unlike WT Rh, mutant Rh^{P23H} displays folding defects, is retained within the ER and is subsequently cleared by the proteasome. Mutant Rh^{P23H} recruits the WT Rh into aggregates and might thus impair its trafficking through the secretory pathway (dominant-negative effect). Misfolded Rh^{P23H} might also exert toxic effects in the cell, by inhibiting the proteasome, by altering the cellular transport of other proteins or by activating ER stress pathways (gain-of-function effects). Despite extensive research, the molecular mechanisms that link mutant Rh^{P23H} to retinal degeneration in RP remain elusive.

The present work identifies the ERAD effector VCP as a critical regulator of Rh^{P23H} retrotranslocation and proteasomal clearance. VCP co-localizes and interacts with misfolded Rh^{P23H} in mammalian cell cultures and uses its D2 ATPase domain to promote the extraction of Rh^{P23H} from the ER and its delivery to the proteasome. Using *Drosophila* genetics, I provide the first evidence that VCP is required *in vivo* for clearance of misfolded Rh1. Partial inactivation of *VCP* exerts a strong suppressing effect on the retinal pathology triggered by misfolded $Rh1^{P37H}$ in *Drosophila*. Histological, behavioural and electrophysiological measurements confirm the rescue of retinal degeneration and visual recovery in $Rh1^{P37H}$ -expressing flies with decreased *VCP* function. Despite this dramatic improvement in visual function, $Rh1^{P37H}$ flies with decreased *VCP* function display higher levels of Rh1-containing aggregates and increased activation of the Ire1/Xbp1 UPR pathway, suggesting that moderate activation of the Ire1/Xbp1 UPR branch might exert protective effects in the retina. Finally, pharmacological inhibition of the VCP/ERAD/proteasome axis in $Rh1^{P37H}$ flies, using the VCP/ERAD inhibitor EerI or the proteasome inhibitor MG13, also exerts a powerful rescuing effect on $Rh1^{P37H}$ -mediated retinal pathology.

Taken together, these results indicate that excessive VCP activity, leading to enhanced retrotranslocation and/or proteasomal degradation of visual pigment might cause RP. Our results suggest that selective inhibition of the VCP/ERAD/proteasome axis might prevent vision loss in RP patients carrying Rh^{P23H} mutations.

1. The ERAD effector VCP co-localizes and interacts with misfolded Rh *in vitro*

Using mammalian cell cultures in which misfolded Rh^{P23H} (or Rh^{WT} as control) was transfected, we found that class II mutant Rh^{P23H} forms aggregates that co-localize and form a complex with the ERAD effector VCP (Figures 13-15 and 18).

Misfolded Rh^{P23H} aggregates showed a partial co-localization with the ER marker Calnexin and with VCP, further confirming that they were localized in the ER. These findings parallel previous studies in which misfolded Rh^{P23H} localized to the ER (Galy et al., 2005; Mendes and Cheetham, 2008; Saliba et al., 2002). Interestingly, we also observed that, in these cells transfected with Rh^{P23H}, some of the Rh-containing cytoplasmic aggregates did not co-localize with the ER marker or with VCP (Figures 13 and 18). We suggest that these species represent misfolded Rh^{P23H} that was extracted from the ER (probably by VCP) and accumulated in the cytosol.

We also followed the subcellular localization of VCP in cells transfected with either WT or P23H Rh. While the localization of endogenous VCP is mainly nuclear in cells transfected with Rh^{WT}, VCP is localized to the ER in cells expressing mutant Rh^{P23H}. (Figure 13). We believe that the overexpression of misfolded Rh causes VCP to re-localize at the ER membrane, in order to perform its function during ERAD. This hypothesis is supported by another study showing that endogenous VCP displays diffuse distribution in the cytosol and nuclei in U2OS cells transfected with empty vector, while co-expression with the ubiquitin ligase gp78 (a VCP-interacting partner in ERAD) mediates re-localization of VCP from the cytosol to the ER membrane (Ballar et al., 2006).

In cells transfected with Rh^{P23H}, we found the endogenous VCP in a complex with Rh^{P23H} aggregates (Figures 14 and 15). These Rh^{P23H} aggregates were polyubiquitinated, suggesting that they were destined for proteasomal delivery. Interestingly, we found that VCP has a broader role in binding to HMW aggregates, as polyubiquitinated aggregates devoid of Rh were also in complex with VCP (Figure 14). These results do not rule out, however, that VCP itself might be ubiquitinated, and additional studies could address this possibility. Emerging evidence suggest that VCP interacts with various cellular aggregates; thus, VCP co-localizes with Ataxin-3 and TDP-43 containing neuronal inclusions (Boeddrich et al., 2006; Gitcho et al., 2009), and with ubiquitin-positive intraneuronal aggregates in Alzheimer's and Parkinson's diseases (Mizuno et al., 2003). These observations raise the possibility that VCP plays an important role in aggregate clearance in different neuronal populations and has a broader role in aggregate recognition that extends beyond misfolded Rh.

Transfection with Rh^{P23H} led to aggregate formation, but also to a pool of mature Rh^{P23H}, that passed beyond the Golgi apparatus and probably reached the plasma membrane. However, we observed no interaction between the mature form of Rh^{P23H} and VCP (Figure 14), suggesting that only misfolded and immature Rh is a substrate of VCP. In contrast to VCP, another ERAD effector, EDEM1, interacts with both mature and misfolded Rh (Kosmaoglou et al., 2009). EDEM1 appears thus to have a dual function in Rh processing, participating in both the correct folding and the enhanced degradation of Rh. The differences between these ERAD effectors can be due to the fact that VCP is a cytoplasmic ERAD effector required for retrotranslocation of misfolded proteins (Vembar and Brodsky, 2008), while EDEM1 is localized in the ER lumen; in the ER lumen, EDEM1 can enhance the release of misfolded glycoproteins (e.g. Rhodopsin) from the

Calnexin/Calreticulin cycle and their demannosylation, thereby promoting ERAD (Hebert and Molinari, 2007).

We observed that the co-localization and the interaction between VCP and Rh^{P23H}-containing aggregates are enhanced after proteasome inhibition (Figures 13 and 15). Proteasome inhibition increased the levels of Rh^{P23H} aggregates, in agreement with the involvement of the proteasome in the clearance of misfolded Rh^{P23H}. Increased levels of misfolded Rh^{P23H} could therefore lead to enhanced interaction between Rh^{P23H} and VCP; VCP might interact with two species of misfolded Rh^{P23H}: both the ER-localized Rh (before retrotranslocation) and the cytosolic Rh (after retrotranslocation). These results are similar to those obtained in another study where the interaction between VCP and CFTR was found to be increased after proteasome inactivation (Goldstein et al., 2007).

Why would the co-localization between mutant Rh^{P23H} and VCP be increased upon proteasome inactivation? Retrotranslocation of some ERAD candidates is inhibited upon proteasome inactivation, showing that retrotranslocation and degradation are coupled events (Chillaron and Haas, 2000; Mancini et al., 2000). The proteasome has also been suggested to participate in the retrotranslocation of mutant Rh (Saliba et al., 2002). It is thus possible that in the presence of an active UPS, VCP co-localizes with misfolded Rh only transiently due to the fact that it extracts the misfolded Rh and delivers it right away to the proteasome for degradation. Under baseline conditions, the co-localization between VCP and misfolded Rh would be only partial and transient. When the proteasome is inhibited, an increased load of ER-based Rh aggregates would result in the accumulation of ER membrane-associated VCP, which senses misfolded Rh. VCP might stay attached to the ER membrane given the difficulty of delivering Rh to the impaired proteasome. An enhanced interaction between an ERAD effector (Ubiquilin) and an ER membrane protein (Erasin) was also observed upon proteasome inhibition; Erasin serves as a platform for recruiting cytoplasmic VCP and Ubiquilin to the ER, thereby allowing the formation of the ERAD complex (Liang et al., 2006; Lim et al., 2009). Thus, proteasome inhibition might lead to intensive recruitment of cytoplasmic ERAD effectors (e.g. VCP, Ubiquilin) to the site of ERAD retrotranslocation, and might explain the enhanced interaction between VCP and misfolded substrates like Rh^{P23H}.

We found that cells transfected with Rh^{WT} also displayed some intracellular Rh aggregates (Figures 13, 14 and 18). We believe this effect is due to overexpression, and has been previously observed with Rh^{WT} (Illing et al., 2002). Rh^{WT}-containing aggregates were also found to co-IP with VCP (Figure 14), further confirming the capacity of VCP to interact with HMW aggregates. Interestingly, proteasome inhibition also increased the levels of Rh^{WT} aggregates, suggesting that Rh^{WT} is also a substrate of the proteasome. Indeed, WT Rh is known to undergo repeated cycles of internalization-degradation during visual processing (Satoh and Ready, 2005), and proteasomal degradation is probably one/the pathway that mediates Rh^{WT} degradation during this process. In their study, Cheetham and colleagues found nonetheless that proteasome inhibition did not affect the processing of Rh^{WT}, nor led to formation of Rh^{WT}-containing cytoplasmic aggregates (Saliba et al., 2002). Although the effects they observed were not quantified, one possibility for this discrepancy is the level of Rh^{WT} expression achieved after transfection. Cheetham and colleagues might have achieved lower levels of Rh expression which prevented the formation of aggregates after proteasome inhibition. Another difference is that Cheetham et al. performed transfections in kidney COS7 cell line, while our experiments were performed in retinal and neuroblastoma cell lines.

Discussion

To determine the structural requirements of VCP for its interaction with misfolded Rh, we analyzed the binding capacity of truncated VCP versions. We found that the N and D2 domains of VCP were dispensable for the interaction with Rh^{P23H} aggregates, while D1 and D1D2 domains were required for binding, indicating that the D1 ATPase domain of VCP is necessary for its interaction with aggregates (Figure 16). The D1 ATPase domain of VCP was previously shown to be required for VCP to form its hexameric and catalytically active structure (Wang et al., 2003); thus, a proper VCP oligomeric structure is not only required for substrate processing but might also be involved in substrate recognition. Our findings are in agreement with another study in which the D1 domain of VCP was found to be required for binding to Luciferase aggregates (Song et al., 2007). While the D1 domain of VCP is required for interaction with Rh^{P23H} aggregates, it alone was not sufficient to allow maximal interaction (i.e. the same binding capacity as WT VCP) with Rh aggregates. We found that the presence of both the D1 ATPase and N-terminal domains of VCP is required for maximal interaction between VCP and Rh^{P23H} aggregates. The N-terminal domain of VCP is known to recruit the Ufd1–Npl4 adaptor complex, which recognizes and binds misfolded proteins destined for ERAD (Meyer et al., 2002; Ye et al., 2003). Therefore, the presence of the Ufd1–Npl4 adaptor complex is required for maximal interaction between VCP and misfolded Rh. Taken together, these results suggest that both a proper higher-order structure and access to aggregate-bound adaptors are needed for VCP to exert its functions during ERAD.

2. VCP is required for clearance of misfolded Rh *in vitro* and *in vivo*

Class II mutant Rh^{P23H} forms insoluble aggregates in the ER (Mendes and Cheetham, 2008; Sung et al., 1991b) and impairs the proteasome (Illing et al., 2002), however, the mechanisms that allow exit of misfolded Rh from the ER and proteasome targeting remained unclear. Since misfolded Rh^{P23H} co-localized and interacted with VCP, we hypothesized that misfolded Rh^{P23H} is a substrate of VCP during ERAD.

We found that VCP is required for the degradation of Rh^{P23H} aggregates *in vitro*, since decreasing VCP activity using siRNA strongly impaired the clearance of misfolded Rh (Figure 17). Conversely, when VCP was overexpressed in cells expressing Rh^{P23H}, a dose-dependent reduction in Rh aggregates was observed, indicating that VCP is sufficient to promote degradation of Rh aggregates (Figure 17). These results suggest that VCP is both required and sufficient to promote the degradation of Rh^{P23H}-containing aggregates.

Previous studies suggested that VCP uses ATP hydrolysis via its D2 ATPase domain to promote substrate retrotranslocation from the ER to the cytosol and delivery to the proteasome (DeLaBarre et al., 2006; Song et al., 2003). The K524A mutation in the D2 domain of VCP was shown to abolish the ATPase activity associated with this domain and to induce accumulation of misfolded ΔF508-CFTR (Kobayashi et al., 2002), whereas the R155H mutation in the N-terminal domain of VCP did not impair the ATPase activity (Weihl et al., 2006). In cells transfected with WT or P23H Rh and with several VCP constructs, we found that overexpression of WT and N-terminal R155H mutant VCP effectively reduced Rh aggregate load; in contrast, overexpression of D2 ATPase deficient K524A VCP failed to do so (Figures 18 and 19). VCP^{K524A} transfection led to high levels of Rh^{WT}- and Rh^{P23H}-containing aggregates, and to extensive co-localization between these aggregates and the ER marker Calnexin, or the VCP^{K524A} (Figure 18). This suggests that inhibition of VCP D2 ATPase activity impairs the clearance of both Rh^{WT} and misfolded Rh^{P23H}. Thus, the D2 domain-associated ATPase activity of VCP is

dispensable for its interaction with Rh aggregates, yet appears to be specifically required for their clearance and proper delivery to the proteasome for degradation. Hence, we suggest that the D2 ATPase activity of VCP is the driving force for retrotranslocation and proteasomal delivery of misfolded Rh^{P23H} during ERAD.

The observation that the VCP^{R155H} mutant, in contrast to VCP^{K524A}, did not impair the clearance of misfolded Rh is interesting. Patients carrying *VCP*^{R155H} mutant alleles display severe myopathy caused by enhanced accumulation of ubiquitinated aggregates (Kimonis et al., 2008), highlighting the crucial role played by VCP in the clearance of misfolded proteins in the muscle. Expression of the VCP^{R155H} variant also prevented the ERAD of misfolded ΔF508-CFTR (Weihl et al., 2006). Our results indicating that expression of VCP^{R155H} did not impair the clearance of Rh^{P23H} suggest that this N-terminally situated residue might be involved in the clearance of specific protein substrates (probably involving defined sets of interactors). In agreement with this interpretation, one study found that the VCP^{R155H} variant did not cause an increase in the overall level of ubiquitin-conjugated proteins (Hubbers et al., 2007), suggesting that R155H mutation is not sufficient to impair the function of VCP during ERAD. A better understanding of the molecular interactions involved in the ERAD of the different VCP substrates will hopefully provide new insights into the pathobiology of VCP.

VCP mutants that have reduced basal ATPase activity often exhibit reduced ERAD (DeLaBarre et al., 2006; Kobayashi et al., 2002). However, the converse did not always turn out to be true, i.e. some VCP variants have optimal ATPase activity but decreased capacity to mediate ERAD. Coordinated ATP hydrolysis and substrate binding are both necessary to dislocate misfolded substrates during ERAD, and DeLaBarre et al. found that certain residues situated within the D2 pore of VCP are essential for substrate interaction and subsequently for ERAD; this raises the possibility that the interactions involving these residues facilitate substrate dislocation (DeLaBarre et al., 2006; Halawani and Latterich, 2006). Our work showed that VCP D2 ATPase activity is required for retrotranslocation of misfolded Rh. However, it is possible that other residues of VCP (including the ones situated in the D2 pore) are required for optimal retrotranslocation of misfolded Rh. Future studies could therefore investigate whether the interaction between misfolded Rh and the VCP D2 pore is required for Rh retrotranslocation.

Is VCP required *in vivo* for the degradation of misfolded Rh, similar to the situation in mammalian cell cultures? To address this possibility, we used *Drosophila* mutants that overexpressed either WT or P37H (the fly equivalent of mammalian P23H) Rh1 in PNs, under the control of the endogenous *Rh1* promoter (Galy et al., 2005). The ectopic protein (either WT or P37H Rh1) was tagged with hsv, to allow the distinction between endogenous and transgenic Rh1. We used two *LOF* alleles of *VCP* to achieve a decrease in VCP levels and activity in flies expressing Rh1. Reducing VCP levels in the fly led to an increase of both WT and mutant P37H Rh1-containing aggregates (Figure 24). These observations suggest that VCP functions as an ERAD effector to clear misfolded Rh1 *in vivo*.

Why is there an increased level of endogenous Rh1^{WT} containing aggregates in control flies with decreased *VCP* function? One explanation for this observation is the trafficking of the endogenous Rh1, which is known to undergo repeated cycles of endocytosis and degradation during visual processing (Satoh and Ready, 2005). It remains therefore possible that the light-induced degradation of Rh1^{WT} proceeds via ERAD, and that VCP is involved in the retrotranslocation and the degradation of mature Rh1 in each visual cycle.

Discussion

A second possibility is that VCP is involved in alternative degradation processes, and that Rh1^{WT} is degraded via an alternative mechanism, which is also VCP-dependent. Recent evidence (Ju et al., 2009; Tresse et al., 2010) suggests that VCP is also a mediator of autophagy, a process that involves the lysosomes (Kirkin et al., 2009). Further studies will determine whether WT and P37H Rh1 are degraded by autophagy and whether VCP is implicated in this process.

After determining how VCP interacts with and extracts Rh1 aggregates from the ER, we sought to determine whether the degradation of misfolded Rh proceeds via the proteasome. To test this possibility, we inhibited the proteasome in cells transfected with mutant Rh^{P23H} and with increasing amounts of VCP. While in the absence of proteasome inhibitor VCP mediated a dose-dependent reduction in misfolded Rh, proteasome inhibition blocked the degradation of misfolded Rh (Figure 17). A previous study also found that the proteasome was required for efficient degradation of misfolded Rh (Saliba et al., 2002). The study by Saliba et al. also suggested that the proteasome is implicated in the retrotranslocation of misfolded Rh from the ER (Saliba et al., 2002) and independent evidence also supports this possibility (Chillaron and Haas, 2000; Mancini et al., 2000). Therefore, besides protein clearance, the proteasome might also participate in the retrotranslocation of misfolded substrates. It would be interesting to determine whether VCP cooperates with the proteasome to promote retrotranslocation of misfolded proteins.

Our findings that misfolded Rh^{P23H} is an ERAD substrate are in agreement with two very recent studies that found Rh to be a substrate of other ERAD effectors. The first study reported that mutant Rh is a substrate of the ERAD effector E3 ubiquitin ligase Hrd1 (Ray-Sinha et al., 2009). The second study found that EDEM1 (also a member of the ERAD machinery) promotes degradation of Rh^{P23H} and decreases its aggregation. Similarly to our VCP knock-down, shRNA-mediated knock-down of EDEM1 in cell cultures increased the amount of Rh^{P23H}-containing aggregates (Kosmaoglou et al., 2009). Collectively, these recent studies and our current study establish that misfolded Rh is an ERAD substrate and is submitted to a selective degradation process, in order to limit its toxicity.

The above observations allow the establishment of a working model for the ERAD of misfolded Rh (see Figure 34). Misfolded Rh might first be subjected to the Calnexin/Calreticulin refolding cycle, although the molecular details of this process are still lacking. While *Drosophila* Calnexin is required for Rh1 maturation (Rosenbaum et al., 2006), mammalian Rh biogenesis does not appear to have an absolute requirement for Calnexin (Kosmaoglou and Cheetham, 2008); therefore, the identity and role of the other enzymes in Rh folding can be evaluated. After the initial refolding cycle (e.g. Calnexin/Calreticulin cycle), misfolded Rh is targeted to the ERAD retrotranslocation site by EDEM1 that facilitates the disposal of glycoproteins from the ER (Kosmaoglou et al., 2009; Olivari et al., 2006).

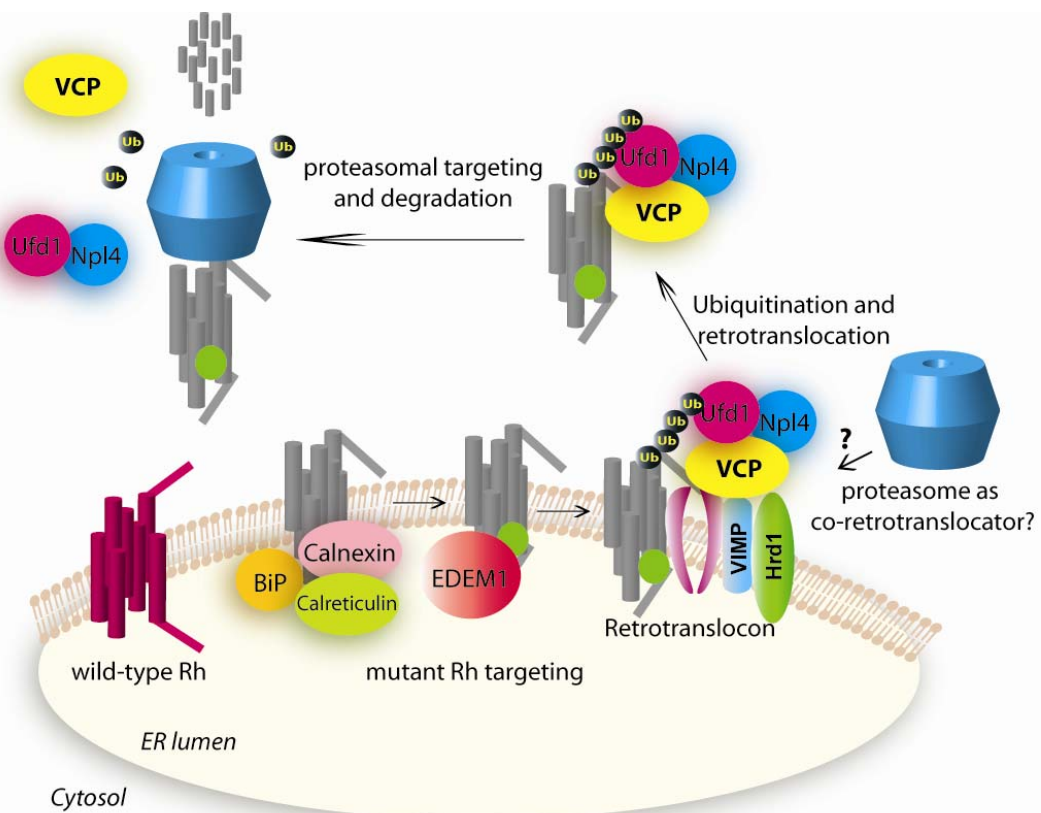


Figure 34. Working model for ERAD of misfolded Rh. Misfolded Rh might be first recognized by ER chaperones (such as BiP, Calnexin/Calreticulin). After failure to refold, misfolded Rh is targeted to the ERAD retrotranslocation site by EDEM1, which facilitates the disposal of glycoproteins from the ER. The ERAD retrotranslocation machinery probably comprises the putative retrotranslocation channel Derlin1, the ER membrane protein VIMP and the E3 ubiquitin ligase Hrd1. Misfolded Rh might be ubiquitinated by the Hrd1 ligase. Then, the cytoplasmic VCP-Ufd1-Npl4 complex is recruited to the retrotranslocation site by the ER membrane protein VIMP or Erasin. Ubiquitinated Rh interacts with the VCP complex and is retrotranslocated into the cytosol. Then, the VCP complex delivers mutant Rh to the proteasome for degradation. Note that the VCP complex and the proteasome could associate transiently at the ERAD retrotranslocation site to promote Rh retrotranslocation and subsequent degradation.

At the ERAD retrotranslocation site, which is probably composed by Derlin1, VIMP and the E3 ubiquitin ligase Hrd1 (Ye et al., 2005), mutant Rh might be ubiquitinated by the Hrd1 ligase (Ray-Sinha et al., 2009). Then, mutant Rh interacts with the cytoplasmic VCP complex and is retrotranslocated into the cytosol. The cytoplasmic VCP complex could be recruited to the ER membrane by VIMP (Ye et al., 2005) or by Erasin (Liang et al., 2006; Lim et al., 2009). Once retrotranslocated, mutant Rh is delivered to the proteasome for degradation; alternatively, the VCP complex and the proteasome temporarily associate to promote Rh retrotranslocation and subsequent degradation. Further studies will determine the molecular details of this process and, in particular, i) whether other E3 ubiquitin ligases (e.g. gp78, Teb4) are necessary for Rh ubiquitination ii) whether the VCP cofactors Ufd1-Npl4 are also required for Rh retrotranslocation, similar to other ERAD substrates (Meyer et al., 2000; Ye, 2006) and iii) whether and how the VCP complex and the proteasome associate/cooperate in promoting Rh retrotranslocation and degradation.

3. Dramatic retinal degeneration and blindness are triggered by misfolded Rh in a light- and age-dependent manner in *Drosophila*

In order to successfully treat Rh^{P23H} -linked RP, a good understanding of the cell death mechanisms triggered by Rh^{P23H} is required. The correlation between Rh aggregates and death is difficult to establish in cell culture systems. Thus, we only observed a minor decrease of cell viability in cells expressing Rh^{P23H} vs. Rh^{WT} and these moderate defects prevented us from analyzing the rescuing effects of VCP manipulation in these systems (Figure 20). In addition, decreasing VCP function by siRNA or by expression of VCP^{K524A} led to a significant decrease in cell viability (Figure 20), presumably via both ERAD-dependent (Hirabayashi et al., 2001; Kobayashi et al., 2002) and independent (e.g. effects on cell proliferation and strong inhibition of NF κ B activation by FGF-2) mechanisms (Vandermoere et al., 2006; Wojcik et al., 2004). Further improvements of the existent cell-based assays appear necessary in order to address the connection between Rh aggregates, VCP function and cell dysfunction *in vitro*. The use of postmitotic neurons (e.g. derived from WT or transgenic mice) might overcome the effects of VCP on cell proliferation and might maintain a high Rh aggregate load in the postmitotic cell, similar to the situation in RP. In addition, a recent study (Mosharov et al., 2009) suggests that postnatal neurons could be maintained in culture, raising the possibility that manipulation of Rh and VCP functions could be addressed in postmitotic and postnatal neurons maintained *in vitro*.

To gain access to the pathogenic mechanisms mediated by misfolded Rh^{P23H} , we used a previously established *Drosophila* model of Rh^{P23H} -linked RP, in which mutant $Rh1^{P37H}$ (the equivalent of mammalian Rh^{P23H}) is expressed in PNs, under the control of a promoter identical to the endogenous $Rh1$ promoter (Galy et al., 2005). $Rh1^{P37H}$ expression leads to a severe light- and age-dependent retinal degeneration and to progressive blindness (Galy et al., 2005).

We first reproduced the previously published retinal pathology in these $Rh1^{P37H}$ flies (Galy et al., 2005). We investigated photoreceptor morphology in $Rh1^{P37H}$ and in $Rh1^{WT}$ flies as a function of age and of light. Rhabdomeres of $Rh1^{P37H}$ flies reared under light conditions showed no sign of photoreceptor degeneration at eclosion (Figure 21). Similarly, $Rh1^{P37H}$ flies reared in the dark did not display a degenerative phenotype, even after 30 days of post-eclosion (Figure 21). However, after 20 days of light exposure, $Rh1^{P37H}$ flies displayed pronounced retinal degeneration, in contrast to $Rh1^{WT}$ flies (Figure 22) and after 30 days of light exposure, the $Rh1^{P37H}$ retina exhibited dramatic retinal degeneration with only 1.7 photoreceptors per ommatidium left on average, compared to 5.5 in $Rh1^{WT}$ (Figure 22). Rh^{P23H} -induced photoreceptor degeneration is associated with progressive blindness (Berson et al., 1991; Dryja et al., 1990) and $Rh1^{P37H}$ was also shown to cause progressive blindness in *Drosophila* (Galy et al., 2005). We analyzed the visual activity of $Rh1^{P37H}$ flies at different ages (Figures 31 and 32) and confirmed that $Rh1^{P37H}$ induces progressive blindness. Thus, $Rh1^{P37H}$ transgenic flies faithfully reproduce the pathological events occurring in ADRP patients that carry the Rh^{P23H} mutation.

The retinal degeneration in $Rh1^{P37H}$ flies has an adult-onset, is progressive, and light- and age-dependent. Similarly, Rh^{P23H} patients and mice carrying mutant Rh^{P23H} present no retinal dysfunction at birth (Berson et al., 1991; Dryja, 1990; Naash et al., 1993; Olsson et al., 1992). In mice, Rh^{P23H} -induced retinal degeneration is also light-sensitive. Rearing Rh^{P23H} mice in the dark slows down, although it does not completely abolish retinal degeneration (Naash et al., 1996); conversely, exposure to bright light accelerates the

Rh^{P23H} -mediated degeneration (Wang et al., 1997). Dark or dim light rearing also slows the rate of retinal degeneration in Rh^{P23H} rats (Organisciak et al., 2003; Walsh et al., 2004), while exposure to bright light accelerates it (Vaughan et al., 2003).

Light appears to be an important risk factor in developing RP. Although it was hypothesized that light deprivation might protect ADRP patients in the earliest stages against retinal degeneration (Berson, 1971), no benefit of light deprivation has been convincingly demonstrated in patients with RP (Berson, 1980; Miyake et al., 1990). One drawback of these studies is that the numbers of patients that were tested were very small and they were genetically heterogenous (Paskowitz et al., 2006). It remains therefore possible that light deprivation might slow down retinal degeneration in patients carrying $P23H$ mutations, similar to the above mentioned results in rodents and flies.

Why and how does light accelerate neurodegeneration in $Rh1^{P37H}$ flies? Classical studies performed by Kurada and O'Tousa showed that class II $Rh1$ fly mutants ($Rh1^{D1}/Rh1^+$ and $Rh1^{D2}/Rh1^+$), similar to $Rh1^{P37H}$ flies, suffer of age- and light-dependent retinal degeneration and that light enhances the rate of degeneration in these flies (Kurada and O'Tousa, 1995). However, up to now, no clear explanation exists to explain why the class II type mutant Rh1-expressing photoreceptors are more sensitive to light. Several possibilities might explain the increased vulnerability of Rh^{P23H} photoreceptors following light exposure. First, genetically defective photoreceptors could be abnormally sensitive to photo-oxidation/oxidative stress following exposure to light (Organisciak et al., 2003). Second, mutant Rh may cause abnormalities in phototransduction. ERG analyses of Rh^{P23H} patients and mice have suggested that the lifetime of activated Rh is prolonged, although it could not be determined whether these species represented mutant Rh, WT Rh, or both (Birch et al., 1995; Goto et al., 1996). Moreover, Rh^{P23H} mice lacking Transducin showed slower retinal degeneration, suggesting that excessive phototransduction might cause retinal degeneration (Samardzija et al., 2006). In contrast, $Rh1^{P37H}$ was shown to properly activate the visual cascade, suggesting that abnormal phototransduction is not the cause of $Rh1^{P37H}$ photoreceptor sensitivity to light. Third, misfolded Rh destabilises outer segment discs, leading to excessive shedding in response to light, which may contribute to photoreceptor stress and eventual death (Berson, 1996). Fourth, light might impact on photoreceptors already stressed by the effects of a mutation (e.g. $Rh1^{P37H}$) by accelerating the cycling of Rh which undergoes repeated cycles of endocytosis and degradation during visual processing (Kiselev et al., 2000; Satoh and Ready, 2005).

In summary, the interaction between Rh misfolding, aging and light exposure triggers a RP-like phenotype in *Drosophila*.

4. Endogenous Rh^{WT} is recruited by misfolded Rh into aggregates

Misfolded Rh^{P23H} might cause photoreceptor neuron degeneration via two major routes. First, Rh^{P23H} is able to recruit the endogenous WT Rh into the ER (dominant-negative effect) and thereby affects the maturation of WT Rh (Colley et al., 1995; Kurada and O'Tousa, 1995; Kurada et al., 1998; Rajan and Kopito, 2005; Saliba et al., 2002). Second, the mutant Rh^{P23H} might acquire novel properties (gain-of-function mechanism) that could include: aggregate formation in the ER or inclusion formation in the cytosol; generation of ER stress and activation of the UPR pathways; other toxic effects on diverse cellular processes (Galy et al., 2005; Lin et al., 2007; Mendes et al., 2005; Ryoo et al., 2007; Saliba et al., 2002). Therefore, a better understanding of the cellular and molecular

Discussion

mechanisms mediating dominance in Rh^{P23H} -linked RP is required for the development of effective therapies (Mendes et al., 2005). We found that in $Rh1^{P37H}$ flies the endogenous WT Rh1 gets recruited into high molecular weight aggregates (Figure 22I). Despite this recruitment, lack of mature Rh1 is not the cause of PN degeneration (Figure 22J)

4.1 Misfolded $Rh1^{P37H}$ forms aggregates in *Drosophila*

To separately follow the fate of the endogenous vs. ectopic Rh1, the mutant $Rh1^{P37H}$ was hsv-tagged; moreover, we monitored the expression pattern of the mature (soluble) vs. aggregated (insoluble) forms of Rh1 during time. We found that loss of mature Rh1 (endogenous and ectopic) parallels the loss of PNs, and is very pronounced after 20 dle in $Rh1^{P37H}$ flies, but not in $Rh1^{WT}$ flies (Figure 22). We also assessed the situation of insoluble Rh1-containing species and found a significant increase in Rh1-containing aggregates in both $Rh1^{WT}$ and $Rh1^{P37H}$ flies after 20 dle (Figure 22). Remarkably, hsv labeling was absent in the insoluble fraction from $Rh1^{P37H}$, but not in $Rh1^{WT}$ flies indicating that endogenous Rh1 is the major component of insoluble aggregates in the $Rh1^{P37H}$ retina (Figure 22). Accumulation of endogenous Rh1 in the insoluble fraction suggests that mutant $Rh1^{P37H}$ recruits its endogenous WT counterpart into aggregates, in accordance with previous studies (Colley et al., 1995; Kurada and O'Tousa, 1995; Kurada et al., 1998; Rajan and Kopito, 2005; Saliba et al., 2002).

Rh^{P23H} is prone to aggregation *ex vivo* in the highly oxidizing environment of SDS-PAGE (Crow et al., 2001; Illing et al., 2002). The hydrophobic nature of Rh or an increased propensity to form β -sheet structures, which underlie the aggregation of many other proteins, might also contribute to Rh aggregation (Fink, 1998). Although it is formally possible that the HMW Rh1 aggregates observed in this study were generated *ex vivo* during sample preparation, we strongly believe that Rh1-containing aggregates were formed *in vivo* since they were detected in a time-dependent manner (Figure 22). At eclosion and up to 10 days of light exposure, when in both $Rh1^{P37H}$ and $Rh1^{WT}$ flies the endogenous Rh1 is properly localized to rhabdomeres, no HMW Rh1 aggregates were detected. In contrast, after 20 days of light exposure, when the $Rh1^{P37H}$ flies show a pronounced retinal degeneration, high levels of HMW Rh1-containing aggregates are detected and the levels were further increased after 30 days of light exposure (Figure 22), suggesting that $Rh1^{WT}$ was recruited into insoluble aggregates as a function of time and light exposure.

Why no ectopic $Rh1^{P37H}$ -containing aggregates (hsv-labeled) were detected in $Rh1^{P37H}$ flies (Figure 22)? Three possibilities might explain this observation: i) these Rh1-containing aggregates were rapidly cleared from the system; ii) the aggregates were not labeled by our anti-hsv antibodies; iii) the size of these aggregates prevented them from entering the polyacrylamide gel. It is conceivable that misfolded $Rh1^{P37H}$ might be rapidly cleared from the system, to limit its toxicity. Thus, excessive degradation of this mutant protein (between the onset of its expression [approx. two days before eclosion] and the first time point of the analysis [posteclosion day 1]) might have removed the mutant $Rh1^{P37H}$. The second possibility is that $Rh1^{P37H-hsv}$ aggregation masks hsv epitope availability. The fact that the hsv tagged $Rh1^{P37H}$ is hardly ever detectable could indicate that the protein has aggregated to a point where the epitope is not available. An alternative explanation for the lack of hsv sensitivity is that the hsv tag might have been cleaved away from the mutant $Rh1^{P37H}$ (but not from $Rh1^{WT}$), although this is very unlikely. The third possibility is that the ectopic $Rh1^{P37H}$ aggregates are very large and do not enter the polyacrylamide gel. Studying the nature of protein aggregates is difficult and

more powerful techniques (including immuno-electron microscopy) might be required in order to visualize these Rh1-containing insoluble aggregates.

4.2 The endogenous Rh1 is required for $Rh1^{P37H}$ toxicity

To determine whether the loss of mature Rh1 in aging $Rh1^{P37H}$ flies (Figure 22) is the cause or the consequence of retinal degeneration in the $Rh1^{P37H}$ retina, we compared the profile of mature Rh1, PN cell death and of the rhabdomeric marker TRP as a function of time. The rhabdomeric marker TRP was used to independently assess the rhabdomere integrity. No loss of mature Rh1 preceded the loss of PNs (or loss of TRP), suggesting that retinal degeneration was responsible for the loss of mature Rh1, and not vice versa.

Because we found the endogenous Rh1 to be recruited into insoluble aggregates, we set up to determine the role of the endogenous Rh1 in the $Rh1^{P37H}$ -mediated retinal pathology. We reduced the dosage of the endogenous Rh1 in $Rh1^{P37H}$ flies and obtained a strong suppression of retinal degeneration in $Rh1^{P37H};Rh1^{KO/+}$ flies (Figure 23). Consistent with the rescue of PN degeneration, the levels of TRP were partially restored in $Rh1^{P37H};Rh1^{KO/+}$ flies. The level of total mature, but not P37H ectopic Rh1 was also partially restored (Figure 23), indicating that rescue of retinal degeneration in $Rh1^{P37H};Rh1^{KO/+}$ flies correlated with decreased degradation of endogenous Rh1. Interestingly, increased dosage of the mutant $Rh1^{P37H}$ transgene relative to endogenous $Rh1$ led to an increased level of Rh1 aggregates that contained a large fraction of endogenous Rh1 in $Rh1^{P37H};Rh1^{KO/+}$ flies (Figure 23).

The fact that reducing the dosage of the endogenous Rh1 leads to suppression of retinal degeneration in $Rh1^{P37H};Rh1^{KO/+}$ flies suggests that the endogenous Rh1 is required for $Rh1^{P37H}$ -mediated PN degeneration (GOF effect), most likely as a result of its recruitment into aggregates. This observation - together with the loss of mature Rh1 which results from retinal degeneration, and not vice versa - rules out that a DN effect of $Rh1^{P37H}$ on the maturation of the endogenous Rh1 is directly responsible for PN degeneration. Moreover, the fact that the suppression of retinal degeneration is associated with more endogenous Rh1-containing aggregates in $Rh1^{P37H};Rh1^{KO/+}$ flies suggests that clearance of endogenous Rh1 might be pathogenic in the $Rh1^{P37H}$ retina.

Previous studies have found that, in mammalian cells, mutant Rh^{P23H} recruits WT Rh into aggregates and enhances the proteasome-mediated degradation of WT Rh (Rajan and Kopito, 2005; Saliba et al., 2002). Our present results suggest that recruited endogenous Rh1 causes cell death in an “active” manner (via a GOF mechanism) rather than “passively” (due to its absence from the rhabdomeres; DN mechanism). Another class II mutant Rh1, Rh1^{D1}, was shown to recruit the endogenous Rh1 into aggregates (Kurada et al., 1998) and to require the endogenous Rh1 for full pathogenicity (Kurada and O’Tousa, 1995). Evidence from other neurodegenerative disorders suggest that several mutant proteins, including Tau in Alzheimer’s disease (Clavaguera et al., 2009), Huntingtin in Huntington’s disease (Busch et al., 2003); or PrP^{Sc} in prion disease (Aguzzi and Polymenidou, 2004) are to recruit their WT counterpart into aggregates. Remarkably, similar to mutant PrP^{Sc}, increasing evidence suggests a prion-like mechanism of action for these mutant proteins which can induce long-term conformational defects in the endogenous protein (Brundin et al., 2010; Krammer et al., 2009). To our knowledge, no evidence exists so far to suggest a prion-like mechanism at work in RP, and future investigations on the mechanisms of Rh misfolding and aggregation will better characterize the behaviour and interactions of mutant and WT Rh conformers.

Discussion

The finding that removal of one WT allele of *Rh1* in *Rh1^{P37H}* flies rescues retinal degeneration is in agreement with results obtained with other *Drosophila* mutants. The presence of mutant *Rh1^{D1}* triggers a dominant form of retinal degeneration, which is also light- and age-dependent. Interestingly, the rate of light-dependent retinal degeneration in *Rh1^{D1}/Rh1⁻* and *Rh1^{D1}/Rh1^{D1}* flies is slower compared to *Rh1^{D1}/Rh1⁺* flies (Kurada and O'Tousa, 1995), suggesting that degeneration in *Drosophila* does not result from low Rh1 content, but rather from an abnormal cellular environment caused by expression of both WT and mutant Rh1 (in agreement to our observations).

These results obtained in fly models are in contrast to the results obtained with *Rh* transgenic mice. In mice carrying three *Rh* mutations (*V20G*, *P23H*, *P27L*, i.e. *Rh^{GHL}*) the severity of retinal degeneration is inversely correlated with the *Rh^{WT}* gene copy number. The degeneration is most severe in the absence of both *Rh^{WT}* alleles, moderate in the presence of one *Rh^{WT}* allele and least severe in the presence of two *Rh^{WT}* alleles (Frederick et al., 2001).

Why would removal of one *Rh^{WT}* allele accelerate retinal degeneration in *Rh^{P23H}* mice and suppress it in *Rh1^{P37H}* flies? One possibility is that the triple *Rh^{GHL}* mutation does not reflect the behavior of the single mutant *Rh^{P23H}* anymore. Therefore, the same experiments should also be performed in *Rh^{P23H}* mice, which are available. A second possibility is that different mechanisms mediate neurodegeneration in mice and in *Drosophila*. One such mechanism might be related to the role played by light in retinal degeneration. In *Rh^{P23H}* mice, retinal degeneration is relatively rapid and also happens in the absence of light. In contrast, the degeneration in flies is very dependent on light exposure. In *Drosophila*, Rh1 is endocytosed upon light activation via an Arrestin-dependent mechanism. Continuous light exposure could thus lead to an increase of stable Rh1/Arrestin complexes and subsequent excessive degradation of Rh1 (Alloway et al., 2000; Lee and Montell, 2004). In this way, exposure to light might lead to massive endocytosis of Rh1, thereby overwhelming the endocytic machinery, resulting in accumulation of late endosomes which trigger cell death by unknown mechanisms (Chinchore et al., 2009). Thus, the more Rh1 is present in the fly photoreceptor environment, the more Rh1 gets endocytosed due to light activation, which leads to enhanced retinal degeneration. Decreasing the dosage of the endogenous *Rh1^{WT}* might therefore suppress the degeneration triggered by excessive endocytosis/degradation of Rh1. It is therefore possible that the *Rh1^{P37H}*-expressing photoreceptors, already stressed by the presence of misfolded *Rh1^{P37H}* in the ER, cannot cope with the additional Rh1 massive endocytosis/degradation caused by exposure to light.

5. Dramatic rescue of blindness in *Rh1^{P37H}* flies by decreasing *VCP* activity

Reducing *VCP* function in *Rh1^{P37H}* flies leads to a complete restoration of endogenous mature Rh1 levels and to a partial rescue of mature mutant *Rh1^{P37H}* from degradation (Figure 25). This correlates with an almost complete rescue of blindness in *VCP^{26-8/+;Rh1^{P37H}/+}* flies, as assessed by the behavioural assay phototaxis (Figure 31) and ERG measurements (Figure 32). Moreover, the rescuing effect of *VCP* inactivation also extends to another class II Rh1 mutation, *Rh1^{D1}* (Figure 33). *VCP^{26-8/+;Rh1^{D1}/+}* flies show preserved retinal structure and are attracted to light when compared to *Rh1^{D1}* flies. This suggests that inactivation of *VCP* has beneficial effects for class II Rh1-mediated retinal pathologies.

The electrophysiological measurements confirm that the levels of mature Rh1 at the plasma membrane are completely restored in $VCP^{26-8}/+;Rh1^{P37H}/+$ flies. We believe a combination of at least two events could lead to this strong rescue: i) partial inactivation of VCP and thus of ERAD leads to higher Rh1 aggregates which ii) in the presence of moderate ER stress are solubilised by the UPR-mediated increase in ER folding capacity (Lin et al., 2007; Ron and Walter, 2007). In this way, a considerable portion of the Rh1 found in the ER re-enters the secretory pathway and reaches the plasma membrane. However, it is also possible that Rh1 mature form is preserved at the plasma membrane in $VCP^{26-8}/+;Rh1^{P37H}/+$ flies simply due to the fact that VCP inactivation leads to suppression of photoreceptor cell death in these flies.

Our study also allowed us to genetically uncouple retinal degeneration from blindness. While blindness was almost completely rescued in $VCP^{26-8}/+;Rh1^{P37H}/+$ vs. $Rh1^{P37H}$ flies, degeneration was considerably, but only partially prevented. Although it remains possible that sensitivities of the methods we used to evaluate retinal degeneration vs. the content of Rh/visual acuity are responsible for these differences, these results raise the possibility that at least some mechanisms cause blindness but not retinal degeneration. Indeed, it was shown that inhibition of Rh1 degradation pathway leads to suppression of blindness but not of retinal degeneration in flies exposed to bright light (Lee and Montell, 2004). Further research will determine which common and distinct mechanisms mediate blindness and retinal degeneration.

6. Upregulation of the Ire1/Xbp1 pathway might be protective in the $Rh1^{P37H}$ retina

Inhibition of VCP activity or reduced dosage of the endogenous $Rh1$ both led to a potent suppression of retinal degeneration in $Rh1^{P37H}$ flies and were both associated with increased levels of Rh1 aggregates and with increased UPR activation, via the Ire1/Xbp1 pathway (Figures 23, 26 and 29). Similarly, we saw increased $Xbp1$ splicing in $GMR/UAS-Rh1^{G69D}$ flies carrying a VCP^{LOF} allele and detected increased Hsc3/BiP levels in flies expressing another class II Rh1 mutant, $Rh1^{G69D}$ (Colley et al., 1995; Ryoo et al., 2007) in a VCP^{26-8} background (Figure 27). Therefore, partial removal of VCP function leads to an early increase in the activation of the Ire1/Xbp1 pathway and to a long-term protection against retinal degeneration in class II Rh1 fly mutants.

How might upregulation of the Ire1/Xbp1 pathway protect $Rh1^{P37H}$ PNs from degeneration? A recent study found that Rh1 aggregation within the ER and moderate activation of the Ire1/Xbp1 pathway induces long-term pro-survival effects, via inhibition of caspase activation and induction of an antioxidant response (Mendes et al., 2009). Adenoviral delivery of Xbp1 also protected mouse dopaminergic neurons from 1-methyl-4-phenyl-1,2,3,6-tetrahydropyridine (MPTP)-induced cell death *in vivo* (Sado et al., 2009). We also found a moderate activation of the Ire1/Xbp1 branch (e.g. enhanced non-conventional $Xbp1$ splicing and increased Hsc3/BiP levels) of the UPR in our rescued $Rh1^{P37H}$ retinas (with reduced VCP or endogenous Rh1 levels; Figure 26), consistent with the observation that Ire1/Xbp1 activation is protective for PNs under stress. It is therefore tempting to hypothesize that moderate activation of Ire1/Xbp1 is one pro-survival signal in $Rh1^{P37H}$ flies with reduced VCP or $Rh1$ function.

It should also be noted that, besides the Ire1/Xbp1 branch, UPR induces two other pathways, mediated by the ER stress sensors Perk and Atf6 (Ron and Walter, 2007; Szegezdi et al., 2006). Lin and collaborators found that, in mammalian cells treated with ER stress inducers, activation of Ire1 occurred during the survival phase, while activation

Discussion

of Atf6 and Perk persisted late in the apoptotic phase. Moreover, forced activation of the Ire1 pathway prolonged cell survival. When analysing Rh^{P23H} transgenic rats, the decrease in BiP levels coincided with the onset of PN degeneration in the outer nuclear layer, while increased levels of the CHOP transcription factor (acting downstream of Perk) were detected during the retinal degeneration phase (Lin et al., 2007). Another very recent study showed that gene delivery of BiP to transgenic Rh^{P23H} rats led to reduced levels of CHOP and rescued PN degeneration and blindness in these rats. Interestingly, BiP was found in complex with caspase-12 and with the BH3-only protein BiK, that may contribute to the anti-apoptotic activity of BiP (Gorbatyuk et al., 2010). Taken together, these observations suggest a protective role for Ire1/Xbp1 signalling in stressed PNs and suggest that a better understanding of the differential regulation of UPR pathways during ER stress might provide further clues about the regulation of cellular survival vs. apoptosis in PNs expressing misfolded Rh^{P23H} .

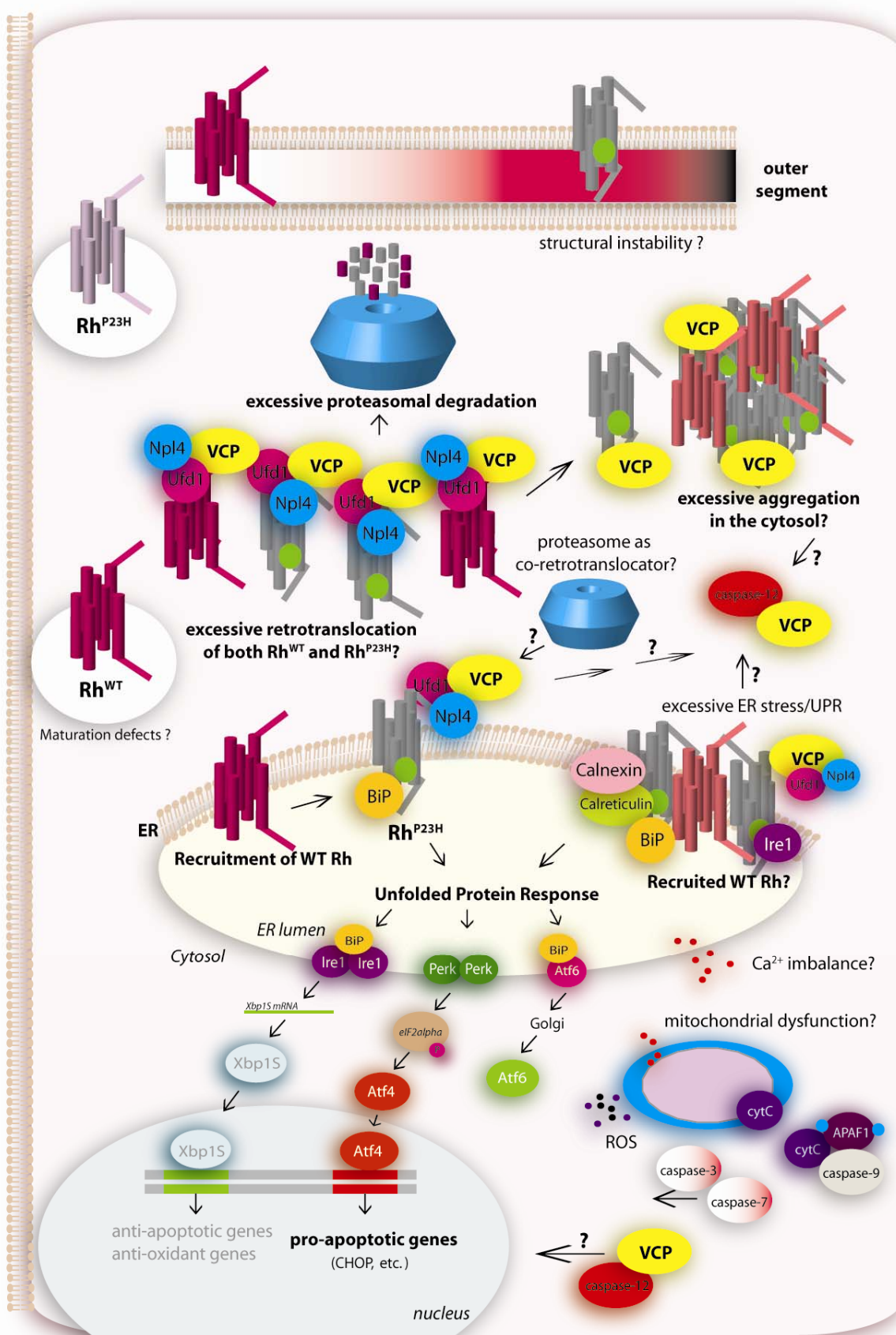
7. Potential pro-apoptotic effects of the VCP/ERAD/proteasome axis in the $Rh1^{P37H}$ retina

The rescuing effect on $Rh1^{P37H}$ PN degeneration after genetic inactivation of the ERAD/retrotranslocation effector *VCP* (Figure 29), or after pharmacological inhibition of the VCP/ERAD/proteasome axis (Figure 30) suggests that excessive VCP/ERAD/proteasome activity causes cell loss in the presence of mutant $Rh^{P23H}/Rh1^{P37H}$.

Can VCP cause cell death independently of ERAD in the $Rh1^{P37H}$ retina?

One possibility is that VCP can be a direct regulator of cell death pathways. VCP might associate with caspase-12 under prolonged ER stress conditions or under excessive Rh1 aggregation in the cytosol, or under chronic and excessive retrotranslocation, and induce cell death (see Figure 35). It was suggested that VCP is a pro-apoptotic effector under conditions of chronic ER stress. Indeed, it was shown that the *Drosophila* homologue of *VCP*, *Ter94*, is a mediator of polyglutamine-induced neurodegeneration (Higashiyama et al., 2002). VCP also seems to mediate a form of ER stress-induced cell death by forming a complex with caspase-9 and caspase-12 and being required for processing of caspase-9 in cell culture systems (Rao et al., 2004).

Figure 35. Potential pro-apoptotic effects of the VCP/ERAD/proteasome axis in the $Rh1^{P37H}$ retina. Our cellular and *Drosophila* studies indicate that excessive VCP/ERAD/proteasome activity causes cell loss in the presence of mutant $Rh^{P23H}/Rh1^{P37H}$. Excessive retrotranslocation (VCP-mediated) of mutant Rh might lead to excess of Rh^{P23H} in the cytosol and to increased cytosolic Rh^{P23H} -containing aggregates. Mutant Rh^{P23H} also recruits its WT counterpart into aggregates. Chronic and excessive degradation (proteasome-mediated) of both Rh^{P23H} and Rh^{WT} might activate yet unidentified pro-apoptotic signals. Chronic and excessive retrotranslocation (VCP-mediated) might activate pro-apoptotic signals as well. The proteasome might also be involved in the retrotranslocation of Rh^{P23H} , thereby accelerating the degenerative process. Previous studies suggested that VCP might associate with caspase-12 under prolonged ER stress conditions, and caspase-12 might induce cell death directly. Misfolded Rh^{P23H} in the ER might also activate the unfolded protein response (UPR) which can be pro-apoptotic (via Perk/Atf4 activation) or anti-apoptotic (via generation of Xbp1S). Excessive ER stress might also lead to calcium imbalance and to mitochondrial dysfunction; dysfunctional mitochondria produce many reactive oxygen species (ROS) and might release cytochrome c (cytC) in the cytosol, thus initiating the mitochondrial-mediated apoptosis (via apoptosome formation [cytC, APAF1 and caspase-9] and subsequent activation of caspases). Mutant Rh^{P23H} present in the outer segment might also be pathologic, although in our model Rh^{P23H} displayed an enhanced degradation and very little Rh^{P23H} actually reached the outer segment (i.e. the rhabdomeres in the fly). Our results suggest that cell death is triggered by GOF effect of mutant Rh^{P23H} . This GOF effect might be either i) excessive retrotranslocation and/or ii) excessive proteasomal degradation, although alternative explanation (which incorporates these two mechanisms) might exist.



Discussion

Even though VCP might directly induce cell death, two lines of evidence suggest that the effect of VCP on the *Rh1^{P37H}* pathology involves its activity as ERAD effector. First, the levels of VCP were found to be increased very early (after 1 dle) in *Rh1^{P37H}* vs. *Rh1^{WT}* flies (Figure 29), which did not match with the late rescuing effect we observed in *VCP^{26-8/+;Rh1^{P37H}/+}* flies. Although an initial increase in VCP levels might induce long-term cellular changes that contribute to PN degeneration and/or regulation of VCP at post-translational level (e.g. phosphorylation, acetylation or subcellular localization) may account for a late pro-apoptotic effect, we believe that changes in VCP levels play little, if any, direct pro-apoptotic role in *Rh1^{P37H}*-induced degeneration. Second, our pharmacological treatment with the VCP/ERAD inhibitor EerI potently suppressed retinal degeneration in *Rh1^{P37H}* flies (Figure 30). Moreover, proteasome inactivation with MG132 inhibitor also led to a dramatic suppression of retinal degeneration in the *Rh1^{P37H}* retina and the proteasome was shown to be tightly coupled to substrate retrotranslocation during ERAD (Chillaron and Haas, 2000; Mancini et al., 2000; Saliba et al., 2002) (Figure 30). Therefore, we strongly suggest that excessive VCP-mediated ERAD and the linked proteasome activity cause cell death in the *Rh1^{P37H}* retina.

How does excessive activity of the VCP/ERAD/proteasome axis lead to PN degeneration in the *Rh1^{P37H}* retina?

Excessive degradation of the visual pigment Rh1 might generate a yet unidentified pro-apoptotic signal, under conditions of chronic ERAD/proteasome activity. ERAD activation is one adaptive response triggered by UPR in the presence of misfolded proteins within the ER (Ron and Walter, 2007; Vembar and Brodsky, 2008). Chronic ERAD/proteasome functioning, downstream or in parallel to VCP activity, might generate pro-apoptotic signals. Although the molecular mechanisms behind such a molecular switch are obscure, recent evidence suggests that several molecules and mechanisms might mediate such a transition from an adaptive stress response to apoptosis; the CHOP transcription factor, caspase activation, Ca²⁺ release and mitochondrial signaling might control this pro-apoptotic switch (Mendes et al., 2005) downstream or in parallel to Rh1 aggregate retrotranslocation and clearance (see Figure 35).

Excessive retrotranslocation of Rh1, coupled to delayed proteasomal degradation might generate cytosolic Rh1 aggregates that might be toxic for PNs. It was found previously that misfolded proteins that have been retrotranslocated from the ER and not degraded by the proteasome can aggregate within the cytoplasm (Kaganovich et al., 2008) and become toxic via a GOF mechanism (e.g. ectopic signalling, recruitment of chaperones, cytoskeleton inhibition, increase of reactive oxygen species and/or free Ca²⁺ levels) (Bucciantini et al., 2004; Mendes et al., 2005) (Figure 35). It is possible that the subcellular localization of aggregates may be critical to their pathogenicity. If Rh1 cytosolic aggregates would be the toxic species as opposed to the Rh1 ER resident species, then blocking retrotranslocation of misfolded Rh1 from the ER by inhibiting VCP- or proteasome-coupled retrotranslocation functions would lead to suppression of retinal degeneration that we see in our treated *Rh1^{P37H}* flies. Further experiments (e.g. immuno-electron microscopy) are needed to determine the subcellular localization of Rh1 aggregates in treated versus untreated *Rh1^{P37H}* flies.

Retrotranslocation of misfolded proteins (like Rh1^{P37H}) during ERAD requires a lot of mechanical force and energy (e.g. ATP hydrolysis) (Wang et al., 2004; Ye, 2006) and this could lead to death of photoreceptor cells by depleting them of energy. Therefore,

inhibition of retrotranslocation might prevent a severe energy imbalance and might thus have protective effects.

8. How does decreased VCP/ERAD/proteasome activity prevent photoreceptor neuron cell death in the *Rh1^{P37H}* retina?

We were interested to determine whether manipulation of VCP activity in *Drosophila* has any impact on the retinal pathology triggered by the mutant *Rh1^{P37H}*. We employed two *VCP LOF* alleles, which decrease the levels and the VCP activity. After generating and aging flies expressing either *Rh1^{WT}* or *Rh1^{P37H}* in a *VCP^{LOF}* background, we compared the retinal pathology in these flies to that in flies expressing WT or P37H *Rh1* in a wild-type background. Our histological analysis revealed a very potent protective effect of *VCP* inactivation on PN degeneration (Figure 29). Partial *VCP* inactivation using the weaker *LOF* allele *VCP²⁶⁻⁸* rescued retinal degeneration in *Rh1^{P37H}* flies only at P30, while PN degeneration was more potently suppressed in *Rh1^{P37H}* flies carrying the stronger *VCP LOF* allele *VCP^{k15502}* both at P20 and P30 (Figure 29).

Our finding that *VCP* inhibition rescues retinal degeneration in *Rh1^{P37H}* flies suggests that inhibition of the ERAD activity might exert long-term protective effects in *Rh1^{P37H}* PNs. The tight coupling between VCP and proteasome activities is essential for substrate delivery and clearance during ERAD (Dai and Li, 2001) and interestingly, proteasome activity is required for proper substrate retrotranslocation (Chillaron and Haas, 2000; Mancini et al., 2000; Saliba et al., 2002).

To independently test whether inhibition of the VCP/ERAD/proteasome axis is protective for *Rh1^{P37H}*-expressing PNs, we treated our *Rh1^{P37H}* flies with a newly characterized ERAD inhibitor, EerI or with the classical proteasome inhibitor MG132. Our pharmacological treatment with the inhibitor EerI potently suppressed retinal degeneration in *Rh1^{P37H}* flies (Figure 30). EerI was reported to inhibit the activity of deubiquitinating enzymes acting downstream of VCP during ERAD, therefore inhibiting an ERAD-associated VCP activity (Fiebiger et al., 2004; Wang et al., 2008). In addition, our pharmacological treatment with the proteasome inhibitor MG132 also led to a dramatic suppression of retinal degeneration in the *Rh1^{P37H}* retina (Figure 30). Although the treatment with EerI led to a substantial rescue, it was less spectacular than the rescue resulting after the treatment with the highest dose of MG132, suggesting that i) either the EerI dose could be further increased to achieve more complete protection or that ii) EerI only inhibits some, but not all, ERAD-related VCP functions, or that iii) other retrotranslocation pathways, VCP/ERAD-independent are responsible for proteasomal targeting of misfolded *Rh1^{P37H}*. In support of this possibility, the ATPases of the proteasome 19S RP were shown to also function as retrotranslocators during ERAD (Meusser et al., 2005; Wahlman et al., 2007).

How does inhibition of the VCP/ERAD/proteasome axis prevent photoreceptor neuron degeneration?

The first explanation for the suppression of retinal degeneration in *VCP^{26-8/+;Rh1^{P37H/+}}*

 flies is that the restoration of mature *Rh1* levels by *VCP^{LOF}* exerts a stabilizing effect on the rhabdomeres and thus prevents cell dysfunction and death. Indeed, complete lack of Rh in mice (Humphries et al., 1997; Lem et al., 1999) leads to absence of rod outer segments and photoreceptor cell death. While flies with one functional and one *Rh1* knockout allele (50 % *Rh1* levels) have a normal retina, further reduction of endogenous

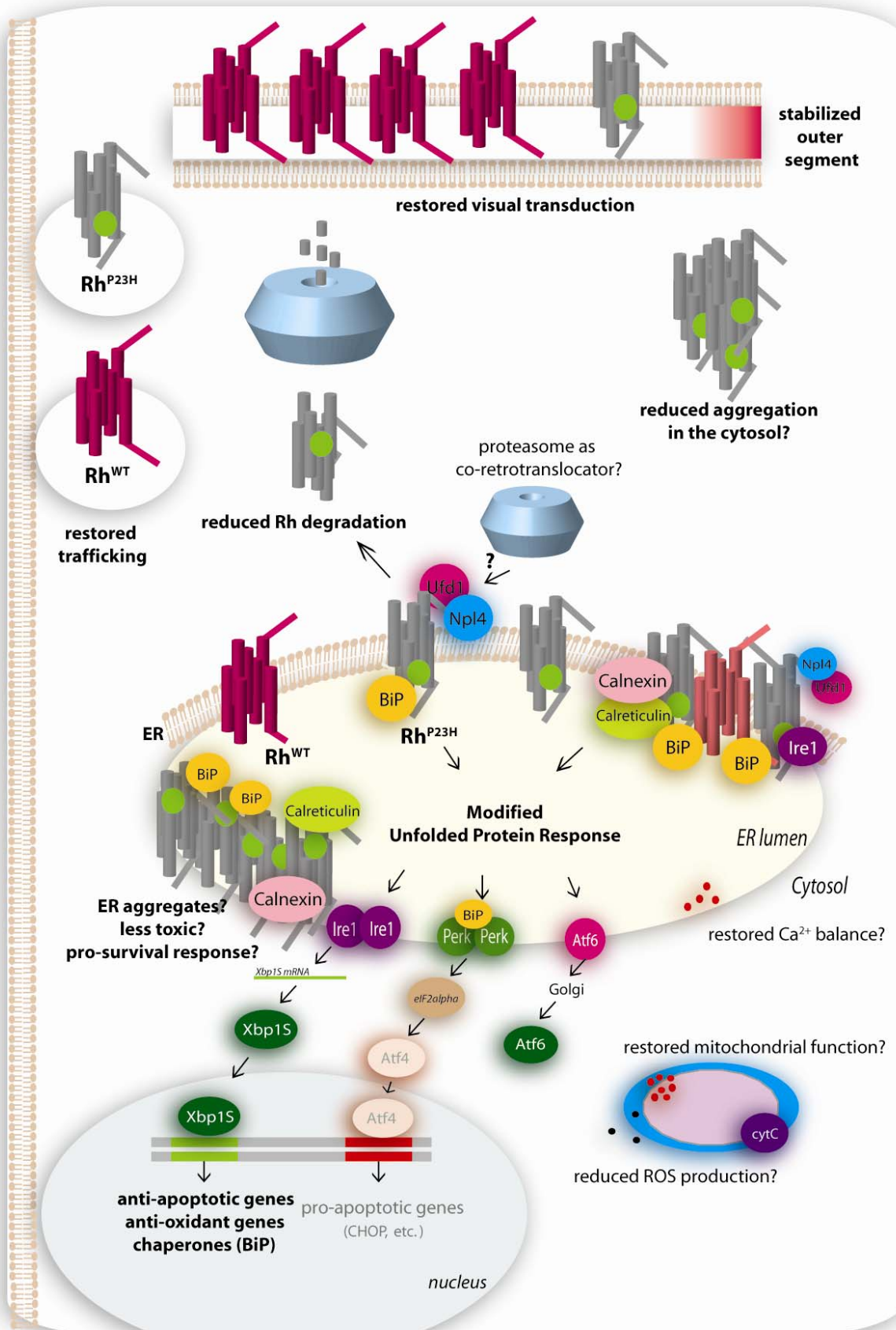
Discussion

Rh1 levels (when using a dominant Rh1 allele; Colley et al., 1995; Kurada and O'Tousa, 1995; and our study) causes degeneration, suggesting the existence of a Rh1 "threshold" between 0 and 50 % that is required for photoreceptor integrity. However, in our *Rh1^{P37H}* flies, the levels of mature Rh1 drop to almost zero concomitantly with retinal degeneration. Loss of mature Rh1 at the plasma membrane does not precede death of PNs or loss of the rhabdomere marker TRP, suggesting that mature Rh1 is lost subsequently to photoreceptor death and not vice versa (Figure 22). Therefore, if loss of mature Rh1 does not cause cell death in *Rh1^{P37H}* flies, then partial *VCP* inactivation probably does not lead to suppression of retinal degeneration by restoring levels of mature Rh1 at the plasma membrane.

A second explanation for the rescue of degeneration after VCP/ERAD/proteasome inhibition in *Rh1^{P37H}* flies is that accumulation of insoluble Rh1 aggregates might protect *Rh1^{P37H}* PNs from degeneration. Evidence from several neurodegenerative disorders suggests that, in contrast to prefibrillar protein species (protofibrils) which are toxic for cells, insoluble aggregates might have beneficial effects (Caughey and Lansbury, 2003; Ross and Poirier, 2004). For example, in a cellular model of HD, formation of insoluble aggregates prolonged survival of striatal neurons, by decreasing the levels of soluble (toxic) Huntingtin (Arrasate et al., 2004). It is therefore possible that insoluble Rh1 aggregates sequester Rh1 protofibrils and thus limit their toxicity. Further support for this hypothesis comes from the analysis of the *VCP^{LOF/+;Rh1^{P37H/+}}* and *Rh1^{P37H;Rh1^{KO/+}}* flies, in which suppression of retinal degeneration was associated with more insoluble Rh1 aggregates (Figures 23, 24 and 29).

A third possibility is that decreased VCP-mediated retrotranslocation might prevent the misfolded *Rh1^{P37H}* from gaining access to the cytoplasm, where it might aggregate and impair the proteasome (Figure 36). It is conceivable that excessive retrotranslocation of mutant *Rh1^{P37H}* leads to its accumulation in the cytosol, should the degrading capacity of the proteasome not suffice to clear all retrotranslocated *Rh1^{P37H}*. Indeed, there is strong evidence to suggest that cytosolic aggregates exert toxic effects in neurodegenerative disorders like AD or PD (Rubinsztein, 2006). Additional support for this hypothesis comes from our pharmacological experiments in which the VCP/ERAD (the EerI inhibitor) and the proteasome (MG132 inhibitor) were inhibited. Inhibition of the proteasome alone protected PNs expressing misfolded Rh1, suggesting that excessive and chronic proteasome activity might generate yet unidentified pro-apoptotic signals. The proteasome might also assist in substrate retrotranslocation (see point 1), and an overactive VCP/ERAD/proteasome axis might be deleterious for PNs (see Figure 36).

Figure 36. Protective effect of VCP/ERAD/proteasome inhibition in the *Rh1^{P37H}* retina. Decreasing VCP activity leads to accumulation of mutant *Rh1^{P37H}* in the ER. The lack of aggregated *Rh1^{P37H}* from the cytosol might prevent cell loss. Another possibility is that an increase in ER-based *Rh1^{P37H}* induces a pro-survival response via activation of the Ire1/Xbp1 pathway and increased production of chaperones, like BiP. Increased BiP might allow enhanced Rh1 refolding and might restore the traffic of Rh1 towards the outer segment (i.e. the rhabdomere in the fly). Proteasome inhibition also exerts a potent rescuing effect in the *Rh1^{P37H}* retina, suggesting that decreased proteasomal degradation might be protective. However, since the proteasome itself might mediate protein retrotranslocation, we cannot rule out that decreased *Rh1^{P37H}* retrotranslocation is the protective mechanism in the *Rh1^{P37H}* retina. The protective mechanisms might also show convergence. Thus, reduced *Rh1^{P37H}* retrotranslocation and proteasome degradation, reduced VCP activation, moderate ER stress, increased Ire1/Xbp1 activation and BiP production might collectively promote survival in the *Rh1^{P37H}* retina. However, inactivation of a single protein (VCP) or a single process (proteasome function) allows a dramatic suppression of retinal degeneration, suggesting that compounds that target VCP or the proteasome activity might represent a potential therapy for *Rh1^{P37H}*-linked RP.



Discussion

Not only might, ER-localized Rh1 aggregates (formed after VCP or proteasome inhibition) be less toxic as compared to cytosolic aggregates, but the presence of excess of misfolded Rh in the ER might induce pro-survival signalling via induction of the UPR. Indeed, inhibition of *VCP* activity or reduced dosage of the endogenous *Rh1* both led to a potent suppression of retinal degeneration in *Rh1^{P37H}* flies (Figures 23 and 29) which were both associated with increased levels of Rh1 aggregates (Figures 23 and 24) and with increased UPR activation via the pro-survival *Ire1/Xbp1* pathway (Figure 26). A recent study reported that mutations affecting Rh1 maturation and folding show protective activity in *Drosophila* retina because misfolded Rh1 in the ER can induce a moderate ER stress with anti-apoptotic effects (Mendes et al., 2009). In this study, prolonged and moderate ER stress protects against apoptosis induced by *p53*, *rpr* or the caspase *dcp-1*. It is thus tempting to speculate that in our *VCP^{26-8/+;Rh1^{P37H/+}}* flies, the increased level of Rh1 aggregates in the ER have a moderate GOF effect resulting in a long-term pro-survival response (see point 6 and Figure 36).

The inactivation of the proteasome itself could also lead to rescue of *Rh1^{P37H}*-caused cell death by inducing pro-survival UPR pathways (Ron and Walter, 2007; Schröder and Kaufman, 2005). Proteasome impairment (with the MG132 inhibitor) was shown to increase the UPR-induced chaperone (BiP, Grp94, Calreticulin) expression levels (Bush et al., 1997; Mu et al., 2008) and to induce the three branches of the UPR (*Ire1*, *Atf6* and *Perk*) in cell culture systems (Mu et al., 2008). Thus, increase of Rh1 aggregate levels in the ER, following impaired retrotranslocation, could lead to induction of UPR in the *Rh1^{P37H}* retina and thereby to cytoprotection. It would be interesting to asses whether upregulation of UPR also occurs in our MG132-treated *Rh1^{P37H}* flies.

Finally, another possible explanation for the suppression of cell death in *Rh1^{P37H}* flies treated with proteasome inhibitor is that the PNs might display increased autophagy. Autophagy might have protective effects against neurodegeneration. Impairment of the UPS *in vitro* has been found to induce autophagy (Iwata et al., 2005; Rideout et al., 2004). It was also shown that compensatory autophagy was induced in response to UPS impairment in a fly model of the neurodegenerative disease spinobulbar muscular atrophy and had a cytoprotective role (Pandey et al., 2007). Inducing autophagy also suppressed cell death in *Drosophila* models of Huntington's disease (Sarkar et al., 2008; Wang et al., 2009). However, induction of autophagy did not suppress cell death caused by the dominant *Rh1^{R27H}* mutant (Wang et al., 2009) which was previously shown to cause retinal cell death (Davidson and Steller, 1998). Thus, induction of autophagy does not protect against cell death in all animal models. Therefore, it would be interesting to study if direct stimulation of autophagy (genetically or pharmacologically) rescues the *Rh1^{P37H}*-induced cell death in *Drosophila*.

In summary, we believe that excessive retrotranslocation and/or degradation of visual pigment Rh1 is pathogenic and inhibition of the VCP/ERAD/proteasome axis is protective for *Rh1^{P37H}* PNs. Increased levels of insoluble Rh1 aggregates accumulating after VCP or proteasome inactivation might be protective indirectly, by inducing UPR and other cytoprotective pathways (including stimulation of autophagy). The protective mechanisms might also show convergence. Thus, reduced *Rh1^{P37H}* retrotranslocation and proteasome degradation, reduced VCP activation, moderate ER stress, increased *Ire1/Xbp1* activation and BiP production might collectively promote survival in the *Rh1^{P37H}* retina.

9. Interaction between misfolded Rh^{P23H}, VCP activity, aging and light exposure might cause *retinitis pigmentosa*

Common risk factors for *Rh*^{P23H}-associated RP are aging and light. It has been proposed that faster progression of the degeneration in *Rh*^{P23H} patients in the inferior retina may result from a modifying effect of light (Paskowitz et al., 2006). Our *Rh1*^{P37H} flies represent a slowly progressive ADRP model in which the interplay between four factors (misfolded *Rh1*^{P37H}, VCP activity, aging and light exposure) is sufficient to cause degeneration of most R1-R6 photoreceptors in the fly retina. These mechanistic insights, facilitated by the analysis of *VCP*^{LOF}/+; *Rh1*^{P37H}/+ flies, raise the possibility that this four-component interaction network might cause RP in humans.

Light is the critical component of this interaction network, as *Rh1*^{P37H} flies reared in the dark do not display any retinal degeneration even after 30 days. The second risk factor is aging, which contributes to the progression of the phenotype, as young *Rh1*^{P37H} flies exposed to light do not show any retinal degeneration. *Rh1* misfolding is also a crucial component of the network, as overexpression of WT *Rh1* leads to almost no retinal degeneration. Finally, VCP activity only becomes critical in aging *Rh1*^{P37H} PNs exposed to light. Interference with any of these individual hits alleviates *Rh1*^{P37H} PN cell death. This quadruple-interaction model likely reflects the synergism generated by several independent pathological triggers, acting at sub-threshold levels, and which together induce degeneration of photoreceptor neurons.

Further investigation of the interactions between different pathological changes will lead to a better understanding of the cellular and molecular mechanisms that are critical for the function and survival of *Rh*^{P23H} photoreceptor neurons.

10. Manipulation of Rh proteostasis via VCP/ERAD/proteasome axis as a therapeutic strategy for *Rh*^{P23H}-linked RP?

The *P23H* mutation alters the three dimensional conformation of Rh, thereby leading to defective Rh proteostasis and to autosomal dominant *retinitis pigmentosa*. Misfolding-prone proteins are a serious challenge for cellular proteostasis and gain-of-function diseases (e.g. AD, PD, HD) that appear to arise when aggregation-associated proteotoxicity dominates over cellular protein clearance (Powers et al., 2009). Adapting the cellular proteostasis network by using proteostasis regulators (PR) (e.g. MG132, Celastrol) can partially correct proteostasis deficiencies that contribute to human disease (Balch et al., 2008; Mu et al., 2008). In our case, the PR MG132 was able to prevent the proteostasis defects in *Rh1*^{P37H} flies.

Should VCP/ERAD/proteasome activities be decreased to produce beneficial functional effects on *Rh*^{P23H}-mediated pathology?

The manipulation of VCP and proteasome activities in other situations involving protein aggregates suggests that the effect of modulating VCP activity depends on the nature of the mutant protein. Mutant ΔF508-CFTR, similar to *Rh*^{P23H} is retained in the ER and is degraded by the ERAD machinery (Ward et al., 1995). Inhibition of VCP activity in cells expressing the mutant ΔF508-CFTR allowed a fraction of the mutant protein to reach the plasma membrane and partially rescued the phenotype induced by excessive ERAD of mutant CFTR (Vij et al., 2006). Treatment of ΔF508-CFTR with the PR-proteasome inhibitor PS-341 also rescued mutant CFTR from degradation, although with less

Discussion

efficiency (Vij et al., 2006). In contrast, for aggregation-prone proteins such as Ataxin-3 (Orr and Zoghbi, 2007), an increase of VCP activity mitigated the Ataxin-3-mediated neurodegeneration (Boeddrich et al., 2006).

Since mutant Rh^{P23H} recruits endogenous Rh^{WT} into aggregates (Colley et al., 1995; Kurada and O'Tousa, 1995; Kurada et al., 1998; Rajan and Kopito, 2005), inhibition of VCP/ERAD and/or proteasome might allow the recovery of functional Rh^{WT}. Inhibition of excessive ERAD and proteasome activities might also promote refolding and membrane delivery of mutant Rh^{P23H}, which could escape degradation and mediate light transduction when at the plasma membrane (Galy et al., 2005). Finally, inhibition of VCP/ERAD/proteasome axis and thereby of VCP/proteasome mediated retrotranslocation of misfolded Rh1 could lead to accumulation of ER-localized Rh1 aggregates which are presumably less toxic than cytosolic aggregates and may mediate neuroprotection by inducing a moderate activation of the Ire1/Xbp1 UPR pathway.

A recent study (Kang and Ryoo, 2009) investigated another Rh1 allele (*Rh1*^{G69D}) which, although not found in RP patients, has been classified as class II Rh mutation (Colley et al., 1995). Overexpression (driven by the *Rh1* promoter) of ERAD members *Hrd1* and *EDEM2* partially rescued late-onset PN degeneration and loss of mature Rh1 in *Rh1*^{G69D} flies. Interestingly, reduced *Hrd1* or *EDEM2* function (by RNAi) also rescued mature Rh1 levels, although its effect on PN degeneration was not assessed. These observations might hint at different mechanisms of dominance or different levels of UPR activation among the different *Rh1* alleles (Mendes et al., 2005). Another possibility is that early clearance of the mutant Rh1 (via enhanced ERAD) might have long-term protective effects (Kang and Ryoo, 2009); indeed, early *Rh1*^{P37H} oligomers (protofibrils) might be the toxic species, while late-onset *Rh1*^{P37H} aggregate formation and/or reduced protein retrotranslocation might be protective (our study). Therefore, the manipulation of ERAD activity for therapeutic purposes should take into account the temporal profile of Rh aggregation and the relative contribution of endogenous Rh to aggregates associated with each individual Rh dominant mutation.

Our results suggest that VCP/ERAD inhibitor EerI and the proteasome inhibitor MG132 could be central in the therapeutic strategy for *Rh*^{P23H}-linked RP. However, given the very complex roles played by VCP in different cellular contexts, the systemic delivery of VCP inhibitors does not appear to be a satisfying strategy. For example, inhibition of VCP activity might promote aggregate formation and neurodegeneration in other parts of the central nervous system. One approach is localized (e.g. intravitreal, subretinal) delivery of VCP inhibitors. Another, more realistic approach is the development of more specific inhibitors of VCP/ERAD/proteasome that are more tolerated by the organism. Therefore, further insights into the molecular mechanisms linking Rh aggregate formation, recognition, retrotranslocation and clearance and their interaction with age- and light-dependent cellular processes could uncover new cellular targets for drug development in RP.

11. Perspectives

11.1 Ongoing and planned experiments

The biochemical mechanisms mediating the excessive retrotranslocation and clearance of misfolded Rh remain largely unknown. Our work has identified the ATP-dependent chaperone VCP as a major mediator of Rh retrotranslocation and proteasomal delivery. The identification of VCP interactors, which promote the degradation of Rh^{P23H} will provide essential clues about the molecular, spatial and temporal control of Rh homeostasis. Such an improved understanding of the quality control mechanisms acting on misfolded Rh will hopefully provide new clues about potential therapies for RP.

Our ongoing experiments are addressing the identity and integration of ER stress-generated signals which modulate Rh degradation and orchestrate the variety of cellular responses to the increased load of ER-based misfolded Rh. We are also evaluating the relevance of autophagy, a second major route for protein clearance in the cell, to the pathology triggered by Rh^{P23H}. The potent suppression of retinal degeneration in *Rh1P37H* flies after treatment with the proteasome inhibitor MG132 prompted us to ask whether a similar suppression of retinal pathology takes place in the *Rh^{P23H}* transgenic mouse model; we are currently addressing this possibility in collaboration with the laboratory of Dr. Jane Farrar (Trinity College Dublin, Ireland). Finally, we are interested to determine whether a combination of proteostasis regulators (such as proteasome inhibitors, chaperones) and anti-apoptotic regulators might succeed in preventing the retinal pathology triggered by Rh^{P23H}.

11.2 Towards differential (personalized) and integrative (multi-target) treatments of *retinitis pigmentosa*?

The multitude of *Rh* mutations that cause RP and the molecular and cellular differences between the different classes of mutations suggest that the pathological mechanisms that trigger RP might be complex and potentially class-dependent. Further insights into the molecular and cellular alterations triggered by these individual mutations will establish the differences and similarities between these mechanisms. One possibility is that a differential (personalized) treatment might be most effective if targeted to a specific class of mutations. A second possibility is that several key pathological mechanisms are shared by all Rh mutants, therefore suggesting that the development of integrative therapies for RP (directed against both common and class-specific disease-causing agents) will effectively fight this debilitating disorder. Further pre-clinical and clinical research efforts will undoubtedly provide the key to a successful RP therapy.

Discussion

IV. MATERIALS AND METHODS

Materials and Methods

A. Materials

A.1 Chemicals, reagents, commercial kits and enzymes

Name	Supplier
4,6-diaminodiphenyl-2-phenylindole (DAPI)	Sigma
30 % (w/v) Acrylamide/Bis solution 37.5:1	Serva
Adenosine triphosphate (dATP)	Fermentas
Agarose	Biomol
Antarctic phosphatase	New England Biolabs
Ammonium persulfate (APS)	BioRad
β-Mercaptoethanol	Sigma
BCIP/NBT substrate	Sigma
Big Dye Terminator v3.1 Cycle Sequencing Kit	Applied Biosystems
BioRad DC Protein Assay	BioRad
Blotting grade milk powder	BioRad
Bovine serum albumin (BSA, lyophilized)	Sigma
Clarion, non-aqueous mounting medium	Sigma
Complete, protease inhibitor cocktail tablets	Roche
Cytotoxicity Detection Kit Plus	Roche
Dimethyl sulfoxide (DMSO)	Fluka
Dithiothreitol (DTT)	Merck
DNA ladder GeneRuler Ladder mix	Fermentas
Durcupan A/M epoxy resin	Sigma
Durcupan ACM component B, hardener	Sigma
Durcupan ACM component C, accelerator	Sigma
Durcupan ACM component D, plasticiser	Sigma
Eeyarestatin I (Eer I)	ChemBridge
Effectene transfection reagent for lipofection	Qiagen
Enhanced chemiluminescence kit (ECL plus)	GE Healthcare
Ethylendiaminetetraacetate (EDTA)	Sigma
Ethidium bromide	Roth
Anti-Flag M2 agarose	Sigma
Flag peptide	Sigma
FluorSave	Calbiochem
Gateway BP Clonase II enzyme mix	Invitrogen
Gateway LR Clonase II enzyme mix	Invitrogen
Lipofectamine	Invitrogen
Lipofectamine 2000	Invitrogen
MG132 (Z-Leu-Leu-Leu-al)	Sigma
Microspin columns	GE Healthcare
Mouse ImmunoglobulinG	Sigma
N, N, N', N'-tetraethylmethylenediamine (TEMED)	BioRad
Nonidet-P40 (NP-40)	Roche
Normal goat serum	Dianova
OrangeG	Sigma
Osmium Tetroxide	Science Services
Paraformaldehyde (PFA)	VWR
PCR buffer	New England Biolabs
Phophatase inhibitor cocktail	Sigma
Phusion High-fidelity PCR Kit (HF PCR kit)	New England Biolabs

Materials and Methods

Plus Reagent	Invitrogen
Poly-D-Lysine hydrobromide	Sigma
Polyfreeze (Frozen mounting medium)	Polysciences
Ponceau S	Merck
Prestained Protein Ladder	Fermentas
Propylene oxide	Sigma
Protein assay kit	BioRad
Protein G PLUS agarose	Santa Cruz
Pure Yield Plasmid Midiprep System	Promega
QIAprep Spin Plasmid Miniprep Kit	Qiagen
QIAquick Gel Extraction Kit	Qiagen
QIAquick PCR Purification Kit	Qiagen
QuickChange II Site-Directed Mutagenesis Kit	Stratagene
Restriction enzymes	New England Biolabs
Sodium deoxycholate	Sigma
Sodium dodecyl sulfate (SDS)	Serva
Suc-LLVY-AMC	Sigma
Sucrose	Merck
T4 DNA ligase	New England Biolabs
Taq DNA polymerase	New England Biolabs
Toluidine Blue	Serva
Trypsin/EDTA	Invitrogen
Triton X-100	Merck
Tris-(hydroxymethyl)-aminomethan (Tris)	Serva
Tween-20, polyoxyethylene sorbitan monolaurate	Sigma
Ubiquitin enrichment kit	Pierce

dH₂O is referred to as deionised water, while ddH₂O is referred to as ultra-pure water (Milli-Q Biocell).

A.2 Consumable materials

Name	Supplier
Cell culture plates 6-well and 10cm Ø	Nunc
Cell culture plate 96-well	Falcon
Cover slips 12mm Ø	VWR
Cryo-tubes	Nunc
PVDF membrane	GE Healthcare
High performance chemiluminescence films	GE Healthcare
Latex gloves, powder-free	Meditrade
Multiwell cell culture plates, Costar 24 well	Corning
Nitril gloves, powder-free	Kimtech
Parafilm®	Pechiney plastic
PCR plate 96well	ABgene
Pipetboy	Accu-jet pro
Pipetman 2µl 10µl, 20µl, 100 µl, 200µl, 1000µl	Gilson
Pipette tipps 10µl, 20µl, 200µl, 1000µl	Diamond
Plastic pipettes, Cellstar 5ml, 10ml, 50ml	Greiner bio-one
Polypropylene conical tube, Falcon 15ml, 50ml	Becton Dickinson
Pre-sterilized pipette tips 10µl, 20µl, 200µl, 1000µl	Molecular BioProducts
Safe-lock reaction tube 0.5 ml, 1.5ml, 2ml	Eppendorf

A.3 Equipment

Name	Supplier
Agfa Curix 60 Developer	Agfa
Autoclave Bioclav	Schütt Labortechnik
Autoclave Systec 5075 ELV	Systec
Calibrated Imaging Densitometer GS-710	Bio Rad
Centrifuge 5415D with standard rotor	Eppendorf
Centrifuges 6K15 and 4K15C and rotors	Sigma
Chambers for agarose gel electrophoresis	Bio Rad
CO ₂ incubator	Sanyo
Cryo-tank (-196°C)	Messer
Cryostat HM560	Microm AG
DigiTherm fly incubator	Tritech Research
Dissection microscope	Leica
Electron microscope EM10	Zeiss
Genetic Analyzer for DNA sequencing ABI Prism	Applied Biosystems
Glas homogenyzer	Kontes Glass
Hypercassette	GE Healthcare
Incubator for <i>E. coli</i>	Memmert
Incubator Shaker for <i>E. coli</i>	Burgwedel
Inverse table top microscope DMIL	Leica Microsystems
Inverse fluorescence microscope DMIRE2	Leica Microsystems
Laminar flow	BDK
Liquid Nitrogen Tank Chronos, ADURβ	Messer
LSM 510 laser-scanning confocal microscope	Zeiss
Magnetic stirrer RH basic	IKA Labortechnik
Milli-Q Biocell	Millipore
Mini Protean 3 for SDS-PAGE	Bio Rad
Mini Trans Blot Electrophoretic Transfer Cell	Bio Rad
Molds for embedding	Science Services
Optima TLX ultracentrifuge with TLA110 rotor	Beckman Coulter
PCR DNA Engine Tetrad Gradient Cycler PTC-225	MJ Research, Bio-Rad
pH meter	Mettler Toledo
Power Supply Power Pac 3000	Bio Rad
Shaker Duomax 1030	Heidolph Instruments
Shaker KS260 basic	IKA Labortechnik
SpeedVac SPD111V	Fisher Scientific
Synergy HT microplate reader	Biotek
Ultra-low temperature freezer (-80°C)	Sanyo Scientific
Ultramicrotome Ultrotome III	LKB
Ultrasonic bath Transsonic 310/H	Elma Ultrasonic
Ultraspec 3300 pro UV/Vis photometer	GE Healthcare
UV transilluminator UVT-40M	Herolab
Vortex Genie 2	VWR
Water bath HRB 4 digital	IKA Labortechnik

Materials and Methods

A.4 Oligonucleotides

Primers for polymerase chain reaction (PCR), sequencing, site-directed mutagenesis and Gateway cloning were bought from Metabion (Martinsried, Germany). Oligonucleotides for siRNA were purchased from Ambion.

Mutated nucleotides are represented in blue, while restriction sites of specified restriction enzymes are represented in red.

Name	Sequence (5'-3')	Purpose
attB1	GGGGACAAGTTGTACAAAAAAGCAGGC	Cloning
attB2	GGGGACCACTTGTACAAGAAAGCTGGG	Cloning
D1_fw_aatB	AAAAAGCAGGCTTCGAAGTAGGGTATGATGACAT	Cloning
D1_rv_aatB	AAGAAAAGCTGGGTCTACTCTACCACGGTTCCCGCA	Cloning
D2_fw_aatB	AAAAAGCAGGCTTCGTGCCACAGGTAAACCTGGGA	Cloning
D2_rv_aatB	AAGAAAAGCTGGGTTAGCCATACAGGTACATCAT	Cloning
N_fw_aatB	AAAAAGCAGGCTTCATGGCTCTGGAGCCGATT	Cloning
N_rv_aatB	AAGAAAAGCTGGGTCTAATTCAAGGACTCTCCTCAT	Cloning
ND2_1_HindIII_fw	AAAAAGCTTAAATGGCTCTGGAGC	Cloning
ND2_1_BamHI_rv	TTTGGATCCATTCAAGGACTCTTCC	Cloning
ND2_2_BamHI_fw	AAAGGATCCGTGCCACAGGTAAACCT	Cloning
ND2_2_EcoRI_rv	TTTGAATTCCTAGCCATACAGGTCA	Cloning
pcDNA3_fw	GCGGTAGGCGTGTACGGTGGG	Sequencing
pcDNA3_rv	GGGCAAACAAACAGATGGCTGGC	Sequencing
VCP1_fw	CGGTTAATTGTTGATGAAGCC	Sequencing
VCP2_fw	GTGGAGTTCAAAGTGGTGG	Sequencing
VCP3_fw	TGTTGACCCTCATGGATGGC	Sequencing
VCP4_fw	ATCCTGTGGAGCACCCAGAC	Sequencing
VCP5_fw	TAACCTGCGCAAGTCCCCAG	Sequencing
VCP6_fw	GGGAACCAGGGTGGAGC	Sequencing
VCP_K524A_fw	GACCTCCTGGCTGTGGGG G CAACTTGTGGC	Mutagenesis
VCP_K524A_rv	GCCAACAAAGTT G CCCCACAGCCAGGAGGT	Mutagenesis
VCP_R155H_fw	GACATTCTTCTGTCC A TGGTGGGATGCGTG	Mutagenesis
VCP_R155H_rv	GCACGCATCCCACCA T GGACAAGAAAAATGTC	Mutagenesis
VCP_silencer_n1	GGGCACAUGUGAUUGUUAUtt	siRNA
VCP_silencer_n2	GGUAUACCUUAAGCCGUACtt	siRNA

A.5 Plasmids and constructs

Plasmid	Description	Resistance	Supplier
pcDNA3	mammalian expression vector	Ampicillin (100 µg/mL)	Invitrogen
pcDNA3-Strep-GFP	pcDNA3 plasmid with C-terminal streptavidin (Strep)-green fluorescent protein (GFP) tag	Ampicillin (100 µg/mL)	C.J. Gloeckner, Helmholtz Zentrum Munich
pDONR201	Gateway-donor vector	Kanamycin (50 µg/mL)	Invitrogen
pDEST/N-SF-TAP	Gateway-entry vector	Ampicillin (100 µg/mL)	Gloeckner et al. (2007)
pDsRed2-ER tracker	mammalian expression vector encoding a fusion consisting of <i>Discosoma</i> sp. red fluorescent protein (DsRed2), Calreticulin ER targeting sequence fused to the 5' end of DsRed2 and the ER retention sequence KDEL fused to the 3' end of DsRed2a	Kanamycin (50 µg/mL)	Clontech
N-SF-TAP	pcDNA3, N-terminal Strep-Flag- tandem affinity purification (TAP) tag	Ampicillin (100 µg/mL)	Gloeckner et al. (2007)

Construct	cDNA	Plasmid	Supplier
VCP-WT	VCP-WT	pcDNA3	R. J. Braun, our laboratory
VCP-WT-GFP	VCP-WT	pcDNA3-Strep-GFP	R. J. Braun
VCP-K524A-GFP	VCP-K524A	pcDNA3-Strep-GFP	R. J. Braun
VCP-R155H-GFP	VCP-R155H	pcDNA3-Strep-GFP	R. J. Braun
Flag-VCP-WT	VCP-WT	N-SF-TAP	this study
Flag-VCP-K524A	VCP-K524A	N-SF-TAP	this study
Flag-VCP-R155H	VCP-R155H	N-SF-TAP	this study
Flag-N	N (1-199 aa)	N-SF-TAP	this study
Flag-D1	D1 (200-470 aa)	N-SF-TAP	this study
Flag-D2	D2 (471-806 aa)	N-SF-TAP	this study
Flag-ND1	ND1 (1-470 aa)	N-SF-TAP	this study
ND2	ND2 (1-199, 471-806 aa)	pcDNA3	this study
Flag-ND2	ND2 (1-199, 471-806 aa)	N-SF-TAP	this study
Flag-D1D2	D1D2 (200-806 aa)	N-SF-TAP	this study
Rhodopsin-WT	Rhodopsin-WT	pMT3	M.E. Cheetham (Saliba et al., 2002)
Rhodopsin-P23H	Rhodopsin-P23H	pMT3	M.E. Cheetham
Rhodopsin-WT-GFP	Rhodopsin-WT	pEGFP-N1	M.E. Cheetham
Rhodopsin-P23H-GFP	Rhodopsin-P23H	pEGFP-N1	M.E. Cheetham
Rhodopsin-WT	Rhodopsin-WT	pRC-CMV	V. Marigo, TIGEM, Italy
Rhodopsin-P23H	Rhodopsin-P23H	pRC-CMV	V. Marigo

Materials and Methods

A.6 Antibodies

Primary antibodies against fly proteins
(IHC: immunohistochemistry, WB: Western blotting)

Antibody	Species	Application	Supplier
Anti-GFP	rabbit polyclonal	1:400 IHC	A11122, Invitrogen
Anti-Hsc3/BiP	guinea pig	1:2000 WB	H.D. Ryoo, NY University, USA
Anti-Hsv	rabbit polyclonal	1:8000 WB	H6030, Sigma
Anti-Rhodopsin1 (4C5)	mouse monoclonal	1:5000 WB	4C5, DSHB, University of Iowa, USA
Anti-Rhodopsin1	rabbit polyclonal	1:5000 WB	D.F. Ready, Purdue University, USA
Anti-Ter94/VCP	rat polyclonal	1:5000 WB	D. McKearin, University of Texas Southwestern Medical Center, USA
Anti-TRP	rabbit polyclonal	1:8000 WB	A. Huber, University Hohenheim, Germany
Anti-β-Tubulin	mouse monoclonal	1:4000 WB	MAB3408, Chemicon
Anti-Ubiquitin	mouse monoclonal	1:300 WB	13-1600, Invitrogen

Primary antibodies against mammalian proteins
(IF: immunofluorescence, IP: immunoprecipitation)

Antibody	Species	Application	Supplier
Anti-Calnexin	rabbit polyclonal	1:400 IF	C4731, Sigma
Anti-Flag	mouse monoclonal	1:5000 WB	F3165, clone M2, Sigma
Anti-Flag	rabbit polyclonal	1:200 IF	F7425, Sigma
Anti-Rhodopsin	rabbit polyclonal	1:5000 WB	PA1-729, Affinity BioReagents
Anti-Rhodopsin (1D4)	mouse monoclonal	1:200 IF 2 µl/IP 1:5000 WB	R5403, Sigma
Anti-β-Tubulin	mouse monoclonal	1:2000 WB	T4026, Sigma
Anti-Ubiquitin	mouse monoclonal	1:8000 WB	550944, BD Pharmingen
Anti-VCP	mouse monoclonal	1:500 IF 2 µl/IP 1:5000 WB	Ab11433, Abcam
Anti-VCP	mouse monoclonal	1:5000 WB	65278, Progen Biotechnik

Secondary antibodies

Antibody	Species	Application	Supplier
Anti-guinea pig IgG HRP-conjugated	goat polyclonal	1:10000 WB	Jackson ImmunoResearch
Anti-mouse IgG Alexa Fluor 568-conjugated	goat polyclonal	1:1000 IF	Invitrogen
Anti-mouse IgG cy5-conjugated	goat polyclonal	1:1000 IF	Jackson ImmunoResearch
Anti-mouse IgG HRP-conjugated	goat polyclonal	1:10000 WB	Jackson ImmunoResearch
Anti-Rabbit IgG Alkaline Phosphatase-conjugated	goat polyclonal	1:200 IHC	Sigma
Anti-Rabbit IgG Alexa Fluor 488-conjugated	goat polyclonal	1:1000 IF	Invitrogen

Anti-Rabbit IgG Alexa Fluor 568-conjugated	goat polyclonal	1:1000 IF	Invitrogen
Anti-Rabbit IgG cy5-conjugated	goat polyclonal	1:1000 IF	Jackson ImmunoResearch
Anti-Rabbit IgG HRP-conjugated	goat polyclonal	1:10000 WB	Jackson ImmunoResearch
Anti-Rat IgG HRP-conjugated	goat polyclonal	1:10000 WB	Jackson ImmunoResearch

A.7 Cell lines and bacteria

Cell line	Description	Supplier
661W	661W mouse cone photoreceptor cells	M.R. Al-Ubaidi, University of Oklahoma Health Sciences Centre, USA
HEK 293	Human embryonic kidney cells 293	DSMZ, Germany
SK-N-SH	SK-N-SH human neuroblastoma cells	European Collection of Cell Cultures

Chemically competent DH5 α cells were purchased from Invitrogen.

A.8 Media, buffers and standard solutions

A.8.1 Media and antibiotics for bacterial culture

Antibiotics 1000x stock solution	Ampicillin (100 mg/ml) Kanamycin monosulfate (50 mg/ml)
Luria-Bertani (LB) medium (1L)	10 g Bacto-Tryptone 5 g Bacto-Yeast extract 5 g NaCl Dissolve in 1 L distilled water and adjust to pH 7.5. Sterilize by autoclaving and store at room temperature (RT).
LB plates	1 L LB medium 15 g Bacto-agar Autoclave, add corresponding antibiotic once the medium cooled down, pour into petri-disches and store at 4 °C.
SOC medium	2 % Bacto-Tryptone 0.5 % Bacto-Yeast extract 0.05 % NaCl 20 mM Glucose

Materials and Methods

A.8.2 Media and supplements for cell culture

Media for 661W and HEK293 cells	Dulbecco's modified Eagle's medium (DMEM) (Invitrogen) 10 % Fetal bovine serum (FBS) (Invitrogen) 2 mM L-Glutamine (Invitrogen) 25 mM HEPES (Invitrogen) 100 U/ml Penicillin (Invitrogen) 100 µg/ml Streptomycin (Invitrogen)
Media for SK-N-SH cells	DMEM/F12 (Ham) (Invitrogen) 10 % FBS 2 mM L-Glutamine 100 U/ml Penicillin 100 µg/ml Streptomycin

A.8.3 Fly food

Fly food (1L)	15 g yeast (Probio) 11.7 g agar (Probio) 80 g molasses (Grafschaftes Krautfabrik) 60 g corn flower (Primavera) 6.3 ml propionic acid (Sigma) 2.4 g methylparaben (Sigma) Cook for 1 hour at 96 °C and then cool down to 60 °C before adding propionic acid and methylparaben. Pour the food into vials and store at 4 °C. Yeast paste (yeast granules and fly water) was added to vials to enhance egg laying during crosses.
Fly water	0.8 % acetic acid in dd H ₂ O

A.8.4 Buffers and standard solutions

6x Agarose gel-loading buffer	TAE 50 % Glycerol 0.2 % Orange G
Phosphate-buffered saline (PBS)	10 mM Na ₂ HPO ₄ pH 7.4 2 mM KH ₂ PO ₄ 0.137 mM NaCl 2.7 mM KCl
PFA 4 %	40 g PFA in 1 L warm PBS (60 °C) add 400 µl NaOH 5 M to help dissolving then neutralize with 150 µl HCl 37 %

Sodium phosphate buffer pH 7.2
 68.4 ml of 1 M Na₂HPO₄
 31.6 ml of 1 M NaH₂PO₄
 2 % SDS
 add water to 1 L total volume.

Tris-acetate-EDTA (TAE) electrophoresis buffer
 40 mM Tris-acetate
 1 mM EDTA pH 8.0

Tris-buffered saline (TBS)
 50 mM Tris-HCl pH 7.4
 150 mM NaCl

A.8.5. Solutions and buffers for biochemistry, Western Blotting and histology

Solutions for biochemistry

Buffer A
 100 mM Tris-HCl pH 8.0
 0.1 mM Suc-LLVY-AMC

Buffer B
 25 mM Tris-HCl pH 7.5
 2 mM ATP
 5 mM MgCl₂
 1 mM DTT

Cell lysis buffer (CLB)
 PBS
 1 % NP-40
 10 % Glycerol
 Complete, protease inhibitor cocktail tablet
 (1 tablet/50 ml)
 Phophatase inhibitor cocktail (1/100)

Radio-immunoprecipitation assay (RIPA) modified buffer
 20 mM Tris-HCl pH 8.0
 150 mM NaCl
 1 mM EDTA
 1 % Triton X-100
 0.1 % SDS
 0.5 % Sodium deoxycholate
 Complete, protease inhibitor cocktail tablet
 Phophatase inhibitor cocktail

Tandem affinity purification (TAP) lysis buffer
 30 mM Tris-HCl pH 7.4
 150 mM NaCl
 0.5 % NP-40
 Complete, protease inhibitor cocktail tablet
 Phophatase inhibitor cocktail

TAP wash buffer
 30 mM Tris-HCl pH 7.4
 150 mM NaCl
 0.1 % NP-40
 Complete, protease inhibitor cocktail tablet
 Phophatase inhibitor cocktail

Materials and Methods

Tris-SDS solution	10 mM Tris-HCl pH 7.5 1 % SDS Complete, protease inhibitor cocktail
Wash buffer for IP	PBS 0.1 % NP-40 0.1 % Glycerol Complete, protease inhibitor cocktail tablet Phophatase inhibitor cocktail

Solutions for SDS-PAGE and Western Blotting

Gel solution for SDS separating gel (30 ml)	8 %	10 %	12 %
30 % (w/v) Acrylamide/Bis (37.5:1)	8 ml	10 ml	12 ml
1.5 M Tris-HCl pH 8.8	7.5 ml	7.5 ml	7.5 ml
ddH ₂ O	14 ml	12 ml	10 ml
10 % SDS	300 µl	300 µl	300 µl
10 % APS	150 µl	150 µl	150 µl
TEMED	30 µl	30 µl	30 µl
Gel solution for SDS stacking gel (15 ml)	4 %		
30 % (w/v) Acrylamide/Bis (37.5:1)	2 ml		
1.5 M Tris-HCl pH 6.8	1.25 ml		
ddH ₂ O	11.65 ml		
10 % SDS	150 µl		
10 % APS	150 µl		
TEMED	30 µl		

5x SDS sample buffer	5 % SDS 250 mM Tris-HCl pH 6.8 500 mM β-Mercaptoethanol 50 % Glycerol 0.4 % Bromphenol blue
Blocking solution for Immunoblotting (IB)	TBS 5 % Milk powder 0.1 % Tween-20
Ponceau staining solution	0.5 % Ponceau S 1 % Acetic acid
Ponceau destaining solution	10 % Acetic acid 40 % Ethanol
SDS Electrophoresis buffer	50 mM Tris base 384 mM Glycine 0.2 % SDS
Stripping buffer	5 mM Sodium phosphate buffer pH 7.2 2 mM β-Mercaptoethanol

	2 % SDS Add β-Mercaptoethanol right before use.
TBS-Tween (TBST)	TBS 0.1 % Tween-20
Wet blotting buffer	12 mM Tris base 96 mM Glycine 20 % Methanol
Solutions for histology, immunohistochemistry and immunofluorescence	
Alkaline phosphatase buffer	100 mM Tris-HCl pH 9.5 100 mM NaCl 50 mM MgCl ₂ 0.1 % Tween-20 Filter and store aliquots at -20 °C.
Antibody incubation solution for cells	PBS 1 % Normal goat serum 1 % BSA 0.1 % Tween-20
Cell blocking solution	PBS 5 % Normal goat serum 1 % BSA 0.1 % Tween-20
Durcupan epoxy resin mixture	48 % Component A/M 40 % Hardener B 2.25 % Accelerator C 9 % Plasticizer D
PBS-Triton 0.3% (PBST)	PBS 0.3 % Triton X-100
Toluidine blue solution	0.1 % Toluidine blue 2.5 % Sodium carbonate

A.9 Fly stocks

The following *Drosophila melanogaster* lines were used during this study:

<i>Drosophila</i> stocks	Source/donor
<i>WT</i>	Bloomington stock center (No. 1)
<i>w</i> ¹¹¹⁸	Bloomington stock center (No. 5905)
<i>w</i> ¹¹¹⁸	Bloomington stock center (No. 6326)
<i>ninaE</i> ^{S137F} (III) referred to as <i>Rh1</i> ^{D1}	J. O'Tousa, USA
<i>ninaE</i> ^{G69D} (III) referred to as <i>Rh1</i> ^{G69D}	B. Mollereau, ENS, France
<i>Rh1-Rh1</i> ^{WT} (II) referred to as <i>Rh1</i> ^{WT}	A. Giangrande, IGBMC, France

Materials and Methods

<i>Rh1-Rh1</i> ^{WT-hsv} (II) referred to as <i>Rh1</i> ^{WT-hsv}	J. O'Tousa
<i>Rh1-Rh1</i> ^{P37H} (III) referred to as <i>Rh1</i> ^{P37H}	A. Giangrande
<i>Rh1-Rh1</i> ^{P37H-hsv} (III) referred to as <i>Rh1</i> ^{P37H-hsv}	A. Giangrande
<i>ninaE</i> ^{H7} referred to as <i>Rh1</i> ^{KO}	Bloomington stock center (No. 5701)
<i>ter94</i> ²⁶⁻⁸ referred to as <i>VCP</i> ²⁶⁻⁸	Bloomington stock center (No. 9872)
<i>ter94</i> ^{k15502} referred to as <i>VCP</i> ^{k15502}	Bloomington stock center (No. 10454)
<i>Actin-Gal4</i> (II)	Takashi Suzuki, MPI Neurobiology
<i>GMR-Gal4</i> (II)	Takashi Suzuki
<i>Hs-Gal4</i> (II)	Takashi Suzuki
<i>Rh1-Gal4</i> (II)	A. Giangrande
<i>UAS-Xbp1-EGFP</i> (III)	H.D. Ryoo, NY University, USA
<i>UAS-Rh1</i> ^{G69D} (III)	H.D. Ryoo
<i>UAS-Ter94</i> (II) referred to as <i>UAS-VCP</i>	A. Kakizuka, Kyoto University, Japan

The following *Drosophila melanogaster* stocks were generated during this study:

w⁻; Bl/Cyo; Rh1-Rh1^{P37H}/*TM2*
w⁻; +/+; Rh1-Rh1^{P37H}:: *UAS-xbp1-EGFP*/+
w⁻; Actin-Gal4/Cyo; Rh1-Rh1^{P37H}/*TM2*
w⁻; Actin-Gal4/Cyo; Rh1^{KO}/*TM2*
w⁻; Actin-Gal4/Cyo; UAS-xbp1-EGFP/*TM2*
w⁻; GMR-Gal4/Cyo; UAS-Rh1^{G69D}/*TM2*
w⁻; UAS-ter94/Cyo; TM2/TM6

A.10 Software and databases

Software	Supplier
Adobe Illustrator CS	Adobe Systems
Adobe Photoshop CS	Adobe Systems
ImageJ 1.41	W. Rasband
ImageQuant TL software	GE Healthcare
MS Office 2003 (Word, Excel, Powerpoint)	Microsoft
Vector NTI Suite 10.0	Invitrogen

Database	Link
FlyBase	http://flybase.org/
NCBI	http://www.ncbi.nlm.nih.gov/
NCBI Blast	http://blast.ncbi.nlm.nih.gov/Blast.cgi
NCBI Nucleotide	http://www.ncbi.nlm.nih.gov/entrez/query.fcgi?db=nucleotide
NCBI Protein	http://www.ncbi.nlm.nih.gov/entrez/query.fcgi?db=protein
NCBI PubMed	http://www.ncbi.nlm.nih.gov/entrez/query.fcgi
Swiss-Prot	http://us.expasy.org/sprot/

B. Methods

B.1 Molecular biology

B.1.1 E. coli cultures

For liquid cultures, LB medium containing the appropriate antibiotics was inoculated either with an *E. coli* colony grown on LB plates or with a small amount of an *E. coli* cryo culture. Cultures were grown overnight at 37 °C with shaking at 130 rpm in flasks. Cryo cultures were obtained by mixing 500 µl of *E. coli* culture with 500 µl of sterile 80 % Glycerol. Cryo cultures were stored at -80 °C for several years.

B.1.2 Chemical transformation of competent *E. coli*

To transform chemically competent *E. coli*, 10 ng of plasmid DNA or 5 µl of ligation reaction were added to 50 µl of cells, mixed and incubated for 30 minutes (min) on ice. The cells were heat-shocked at 42 °C for 45 seconds (sec) and then cooled down on ice for 2 min. 450 µl of SOC medium without antibiotics were added and the cells were grown for 1 hour (h) at 37 °C with shaking at 200 rpm. Cells were sedimented and 400 µl of the supernatant were discarded. The pellet was resuspended in the remaining 100 µl of supernatant and plated onto LB plate containing the appropriate antibiotic. The LB plate was incubated overnight at 37 °C. Single colonies were later grown in LB medium supplemented with the appropriate antibiotic.

B.1.3 Preparation of plasmid DNA

Plasmid DNA was prepared from small-scale (2ml, miniprep) bacteria cultures using QIAprep Spin Plasmid Miniprep Kit or from large-scale (100 ml) of overnight cultures using the PureYield Plasmid Midiprep System. Bacteria were sedimented at 10000 g for 10 min at room temperature (RT) and plasmid DNA purification was carried out as described in the manufacturer's protocol, including steps of cell lysis, binding of the plasmid to the column, washing, and elution. Plasmid DNA was eluted with ddH₂O that was pre-heated at 60 °C. The concentration and purity of plasmid DNA preparations was determined using a UV spectrometer at 260 nm. A 260 nm/280 nm absorption ratio of 1.8 indicated a pure DNA preparation.

B.1.4 Enzymatic treatment of DNA

DNA cleavage

The recommended reaction volume for digestions is 50 µl. Plasmid DNA (1 µg) or purified cDNA PCR amplicates (300 ng) were digested with 10 U restriction enzyme in the appropriate buffer (1x), with 100 µg/ml BSA if required for 2 h at 37 °C. The reaction was stopped by heat-inactivation of the enzyme at 65 °C for 20 min. Digestion was checked by running 10 µl of the sample in a separating agarose gel.

DNA-fragment dephosphorylation

Treatment of DNA with antarctic phosphatase results in removal of the 5' phosphoryl termini, which is required by ligases. It prevents target vectors from self-ligation. Usual reaction volume is 50 µl including 1 U (1 µl) of antarctic phosphatase and the digested

Materials and Methods

sample in 1x antarctic phosphatase buffer. The reaction takes place during 30 min at 37 °C, followed by heat-inactivation for 5 min at 65 °C.

Ligation of DNA fragments and target vectors

The enzyme T4 ligase catalyses the formation of a phosphodiester bond between 5' phosphate and 3' hydroxyl termini in double stranded DNA or RNA and is therefore used to join DNA inserts, into open vectors. In a 20 µl volume, cleaved vector (0.1 µg) and DNA inserts of a 1:5 ratio, 1 µl of T4 ligase in 1x T4 ligase buffer were incubated overnight (o/n) at 16 °C or for 2 h at RT, followed by heat inactivation of the enzyme at 65 °C for 10 min and subsequent transformation of bacteria.

B.1.5 Agarose gel electrophoresis

To separate different sized DNA fragments and/or to determine their length and amount, DNA samples were run on agarose gels of 1-2 % and separated by electrophoresis. Agarose was dissolved in 1x TAE buffer by microwaving, mixed with 1 µl/100 ml ethidium bromide to visualize the DNA, poured into an electrophoresis gel chamber and cooled to RT while polymerizing. DNA samples were mixed with agarose gel loading buffer (6:1) loaded into the gel pockets and separated for approximately 30-45 min at 100-200 V depending on the gel size. DNA fragments were visualized by an UV transilluminator and their size was determined thanks to the DNA ladder. For preparative gels, the DNA band of interest was excised from the agarose gel using a clean, sharp blade and purified as described below.

B.1.6 DNA purification

From agarose gels

After excising the DNA band of interest from an agarose gel, the DNA fragments were purified using the QIAquick Gel Extraction Kit following the enclosed Qiagen protocol.

From enzymatic reactions

After enzymatic reactions, *e.g.*, PCRs, DNA digestion, DNA fragments were cleaned from salts, enzymes, and remnant nucleotides using the QIAquick PCR purification Kit following the enclosed protocol of the provider.

B.1.7 DNA sequencing

DNA sequencing was performed in a capillary-based automated sequencer after a cycle-sequence reaction done with the BigDye-Terminator v3.1 Cycle Sequencing Kit. 200 ng of plasmid DNA template were mixed with 2 µl of BigDye Terminator containing DNA polymerase and the fluorescence-labeled ddNTPs, 0.5 µl primer (10 pmol/µl) and ddH₂O up to 10 µl of final volume. Oligonucleotides used as primers for sequencing are supposed to have a melting temperature of ~ 50 °C. A PCR thermocycler was used with the following cycling program with 30 cycles from step 2 to 4:

1	96 °C	2 min	first denaturation of the double-stranded DNA template
2	96 °C	30 sec	denaturation of the DNA template
3	50 °C	15 sec	annealing of the primer to the DNA template
4	60 °C	4 min	elongation of the primer catalyzed by the polymerase
5	60 °C	4 min	final elongation

After the cycle-sequence reaction, the DNA was precipitated by adding 8 µl ddH₂O and 32 µl 95 % ethanol. After 15 min incubation at RT in the dark, the reaction mixtures were centrifuged for 15 min at 16000 g at RT. The DNA pellet was then washed with 200 µl 70 % ethanol and centrifuged during 10 min at 16000 g. The DNA pellet was dried at RT for 5 min and was dissolved in 75 µl H₂O. 25 µl of dissolved DNA were transferred onto a sequencing plate, which was placed into the automated sequencer. The resulting data were analyzed using ContigExpress in the Vector NTI Suite 10.0 software.

B.1.8 Polymerase chain reaction

PCR was performed according to standard conditions. The reaction mixture consisted of 50 ng cDNA template, 1x PCR buffer, 1.5 mM MgCl₂, 200 µM dNTPs, 0.5 µM forward and 0.5 µM reverse primer and 5 U Taq DNA polymerase in ddH₂O. PCR reaction was performed in a thermocycler with the following amplification program:

1	96 °C	1 min	first denaturation of the double-stranded DNA template
2	96 °C	30 sec	denaturation of the DNA template
3	* °C	30 sec	annealing of the primer to the DNA template
4	72 °C	** sec	elongation of the primer catalyzed by the polymerase
5	72 °C	5 min	final elongation

The amplification consisted of 30 cycles from step 2 to 4. The annealing temperature (*) was set as average of the melting temperatures of forward and reverse primers. Primers were designed with the Vector NTI Suite 10.0 software. The time required for elongation (**) depends on the length of the desired PCR product. Taq DNA polymerase needs 1 min elongation/kb of PCR fragment.

B.1.9 DNA cloning

PCR-based cloning

cDNA was amplified by PCR using primer with overhangs containing appropriate restriction sites. The PCR amplified fragments were purified by agarose gel electrophoresis, treated with restriction enzymes and purified with QIAquick PCR purification Kit. Subsequent ligation with the target vector, transformation into *E.coli*, plasmid DNA preparation, validation by restriction analysis and DNA sequencing were done as described before.

Gateway cloning

The Gateway cloning system is based on site-specific recombination mediated by the λ integrase family of recombinases (Hartley et al., 2000). It allows fast and easy cloning of inserts. The Gateway system consists of the donor and the destination vectors. The donor vector is used for the generation of generic entry clone, which contains the coding sequence of the protein of interest. The entry clone is recombined with destination vector in order to obtain a specific expression construct (destination clone).

The cDNA of the protein of interest (or of a domain) is first amplified by PCR. The PCR primers contain the *attB*1/2 recombination sites in order to allow a recombination with the pDONR201 plasmid for the generation of an entry clone. Since the *attB* sites are quite long (29 bp), a two-step PCR strategy is used. For the first PCR, half of the needed *aatB* sites are designed within the primers. In the second PCR, generic *aatB*1/2 primers for all

Materials and Methods

constructs are used to complete the *aatB* sites. The entry clone is then recombined with the appropriate destination plasmid: pDEST N-SF-TAP, to obtain the destination expression clone.

The donor vector as well as the destination vector contain *ccdB* marker for negative selection to avoid background caused by empty pDONR and pDEST vectors in the Gateway BP and LR reactions, respectively. The *ccdB* gene is toxic for *E. coli* K12 strains such as DH5 α . Gene specific primers were designed for the cDNA of interest flanked by *aatB* linker sequences (see A.4 Oligonucleotides). For the first PCR; 5 μ l high-fidelity (HF) Reaction Buffer and 0.5 μ l dNTP mix (provided with the fusion HF PCR Kit) were mixed with 1.3 μ l forward/ reverse gene-specific primer stocks 810 μ M), X μ l template (5-10 ng) and 0.5 μ l Phusion polymerase. The final volume was adjusted with water to 25 μ l. The following program for the thermocycler was used:

1cycle:	98 °C/ 1 min
10 cycles:	96 °C/ 20 sec
	55 °C/ 40 sec
	72 °C/ 1 min/ kb insert size

For the second PCR; to 10 μ l of the first PCR reaction 10 μ l HF-Reaction Buffer and 0.5 μ l dNTP mix were added, as well as 1.5 μ l of *attB1* and *attB2* primer stocks (10 μ M) and 1 μ l Phusion polymerase. The total volume was adjusted with water to 50 μ l. The following PCR program for the thermocycler was used:

1cycle:	98° C/ 1 min
10 cycles:	96 °C/ 20 sec
	55 °C/ 40 sec
	72 °C/ 1 min/ kb insert size
20 cycles:	95 °C/ 20 sec
	55 °C/ 40 sec
	72 °C/ 1 min/ kb insert size

The size of the PCR product was checked by agarose gel electrophoresis. Afterwards, for the Gateway BP reaction, 3 μ l of PCR product were added to 1 μ l pDONR201 plasmid (90 ng/ μ l) and 1 μ l BP Clonase Mix II. Following incubation for 2 h at 25 °C, 0.5 μ l Proteinase K were added and the reaction mix was incubated for 10 min at 37 °C. 5 μ l of the BP reaction were transformed into DH5 α cells and the cells were plated onto kanamycin LB agar plates. Clones were collected and inoculated with 2 ml of LB containing kanamycin. Entry clone plasmids were isolated from cultures and the inserts were verified by sequencing.

For the LR reaction, 1 μ l entry plasmid (90 ng/ μ l) was added to 2 μ l 10 mM Tris-HCl pH 8.0, 1 μ l pDEST/ N-SF-TAP plasmid (90 ng/ μ l) and 1 μ l LR Clonase Mix II. Following incubation for 2 h at 25 °C, the reaction was stopped by addition of 0.5 μ l Proteinase K and incubation for 10 min at 37 °C. 5 μ l of the LR reaction were transformed into DH5 α cells. The cells were plated onto ampicillin LB agar plates. Clones were collected and inoculated with 2 ml of LB containing ampicillin. Plasmids were isolated and inserts were verified by sequencing.

B.1.10 Site-directed mutagenesis

Point-mutated VCP constructs (VCP^{K524A} , VCP^{R155H}) were generated from VCP^{WT} construct by site-directed mutagenesis using the QuikChange II Site-Directed Mutagenesis Kit. Mutagenesis primer pairs (see A.4 Oligonucleotides) were designed considering the manufacturer's protocol with a melting temperature of $> 78\text{ }^{\circ}\text{C}$. Both primers (sense and antisense) comprised the nucleotide exchange. The whole plasmid was amplified by PCR with the *PfuUltra* High-Fidelity DNA polymerase, resulting in amplified plasmid containing the mutation of interest. 10 ng cDNA template were used for a 50 μl reaction mixture containing 5 μl 10x reaction buffer, 125 ng forward primer, 125 ng reverse primer, 1 μl dNTP mix and 1 μl *PfuUltra* High-Fidelity DNA polymerase (2.5 U/ μl) in ddH₂O. PCR reaction was performed in a thermocycler with the following settings:

1	95 °C	30 sec	first denaturation of the double-stranded DNA template
2	95 °C	30 sec	denaturation of the DNA template
3	55 °C	1 min	annealing of the primer to the DNA template
4	68 °C	1 min/kb	elongation
5	68 °C	5 min	final elongation

The amplification stage comprised (step 2 to 4) 12 cycles for point mutations. The non-mutated methylated DNA template was selectively degraded by *DpnI* endonuclease by adding 1 μl *DpnI* (10 U/ μl) per reaction mixture and incubation at 37 °C for 1 h. The non-methylated amplified mutation-carrying plasmid was then transformed into XL1-Blue supercompetent cells by mixing 1 μl of *DpnI* treated DNA with 50 μl cells. Plasmid DNA was prepared from the transformed colonies and validated by DNA sequencing.

B.1.11 Generation of VCP constructs

pcDNA3-VCP^{WT} and pcDNA3-VCP^{WT/K524/R155H}-Strep-GFP constructs were kindly offered by R. J. Braun. Briefly, to clone human VCP into the pcDNA3 vector, the full-length VCP cDNA from the pOTB7 library vector was used. VCP^{K524A} and VCP^{R155H} mutants were generated from the VCP^{WT} construct using QuickChangeII Site-Directed Mutagenesis Kit. To obtain C-terminal GFP-tagged VCP, VCP^{WT} and its variants were subcloned into the pcDNA3-Strep-GFP.

During this study, SF-tagged human full-length VCP and VCP domains (N, D1, D2, ND1, D1D2) were obtained by PCR amplification using pcDNA3-VCP^{WT} as template and further cloning into the pcDNA3-SF-TAP vector by using Gateway system. For the ND2 chimeric domain (1-199, 471-806), individual N and D2 domains were amplified by PCR using pcDNA3-VCP^{WT} as template and then cloned into pcDNA3 vector using *BamHI*, *EcoRI* and *HindIII* restriction sites. ND2 domain was then PCR-amplified and cloned into the pcDNA3-SF-TAP plasmid via Gateway system. pcDNA3-VCP^{K524/R155H}-SF-TAP were generated from pcDNA3-VCP^{WT}-SF-TAP by using QuickChangeII Site-Directed Mutagenesis Kit.

B.2 Analysis of mammalian cell cultures

B.2.1 Maintenance of mammalian cell cultures

Propagation

HEK293, 661W or SK-N-SH cells were maintained at 37 °C and 5 % CO₂ below total confluence. For splitting, the cells were washed with sterile PBS, treated with trypsin/EDTA at 37 °C until the cells started to detach from the culture dish, and collected in the appropriate volume of growth medium. The cells were then distributed in the desired dilution onto fresh culture plates with pre-warmed growth medium.

Freezing and thawing

Cells were harvested using trypsin/EDTA as described above, collected by centrifugation at 180 g for 5 min at RT and re-suspended in FBS with 10 % DMSO and distributed into cryo-tubes of 1 ml volume. Cryo-tubes were placed at 4 °C for 30 min, at -20 °C for 1 h and at -80 °C overnight. Long-term storage of cryo cultures was done in a cryo-tank filled with liquid nitrogen. To thaw frozen cells, the cryo-tube was quickly placed into a 37 °C water bath and 10 ml of pre-warmed growth medium was added as soon as its content was thawed. The cells were collected by centrifugation at 180 g for 5 min at RT, re-suspended and seeded onto culture plates with pre-warmed growth medium.

B.2.2 Treatment and coating of coverslips

For immunofluorescence experiments, coverslips were treated with ethanol in a glass beaker twice for 30 min at RT. Coverslips were then dried under the laminar flow and baked in a glass Petri dish in the oven at 180 °C for 3 h. Sterile coverslips were then placed into 24-well plates and coated with sterile 1 mg/ml poly-D-lysine dissolved in ddH₂O (400 µl/well) at 37 °C for minimum 4 h. Then the coverslips were washed 3 times with sterile ddH₂O and left to dry under the laminar flow.

B.2.3 Transient transfection of mammalian cell cultures

Transient transfection of 661W and HEK293 cell cultures was done by lipofection using the effectene transfection reagent according to manufacturer's instructions. 24 h prior transfection, 661W cells or HEK293 were seeded at 1.5 x 10⁴ cells/well in 24-well plates for immunofluorescence experiments. For generation of protein extracts, HEK293 cells were splitted to achieve the appropriate density (60 %) for transfection onto 6-well or 10 cm culture plates. Plasmid cDNA was added to EC buffer, supplemented with enhancer solution and the mixture was shortly vortexed and incubated for 5 min at RT. Liposome formation was initiated by adding effectene. The solution was mixed and incubated at RT for 10 min. The medium was removed from the wells, and the liposome solution mixed with fresh medium was gently added to the cells for 48 h at 37 °C. Following proportions were followed for transfection:

Culture format	cDNA (µg)	Enhancer (µl)	EC buffer (µl)	Effectene (µl)	Medium to add to cells (Volume: µl)	Medium to add to complexes (Volume: µl)
24-well	0.3	1.6	60	5	300	350
6-well	0.5	3.2	100	10	1600	600
10 cm	1	16.0	300	60	7000	3000

For immunofluorescence or for cytotoxicity experiments, SK-N-SH cells were transiently transfected with plasmid cDNA using Lipofectamine and Plus reagent according to manufacturer's protocol. 24 h prior transfection, SK-N-SH cells were seeded in the appropriate growth medium. cDNA was dissolved in DMEM/F12 medium without serum or antibiotics and Plus reagent was added. The mixture was incubated for 15 min at RT. Lipofectamine was diluted separately in DMEM/F12 medium without serum or antibiotics. Pre-complexed cDNA was combined with the diluted Lipofectamine and incubated for 15 min at RT. Medium on cells was replaced with growth medium without serum or antibiotics and the DNA-Lipofectamine mixture was added to the cells for 3 h at 37 °C. After 3 h, the transfection medium was replaced by the appropriate growth medium. Following proportions were followed for transfection:

Culture format	Cell type and density	Volume of plating medium	cDNA (µg) and Plus reagent (µl) and dilution volume	Lipofectamine and dilution volume	Volume of medium (without serum) to add to cells
96-well	SK-N-SH 7 x 10 ³ / well	100 µl	0.1 µg and 0.8 µl in 12.5 µl	0.4 µl in 12.5 µl	25 µl
24-well	SK-N-SH 7 x 10 ⁴ / well	500 µl	0.4 µg and 4 µl in 25 µl	1 µl in 25 µl	200 µl

VCP siRNA silencer n1, n2 (see A.4 Oligonucleotides) and negative control n1 (non-sense sequence) were purchased from Ambion. For transfection of silencers, Lipofectamine 2000 was used according to manufacturer's protocol. Briefly, HEK293 or SK-N-SH cells were seeded in the appropriate growth medium, but without antibiotics. 20 h later, cells were transfected with VCP siRNA. For transfection, siRNA was diluted in DMEM (for HEK293) or DMEM/F12 medium (for SK-N-SH) without serum or antibiotics. Lipofectamine 2000 was separately diluted in DMEM or DMEM/F12 medium and incubated for 15 min at RT. Then the diluted siRNA was combined with the diluted Lipofectamine 2000 and incubated at RT for 15 min. DNA-Lipofectamine 2000 complexes were added to each well. Cells were assessed for knock-down levels 48 h later. Following proportions were followed for transfection:

Culture format	Cell type and density	Volume of plating medium	siRNA and dilution volume	Lipofectamine 2000 and dilution volume
96-well	SK-N-SH 7 x 10 ³ / well	100 µl	5 µM in 12.5 µl	0.4 µl in 12.5 µl
6-well	HEK293 2 x 10 ⁵ / well	2 ml	50 µM in 250 µl	4 µl in 250 µl

The transfection efficiency for different cell lines was: 80 % for HEK293, 15 % for SK-N-SH and 10 % for retinal 661W. All the constructs had similar expression levels. The ratio between GFP-transfected cells and the total number of living cells (*i.e.* the transfection efficiency) was calculated for each condition using at least two fields of ~50 cells.

B.2.4 Rh degradation and proteasome inhibition assay

Cells were transfected with VCP siRNA or control, and after 20 h were transfected with Rh construct. 20 h after Rh transfection, cell lysates were collected at different time points within a 7.5 h period after inhibition of protein synthesis by cycloheximide (100 µM).

Materials and Methods

Proteasome inhibition was achieved by exposing HEK293 cells, 32 h after transfection, to 5 µM MG132. For the VCP-dependent degradation assay of Rh, cells were lysed after 16 h of incubation with MG132 and the lysates were analyzed by WB. For the co-IP experiment, cells were lysed after 8h of incubation with MG132 and the IP experiment was performed. For immunofluorescence, 661W retinal cells and SK-N-SH cells were fixed and labelled after 8h of incubation with 5 µM MG132 inhibitor.

B.2.5 Cell lysis

Medium was removed from HEK293 cells and cells were washed 3 times with ice-cold PBS. Cells were then scraped and lysed with ice-cold cell lysis buffer (CLB). 200 µl of CLB/well were used for 6 well-plates and 500 µl for 10 cm cultures dishes. Cell lysates were transferred into Eppendorf tubes and lysis was continued for 30 min on a spinning wheel at 4 °C. Lysate were then centrifuged (10 min, 16000 g, 4 °C), in order to discard cell debris. The supernatants were transferred into tubes and used right away or shock frozen in liquid nitrogen and stored at -80 °C until further use.

B.2.6 Lactate dehydrogenase assay

Quantification of cytotoxicity induced by expression of misfolded Rh or of VCP siRNA was performed via measurement of cytoplasmic lactate dehydrogenase (LDH) release into the cell culture supernatant from damaged cells using the Cytotoxicity Detection Kit Plus. The LDH activity is determined in an enzymatic test: in the first step NAD⁺ is reduced to NADH/H⁺ by the LDH-catalyzed conversion of lactate to pyruvate. In the second step the catalyst (diaphorase) transfers H/H⁺ from NADH/H⁺ to the tetrazolium salt INT (pale yellow) which is reduced to formazan salt (red). An increase in the amount of dead or plasma membrane-damaged cells results in an increase of LDH activity in the culture supernatant. This increase in the amount of enzyme activity in the supernatant directly correlates to the amount of formazan formed during a limited time period. The formazan dye formed is water-soluble and has a broad absorption maximum at about 500 nm, whereas the tetrazolium salt INT has no significant absorption at these wavelengths.

The LDH assay was performed on SK-N-SH cells seeded onto 96-well pates, 48 h after transfection, according to the manufacturer's instructions. Reaction mixture was prepared just before the assay, by mixing catalyst solution (diaphorose, NAD⁺ mixture) with the dye solution (tetrazolium salt INT and sodium lactate). 100 µl of reaction mixture were added to the cell supernatant of each well of the 96-well plate and incubated in the dark at RT for 20 min. 50 µl of stop solution were then added to each well and the amount of formed formazan was measured by absorbance at 492 nm using a Synergy HT microplate reader.

B.2.7 Immunofluorescence microscopy

48 h post-transfection, cells were fixed by adding 400 µl of pre-warmed (37 °C) 4 % PFA for 15 min at RT. PFA was then discarded and cells were washed 3 times with PBS. Fixed cells were permeabilized with 100 µl of 0.1 % Triton X-100 in PBS/coverslip for 5 min at RT. Cells were washed with PBS and were then blocked with cell blocking solution for 30 min at RT. Coverslips were afterwards incubated for 3 h at RT with the primary antibody in an appropriate dilution (see A.6 Antibodies) in 75µl/coverslip of antibody incubation solution for cells. Cells were then washed five times for 5 min each with PBS and were incubated for 1 h at RT with the appropriate fluorochrome-coupled secondary

antibodies (see A.6 Antibodies) diluted in antibody incubation solution for cells. After five washes for 5 min each with PBS, coverslips were briefly rinsed in ddH₂O and mounted with fluorsave on glass slides. Images were acquired using a 63x objective of a Carl Zeiss LSM 510 laser-scanning confocal microscope.

B.2.8 Quantification of average levels of intracellular Rh aggregates

Pictures displaying the distribution of Rh in transfected cells were used. The area corresponding to intracellular Rh aggregates was carefully delineated and the average intensity of the signal was determined within this area. To correct for differences in background intensity, an area devoid of aggregates (generally the nucleus, inferred from the Calnexin/ER labeling) was used and the average intensity in this area was subtracted from the average intensity of Rh aggregates. The quantifications were performed using the ImageJ software and the values are represented in arbitrary units. At least 15 cells were analyzed per condition. Results were considered significant for a p-value inferior to 0.05, using the Student's t-test.

B.3 Protein chemistry and Western blotting

B.3.1 Protein concentration measurement

The concentration of proteins in cell lysates was determined using the Bio-Rad Protein Assay Kit, based on Bradford assay, following manufacturer's instructions. 1 volume of dye reagent concentrate was diluted with 4 volumes of ddH₂O. 1 ml of the diluted reagent was mixed with 2-5 µl of cell lysates in doublets and incubated for 5 min at RT. Absorption was measured at 595 nm with Ultraspec 3300 photometer. Protein concentrations were calculated using a standard regression curve with BSA as protein standard (2-10 µg BSA). Protein extracts were treated with 5x SDS sample buffer 5 min at 95 °C or for 30 min on ice for membrane proteins.

B.3.2 Immunoprecipitation and chloroform-methanol precipitation

Immunoprecipitation

For co-IP HEK293 cells were lysed with cell lysis buffer and a total amount of 1.5 mg of detergent-soluble protein extracts in a final volume of 500 µl was first pre-cleared with mouse IgG coupled to protein G agarose beads. Prior to incubation with cell lysates, antibodies were coupled to protein G beads for 45 min at RT in 50 µl of PBS. The pre-cleared cell lysates were then incubated with 2 µl of undiluted anti-VCP antibody (mouse monoclonal, Abcam) or anti-Rh antibody (1D4, mouse monoclonal, Sigma) coupled to 20 µl of protein G agarose beads for 5 h at 4 °C. Protein G beads were then centrifuged for 3 min, 0.1 g at 4 °C and the cell lysates were discarded. The beads linked to the immunoprecipitates were then washed 3 times with wash buffer for IP and centrifuged for 3 min each at 0.1 g, 4 °C. Samples were eluted with 2x SDS sample buffer for 5 min at 95 °C or for 30 min on ice for membrane proteins.

Ubiquitin pull-down

For ubiquitin pull-down, ubiquitin enrichment kit was used according to manufacturer's protocol. Briefly, 400 µl of detergent-soluble fractions (obtained with cell lysis buffer) containing at least 0.5 mg of total protein were incubated with 20 µl of polyubiquitin affinity resin for 2 h at 4 °C in provided spin columns. The polyubiquitin affinity resin binds polymers containing four or more ubiquitin subunits. Afterwards, cell lysates were

Materials and Methods

discarded and the resin was 3 times washed with the wash buffer provided by the manufacturer. The samples were then eluted with 2x SDS sample buffer for 30 min on ice. Eluate contains ubiquitin-enriched fraction. A polyubiquitin positive control was also provided by the manufacturer. 1 μ l of this positive control was diluted in cell lysis buffer and incubated with polyubiquitin affinity resin in the same conditions as all the cell lysates.

Flag precipitation assay

For Flag precipitation assay, cells were lysed using tandem affinity purification (TAP) lysis buffer. N-SF-TAP expression constructs allow a two-step purification (for Strep and Flag tags), but in this case, a one-step anti-Flag precipitation was performed. 500 μ l of detergent-soluble fractions containing 1 mg of total protein were incubated with 10 μ l of anti-Flag M2 agarose in microspin columns for 2 h at 4 °C. Afterwards, Flag-coupled beads were washed 3 times with 500 μ l of TAP wash buffer and the proteins were eluted with 200 μ l of 200 μ g/ml Flag peptide in TBS. After chloroform-methanol precipitation, 2x SDS sample buffer was added to samples that were incubated during 30 min on ice.

Chloroform-methanol precipitation

Chloroform-methanol precipitation was performed on aqueous protein samples. 0.8 ml methanol was added to 0.2 ml of protein sample. The solution was vortexed and centrifuged for 10 sec (16000 g, RT). 0.2 ml chloroform was added, and the solution was mixed and centrifuged (10 sec, 16000 g, RT). By adding 0.6 ml ddH₂O and vortexing and centrifuging (1 min, 16000 g, RT), phase separation was induced leading to accumulation of denatured proteins in the interphase. The upper (aqueous) phase was removed and the remaining solution was mixed with 0.6 ml methanol. Denatured proteins were then sedimented (2 min, 16000 g, RT) and air-dried after discarding the supernatant. The pellet was dissolved in 2x SDS sample buffer for analysis by SDS-PAGE.

B.3.3 SDS-PAGE

In order to separate protein mixtures, one-dimensional SDS-polyacrylamide gel electrophoresis (SDS-PAGE) was used. Gels were casted using casting chambers for mini gels with 1/1.5 mm spacers. The casting chamber was filled with separating gel solution (see A.8.5) that was overlaid with isopropanol. After polymerization, isopropanol was removed and the top of the separating gel was washed with dH₂O. The separating gel was overlaid by the stacking gel solution and the combs were inserted. Different concentrations of acrylamide were used for separating gels (8 to 12 %). Gels were then placed into the gel chamber Mini Protean 3 and the buffer chamber was filled with SDS electrophoresis buffer. After loading the samples onto the gel, electrophoresis was done at 60 V until the bromophenol blue front reached the beginning of the separating gel and was then changed to 90 V. Electrophoresis was stopped when the bromophenol blue front reached the end of the separating gel. A pre-stained protein marker was used as protein standard.

B.3.4 Immunoblotting analysis

Western blotting of SDS gels to PVDF membrane was performed with a wet blotting apparatus according to manufacturer's protocol. After electrophoresis, gels were incubated in wet blotting buffer for 5 min. PVDF membranes were activated with methanol, rinsed in dH₂O and incubated in blotting buffer for 5 min. Cut filter papers and fiber pads were soaked in wet blotting buffer prior use. A fiber pad, 2 filter papers and the

PVDF membrane were laid on the anode side of the gel holder cassette. The gel was then placed on top of the membrane avoiding the air bubbles, followed by 2 filter papers and a fiber pad. The gel holder cassette was closed and placed into the blotting system. The blotting system and the cooling unit were inserted into the tank. Proteins were transferred with 90 V for 2 h at 4 °C. After blotting, the membranes were stained for 5 min with Ponceau staining solution. Background staining was removed by incubating the membranes for 5 min with Ponceau destaining solution and then short wash with TBST.

For further immunodetection, membranes were destained with TBST and blocked for 1 h at RT with blocking solution for immunoblotting (IB), incubated with the primary antibody in an appropriate dilution (see A.6 Antibodies) in blocking solution for IB o/n at 4 °C. Membranes were washed 3 times for 10 min with TBST and were then incubated with the appropriate horseradish-peroxidase (HRP)-coupled secondary antibody in a 1:10000 dilution in blocking solution for IB during 1 h at RT. Membranes were washed 3 times for 10 min with TBST. Immunodetection was done using the enhanced chemiluminescence (ECL) plus kit according to manufacturer's protocol. Briefly, 2 ml of solution A were mixed with 50 µl solution B before use. Membranes were incubated for 2 min at RT with the mixed solution. Hyperfilm ECL films and the Agfa Curix 60 developer were further used. The films were afterwards digitalized using a calibrated imaging densitometer. Quantification of band intensity after ECL detection was performed using Image Quant TL software.

For reprobing of the membranes, antibodies bound to PVDF membranes were removed by incubating the membranes in stripping buffer for 20 min at 55 °C on a shaker. Membranes were washed with TBST and blocked, incubated with the primary and secondary antibodies as described above.

B.4 Drosophila genetics, biochemistry, immunohistochemistry, behaviour and ERG

B.4.1 Drosophila maintenance

Flies were raised on standard cornmeal agar medium (see A.8.3 Fly food), under moderate continuous illumination at 25°C. Moderate illumination was obtained by using photosynthetic fluorescent tubes (in total 170 candela/m²). Fly progeny having same eye pigmentation was used during the study.

B.4.2 The Gal4-UAS system

The Gal4-UAS binary system allows the expression of a given transgene under the indirect control of a given promoter (Figure 37). The gene (*X*) to be expressed is positioned downstream of an upstream activating sequence (UAS) found in yeast; flies carrying the UAS-X construct are generated (line 1). Conventional lines exist in which the *Gal4* transactivating yeast gene is placed under the control of a cell/tissue specific promoter (P; line 2), allowing expression of the Gal4 protein in cells/tissue where the promoter P is active. When the two lines 1 and 2 are crossed, the Gal4 protein generated in defined cells/tissue binds specifically the UAS sequence and induces the expression of the X gene in the same cells/tissue. If, for example, P is *Rh1* and X is *Xbp1*, expression of *Xbp1* will be specifically induced in *Rh1*-6 photoreceptor neurons, where *Rh1* is active.

Materials and Methods

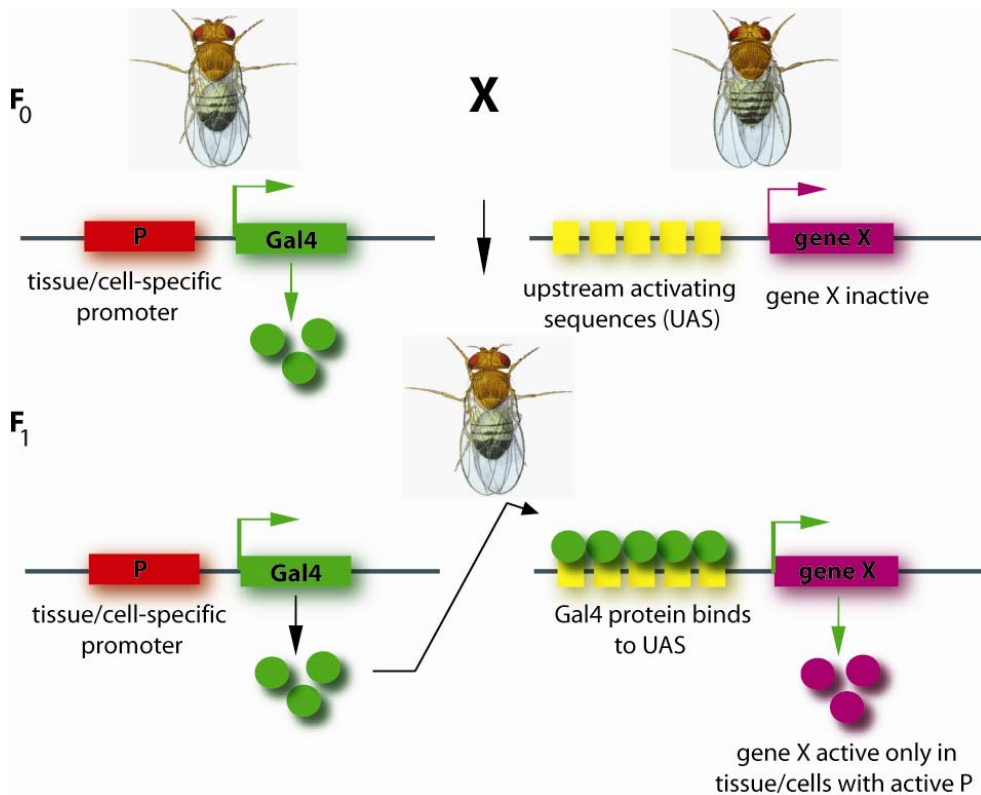


Figure 37. Targeted gene expression using the Gal4-UAS system. The Gal4-UAS system allows the expression of a given gene (*X*) in defined tissue/cells, using a tissue/cell specific promoter (*P*). One fly line carries a transgene in which the coding sequence of the yeast transactivator Gal4 is placed downstream of promoter *P*. Alternatively, the coding sequence of Gal4 can be knocked in downstream of an endogenous promoter. A second fly line carries a transgene in which the gene of interest (*X*) is placed downstream of an upstream activating sequence (UAS). Upon crossing these two fly lines, the resulting progeny will express the Gal4 transactivator in the cells/tissue defined by the promoter *P*; in these cells, Gal4 binds the UAS sequence and leads to activation of transcription downstream of UAS. The gene *X* is therefore active only in *P*-positive cells, while it remains inactive in all other cells/tissues.

B.4.3 Drosophila heat-shock

Transgenic animals carrying UAS-VCP and a transgene driver Hs-Gal4 (heat shock promoter coupled to Gal4) were given a 90 minutes heat-pulse at 37 °C and assayed at different time points after being shifted to 25 °C.

B.4.4 Drosophila biochemistry

Generation of detergent-soluble and insoluble fractions

30 fly heads were homogenized in 60 µl of RIPA modified buffer with a small glass homogenizer. Lysates were centrifuged at 16000 g for 15 min at 4° C and the supernatants containing detergent-soluble fractions were kept for further analysis. For detergent-insoluble fractions, pellets were solubilised in 50 µl of Tris-SDS solution for 8 min at RT. 100 µl of RIPA modified buffer was added, and the pellets were then sonicated six times 10 sec each at 4 °C. Following sonication, the fractions were incubated on a spinning wheel for 30 min at 4 °C. Detergent-insoluble fractions were then centrifuged at 100 g for 10 min at 4 °C and tissue debris were discarded. For WB, fractions were normalised for total protein using the *Dc* protein kit based on Lowry assay. An equal volume of 2x SDS sample buffer was added to fractions separated by 1 mm

thick 10-12 % SDS-PAGE for detergent-soluble and by 1.5 mm thick 8 % SDS-PAGE for detergent-insoluble fractions.

Immunoblotting

Immunodetection was performed as described before. All primary antibodies are indicated in A.6 Antibodies section. Anti-Rh1 (rabbit polyclonal, gift from D. Ready) was used for detecting Rh1 in detergent-insoluble fractions, while 4C5 (mouse monoclonal, DSHB) was used to detect Rh1 in detergent-soluble fractions. Quantification of protein immunoband intensity after chemiluminescence detection was performed using Image Quant TL software.

Crude proteasome extraction and measurement of proteasome activity

Proteasome chymotrypsin-like activity in *Drosophila* lysates was assessed colorimetrically using a synthetic peptide substrate, succinyl-Leu-Leu-Val-Tyr-7-amino-4-methyl-coumarin (Suc-LLVY-AMC) as previously described (Tonoki et al., 2009). When a C-terminal 7-amino-4-methylcoumarin-containing peptide is hydrolyzed, the fluorescent compound 7-amino-4-methylcoumarin is released. This compound is monitored by excitation at 380 nm and emission at 460 nm. The more compound is released, the more active is the proteasome.

Proteasome activity was measured in the presence and absence of the proteasome inhibitor MG132. In order to preserve the proteasome activity, freshly collected control *Drosophila* heads were gently homogenized using a small glass homogenizer in buffer B and incubated during 30 min on ice. Homogenates were centrifuged at 20000 g for 20 min at 4 °C. Supernatants were then centrifuged again at 20000 g for 10 min at 4 °C. Cleared supernatants were normalised for total protein using Protein Assay kit based on Bradford assay. A protein concentration of 0.3-0.5 µg/µl is suitable for this assay. 10 µl of lysates were added in a 96 well-plate on ice. Then, 90 µl of buffer A containing the proteasome substrate Suc-LLVY-AMC and supplemented with either 50 µM MG132 in 0.5 % DMSO or only 0.5 % DMSO were added in the dark and the plate was incubated at 37 °C during 1 h in the dark. Fluorescence was read using a 380/460 nm filter set of a Synergy HT microplate reader.

B.4.5 Drosophila histology, electron microscopy and immunohistochemistry

Histology, toluidine blue staining and analysis

To highlight the cellular anatomy of the fly retina and to visualize the sub-cellular morphology of photoreceptor neurons, toluidine blue was used as contrasting agent. Fly heads were dissected and post-fixed in 2.5 % glutaraldehyde in PBS o/n at 4 °C. After washing with PBS, heads were incubated in a 1 % osmium tetroxide solution and then dehydrated in ethanol solutions of increasing concentrations (25-100 %), followed by a 10 min incubation in propylene oxide. Heads were then incubated o/n in a solution containing 50 % propylene oxide and 50 % durcupan epoxy resin mixture. Then, heads were incubated overnight in 100 % durcupan epoxy resin mixture. The next day, heads and fresh durcupan epoxy resin mixture were transferred to molds; heads were oriented tangentially and then cooked overnight at 60 °C. The polymerized resin containing the specimens was then removed from molds and cut using an ultramicrotome. Semi-thin sections of 2 µm were collected, mounted and then stained using a prewarmed toluidine blue solution. After a quick wash in water, sections were allowed to dry and were then covered with paraffin oil. Pictures at different retinal depths were acquired for each head (at 40x magnification). To determine the number of photoreceptor neurons/ommatidium

Materials and Methods

(P/O), at least 150 ommatidia were scored per animal from at least 6 animals per genotype.

Electron microscopy

Electron microscopy experiments were performed with the help of Luise Jennen (Institute of Pathology, Helmholtz Zentrum München). For electron microscopy, the specimens were embedded the same way as described above for toluidine blue staining experiments. However, 70 nm ultra-thin sections (instead of 2 µm) were collected on nickel grids and contrasted with 5 % uranyl acetate and lead citrate, and analyzed with a Zeiss electron microscope EM 10.

Xbp1-EGFP ER stress reporter and immunohistochemistry

The *Drosophila* *Xbp1* mRNA undergoes Ire1-mediated unconventional splicing in response to ER stress. *Drosophila* has two *Xbp1* isoforms: the RA isoform containing an extra 23-base sequence compared to the RB isoform. The splicing of this 23-nucleotide sequence by Ire1 is predicted to cause a frame shift during protein translation. As a result, the putative RA transcript encodes a 307 amino acid protein whereas the RB transcript encodes a 498 amino acid protein (Figure 38A). The property of unconventional slicing of *Xbp1* was used to develop a specific ER stress reporter, Xbp1-EGFP, in which EGFP is expressed in frame only after ER stress (Figure 38B) (Ryoo et al., 2007). To detect non-conventional *Xbp1* mRNA splicing of the *Xbp1-EGFP* construct, an anti-GFP antibody was used to label GFP expressed in fly retinas upon ER stress activation, followed by alkaline phosphatase staining and quantification of GFP-positive cells/area. For example, in *Rh1^{P37H}* retinas there are significantly more GFP-positive cells compared to control flies (Figure 38C).

Immunohistochemistry procedure was performed as described (Galy et al., 2005). Fly heads were dissected and fixed for 15 min in 4 % PFA, incubated in 10 % sucrose in PBS during 2 h and in 25 % sucrose o/n at 4 °C, then embedded in cryomedium. 16 µm-thick cryostat sections were fixed for 15 min with 4 % PFA, permeated with PBST during 30 min and blocked during 1h with 5 % normal goat serum in PBST. To detect *Xbp1* mRNA splicing an anti-GFP antibody diluted in blocking solution was used. After o/n incubation with primary antibody, sections were washed 3 times 10 min each with PBST. Afterwards, an alkaline phosphatase-linked anti-rabbit secondary antibody was added for 2h at RT. Sections were then washed 2 times with PBST and 3 times with alkaline phosphatase buffer 10 min each. Sections were incubated with 5-bromo-4-chloro-3-indolyl phosphate (BCIP)/nitro blue tetrazolium (NBT) substrate during 30 min, washed with ddH₂O, air-dried and mounted in a non-aqueous mounting medium Clarion. Number of GFP-positive nuclei/area was quantified for each genotype.

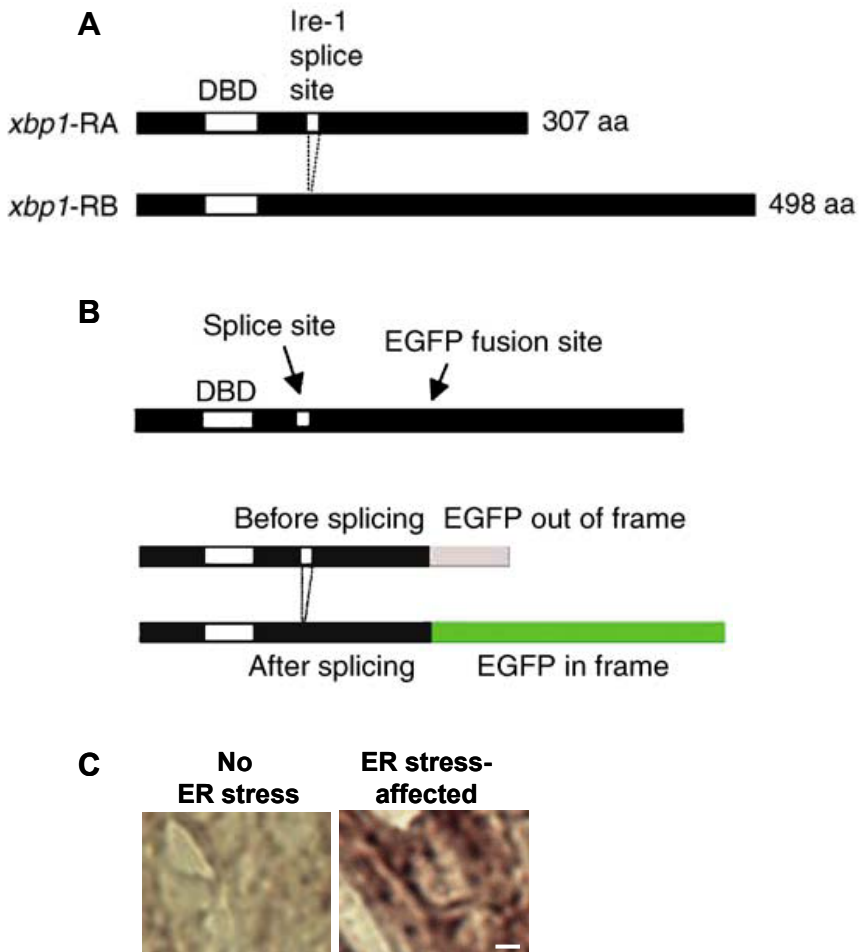


Figure 38. ER stress activates Xbp1 splicing. (A) The two predicted *Drosophila* *Xbp1* isoforms. After Ire1-mediated splicing, a frameshift in *Xbp1* translation takes place, converting a 307 amino acid (aa) protein into a 498 aa protein. The first white box indicates the DNA-binding domain (DBD). The second white box indicates the putative Ire1 splice site. (B) The design of the *Xbp1*-EGFP reporter. EGFP was inserted 3' to the putative Ire1 splice site, giving rise to a fusion protein that lacks the *Xbp1* C-terminal region (upper). EGFP is out of frame without Ire1-mediated splicing (middle), but comes in frame after splicing (lower). (C) Horizontal retinal cryosections from flies after 10 days of light exposure (dle) were stained with an anti-GFP antibody. *Xbp1*-EGFP is expressed under the control of *Actin* promoter. Unconventional *Xbp1* mRNA splicing is increased in the *Rh1*^{P37H} retina compared to control flies, revealed by EGFP expression. Scale bar is 10 μ m. Adapted from Ryoo et al. (2007).

B.4.6 Pharmacological treatments

Flies were treated with EerI or MG132 inhibitors (Figure 39) dissolved in fly food. 2 doses of EerI (1 mM and 10 mM) and 2 doses of MG132 (5 μ M and 50 μ M) were used. These compounds were first dissolved in DMSO and the solution was then added to fly food cooled down to 30 °C. The food was then dispensed into empty vials and allowed to solidify. It was kept at 4 °C in the dark for maximum 3-4 days. The above-mentioned concentrations correspond to the final concentrations in fly food. Flies were transferred in vials containing this modified food right after birth, were reared as described above and transferred to fresh vials every day. The control food contained all the ingredients (including DMSO) except the active compound. After 30 days of light exposure, flies fed on control food (2 % DMSO) and on drug food (EerI or MG132 in 2 % DMSO) were sacrificed and their retinal integrity was assessed histologically.

Materials and Methods

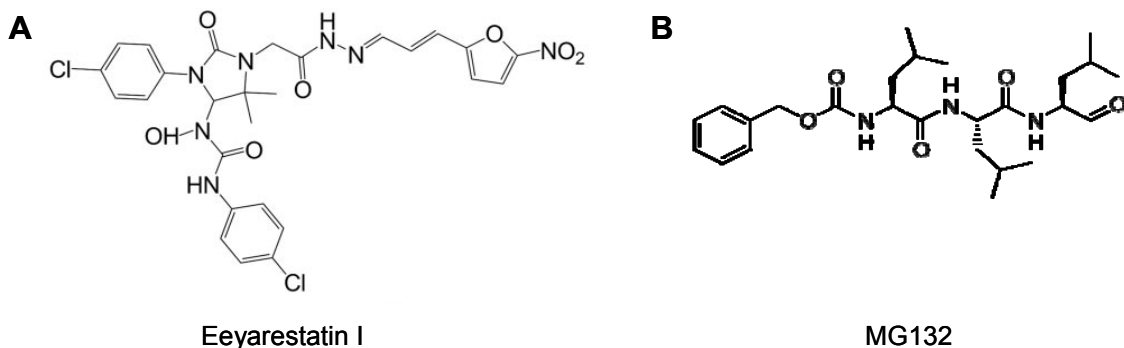


Figure 39. Chemical structures of Eeyarestatin I and MG132. Chemical structures of the VCP/ERAD inhibitor Eeyarestatin I (A) and of the proteasome inhibitor MG132 (B).

B.4.7 Behavioural assays

Phototaxis

Fast phototaxis was performed as described (Galy et al., 2005). Around 20 flies were placed in tube 1 of a countercurrent apparatus with six tubes and gently tapped to the bottom of the tube (Figure 40). The apparatus was placed horizontally, the light source was switched on and the flies were allowed to walk toward the light during 30 sec. The flies that moved toward the light were shifted to the second tube and this procedure was repeated five times. At the end of the test, the number of flies was counted in each of the six tubes. The flies that see well reach the tubes 5 and 6. Between 277-451 flies were scored per genotype, in 3 independent experiments. The phototactic score (PS) quantifies the visual activity of a fly population following a weighted equation $(\sum iN_i)/\sum N_i$, where N is the number of flies in the i^{th} tube.

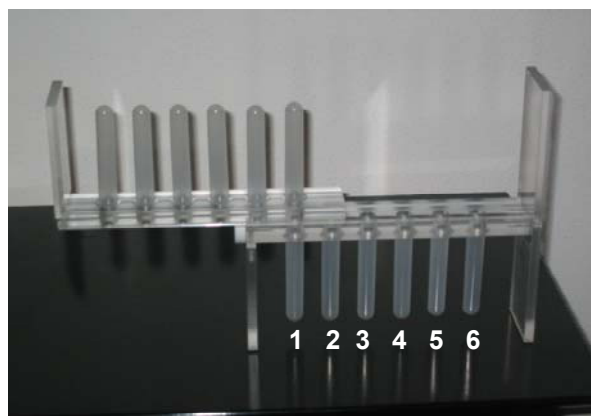


Figure 40. Phototaxis system. Phototaxis apparatus is represented in the figure. Principle of phototactic assay: 1 to 6 indicate tube numbers. Prior to the test, flies are placed at the bottom of tube 1 (white arrow). The apparatus is placed horizontally, flies are allowed to walk towards light during 30 sec. Tubes are shifted towards right and flies are placed at the bottom of the following tube to start the test again. Flies that have responded to light are in tube 2, whereas others stay in tube 1. The test is reiterated five times.

Geotaxis

Geotaxis was used to assess motor performance in flies chronically exposed to light. About 20 flies/ tube were gently tapped to the bottom of the tube and then allowed to climb during 20 sec. The number of flies that climbed 4 cm or above was scored. Each tube was tested twice. The results represent the % of flies that reached 4 cm or above after 20 sec.

B.4.8 Electroretinogram recordings

Electroretinogram (ERG) analysis was performed as described (Galy et al., 2005) in collaboration with Dr. Michel Roux, IGBMC, Strasbourg. Cold-anesthetized flies were immobilized in clay (Figure 41A). A tungsten electrode ($0.5\text{--}1\text{ M}\Omega$, Intracell) was introduced in the back of the fly head and a glass electrode filled with 3 M KCl ($2\text{--}6\text{ M}\Omega$) was introduced through the cornea (Figure 41B). Flies were dark-adapted for 5 min before recordings. The light intensity reaching the eye was $\sim 300\text{ }\mu\text{W/cm}^2$, from a white LED (Nichia, NSPW510BS) emitting from 425 to 750 nm with two peaks at 460 and 560 nm, with a 45° viewing angle, placed at 1.5 cm from the fly eye. Six 1sec light pulses were used to stimulate the eye and their responses averaged. The flash intensity (700 candela/m^2) was chosen as the minimal intensity that consistently produces maximal ERG Plateau (Figure 41C). Signals were filtered at 2 kHz and digitized at 10 kHz, using a MultiClamp 700 A amplifier, Digidata 1322 A interface and pClamp-8 software (Axon Instruments).

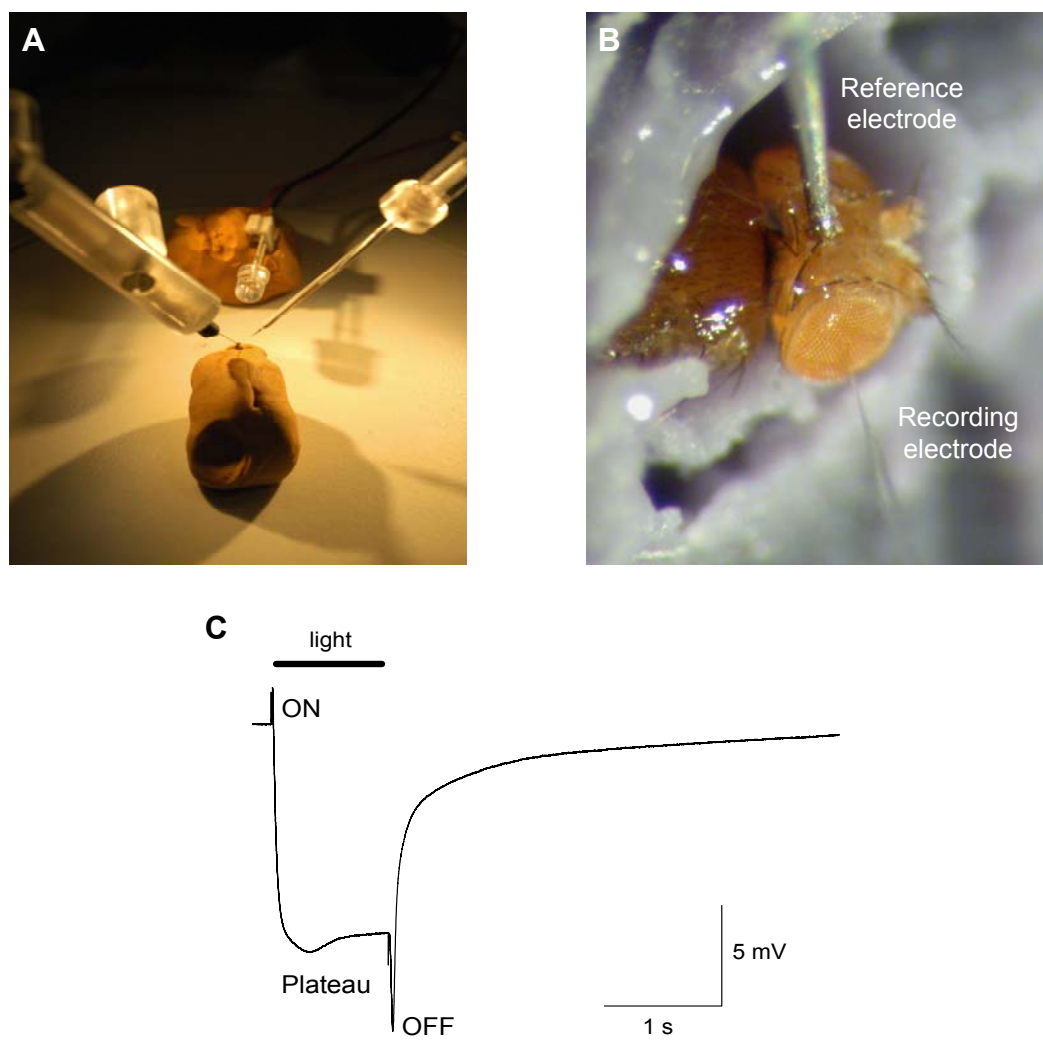


Figure 41. ERG setup. (A) Cold-anesthetized flies are immobilized in clay. (B) A tungsten electrode (reference) is introduced in the back of the fly head and a glass electrode (recording) filled with 3 M KCl is poked through the cornea. (C) ERG tracing of a WT fly. Plateau represents photoreceptor depolarization. ON and OFF spikes represent synaptic transmission from photoreceptors to the lamina.

Materials and Methods

B.4.9 Statistics

Unpaired Student's t-test was used to compare mean values and to evaluate significance. Differences were considered statistically significant for *p*-values inferior to 0.05.

V. REFERENCES

References

- Adler, R. (1996). Mechanisms of photoreceptor death in retinal degenerations. From the cell biology of the 1990s to the ophthalmology of the 21st century? *Arch Ophthalmol* *114*, 79-83.
- Aguzzi, A., and Polymenidou, M. (2004). Mammalian prion biology: one century of evolving concepts. *Cell* *116*, 313-327.
- Ahnelt, P. K., and Kolb, H. (2000). The mammalian photoreceptor mosaic-adaptive design. *Prog Retin Eye Res* *19*, 711-777.
- Alloway, P. G., Howard, L., and Dolph, P. J. (2000). The formation of stable rhodopsin-arrestin complexes induces apoptosis and photoreceptor cell degeneration. *Neuron* *28*, 129-138.
- Amerik, A. Y., and Hochstrasser, M. (2004). Mechanism and function of deubiquitinating enzymes. *Biochim Biophys Acta* *1695*, 189-207.
- Anelli, T., and Sitia, R. (2008). Protein quality control in the early secretory pathway. *EMBO J* *27*, 315-327.
- Arendt, D. (2003). Evolution of eyes and photoreceptor cell types. *Int J Dev Biol* *47*, 563-571.
- Arrasate, M., Mitra, S., Schweitzer, E. S., Segal, M. R., and Finkbeiner, S. (2004). Inclusion body formation reduces levels of mutant huntingtin and the risk of neuronal death. *Nature* *431*, 805-810.
- Balch, W. E., Morimoto, R. I., Dillin, A., and Kelly, J. W. (2008). Adapting proteostasis for disease intervention. *Science* *319*, 916-919.
- Ballar, P., Shen, Y., Yang, H., and Fang, S. (2006). The role of a novel p97/valosin-containing protein-interacting motif of gp78 in endoplasmic reticulum-associated degradation. *J Biol Chem* *281*, 35359-35368.
- Ballar, P., Zhong, Y., Nagahama, M., Tagaya, M., Shen, Y., and Fang, S. (2007). Identification of SVIP as an endogenous inhibitor of endoplasmic reticulum-associated degradation. *J Biol Chem* *282*, 33908-33914.
- Bernales, S., Papa, F. R., and Walter, P. (2006). Intracellular signaling by the unfolded protein response. *Annu Rev Cell Dev Biol* *22*, 487-508.
- Berson, E. L. (1971). Light deprivation for early retinitis pigmentosa. A hypothesis. *Arch Ophthalmol* *85*, 521-529.
- Berson, E. L. (1980). Light deprivation and retinitis pigmentosa. *Vision Res* *20*, 1179-1184.
- Berson, E. L. (1996). Retinitis pigmentosa: unfolding its mystery. *Proc Natl Acad Sci U S A* *93*, 4526-4528.
- Berson, E. L., Rosner, B., Sandberg, M. A., and Dryja, T. P. (1991). Ocular findings in patients with autosomal dominant retinitis pigmentosa and a rhodopsin gene defect (Pro-23-His). *Arch Ophthalmol* *109*, 92-101.
- Birch, D. G., Hood, D. C., Nusinowitz, S., and Pepperberg, D. R. (1995). Abnormal activation and inactivation mechanisms of rod transduction in patients with autosomal dominant retinitis pigmentosa and the pro-23-his mutation. *Invest Ophthalmol Vis Sci* *36*, 1603-1614.
- Boeddrich, A., Gaumer, S., Haacke, A., Tzvetkov, N., Albrecht, M., Evert, B. O., Muller, E. C., Lurz, R., Breuer, P., Schugardt, N., et al. (2006). An arginine/lysine-rich motif is crucial for VCP/p97-mediated modulation of ataxin-3 fibrillogenesis. *EMBO J* *25*, 1547-1558.
- Boughman, J. A., and Fishman, G. A. (1983). A genetic analysis of retinitis pigmentosa. *Br J Ophthalmol* *67*, 449-454.
- Bourne, H. R., and Meng, E. C. (2000). Structure. Rhodopsin sees the light. *Science* *289*, 733-734.

References

- Brundin, P., Melki, R., and Kopito, R. (2010). Prion-like transmission of protein aggregates in neurodegenerative diseases. *Nat Rev Mol Cell Biol* 11, 301-307.
- Bucciantini, M., Calloni, G., Chiti, F., Formigli, L., Nosi, D., Dobson, C. M., and Stefani, M. (2004). Prefibrillar amyloid protein aggregates share common features of cytotoxicity. *J Biol Chem* 279, 31374-31382.
- Busch, A., Engemann, S., Lurz, R., Okazawa, H., Lehrach, H., and Wanker, E. E. (2003). Mutant huntingtin promotes the fibrillogenesis of wild-type huntingtin: a potential mechanism for loss of huntingtin function in Huntington's disease. *J Biol Chem* 278, 41452-41461.
- Bush, K. T., Goldberg, A. L., and Nigam, S. K. (1997). Proteasome inhibition leads to a heat-shock response, induction of endoplasmic reticulum chaperones, and thermotolerance. *J Biol Chem* 272, 9086-9092.
- Carvalho, P., Goder, V., and Rapoport, T. A. (2006). Distinct ubiquitin-ligase complexes define convergent pathways for the degradation of ER proteins. *Cell* 126, 361-373.
- Caughey, B., and Lansbury, P. T. (2003). Protofibrils, pores, fibrils, and neurodegeneration: separating the responsible protein aggregates from the innocent bystanders. *Annu Rev Neurosci* 26, 267-298.
- Chang, H. Y., and Ready, D. F. (2000). Rescue of photoreceptor degeneration in rhodopsin-null *Drosophila* mutants by activated Rac1. *Science* 290, 1978-1980.
- Chapple, J. P., and Cheetham, M. E. (2003). The chaperone environment at the cytoplasmic face of the endoplasmic reticulum can modulate rhodopsin processing and inclusion formation. *J Biol Chem* 278, 19087-19094.
- Chillaron, J., and Haas, I. G. (2000). Dissociation from BiP and retrotranslocation of unassembled immunoglobulin light chains are tightly coupled to proteasome activity. *Mol Biol Cell* 11, 217-226.
- Chinchore, Y., Mitra, A., and Dolph, P. J. (2009). Accumulation of rhodopsin in late endosomes triggers photoreceptor cell degeneration. *PLoS Genet* 5, e1000377.
- Chuang, J. Z., Vega, C., Jun, W., and Sung, C. H. (2004). Structural and functional impairment of endocytic pathways by retinitis pigmentosa mutant rhodopsin-arrestin complexes. *J Clin Invest* 114, 131-140.
- Clavaguera, F., Bolmont, T., Crowther, R. A., Abramowski, D., Frank, S., Probst, A., Fraser, G., Stalder, A. K., Beibel, M., Staufenbiel, M., et al. (2009). Transmission and spreading of tauopathy in transgenic mouse brain. *Nat Cell Biol* 11, 909-913.
- Colley, N. J., Cassill, J. A., Baker, E. K., and Zuker, C. S. (1995). Defective intracellular transport is the molecular basis of rhodopsin-dependent dominant retinal degeneration. *Proc Natl Acad Sci U S A* 92, 3070-3074.
- Cook, T., and Desplan, C. (2001). Photoreceptor subtype specification: from flies to humans. *Semin Cell Dev Biol* 12, 509-518.
- Cooper, A. A., Gitler, A. D., Cashikar, A., Haynes, C. M., Hill, K. J., Bhullar, B., Liu, K., Xu, K., Strathearn, K. E., Liu, F., et al. (2006). Alpha-synuclein blocks ER-Golgi traffic and Rab1 rescues neuron loss in Parkinson's models. *Science* 313, 324-328.
- Crow, M. K., Karasavvas, N., and Sarris, A. H. (2001). Protein aggregation mediated by cysteine oxidation during the stacking phase of discontinuous buffer SDS-PAGE. *Biotechniques* 30, 311-316.
- Custer, S. K., Neumann, M., Lu, H., Wright, A. C., and Taylor, J. P. (2010). Transgenic mice expressing mutant forms VCP/p97 recapitulate the full spectrum of IBMPFD including degeneration in muscle, brain and bone. *Hum Mol Genet* 19, 1741-1755.
- Dai, R. M., Chen, E., Longo, D. L., Gorbea, C. M., and Li, C. C. (1998). Involvement of valosin-containing protein, an ATPase Co-purified with IkappaBalphalpha and 26 S proteasome, in ubiquitin-proteasome-mediated degradation of IkappaBalphalpha. *J Biol Chem* 273, 3562-3573.

- Dai, R. M., and Li, C. C. (2001). Valosin-containing protein is a multi-ubiquitin chain-targeting factor required in ubiquitin-proteasome degradation. *Nat Cell Biol* 3, 740-744.
- Daiger, S. P. (2004). Identifying retinal disease genes: how far have we come, how far do we have to go? *Novartis Found Symp* 255, 17-27; discussion 27-36, 177-178.
- Daiger, S. P., Bowne, S. J., and Sullivan, L. S. (2007). Perspective on genes and mutations causing retinitis pigmentosa. *Arch Ophthalmol* 125, 151-158.
- Davidson, F. F., and Steller, H. (1998). Blocking apoptosis prevents blindness in *Drosophila* retinal degeneration mutants. *Nature* 391, 587-591.
- DeLaBarre, B., Christianson, J. C., Kopito, R. R., and Brunger, A. T. (2006). Central pore residues mediate the p97/VCP activity required for ERAD. *Mol Cell* 22, 451-462.
- Denic, V., Quan, E. M., and Weissman, J. S. (2006). A luminal surveillance complex that selects misfolded glycoproteins for ER-associated degradation. *Cell* 126, 349-359.
- Dreveny, I., Pye, V. E., Beuron, F., Briggs, L. C., Isaacson, R. L., Matthews, S. J., McKeown, C., Yuan, X., Zhang, X., and Freemont, P. S. (2004). p97 and close encounters of every kind: a brief review. *Biochem Soc Trans* 32, 715-720.
- Dryja, T. P. (1990). Human genetics. Deficiencies in sight with the candidate gene approach. *Nature* 347, 614.
- Dryja, T. P., Hahn, L. B., Cowley, G. S., McGee, T. L., and Berson, E. L. (1991). Mutation spectrum of the rhodopsin gene among patients with autosomal dominant retinitis pigmentosa. *Proc Natl Acad Sci U S A* 88, 9370-9374.
- Dryja, T. P., McGee, T. L., Reichel, E., Hahn, L. B., Cowley, G. S., Yandell, D. W., Sandberg, M. A., and Berson, E. L. (1990). A point mutation of the rhodopsin gene in one form of retinitis pigmentosa. *Nature* 343, 364-366.
- Duennwald, M. L., and Lindquist, S. (2008). Impaired ERAD and ER stress are early and specific events in polyglutamine toxicity. *Genes Dev* 22, 3308-3319.
- Ellgaard, L., and Helenius, A. (2003). Quality control in the endoplasmic reticulum. *Nat Rev Mol Cell Biol* 4, 181-191.
- Fagioli, C., Mezghrani, A., and Sitia, R. (2001). Reduction of interchain disulfide bonds precedes the dislocation of Ig-mu chains from the endoplasmic reticulum to the cytosol for proteasomal degradation. *J Biol Chem* 276, 40962-40967.
- Fagioli, C., and Sitia, R. (2001). Glycoprotein quality control in the endoplasmic reticulum. Mannose trimming by endoplasmic reticulum mannosidase I times the proteasomal degradation of unassembled immunoglobulin subunits. *J Biol Chem* 276, 12885-12892.
- Farrar, G. J., Kenna, P. F., and Humphries, P. (2002). On the genetics of retinitis pigmentosa and on mutation-independent approaches to therapeutic intervention. *EMBO J* 21, 857-864.
- Fiebiger, E., Hirsch, C., Vyas, J. M., Gordon, E., Ploegh, H. L., and Tortorella, D. (2004). Dissection of the dislocation pathway for type I membrane proteins with a new small molecule inhibitor, eeyarestatin. *Mol Biol Cell* 15, 1635-1646.
- Fink, A. L. (1998). Protein aggregation: folding aggregates, inclusion bodies and amyloid. *Fold Des* 3, R9-23.
- Finley, D. (2009). Recognition and processing of ubiquitin-protein conjugates by the proteasome. *Annu Rev Biochem* 78, 477-513.
- Flierman, D., Ye, Y., Dai, M., Chau, V., and Rapoport, T. A. (2003). Polyubiquitin serves as a recognition signal, rather than a ratcheting molecule, during retrotranslocation of proteins across the endoplasmic reticulum membrane. *J Biol Chem* 278, 34774-34782.
- Fotiadis, D., Liang, Y., Filipek, S., Saperstein, D. A., Engel, A., and Palczewski, K. (2003). Atomic-force microscopy: Rhodopsin dimers in native disc membranes. *Nature* 421, 127-128.

References

- Frederick, J. M., Krasnoperova, N. V., Hoffmann, K., Church-Kopish, J., Ruther, K., Howes, K., Lem, J., and Baehr, W. (2001). Mutant rhodopsin transgene expression on a null background. *Invest Ophthalmol Vis Sci* *42*, 826-833.
- Galy, A., Roux, M. J., Sahel, J. A., Leveillard, T., and Giangrande, A. (2005). Rhodopsin maturation defects induce photoreceptor death by apoptosis: a fly model for RhodopsinPro23His human retinitis pigmentosa. *Hum Mol Genet* *14*, 2547-2557.
- Ghislain, M., Dohmen, R. J., Levy, F., and Varshavsky, A. (1996). Cdc48p interacts with Ufd3p, a WD repeat protein required for ubiquitin-mediated proteolysis in *Saccharomyces cerevisiae*. *EMBO J* *15*, 4884-4899.
- Gitcho, M. A., Strider, J., Carter, D., Taylor-Reinwald, L., Forman, M. S., Goate, A. M., and Cairns, N. J. (2009). VCP mutations causing frontotemporal lobar degeneration disrupt localization of TDP-43 and induce cell death. *J Biol Chem* *284*, 12384-12398.
- Gloeckner, C. J., Boldt, K., Schumacher, A., Roepman, R., and Ueffing, M. (2007). A novel tandem affinity purification strategy for the efficient isolation and characterisation of native protein complexes. *Proteomics* *7*, 4228-4234.
- Goldstein, R. F., Niraj, A., Sanderson, T. P., Wilson, L. S., Rab, A., Kim, H., Bebok, Z., and Collawn, J. F. (2007). VCP/p97 AAA-ATPase does not interact with the endogenous wild-type cystic fibrosis transmembrane conductance regulator. *Am J Respir Cell Mol Biol* *36*, 706-714.
- Gorbatyuk, M. S., Knox, T., LaVail, M. M., Gorbatyuk, O. S., Noorwez, S. M., Hauswirth, W. W., Lin, J. H., Muzychka, N., and Lewin, A. S. (2010). Restoration of visual function in P23H rhodopsin transgenic rats by gene delivery of BiP/Grp78. *Proc Natl Acad Sci U S A* *107*, 5961-5966.
- Goto, Y., Peachey, N. S., Ziroli, N. E., Seiple, W. H., Gryczan, C., Pepperberg, D. R., and Naash, M. I. (1996). Rod phototransduction in transgenic mice expressing a mutant opsin gene. *J Opt Soc Am A Opt Image Sci Vis* *13*, 577-585.
- Gregersen, N., Bolund, L., and Bross, P. (2005). Protein misfolding, aggregation, and degradation in disease. *Mol Biotechnol* *31*, 141-150.
- Halawani, D., and Latterich, M. (2006). p97: The cell's molecular purgatory? *Mol Cell* *22*, 713-717.
- Hamel, C. (2006). Retinitis pigmentosa. *Orphanet J Rare Dis* *1*, 40.
- Hartley, J. L., Temple, G. F., and Brasch, M. A. (2000). DNA cloning using in vitro site-specific recombination. *Genome Res* *10*, 1788-1795.
- Hebert, D. N., Foellmer, B., and Helenius, A. (1995). Glucose trimming and reglucosylation determine glycoprotein association with calnexin in the endoplasmic reticulum. *Cell* *81*, 425-433.
- Hebert, D. N., and Molinari, M. (2007). In and out of the ER: protein folding, quality control, degradation, and related human diseases. *Physiol Rev* *87*, 1377-1408.
- Heckenlively, J. R., Rodriguez, J. A., and Daiger, S. P. (1991). Autosomal dominant sectoral retinitis pigmentosa. Two families with transversion mutation in codon 23 of rhodopsin. *Arch Ophthalmol* *109*, 84-91.
- Hendershot, L. M. (2004). The ER function BiP is a master regulator of ER function. *Mt Sinai J Med* *71*, 289-297.
- Higashiyama, H., Hirose, F., Yamaguchi, M., Inoue, Y. H., Fujikake, N., Matsukage, A., and Kakizuka, A. (2002). Identification of ter94, *Drosophila* VCP, as a modulator of polyglutamine-induced neurodegeneration. *Cell Death Differ* *9*, 264-273.
- Hims, M. M., Diager, S. P., and Inglehearn, C. F. (2003). Retinitis pigmentosa: genes, proteins and prospects. *Dev Ophthalmol* *37*, 109-125.
- Hirabayashi, M., Inoue, K., Tanaka, K., Nakadate, K., Ohsawa, Y., Kamei, Y., Popiel, A. H., Sinohara, A., Iwamatsu, A., Kimura, Y., et al. (2001). VCP/p97 in abnormal protein

- aggregates, cytoplasmic vacuoles, and cell death, phenotypes relevant to neurodegeneration. *Cell Death Differ* 8, 977-984.
- Hirsch, C., Jarosch, E., Sommer, T., and Wolf, D. H. (2004). Endoplasmic reticulum-associated protein degradation--one model fits all? *Biochim Biophys Acta* 1695, 215-223.
- Hubbers, C. U., Clemen, C. S., Kesper, K., Boddrich, A., Hofmann, A., Kamarainen, O., Tolksdorf, K., Stumpf, M., Reichelt, J., Roth, U., *et al.* (2007). Pathological consequences of VCP mutations on human striated muscle. *Brain* 130, 381-393.
- Humphries, M. M., Rancourt, D., Farrar, G. J., Kenna, P., Hazel, M., Bush, R. A., Sieving, P. A., Sheils, D. M., McNally, N., Creighton, P., *et al.* (1997). Retinopathy induced in mice by targeted disruption of the rhodopsin gene. *Nat Genet* 15, 216-219.
- Huyton, T., Pye, V. E., Briggs, L. C., Flynn, T. C., Beuron, F., Kondo, H., Ma, J., Zhang, X., and Freemont, P. S. (2003). The crystal structure of murine p97/VCP at 3.6A. *J Struct Biol* 144, 337-348.
- Iakhine, R., Chorna-Ornan, I., Zars, T., Elia, N., Cheng, Y., Selinger, Z., Minke, B., and Hyde, D. R. (2004). Novel dominant rhodopsin mutation triggers two mechanisms of retinal degeneration and photoreceptor desensitization. *J Neurosci* 24, 2516-2526.
- Illing, M. E., Rajan, R. S., Bence, N. F., and Kopito, R. R. (2002). A rhodopsin mutant linked to autosomal dominant retinitis pigmentosa is prone to aggregate and interacts with the ubiquitin proteasome system. *J Biol Chem* 277, 34150-34160.
- Iwata, A., Riley, B. E., Johnston, J. A., and Kopito, R. R. (2005). HDAC6 and microtubules are required for autophagic degradation of aggregated huntingtin. *J Biol Chem* 280, 40282-40292.
- Jahn, T. R., and Radford, S. E. (2005). The Yin and Yang of protein folding. *FEBS J* 272, 5962-5970.
- Jentsch, S., and Rumpf, S. (2007). Cdc48 (p97): a "molecular gearbox" in the ubiquitin pathway? *Trends Biochem Sci* 32, 6-11.
- Johnson, E. C., and Pak, W. L. (1986). Electrophysiological study of Drosophila rhodopsin mutants. *J Gen Physiol* 88, 651-673.
- Ju, J. S., Fuentealba, R. A., Miller, S. E., Jackson, E., Piwnica-Worms, D., Baloh, R. H., and Weihl, C. C. (2009). Valosin-containing protein (VCP) is required for autophagy and is disrupted in VCP disease. *J Cell Biol* 187, 875-888.
- Ju, J. S., Miller, S. E., Hanson, P. I., and Weihl, C. C. (2008). Impaired protein aggregate handling and clearance underlie the pathogenesis of p97/VCP-associated disease. *J Biol Chem* 283, 30289-30299.
- Kaganovich, D., Kopito, R., and Frydman, J. (2008). Misfolded proteins partition between two distinct quality control compartments. *Nature* 454, 1088-1095.
- Kalies, K. U., Allan, S., Sergeyenko, T., Kroger, H., and Romisch, K. (2005). The protein translocation channel binds proteasomes to the endoplasmic reticulum membrane. *EMBO J* 24, 2284-2293.
- Kalloniatis, M., and Fletcher, E. L. (2004). Retinitis pigmentosa: understanding the clinical presentation, mechanisms and treatment options. *Clin Exp Optom* 87, 65-80.
- Kandel, E.R., Schwartz, J., Jessell, T. (2000) Visual processing by the retina. In *Principles of Neural Science*, Elsevier, pp. 507-522.
- Kang, M. J., and Ryoo, H. D. (2009). Suppression of retinal degeneration in Drosophila by stimulation of ER-associated degradation. *Proc Natl Acad Sci U S A* 106, 17043-17048.
- Kaushal, S., and Khorana, H. G. (1994). Structure and function in rhodopsin. 7. Point mutations associated with autosomal dominant retinitis pigmentosa. *Biochemistry* 33, 6121-6128.
- Kennan, A., Aherne, A., and Humphries, P. (2005). Light in retinitis pigmentosa. *Trends Genet* 21, 103-110.

References

- Kimonis, V. E., Fulchiero, E., Vesa, J., and Watts, G. (2008). VCP disease associated with myopathy, Paget disease of bone and frontotemporal dementia: review of a unique disorder. *Biochim Biophys Acta* *1782*, 744-748.
- Kimonis, V. E., and Watts, G. D. (2005). Autosomal dominant inclusion body myopathy, Paget disease of bone, and frontotemporal dementia. *Alzheimer Dis Assoc Disord* *19 Suppl 1*, S44-47.
- Kirkin, V., McEwan, D. G., Novak, I., and Dikic, I. (2009). A role for ubiquitin in selective autophagy. *Mol Cell* *34*, 259-269.
- Kiselev, A., Socolich, M., Vinos, J., Hardy, R. W., Zuker, C. S., and Ranganathan, R. (2000). A molecular pathway for light-dependent photoreceptor apoptosis in *Drosophila*. *Neuron* *28*, 139-152.
- Klausner, R. D., and Sitia, R. (1990). Protein degradation in the endoplasmic reticulum. *Cell* *62*, 611-614.
- Klein, J. B., Barati, M. T., Wu, R., Gozal, D., Sachleben, L. R., Jr., Kausar, H., Trent, J. O., Gozal, E., and Rane, M. J. (2005). Akt-mediated valosin-containing protein 97 phosphorylation regulates its association with ubiquitinated proteins. *J Biol Chem* *280*, 31870-31881.
- Knecht, E., Aguado, C., Carcel, J., Esteban, I., Esteve, J. M., Ghislaut, G., Moruno, J. F., Vidal, J. M., and Saez, R. (2009). Intracellular protein degradation in mammalian cells: recent developments. *Cell Mol Life Sci* *66*, 2427-2443.
- Kobayashi, T., Tanaka, K., Inoue, K., and Kakizuka, A. (2002). Functional ATPase activity of p97/valosin-containing protein (VCP) is required for the quality control of endoplasmic reticulum in neuronally differentiated mammalian PC12 cells. *J Biol Chem* *277*, 47358-47365.
- Koller, K. J., and Brownstein, M. J. (1987). Use of a cDNA clone to identify a supposed precursor protein containing valosin. *Nature* *325*, 542-545.
- Kopito, R. R. (2000). Aggresomes, inclusion bodies and protein aggregation. *Trends Cell Biol* *10*, 524-530.
- Kornfeld, R., and Kornfeld, S. (1985). Assembly of asparagine-linked oligosaccharides. *Annu Rev Biochem* *54*, 631-664.
- Kosmaoglou, M., and Cheetham, M. E. (2008). Calnexin is not essential for mammalian rod opsin biogenesis. *Mol Vis* *14*, 2466-2474.
- Kosmaoglou, M., Kanuga, N., Aguila, M., Garriga, P., and Cheetham, M. E. (2009). A dual role for EDEM1 in the processing of rod opsin. *J Cell Sci* *122*, 4465-4472.
- Kostova, Z., Tsai, Y. C., and Weissman, A. M. (2007). Ubiquitin ligases, critical mediators of endoplasmic reticulum-associated degradation. *Semin Cell Dev Biol* *18*, 770-779.
- Krammer, C., Schatzl, H. M., and Vorberg, I. (2009). Prion-like propagation of cytosolic protein aggregates: insights from cell culture models. *Prion* *3*, 206-212.
- Kurada, P., and O'Tousa, J. E. (1995). Retinal degeneration caused by dominant rhodopsin mutations in *Drosophila*. *Neuron* *14*, 571-579.
- Kurada, P., Tonini, T. D., Serikaku, M. A., Piccini, J. P., and O'Tousa, J. E. (1998). Rhodopsin maturation antagonized by dominant rhodopsin mutants. *Vis Neurosci* *15*, 693-700.
- Lansbury, P. T., and Lashuel, H. A. (2006). A century-old debate on protein aggregation and neurodegeneration enters the clinic. *Nature* *443*, 774-779.
- Latterich, M., Fröhlich, K. U., and Schekman, R. (1995). Membrane fusion and the cell cycle: Cdc48p participates in the fusion of ER membranes. *Cell* *82*, 885-893.
- Lee, R. J., Liu, C. W., Harty, C., McCracken, A. A., Latterich, M., Romisch, K., DeMartino, G. N., Thomas, P. J., and Brodsky, J. L. (2004). Uncoupling retro-

- translocation and degradation in the ER-associated degradation of a soluble protein. *EMBO J* 23, 2206-2215.
- Lee, S. J., and Montell, C. (2004). Suppression of constant-light-induced blindness but not retinal degeneration by inhibition of the rhodopsin degradation pathway. *Curr Biol* 14, 2076-2085.
- Lem, J., Krasnoperova, N. V., Calvert, P. D., Kosaras, B., Cameron, D. A., Nicolo, M., Makino, C. L., and Sidman, R. L. (1999). Morphological, physiological, and biochemical changes in rhodopsin knockout mice. *Proc Natl Acad Sci U S A* 96, 736-741.
- Leon, A., and McKearin, D. (1999). Identification of TER94, an AAA ATPase protein, as a Bam-dependent component of the *Drosophila* fusome. *Mol Biol Cell* 10, 3825-3834.
- Leonard, D. S., Bowman, V. D., Ready, D. F., and Pak, W. L. (1992). Degeneration of photoreceptors in rhodopsin mutants of *Drosophila*. *J Neurobiol* 23, 605-626.
- Li, G., Zhao, G., Schindelin, H., and Lennarz, W. J. (2008). Tyrosine phosphorylation of ATPase p97 regulates its activity during ERAD. *Biochem Biophys Res Commun* 375, 247-251.
- Liang, J., Yin, C., Doong, H., Fang, S., Peterhoff, C., Nixon, R. A., and Monteiro, M. J. (2006). Characterization of erasin (UBXD2): a new ER protein that promotes ER-associated protein degradation. *J Cell Sci* 119, 4011-4024.
- Lim, P. J., Danner, R., Liang, J., Doong, H., Harman, C., Srinivasan, D., Rothenberg, C., Wang, H., Ye, Y., Fang, S., and Monteiro, M. J. (2009). Ubiquilin and p97/VCP bind erasin, forming a complex involved in ERAD. *J Cell Biol* 187, 201-217.
- Lin, J. H., Li, H., Yasumura, D., Cohen, H. R., Zhang, C., Panning, B., Shokat, K. M., Lavail, M. M., and Walter, P. (2007). IRE1 signaling affects cell fate during the unfolded protein response. *Science* 318, 944-949.
- Lippincott-Schwartz, J., Bonifacino, J. S., Yuan, L. C., and Klausner, R. D. (1988). Degradation from the endoplasmic reticulum: disposing of newly synthesized proteins. *Cell* 54, 209-220.
- Lundgren, J., Masson, P., Mirzaei, Z., and Young, P. (2005). Identification and characterization of a *Drosophila* proteasome regulatory network. *Mol Cell Biol* 25, 4662-4675.
- Lupas, A. N., and Martin, J. (2002). AAA proteins. *Curr Opin Struct Biol* 12, 746-753.
- Madeo, F., Schlauer, J., Zischka, H., Mecke, D., and Frohlich, K. U. (1998). Tyrosine phosphorylation regulates cell cycle-dependent nuclear localization of Cdc48p. *Mol Biol Cell* 9, 131-141.
- Mancini, R., Fagioli, C., Fra, A. M., Maggioni, C., and Sitia, R. (2000). Degradation of unassembled soluble Ig subunits by cytosolic proteasomes: evidence that retrotranslocation and degradation are coupled events. *FASEB J* 14, 769-778.
- Mayer, T. U., Braun, T., and Jentsch, S. (1998). Role of the proteasome in membrane extraction of a short-lived ER-transmembrane protein. *EMBO J* 17, 3251-3257.
- Medicherla, B., Kostova, Z., Schaefer, A., and Wolf, D. H. (2004). A genomic screen identifies Dsk2p and Rad23p as essential components of ER-associated degradation. *EMBO Rep* 5, 692-697.
- Mendes, C. S., Levet, C., Chatelain, G., Dourlen, P., Fouillet, A., Dichtel-Danjoy, M. L., Gambis, A., Ryoo, H. D., Steller, H., and Mollereau, B. (2009). ER stress protects from retinal degeneration. *EMBO J* 28, 1296-1307.
- Mendes, H. F., and Cheetham, M. E. (2008). Pharmacological manipulation of gain-of-function and dominant-negative mechanisms in rhodopsin retinitis pigmentosa. *Hum Mol Genet* 17, 3043-3054.
- Mendes, H. F., van der Spuy, J., Chapple, J. P., and Cheetham, M. E. (2005). Mechanisms of cell death in rhodopsin retinitis pigmentosa: implications for therapy. *Trends Mol Med* 11, 177-185.

References

- Meusser, B., Hirsch, C., Jarosch, E., and Sommer, T. (2005). ERAD: the long road to destruction. *Nat Cell Biol* 7, 766-772.
- Meyer, H. H., Shorter, J. G., Seemann, J., Pappin, D., and Warren, G. (2000). A complex of mammalian ufd1 and npl4 links the AAA-ATPase, p97, to ubiquitin and nuclear transport pathways. *EMBO J* 19, 2181-2192.
- Meyer, H. H., Wang, Y., and Warren, G. (2002). Direct binding of ubiquitin conjugates by the mammalian p97 adaptor complexes, p47 and Ufd1-Npl4. *EMBO J* 21, 5645-5652.
- Mimura, N., Yuasa, S., Soma, M., Jin, H., Kimura, K., Goto, S., Koseki, H., and Aoe, T. (2008). Altered quality control in the endoplasmic reticulum causes cortical dysplasia in knock-in mice expressing a mutant BiP. *Mol Cell Biol* 28, 293-301.
- Miyake, Y., Sugita, S., Horiguchi, M., and Yagasaki, K. (1990). Light deprivation and retinitis pigmentosa. *Am J Ophthalmol* 110, 305-306.
- Mizuno, Y., Hori, S., Kakizuka, A., and Okamoto, K. (2003). Vacuole-creating protein in neurodegenerative diseases in humans. *Neurosci Lett* 343, 77-80.
- Moir, D., Stewart, S. E., Osmond, B. C., and Botstein, D. (1982). Cold-sensitive cell-division-cycle mutants of yeast: isolation, properties, and pseudoreversion studies. *Genetics* 100, 547-563.
- Mollereau, B., and Domingos, P. M. (2005). Photoreceptor differentiation in *Drosophila*: from immature neurons to functional photoreceptors. *Dev Dyn* 232, 585-592.
- Mosharov, E. V., Larsen, K. E., Kanter, E., Phillips, K. A., Wilson, K., Schmitz, Y., Krantz, D. E., Kobayashi, K., Edwards, R. H., and Sulzer, D. (2009). Interplay between cytosolic dopamine, calcium, and alpha-synuclein causes selective death of substantia nigra neurons. *Neuron* 62, 218-229.
- Mu, T. W., Ong, D. S., Wang, Y. J., Balch, W. E., Yates, J. R., 3rd, Segatori, L., and Kelly, J. W. (2008). Chemical and biological approaches synergize to ameliorate protein-folding diseases. *Cell* 134, 769-781.
- Muller, J. M., Deinhardt, K., Rosewell, I., Warren, G., and Shima, D. T. (2007). Targeted deletion of p97 (VCP/CDC48) in mouse results in early embryonic lethality. *Biochem Biophys Res Commun* 354, 459-465.
- Muro, I., Hay, B. A., and Clem, R. J. (2002). The *Drosophila* DIAP1 protein is required to prevent accumulation of a continuously generated, processed form of the apical caspase DRONC. *J Biol Chem* 277, 49644-49650.
- Naash, M. I., Hollyfield, J. G., al-Ubaidi, M. R., and Baehr, W. (1993). Simulation of human autosomal dominant retinitis pigmentosa in transgenic mice expressing a mutated murine opsin gene. *Proc Natl Acad Sci U S A* 90, 5499-5503.
- Naash, M. L., Peachey, N. S., Li, Z. Y., Gryczan, C. C., Goto, Y., Blanks, J., Milam, A. H., and Ripps, H. (1996). Light-induced acceleration of photoreceptor degeneration in transgenic mice expressing mutant rhodopsin. *Invest Ophthalmol Vis Sci* 37, 775-782.
- Nathans, J., Thomas, D., and Hogness, D. S. (1986). Molecular genetics of human color vision: the genes encoding blue, green, and red pigments. *Science* 232, 193-202.
- O'Tousa, J. E., Baehr, W., Martin, R. L., Hirsh, J., Pak, W. L., and Applebury, M. L. (1985). The *Drosophila* ninaE gene encodes an opsin. *Cell* 40, 839-850.
- O'Tousa, J. E., Leonard, D. S., and Pak, W. L. (1989). Morphological defects in oraJK84 photoreceptors caused by mutation in R1-6 opsin gene of *Drosophila*. *J Neurogenet* 6, 41-52.
- Olivari, S., Cali, T., Salo, K. E., Paganetti, P., Ruddock, L. W., and Molinari, M. (2006). EDEM1 regulates ER-associated degradation by accelerating de-mannosylation of folding-defective polypeptides and by inhibiting their covalent aggregation. *Biochem Biophys Res Commun* 349, 1278-1284.
- Olsson, J. E., Gordon, J. W., Pawlyk, B. S., Roof, D., Hayes, A., Molday, R. S., Mukai, S., Cowley, G. S., Berson, E. L., and Dryja, T. P. (1992). Transgenic mice with a

- rhodopsin mutation (Pro23His): a mouse model of autosomal dominant retinitis pigmentosa. *Neuron* 9, 815-830.
- Organisciak, D. T., Darrow, R. M., Barsalou, L., Kutty, R. K., and Wiggert, B. (2003). Susceptibility to retinal light damage in transgenic rats with rhodopsin mutations. *Invest Ophthalmol Vis Sci* 44, 486-492.
- Orr, H. T., and Zoghbi, H. Y. (2007). Trinucleotide repeat disorders. *Annu Rev Neurosci* 30, 575-621.
- Otsuna, H., and Ito, K. (2006). Systematic analysis of the visual projection neurons of *Drosophila melanogaster*. I. Lobula-specific pathways. *J Comp Neurol* 497, 928-958.
- Palczewski, K. (2006). G protein-coupled receptor rhodopsin. *Annu Rev Biochem* 75, 743-767.
- Palczewski, K., Kumada, T., Hori, T., Behnke, C. A., Motoshima, H., Fox, B. A., Le Trong, I., Teller, D. C., Okada, T., Stenkamp, R. E., et al. (2000). Crystal structure of rhodopsin: A G protein-coupled receptor. *Science* 289, 739-745.
- Pandey, U. B., Nie, Z., Batlevi, Y., McCray, B. A., Ritson, G. P., Nedelsky, N. B., Schwartz, S. L., DiProspero, N. A., Knight, M. A., Schulziner, O., et al. (2007). HDAC6 rescues neurodegeneration and provides an essential link between autophagy and the UPS. *Nature* 447, 859-863.
- Paskowitz, D. M., LaVail, M. M., and Duncan, J. L. (2006). Light and inherited retinal degeneration. *Br J Ophthalmol* 90, 1060-1066.
- Petters, R. M., Alexander, C. A., Wells, K. D., Collins, E. B., Sommer, J. R., Blanton, M. R., Rojas, G., Hao, Y., Flowers, W. L., Banin, E., et al. (1997). Genetically engineered large animal model for studying cone photoreceptor survival and degeneration in retinitis pigmentosa. *Nat Biotechnol* 15, 965-970.
- Pichaud, F., Briscoe, A., and Desplan, C. (1999). Evolution of color vision. *Curr Opin Neurobiol* 9, 622-627.
- Pickart, C. M., and Cohen, R. E. (2004). Proteasomes and their kin: proteases in the machine age. *Nat Rev Mol Cell Biol* 5, 177-187.
- Plempner, R. K., Bohmler, S., Bordallo, J., Sommer, T., and Wolf, D. H. (1997). Mutant analysis links the translocon and BiP to retrograde protein transport for ER degradation. *Nature* 388, 891-895.
- Powers, E. T., Morimoto, R. I., Dillin, A., Kelly, J. W., and Balch, W. E. (2009). Biological and chemical approaches to diseases of proteostasis deficiency. *Annu Rev Biochem* 78, 959-991.
- Rabouille, C., Levine, T. P., Peters, J. M., and Warren, G. (1995). An NSF-like ATPase, p97, and NSF mediate cisternal regrowth from mitotic Golgi fragments. *Cell* 82, 905-914.
- Rajan, R. S., and Kopito, R. R. (2005). Suppression of wild-type rhodopsin maturation by mutants linked to autosomal dominant retinitis pigmentosa. *J Biol Chem* 280, 1284-1291.
- Rao, R. V., Poksay, K. S., Castro-Obregon, S., Schilling, B., Row, R. H., del Rio, G., Gibson, B. W., Ellerby, H. M., and Bredesen, D. E. (2004). Molecular components of a cell death pathway activated by endoplasmic reticulum stress. *J Biol Chem* 279, 177-187.
- Ray-Sinha, A., Cross, B. C., Mironov, A., Wiertz, E., and High, S. (2009). Endoplasmic reticulum-associated degradation of a degron-containing polytopic membrane protein. *Mol Membr Biol* 26, 448-464.
- Read, R. D., Goodfellow, P. J., Mardis, E. R., Novak, N., Armstrong, J. R., and Cagan, R. L. (2005). A *Drosophila* model of multiple endocrine neoplasia type 2. *Genetics* 171, 1057-1081.
- Rideout, H. J., Lang-Rollin, I., and Stefanis, L. (2004). Involvement of macroautophagy in the dissolution of neuronal inclusions. *Int J Biochem Cell Biol* 36, 2551-2562.
- Rivett, A. J., and Knecht, E. (1993). Protein turnover: proteasome location. *Curr Biol* 3, 127-129.

References

- Romisch, K. (2005). Endoplasmic reticulum-associated degradation. *Annu Rev Cell Dev Biol* *21*, 435-456.
- Ron, D., and Walter, P. (2007). Signal integration in the endoplasmic reticulum unfolded protein response. *Nat Rev Mol Cell Biol* *8*, 519-529.
- Rosenbaum, E. E., Hardie, R. C., and Colley, N. J. (2006). Calnexin is essential for rhodopsin maturation, Ca²⁺ regulation, and photoreceptor cell survival. *Neuron* *49*, 229-241.
- Ross, C. A., and Poirier, M. A. (2004). Protein aggregation and neurodegenerative disease. *Nat Med* *10 Suppl*, S10-17.
- Rubinsztein, D. C. (2006). The roles of intracellular protein-degradation pathways in neurodegeneration. *Nature* *443*, 780-786.
- Ruden, D. M., Sollars, V., Wang, X., Mori, D., Alterman, M., and Lu, X. (2000). Membrane fusion proteins are required for oskar mRNA localization in the Drosophila egg chamber. *Dev Biol* *218*, 314-325.
- Rutkowski, D. T., and Kaufman, R. J. (2007). That which does not kill me makes me stronger: adapting to chronic ER stress. *Trends Biochem Sci* *32*, 469-476.
- Ryoo, H. D., Domingos, P. M., Kang, M. J., and Steller, H. (2007). Unfolded protein response in a Drosophila model for retinal degeneration. *EMBO J* *26*, 242-252.
- Sado, M., Yamasaki, Y., Iwanaga, T., Onaka, Y., Ibuki, T., Nishihara, S., Mizuguchi, H., Momota, H., Kishibuchi, R., Hashimoto, T., et al. (2009). Protective effect against Parkinson's disease-related insults through the activation of XBP1. *Brain Res* *1257*, 16-24.
- Saliba, R. S., Munro, P. M., Luthert, P. J., and Cheetham, M. E. (2002). The cellular fate of mutant rhodopsin: quality control, degradation and aggresome formation. *J Cell Sci* *115*, 2907-2918.
- Samardzija, M., Wenzel, A., Naash, M., Reme, C. E., and Grimm, C. (2006). Rpe65 as a modifier gene for inherited retinal degeneration. *Eur J Neurosci* *23*, 1028-1034.
- Sancho-Pelluz, J., Arango-Gonzalez, B., Kustermann, S., Romero, F. J., van Veen, T., Zrenner, E., Ekstrom, P., and Paquet-Durand, F. (2008). Photoreceptor cell death mechanisms in inherited retinal degeneration. *Mol Neurobiol* *38*, 253-269.
- Sanes, J.R., Zipursky, S.L. (2010). Design principles of insect and vertebrate visual systems. *Neuron* *66*, 15-36.
- Sarkar, S., Krishna, G., Imarisio, S., Saiki, S., O'Kane, C. J., and Rubinsztein, D. C. (2008). A rational mechanism for combination treatment of Huntington's disease using lithium and rapamycin. *Hum Mol Genet* *17*, 170-178.
- Satoh, A. K., and Ready, D. F. (2005). Arrestin1 mediates light-dependent rhodopsin endocytosis and cell survival. *Curr Biol* *15*, 1722-1733.
- Schroder, M., and Kaufman, R. J. (2005). ER stress and the unfolded protein response. *Mutat Res* *569*, 29-63.
- Schroder, R., Watts, G. D., Mehta, S. G., Evert, B. O., Broich, P., Fliessbach, K., Pauls, K., Hans, V. H., Kimonis, V., and Thal, D. R. (2005). Mutant valosin-containing protein causes a novel type of frontotemporal dementia. *Ann Neurol* *57*, 457-461.
- Schuberth, C., and Buchberger, A. (2005). Membrane-bound Ubx2 recruits Cdc48 to ubiquitin ligases and their substrates to ensure efficient ER-associated protein degradation. *Nat Cell Biol* *7*, 999-1006.
- Schuberth, C., and Buchberger, A. (2008). UBX domain proteins: major regulators of the AAA ATPase Cdc48/p97. *Cell Mol Life Sci* *65*, 2360-2371.
- Schwieger, I., Lautz, K., Krause, E., Rosenthal, W., Wiesner, B., and Hermosilla, R. (2008). Derlin-1 and p97/valosin-containing protein mediate the endoplasmic reticulum-associated degradation of human V2 vasopressin receptors. *Mol Pharmacol* *73*, 697-708.

- Shintani, K., Shechtman, D. L., and Gurwood, A. S. (2009). Review and update: current treatment trends for patients with retinitis pigmentosa. *Optometry* 80, 384-401.
- Sohocki, M. M., Daiger, S. P., Bowne, S. J., Rodriguez, J. A., Northrup, H., Heckenlively, J. R., Birch, D. G., Mintz-Hittner, H., Ruiz, R. S., Lewis, R. A., *et al.* (2001). Prevalence of mutations causing retinitis pigmentosa and other inherited retinopathies. *Hum Mutat* 17, 42-51.
- Sommer, T., and Jentsch, S. (1993). A protein translocation defect linked to ubiquitin conjugation at the endoplasmic reticulum. *Nature* 365, 176-179.
- Song, C., Wang, Q., and Li, C. C. (2003). ATPase activity of p97-valosin-containing protein (VCP). D2 mediates the major enzyme activity, and D1 contributes to the heat-induced activity. *J Biol Chem* 278, 3648-3655.
- Song, C., Wang, Q., and Li, C. C. (2007). Characterization of the aggregation-prevention activity of p97/valosin-containing protein. *Biochemistry* 46, 14889-14898.
- Spiro, R. G., Zhu, Q., Bhoyroo, V., and Soling, H. D. (1996). Definition of the lectin-like properties of the molecular chaperone, calreticulin, and demonstration of its copurification with endomannosidase from rat liver Golgi. *J Biol Chem* 271, 11588-11594.
- Stone, E. M., Kimura, A. E., Nichols, B. E., Khadivi, P., Fishman, G. A., and Sheffield, V. C. (1991). Regional distribution of retinal degeneration in patients with the proline to histidine mutation in codon 23 of the rhodopsin gene. *Ophthalmology* 98, 1806-1813.
- Stone, J., Maslim, J., Valter-Kocsi, K., Mervin, K., Bowers, F., Chu, Y., Barnett, N., Provis, J., Lewis, G., Fisher, S. K., *et al.* (1999). Mechanisms of photoreceptor death and survival in mammalian retina. *Prog Retin Eye Res* 18, 689-735.
- Sung, C. H., Davenport, C. M., Hennessey, J. C., Maumenee, I. H., Jacobson, S. G., Heckenlively, J. R., Nowakowski, R., Fishman, G., Gouras, P., and Nathans, J. (1991a). Rhodopsin mutations in autosomal dominant retinitis pigmentosa. *Proc Natl Acad Sci U S A* 88, 6481-6485.
- Sung, C. H., Davenport, C. M., and Nathans, J. (1993). Rhodopsin mutations responsible for autosomal dominant retinitis pigmentosa. Clustering of functional classes along the polypeptide chain. *J Biol Chem* 268, 26645-26649.
- Sung, C. H., Schneider, B. G., Agarwal, N., Papermaster, D. S., and Nathans, J. (1991b). Functional heterogeneity of mutant rhodopsins responsible for autosomal dominant retinitis pigmentosa. *Proc Natl Acad Sci U S A* 88, 8840-8844.
- Surgucheva, I., Ninkina, N., Buchman, V. L., Grasing, K., and Surguchov, A. (2005). Protein aggregation in retinal cells and approaches to cell protection. *Cell Mol Neurobiol* 25, 1051-1066.
- Szegezdi, E., Logue, S. E., Gorman, A. M., and Samali, A. (2006). Mediators of endoplasmic reticulum stress-induced apoptosis. *EMBO Rep* 7, 880-885.
- Tan, E., Ding, X. Q., Saadi, A., Agarwal, N., Naash, M. I., and Al-Ubaidi, M. R. (2004). Expression of cone-photoreceptor-specific antigens in a cell line derived from retinal tumors in transgenic mice. *Invest Ophthalmol Vis Sci* 45, 764-768.
- Thrower, J. S., Hoffman, L., Rechsteiner, M., and Pickart, C. M. (2000). Recognition of the polyubiquitin proteolytic signal. *EMBO J* 19, 94-102.
- Tirosh, B., Furman, M. H., Tortorella, D., and Ploegh, H. L. (2003). Protein unfolding is not a prerequisite for endoplasmic reticulum-to-cytosol dislocation. *J Biol Chem* 278, 6664-6672.
- Tonoki, A., Kuranaga, E., Tomioka, T., Hamazaki, J., Murata, S., Tanaka, K., and Miura, M. (2009). Genetic evidence linking age-dependent attenuation of the 26S proteasome with the aging process. *Mol Cell Biol* 29, 1095-1106.

References

- Travers, K. J., Patil, C. K., Wodicka, L., Lockhart, D. J., Weissman, J. S., and Walter, P. (2000). Functional and genomic analyses reveal an essential coordination between the unfolded protein response and ER-associated degradation. *Cell* *101*, 249-258.
- Travis, G. H. (1998). Mechanisms of cell death in the inherited retinal degenerations. *Am J Hum Genet* *62*, 503-508.
- Tresse, E., Salomons, F. A., Vesa, J., Bott, L. C., Kimonis, V., Yao, T. P., Dantuma, N. P., and Taylor, J. P. (2010). VCP/p97 is essential for maturation of ubiquitin-containing autophagosomes and this function is impaired by mutations that cause IBMPFD. *Autophagy* *6*, 217-227.
- Vandermoere, F., El Yazidi-Belkoura, I., Slomianny, C., Demont, Y., Bidaux, G., Adriaenssens, E., Lemoine, J., and Hondermarck, H. (2006). The valosin-containing protein (VCP) is a target of Akt signaling required for cell survival. *J Biol Chem* *281*, 14307-14313.
- Vaughan, D. K., Coulibaly, S. F., Darrow, R. M., and Organisciak, D. T. (2003). A morphometric study of light-induced damage in transgenic rat models of retinitis pigmentosa. *Invest Ophthalmol Vis Sci* *44*, 848-855.
- Vembar, S. S., and Brodsky, J. L. (2008). One step at a time: endoplasmic reticulum-associated degradation. *Nat Rev Mol Cell Biol* *9*, 944-957.
- Verma, R., Chen, S., Feldman, R., Schieltz, D., Yates, J., Dohmen, J., and Deshaies, R. J. (2000). Proteasomal proteomics: identification of nucleotide-sensitive proteasome-interacting proteins by mass spectrometric analysis of affinity-purified proteasomes. *Mol Biol Cell* *11*, 3425-3439.
- Vij, N., Fang, S., and Zeitlin, P. L. (2006). Selective inhibition of endoplasmic reticulum-associated degradation rescues DeltaF508-cystic fibrosis transmembrane regulator and suppresses interleukin-8 levels: therapeutic implications. *J Biol Chem* *281*, 17369-17378.
- Wahlman, J., DeMartino, G. N., Skach, W. R., Bulleid, N. J., Brodsky, J. L., and Johnson, A. E. (2007). Real-time fluorescence detection of ERAD substrate retrotranslocation in a mammalian *in vitro* system. *Cell* *129*, 943-955.
- Walsh, N., van Driel, D., Lee, D., and Stone, J. (2004). Multiple vulnerability of photoreceptors to mesopic ambient light in the P23H transgenic rat. *Brain Res* *1013*, 194-203.
- Wang, M., Lam, T. T., Tso, M. O., and Naash, M. I. (1997). Expression of a mutant opsin gene increases the susceptibility of the retina to light damage. *Vis Neurosci* *14*, 55-62.
- Wang, Q., Li, L., and Ye, Y. (2008). Inhibition of p97-dependent protein degradation by Eeyarestatin I. *J Biol Chem* *283*, 7445-7454.
- Wang, Q., Song, C., and Li, C. C. (2003). Hexamerization of p97-VCP is promoted by ATP binding to the D1 domain and required for ATPase and biological activities. *Biochem Biophys Res Commun* *300*, 253-260.
- Wang, Q., Song, C., and Li, C. C. (2004). Molecular perspectives on p97-VCP: progress in understanding its structure and diverse biological functions. *J Struct Biol* *146*, 44-57.
- Wang, T., Lao, U., and Edgar, B. A. (2009). TOR-mediated autophagy regulates cell death in Drosophila neurodegenerative disease. *J Cell Biol* *186*, 703-711.
- Wang, T., and Montell, C. (2007). Phototransduction and retinal degeneration in Drosophila. *Pflugers Arch* *454*, 821-847.
- Ward, C. L., Omura, S., and Kopito, R. R. (1995). Degradation of CFTR by the ubiquitin-proteasome pathway. *Cell* *83*, 121-127.
- Watts, G. D., Wymer, J., Kovach, M. J., Mehta, S. G., Mumm, S., Darvish, D., Pestronk, A., Whyte, M. P., and Kimonis, V. E. (2004). Inclusion body myopathy associated with Paget disease of bone and frontotemporal dementia is caused by mutant valosin-containing protein. *Nat Genet* *36*, 377-381.

- Weihl, C. C., Dalal, S., Pestronk, A., and Hanson, P. I. (2006). Inclusion body myopathy-associated mutations in p97/VCP impair endoplasmic reticulum-associated degradation. *Hum Mol Genet* *15*, 189-199.
- Weihl, C. C., Miller, S. E., Hanson, P. I., and Pestronk, A. (2007). Transgenic expression of inclusion body myopathy associated mutant p97/VCP causes weakness and ubiquitinated protein inclusions in mice. *Hum Mol Genet* *16*, 919-928.
- Westhoff, B., Chapple, J. P., van der Spuy, J., Hohfeld, J., and Cheetham, M. E. (2005). HSJ1 is a neuronal shuttling factor for the sorting of chaperone clients to the proteasome. *Curr Biol* *15*, 1058-1064.
- Wojcik, C., Yano, M., and DeMartino, G. N. (2004). RNA interference of valosin-containing protein (VCP/p97) reveals multiple cellular roles linked to ubiquitin/proteasome-dependent proteolysis. *J Cell Sci* *117*, 281-292.
- Ye, Y. (2006). Diverse functions with a common regulator: Ubiquitin takes command of an AAA ATPase. *J Struct Biol.* *156*, 29-40.
- Ye, Y., Meyer, H. H., and Rapoport, T. A. (2001). The AAA ATPase Cdc48/p97 and its partners transport proteins from the ER into the cytosol. *Nature* *414*, 652-656.
- Ye, Y., Meyer, H. H., and Rapoport, T. A. (2003). Function of the p97-Ufd1-Npl4 complex in retrotranslocation from the ER to the cytosol: dual recognition of nonubiquitinated polypeptide segments and polyubiquitin chains. *J Cell Biol* *162*, 71-84.
- Ye, Y., Shibata, Y., Kikkert, M., van Voorden, S., Wiertz, E., and Rapoport, T. A. (2005). Inaugural Article: Recruitment of the p97 ATPase and ubiquitin ligases to the site of retrotranslocation at the endoplasmic reticulum membrane. *Proc Natl Acad Sci U S A* *102*, 14132-14138.
- Ye, Y., Shibata, Y., Yun, C., Ron, D., and Rapoport, T. A. (2004). A membrane protein complex mediates retro-translocation from the ER lumen into the cytosol. *Nature* *429*, 841-847.
- Zhang, J. X., Braakman, I., Matlack, K. E., and Helenius, A. (1997). Quality control in the secretory pathway: the role of calreticulin, calnexin and BiP in the retention of glycoproteins with C-terminal truncations. *Mol Biol Cell* *8*, 1943-1954.
- Zhang, X., Shaw, A., Bates, P. A., Newman, R. H., Gowen, B., Orlova, E., Gorman, M. A., Kondo, H., Dokurno, P., Lally, J., et al. (2000). Structure of the AAA ATPase p97. *Mol Cell* *6*, 1473-1484.
- Zhao, G., Zhou, X., Wang, L., Li, G., Schindelin, H., and Lennarz, W. J. (2007). Studies on peptide:N-glycanase-p97 interaction suggest that p97 phosphorylation modulates endoplasmic reticulum-associated degradation. *Proc Natl Acad Sci U S A* *104*, 8785-8790.

References

VI. Annexes

Annexes

1. Index of figures

Figure 1	Components of the vertebrate (left) and <i>Drosophila</i> (right) visual systems	13
Figure 2	The <i>Drosophila</i> retina is made of ommatidia	14
Figure 3	The two types of vertebrate photoreceptor neurons: rods and cones	15
Figure 4	The vertebrate phototransduction cascade	16
Figure 5	Clinical characteristics of <i>retinitis pigmentosa</i>	18
Figure 6	Structure of the visual pigment Rh and the localization of RP-linked mutations	22
Figure 7	Mechanisms of photoreceptor cell death mediated by mutant Rh in <i>retinitis pigmentosa</i>	31
Figure 8	The main steps of the ERAD process	34
Figure 9	Distinct ERAD pathways and machineries	35
Figure 10	The ubiquitination process	37
Figure 11	The Unfolded Protein Response	40
Figure 12	VCP structure	43
Figure 13	VCP co-localizes with aggregated Rh in mouse retinal 661W and SK-N-SH cells	53
Figure 14	VCP forms a complex with Rh aggregates <i>in vitro</i>	55
Figure 15	The interaction between VCP and Rh aggregates is enhanced after proteasome inhibition	57
Figure 16	The D1 domain of VCP is required for interaction with Rh ^{P23H} aggregates	58
Figure 17	VCP is required for degradation of Rh aggregates <i>in vitro</i>	59
Figure 18	D2 ATPase activity of VCP is required for clearance of Rh ^{P23H} aggregates	61
Figure 19	Clearance of misfolded Rh ^{P23H} requires the D2 ATPase activity of VCP	63
Figure 20	Effect of Rh misfolding and of VCP expression on SK-N-SH cell viability	64
Figure 21	Retinal degeneration in <i>Rh1</i> ^{P37H} flies is light- and age-dependent	66
Figure 22	Progressive retinal degeneration and Rh1 loss in <i>Rh1</i> ^{P37H} flies exposed to light	67
Figure 23	Dominant effects in <i>Rh1</i> ^{P37H} flies exposed to light	69
Figure 24	Decreasing <i>VCP</i> function increases Rh1 aggregate load in <i>Rh1</i> ^{P37H} flies	71
Figure 25	Decreasing <i>VCP</i> function restores mature Rh1 levels in <i>Rh1</i> ^{P37H} flies	73
Figure 26	Increased activation of the Ire1/Xbp1 UPR pathway in <i>VCP</i> ^{26-8/+;Rh1^{P37H/+} flies}	75
Figure 27	<i>VCP</i> inactivation increases ER stress in <i>GMR/Rh1</i> ^{G69D} flies and in <i>Rh1</i> ^{G69D} flies	77
Figure 28	<i>VCP</i> inactivation suppresses first signs of retinal degeneration in <i>Rh1</i> ^{P37H} flies	78
Figure 29	Suppression of <i>Rh1</i> ^{P37H} -induced retinal degeneration by <i>VCP</i> <i>loss-of-function</i> alleles	80
Figure 30	<i>VCP</i> /ERAD/proteasome inhibition rescues <i>Rh1</i> ^{P37H} -mediated retinal degeneration	82
Figure 31	Altered phototaxis in <i>Rh1</i> ^{P37H} flies is rescued by <i>VCP</i> <i>loss-of-function</i> alleles	84
Figure 32	Blindness in <i>Rh1</i> ^{P37H} flies is rescued in a hypomorphic <i>VCP</i> ²⁶⁻⁸ background	86
Figure 33	Rescue of <i>Rh1</i> ^{D1} -induced retinal degeneration and visual impairment by <i>VCP</i> ²⁶⁻⁸	87
Figure 34	Working model for ERAD of misfolded Rh	97
Figure 35	Potential pro-apoptotic effects of the <i>VCP</i> /ERAD/proteasome axis in the <i>Rh1</i> ^{P37H} retina	105
Figure 36	Protective effect of <i>VCP</i> /ERAD/proteasome inhibition in the <i>Rh1</i> ^{P37H} retina	109
Figure 37	Targeted gene expression using the Gal4-UAS system	140
Figure 38	ER stress activates Xbp1 splicing	143
Figure 39	Chemical structures of Eeyarestatin I and MG132	144
Figure 40	Phototaxis system	144
Figure 41	ERG setup	145

2. Publications and poster presentations from the work presented in this thesis

2.1 Peer reviewed publications

Griciuc A, Aron L, Piccoli G, Ueffing M. "Clearance of Rhodopsin^{P23H} aggregates requires the ERAD effector VCP" (2010) **BBA Mol Cell Res** **1803**: 424-434

Griciuc A, Aron L, Roux M.J., Giangrande A., Ueffing M. "Inactivation of VCP/ter94 suppresses retinal pathology induced by misfolded Rhodopsin in *Drosophila*" **PLoS Genetics** **6(8)**: e1001075

Griciuc A, Aron L, Ueffing M (2010) Looking into eyes: rhodopsin pathologies in *Drosophila*. **Adv Exp Med Biol** (in press). Review

2.2 Poster presentations

Griciuc A, Aron L, Roux M.J., Giangrande A., Ueffing M. "Cellular pathways modulating Rhodopsin^{P23H}-induced pathology" ARVO 2009 Annual Meeting, Fort Lauderdale, USA, May 2009

Griciuc A, Aron L, Roux M.J., Giangrande A., Ueffing M. "VCP ablation mitigates pathology induced by misfolded Rhodopsin" 8th International Conference on AAA proteins, Toronto, Canada, July 2009

Griciuc A, Aron L, Roux M.J., Giangrande A., Ueffing M. "VCP inactivation rescues blindness and retinal degeneration caused by misfolded Rhodopsin" XIVth International Symposium on Retinal Degeneration, Mont-Tremblant, Canada, July 2010

3. Acknowledgements

During my PhD work at the Helmholtz Zentrum Muenchen I had the privilege to interact with many excellent scientists who shared their experience with me. I would like to thank the following people, who greatly facilitated my work:

Prof. Dr. Marius Ueffing for being a great supervisor, for his scientific and moral support and for the opportunity I had to do my thesis in his laboratory. Thank you for letting me work on a challenging disease-related project, for all the helpful discussions, for the encouragements and for the granted freedom to design by myself many experiments, which helped me mature as a scientist.

Dr. Liviu Aron for his help provided during my thesis project and for sharing with me his enthusiasm for science. I am thankful to Liviu for teaching me *Drosophila* genetics and for his guidance in establishing the fly facility in our laboratory.

Prof. Dr. Jerzy Adamski, my *Doktorvater*, who guided me through my thesis project, for the seminars and discussions that we had in his laboratory, and especially for helping me a lot with all the paper work related to the TU.

Dr. Angela Giangrande (IGBMC, Strasbourg) for kindly sharing with us the Rhodopsin mutant flies, for helpful discussions and for welcoming me in her laboratory. I also thank Celine Diebold for always answering my questions related to the fly lines.

Dr. Michel Roux (IGBMC, Strasbourg) who helped me acquire the ERG recordings. I am grateful to him for sharing his knowledge with me, for his optimism and especially for never giving up on my blind flies.

All members of the Marie Curie Research Training Network “NEUROTRAIN” for the very interesting workshops and annual meetings we spent together. I am also thankful to our network managers who allowed me to visit many interesting laboratories, companies and cities across Europe.

All members of the Ueffing lab for an excellent working atmosphere. In particular, I thank Dr. Stefanie Hauck and Dr. Johannes Glöckner for always being very supportive towards my work and for answering my numerous questions; Dr. Giovanni Piccoli for participating in our *in vitro* Rh-VCP project; Dr. Ralf Braun for supervising me at the beginning of my doctoral training; Saskia Hanf and Dr. Ursula Olazabal for keeping the lab in good shape, for organizing nice retreats and parties; I am also thankful to Saskia for taking care of my contract; I thank Dr. Sybille Regn and Dr. Juliana Merl for help with translation; Mrs. Luise Jennen for help with the electron microscopy experiments; I am grateful to Marieta, Patricia, Matteo, Andreas, Karsten, Caroline, Norbert, Elöd, Gaby, Andrea, Jennifer, Felix and Jack Favor for their support.

My friends Bestia, Rolf, Jukki, Codrut, Ana Barat, Alex, Hansi, Dorina and all the others for the funny moments we spent together and for a lot of moral support.

My dear Yannick who was always by my side during this time. I am thankful for his love and for all the understanding concerning my extra hours spent in the laboratory.

My family for their constant support, in particular my dear parents for their love and for supporting me during all these years.

4. Curriculum vitae

Ana Griciuc

E-mail: griciuc_ana@yahoo.fr
Born on September 30th 1983
Nationality: Romanian

Research experience

- | | |
|-----------------|---|
| Since July 2006 | Ph.D. thesis at the Helmholtz Zentrum Muenchen, Department of Protein Science (Prof. Dr. Marius Ueffing), Munich-Germany. |
| Jan.-June 2006 | M.Sc. research training at the Max-Planck Institute of Neurobiology, Group of Signal Transduction (Prof. Amparo Acker-Palmer), Munich-Germany. |
| July-Aug. 2005 | Internship at the National Institute of Health and Medical Research (INSERM), Laboratory of Metabolic Regulation, Nutrition and Diabetes (Dr. Hubert Vidal), Lyon-France. |

Education

- | | |
|----------------------|--|
| Sept. 2005-June 2006 | M.Sc. in Biochemistry from the Claude Bernard University-Lyon and INSA de Lyon-France. |
| Oct. 2004- Jan. 2005 | Academic exchange at the Technical University of Karlsruhe and Research Center of Karlsruhe-Germany. |
| 2001-2006 | Master of Engineering and Engineering degree in Biochemistry and Biosciences at the National Institute of Applied Sciences (INSA de Lyon), Department of BioSciences, Lyon-France. Bachelor studies at EURINSA (the European Department of INSA de Lyon, 2001-2003) and the Department of BioSciences (2003-2006). |
| 2001 | Baccalaureate in sciences, Chisinau-Moldova. |

Courses and workshops

- | | |
|---------------------|--|
| April 2009 | Cambridge Spring school on “Regeneration and Plasticity of Neural Circuits”, Cambridge University-UK |
| Sept. 2008 | Summer school “From functional proteomics to systems biology” organized by Interaction Proteome Research Network, Spetses-Greece. |
| July 2006-July 2009 | Took part at 3 workshops organized by the NEUROTRAIN research training network: Berlin, Lund, Tuebingen. Each workshop (duration 4 days) consisted of lectures, practicals and company visits. |

Meetings and conferences

July 2010	XIV th International Symposium on Retinal Degeneration, Mont-Tremblant-Canada, presented a poster.
July 2009	8 th International Meeting on AAA proteins, Toronto-Canada, presented a poster.
May 2009	ARVO 2009 Annual Meeting, Fort Lauderdale-USA, presented a poster
Nov. 2008	Society for Neuroscience 38 th Annual Meeting, Washington, DC-USA.
June 2008	Meeting “Enlightened views on life and death of visual cells. A celebratory tribute to Prof. C.E. Remé”, Zürich-Switzerland.
March 2007	Pro-Retina meeting “Retinal Degeneration: Genes-Progression-Therapy”, Potsdam-Germany.

Fellowships

2010	Travel fellowship to attend the XIV th International Symposium on Retinal Degeneration, Mont-Tremblant-Canada.
2006-2009	Ph.D. fellowship from the Marie Curie Research Training Network NEUROTRAIN-official EU research program.
2006	M.Sc. scholarship awarded by the Rhône-Alpes region for research work at Max-Planck Institute of Neurobiology, Munich-Germany.
2004	Erasmus scholarship awarded for one exchange semester at the Technical University Karlsruhe-Germany.
2001-2003	Scholarship awarded by the INSA de Lyon and the Rhône-Alpes region during my training at EURINSA (INSA de Lyon).

Language skills

Romanian, Russian: mother tongues
 English, French: fluent
 German, Spanish: intermediate level